Vitamin B3 salvage and NAD^+ metabolism in skeletal muscle

By

Rachel Fletcher

A thesis submitted to the University of Birmingham

for the degree of

DOCTOR OF PHILOSOPHY

Institute of Metabolism and Systems Research

College of Medical and Dental Sciences

University of Birmingham

June 2017

Abstract

Nicotinamide adenine dinucleotide (NAD^+) is both an essential redox coenzyme and a substrate for NAD^+-consuming enzymes, such as the sirtuins, which adapt transcriptional programmes to increase energy availability. Skeletal muscle is a major regulator of energy metabolism and its function is impaired with ageing. Uncovering the key routes regulating NAD^+ availability may provide valuable insight into novel aspects of skeletal muscle metabolic health. Data presented here identifies a limited set of enzymes important for skeletal muscle NAD^+-biosynthesis namely; nicotinamide phosphoribosyltransferase (NAMPT) and nicotinamide riboside kinases (NMRK) 1 and 2, which salvage vitamin B3s nicotinamide (NAM) and nicotinamide riboside (NR) to NAD^+. NAMPT was confirmed vital for recycling of NAM, with NAD^+ depleted in myotubes following NAMPT inhibition. Single and double NMRK knockout mouse models found NMRK activity non-essential for maintaining basal NAD^+, with activity restricted by NR availability. Exogenous NR delivery enhanced NAD^+ and recovered the effects of NAD^+ depletion following NAMPT inhibition. NMRK2 was determined highly muscle-specific; although energy signalling was mostly unperturbed in NMRK2KOs, *in vivo* data indicated impaired metabolic flexibility following high fat diet. While the muscle-specific role of NMRK2 requires further investigation, this thesis identifies NMRK1/2 as important therapeutic targets for enhancing NAD^+ by NR supplementation.

Acknowledgements

Firstly, and most importantly, I would like to thank my supervisor Prof. Gareth Lavery for all of his help, support, encouragement and time over the past 4 years. I am truly grateful and I know that his excellence as a scientist, innovator and mentor has enabled and inspired me to grow as a researcher. He has listened (a great deal), motivated me through the project difficulties and given me the confidence to become independent with my research ideas. I couldn't have asked for anything more.

Equally I would like to thank all the current and past members of the Lavery lab / Molecular Metabolism Research Group. Together (Craig, Agnieszka, Lucy, Yasir, Antje, Dave and Ganesh) have all contributed to my PhD experience, they have helped to make the difficult times easier and the good times better, so I am truly grateful to them all. They have not only been great colleagues but have also become great friends and I have so many fond memories. I would like to especially thank Craig, as he not only taught me everything I know in the lab (including what not to do) but endlessly supported me throughout this project. His invaluable advice, calm and in lab banter has been much appreciated. He also inspired (or challenged rather) me to take up running, I'm yet to decide how happy I feel about this, but without the 'Shadow Ninjas' I wouldn't have managed to complete two marathons during my PhD.

I would also like to thank everyone in CEDAM and the IMSR for their support and guidance. I feel incredibly lucky to have been part of such a great institute and work alongside such friendly, helpful and exceptional peers.

During my PhD I had the opportunity to partake in two placements at the University of Iowa and the Nestlé Institute of Health Sciences. I would like to thank Prof. Charles Brenner for the time I spent in Iowa City. I am grateful to Charlie and all of the Brenner group for their help and training during my visit. Equally, I would like to thank Dr Carles Canto and Nestlé for providing me with the opportunity to spend time researching in Lausanne. I am truly indebted as this work put the final pieces of my PhD research together, something I could never have done without this opportunity. I am particularly grateful to Joanna for all of her help during my time in Lausanne, we made a great team and I know I have found a true friend through this collaboration.

Finally, I would like to thank my family for a lifetime of love, care and encouragement. Their endless support has allowed me to achieve so much already. I'm incredibly proud to have such amazing parents who have always given me the freedom to thrive in whatever I choose. I'm also extremely lucky to have my brothers, James and Gary, who have inspired me since I can remember. Their successes have always motivated me to follow suit and encouraged me to strive to be the best that I can be. Last, but not least, I would like to thank Chris. We met at the beginning of my PhD journey and I couldn't think of a better person to share this experience with; he is the most hardworking and focused person I have ever met and has made me more determined than ever to succeed.

Table of Contents

List of Figures

List of Tables

Abbreviations

-VE	Negative
+VE	Positive
1C	1 cell
1K	1000 cells
AA	Antimycin A
Acetyl CoA	Acetyl coenzyme A
ACMS	α-amino-β-carboxymuconate-ε-semialdehyde
ADP	Adenosine diphosphate
ADPr	Adenosine diphosphate ribose
AMP	Adenosine monophosphate
AMPK	Adenosine monophosphate kinase
ATP	Adenosine triphosphate
AUC	Area under the curve
bFGF	Fibroblast growth factor-basic
BIOPS	Biopsy preservation solution
BP	Base pair
Brn	Brain
BSA	Bovine serum albumin
C	Carbon
Ca^{2+}	Calcium
cDNA	Complimentary DNA
CE	Collision energy
CEE	Chick embryo extract
CMP	Cytidine monophosphate
CO2	Carbon dioxide
Con	Control
COPD	Chronic obstructive pulmonary disease
COX	Cytochrome c oxidase
CREB	cyclic AMP response element binding protein
CytC	Cytochrome c
D	Deuterium
dCT	Delta cycle threshold
Dia	Diaphragm
DKO	Double Knockout
DM	Differentiation media
DMEM	Dulbecco's modified Eagle's medium
DMSO	Dimethyl sulfoxide
DNA	Deoxyribonucleic acid
dNTP	Deoxynucleotide triphosphates

Dre	Danio rerio (zebrafish)
DTT	Dithiothreitol
ECAR	Extracellular acidification rate
ECL	Electrochemiluminescence
EDL	Extensor digitorum longus
EDTA	Ethylenediaminetetraacetic acid
EGTA	Ethylene glycol-bis(β-aminoethyl ether)-N,N,N',N'-tetraacetic acid
eNAMPT	Extracellular nicotinamide phosphoribosyltransferase
ENT	Equilibrative nucleoside transporters
ES	Embryonic stem
ES	Electrical stimulation
ETC	Electron transport chain
FCCP	Carbonyl cyanide 4-(trifluoromethoxy)phenylhydrazone
FCS	Foetal calf serum
FK	FK866
FOXO	Forkhead box
G3P	Glyceraldehyde 3-phosphate
GF-AFC	Glycylphenylalanyl-aminofluorocoumarin
Glut.	Glutamate
GLUT4	glucose transporter 4
GM	Growth media
GTP	Guanosine triphosphate
GTT	Glucose tolerance test
H2O2	Hydrogen peroxide
HDAC	Histone deacetylase
HDL	High density lipoprotein
HEPES	4-(2-hydroxyethyl)-1-piperazineethanesulfonic acid
HET	Heterozygous
HFD	High fat diet
HPF	Hours post fertilisation
HPLC	High performance liquid chromatography
Hrt	Heart
HS	Horse serum
I.P	Intraperitoneal
IDH2	Isocitrate dehydrogenase 2
IDO	Indoleamine 2,3-dioxygenase
IMP	Inosine monophosphate
IS	Internal standard
K'	Retention capacity
KD	Knockdown
KH2PO4	Potassium dihydrogen phosphate
Kid	Kidney
K-MES	(2-(N-Morpholino)ethanesulfonic acid potassium salt

KO	Knock out
KOMP	Knockout Mouse Phenotyping Program
LC-MS	Liquid chromatography - mass spectrometry
LDL	Low density lipoprotein
Liv	Liver
LOQ	Limits of quantification
m/z	Mass to charge ratio
MA	Malate-aspartate
MeNAM	Methylated Nicotinamide
MgCl2	Magnesium chloride
MgCl2.6H20	Magnesium chloride hexahydrate
MIBP	Muscle-specific β1 integrin binding protein
miR149	MicroRNA 149
MiRO5	Mitochondrial respiration medium
Mm	Mus musculus (house mouse)
MRF	Myogenic regulatory factors
mRNA	Messenger RNA
Myf5	Myogenic factor 5
MYH	Myosin heavy chain
MyoD	Myogenic differentiation
NA	Nicotinic Acid
NAAD	Nicotinic acid adenine dinucleotide
NaCl	Sodium chloride
NAD(H)	Nicotinamide adenine dinucleotide
NADK	Nicotinamide adenine dinucleotide kinase
NADP(H)	Nicotinamide adenine dinucleotide phosphate
NADS	NAD+ synthase
NAM	Nicotinamide
NAMN	Nicotinic acid mononucleotide
NAMPT	Nicotinamide phosphoribosyltransferase
NaOH	Sodium hydroxide
NAPT	Nicotinic acid phosphoribosyltransferase
NaR	Nicotinic acid riboside
NEFA	Non-esterified fatty acids
NFW	Nuclease free water
NMN	Nicotinamide mononucleotide
NMNAT	Nicotinamide mononucleotide adenylyltransferase
NMRK1	Nicotinamide riboside kinase 1
NMRK2	Nicotinamide riboside kinase 2
NNMT1	Nicotinamide N-methyltransferase
NP-40	Nonidet P-40
NR	Nicotinamide Riboside
NRF	Nuclear respiratory factor

O	Oxygen
OAADPr	O-acetyl-ADP-ribose
OCR	Oxygen consumption rate
OCT	Optimal cutting temperature compound
OD	Optical density
P/S	Penicillin/Streptomycin
Palm.	palmitoyl carnitine
PARP	Poly(ADP-ribose) polymerase
Pax-7	paired box 7
PBEF	Pre-B cell colony enhancing factor
PBMC	Peripheral blood mononuclear cell
PBS	Phosphate buffered saline
PBS-T	Phosphate buffered saline-Tween
PCR	Polymerase chain reaction
PDH	Pyruvate dehydrogenase
PDK	Pyruvate dehydrogenase kinase
PGC1a	Peroxisome proliferator-activated receptor gamma coactivator 1-alpha
PNP	Purine nucleoside phosphorylase
PPAR	Peroxisome proliferator-activated receptor
PPi	Pyrophosphate
PRPP	5’-phosphoribosyl-1-pyrophosphate
qPCR	Real-time polymerase chain reaction
QPRT	Quinolinate phosphoribosyl-transferase
QUAD	Quadriceps
RER	Respiratory exchange ratio
RIPA	Radioimmunoprecipitation assay
RNA	Ribonucleic acid
ROS	Reactive oxygen species
rpm	Revolutions per minute
RQ	Respiratory quotient
RT	Reverse transcription
RT	Room temperature
RT	Retention time
SDS	Sodium dodecyl sulfate
SDS-PAGE	Sodium dodecyl sulphate - polyacrylamide gel electrophoresis
ShARM	Shared Ageing Research Models
siRNA	Short interfering RNA
SIRT	Sirtuin
SNS	Somatic nervous system
SOL	Soleus
Sph	Sphere
SR	Sarcoplasmic reticulum
SRM	Selective reaction monitoring

Succ.	Succinate
T2D	Type 2 diabetes mellitus
TA	Tibialis anterior
TBE	Tris-borate-EDTA
TCA	Tricarboxylic acid cycle
TDO	Tryptophan2,3-dioxygenase
TEMED	Tetramethylethylenediamine
TFAM	Mitochondrial transcription factor A
Tris HCl	Trizma hydrochloride
TSA	Trichostatin A
UCP2	Uncoupling protein 2
UMP	Uridine monophosphate
v/v	Volume/volume
w/v	Weight/volume
Wat	White adipose tissue
WT	Wild type
XF	Extracellular flux

Chapter 1 General Introduction

1.1 Skeletal muscle metabolism

Skeletal muscle is an essential contractile tissue made up of myofibres and connective tissue, integrated with neural and vascular networks [1]. As the largest organ by mass, accounting for around 40% of a healthy adult's total body mass, maintaining muscle health and function is vital for preserving systemic homeostasis [1].

1.1.1 Skeletal muscle structure

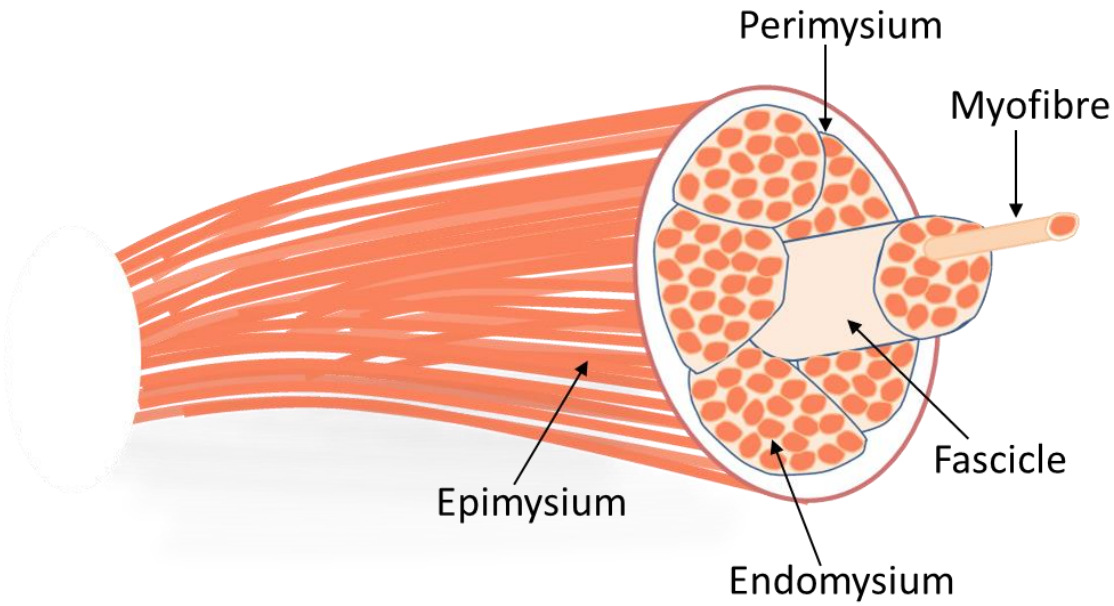

Figure 1.1 Skeletal muscle structure
Individual myofibres are surrounded by connective tissue (endomysium). They are bundled into fascicles and held by further connective tissue (perimysium). Fascicles are grouped together to form muscle tissue and coated by an outer membrane (epimysium).

Skeletal muscle is one of three main muscle types (skeletal, cardiac and smooth muscle) [2] characterised by its multinucleated, long and cylindrical shaped cells and is under the voluntary control of the somatic nervous system (SNS) [1]. These

multinucleated cells are known as myofibres, which are individually coated with a layer of connective tissue called the endomysium. Muscle fibres are bundled together by further connective tissue, the perimysium, to form muscle fascicules and the entire muscle is surrounded by the epimysium, an outer layer of connective tissue (figure 1.1) [3, 4].

Myofibres are composed of filamentous bundles, known as myofibrils, which extend across the whole length of the fibre [5]. Actin and myosin are the two main myofilaments in muscle but troponin and tropomyosin also play an important role. The filaments are grouped by appearance into thin (actin, troponin and tropomyosin) and thick filaments (myosin) [6]. The arrangement of thick and thin myofilaments within individual myofibrils is known as a sarcomere; the striated appearance of skeletal muscle is a result of repeated alignment of sarcomeres within myofibres. Individual sarcomere regions were originally described due to their appearance and named using alphabetical letters. The dark anisotropic region of the sarcomere refracts polarised light and is known as the A band, in contrast the lighter isotropic region does not refract polarised light and is termed the I band. The line dividing the I band is called the Z line and one Z line to the next makes up one sarcomere unit (figure 1.2) [7].

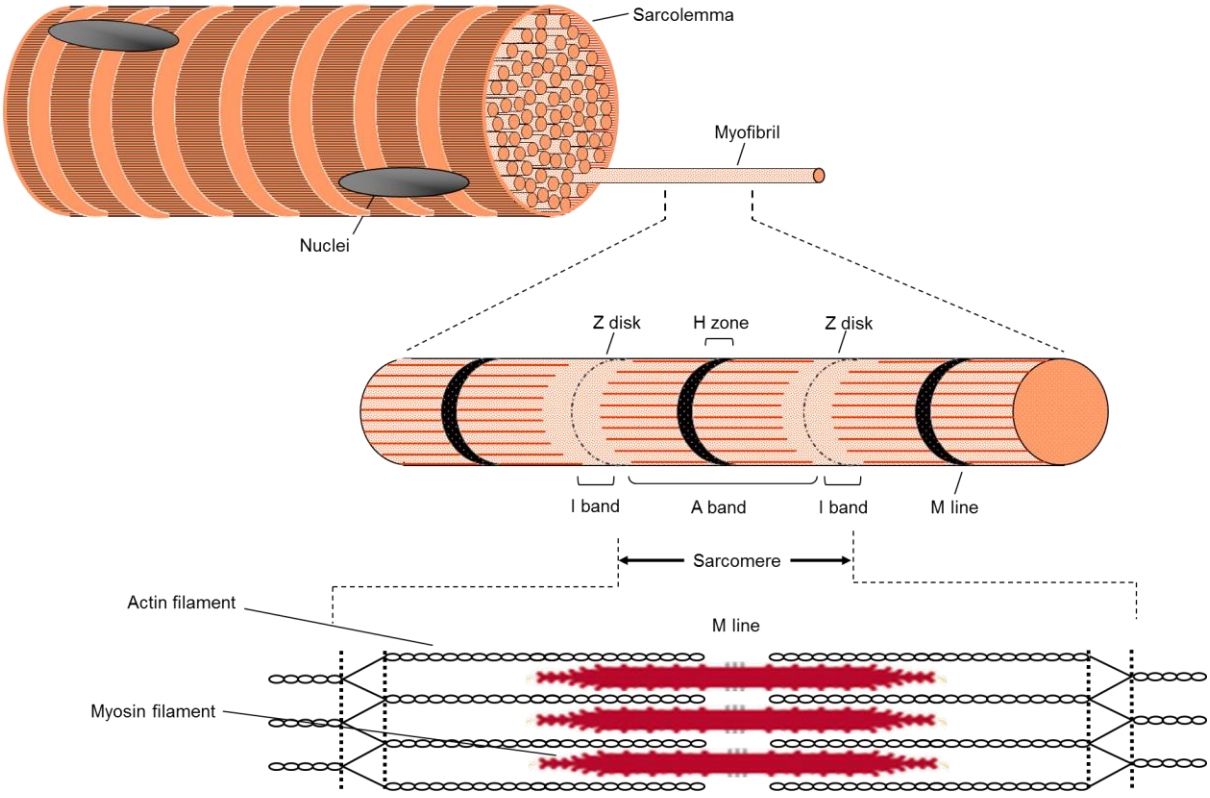

Figure 1.2 Structure of individual myofibres

Different levels of myofibre structure. Myofibrils are packed into a multinucleated myotubes (top). The sarcomere unit of Individual myofibrils consists of aligned myofilaments (bottom).

1.1.2 Myogenesis

During mammalian embryonic development skeletal muscle of the vertebrate mostly originates from lateral plate and paraxial somatic mesoderm [8]. Following somite segmentation, the dermomyotome is formed and involution of these cells gives rise to the myotome. The process of skeletal myogenesis is a 2-step process which firstly requires the commitment of mesodermal cells to myoblasts and then terminal differentiation of myoblasts to myotubes. Both steps are highly regulated by a number of myogenic regulatory factors (MRFs) including Myf5, MyoD, myogenin and MRF4. Myf5 is the earliest MRF to be expressed during muscle

development [9], and is thought to be an important muscle commitment factor, followed by MyoD, MRF4 and myogenin; the latter three are thought to play a role in terminal differentiation (figure 1.3 demonstrates a simplified example of myogenesis). Importantly, numerous single and combined loss of function studies show incredible redundancy of these MRFs during muscle development and their roles are not limited to either stage of myogenesis [10].

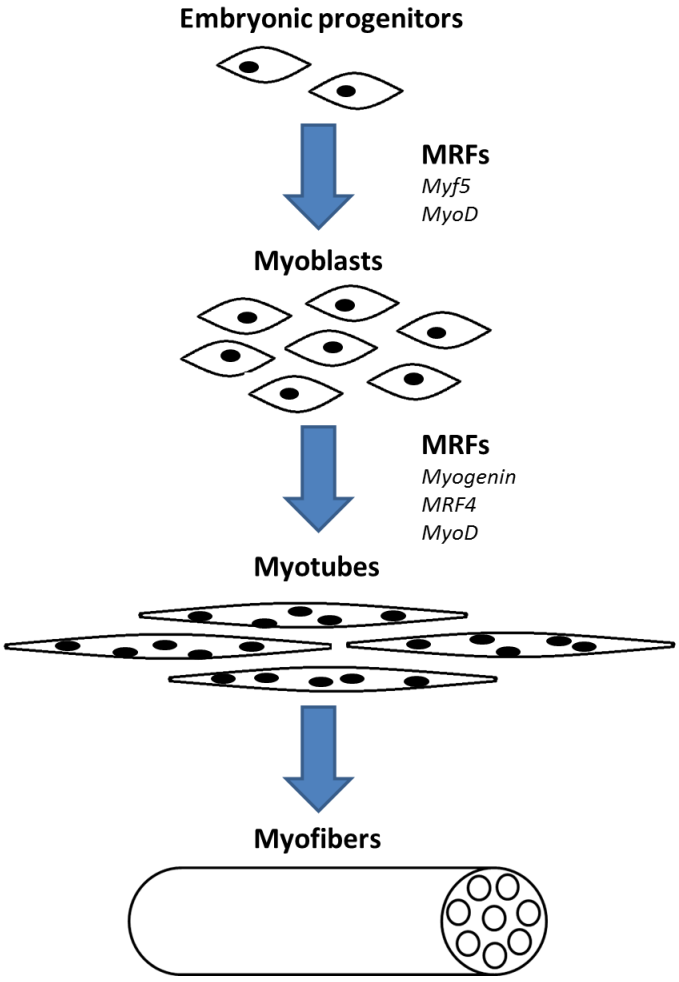

Figure 1.3 Myogenesis

A simplified outline of skeletal muscle myogenesis. This highly regulated process involves several MRFs allowing progenitor cell commitment to myoblasts and differentiation into multinucleated myotubes which are then arranged into myofibres.

As myotubes are post-mitotic, the highly regenerative capacity of muscle is coordinated by a unique subset of cells known as satellite cells. Satellite cells are myogenic precursor cells, with stem-cell like properties, that are located on the surface of terminally differentiated myotubes [11]. In sedentary adult muscle they typically remain quiescent, expressing the transcription factor paired box 7(Pax-7). In response to physiological (exercise) and pathological (muscle cell death or injury) stimuli, satellite cells are taken out of quiescence by the upregulation of Myf5 and MyoD [12]. Activation of satellite cells allows muscle regeneration through cell proliferation, myogenic commitment, and differentiation; in a process regulated by MRFs akin to embryonic muscle development (figure 1.3). Differential expression of these myogenic factors, alongside extensive intracellular and extracellular signalling cascades induced by muscle injury (e.g. downregulation of notch signalling and upregulation of Wnt signalling), subsequently drives activation, proliferation, and differentiation [12].

1.1.3 Skeletal muscle function

Skeletal muscle typically coincides alongside bone and connective tissue to form the musculoskeletal system crucial for stability, locomotion of the body and physiological respiration [13, 14]. These vital physiological processes are coordinated through excitation-contraction coupling in response to motor neuron signalling with tension generated by muscle contraction. Following somatic neural stimulation, an action potential is fired leading to calcium (Ca^{2+}) release from the sarcoplasmic reticulum (SR) into the sarcoplasm of muscle cells. A surge in free Ca^{2+} leads to reformation of the complex formed by actin, troponin and tropomyosin filaments; whereby troponin binds to free Ca^{2+} and changes position. This allows actin to interact with the head groups of myosin filaments. Binding of

adenosine triphosphate (ATP) to myosin heads leads to dissociation from actin filaments and subsequent hydrolysis of ATP causes a change in to angle of the myosin head and results in movement along the actin filament and shortening of the sarcomere. This process is repeated with further ATP, and as the filaments appear to slide over each other this interaction was termed the 'sliding filament theory' (figure 1.4) [15-17]. Although skeletal muscle is both structurally and functionally distinct from cardiac and smooth muscle, the actin-myosin driven contractile process between the three different muscle types remains similar.

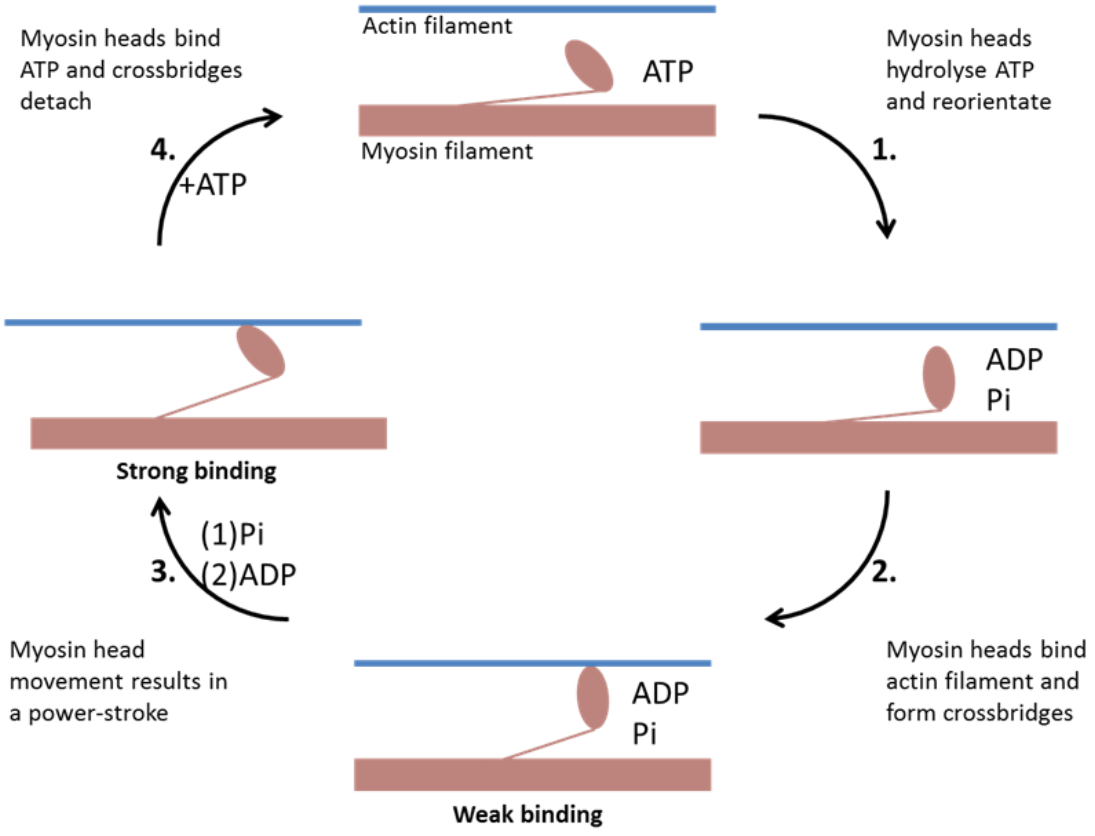

Figure 1.4 The sliding filament theory

(1) ATP hydrolysis by myosin heads leads to a conformational change (2) allowing the myosin heads to bind actin filaments and form crossbridges. (3) Through a 'powerstroke', myosin heads move towards the middle of the sarcomere and (4) then binding of ATP to the myosin heads leads to dissociation of crossbridges ready for the cycle to start again.

1.1.4 Skeletal muscle fibre types

Muscle fibre composition is heterogeneous. The three muscle fibre types in mammalians are type 1, type 2A and type 2X (humans or 2B rodents), determined by the expression of different myosin heavy chain isoforms (MYH7, MYH2 and MYH1 (or MYH4) respectively) [18, 19]. Type 1 and 2A are typically more oxidative while type 2X fibres are glycolytic [20]. Although in most cases fibre type composition is mixed, the distribution of different fibre types that make up an individual muscle mostly depends on the activity the muscle is intended to do. Muscles important for endurance or low intensity activity, such as maintaining posture, are predominantly composed of oxidative (slow-twitch) fibres, whereas muscles intended for high intensity exercise such as weightlifting are mostly composed of glycolytic (fast-twitch) fibres [21]. Table 1.1 demonstrates some of the key differences between the muscle fibre types [19, 22]**.** For example, oxidative fibres have a good blood supply to deliver fuel and oxygen, they resist fatigue and are abundant in mitochondria allowing a high oxidative capacity. On the other hand, glycolytic fibres typically, generate strong force, have lower levels of mitochondria and myoglobin due to their preference of non-oxidative metabolism. Further factors that influence fibre type composition include age, metabolic health and exercise training [23-25].

	Type 1	Type 2A	Type 2X	Type 2b
Activity	Oxidative / aerobic	Oxidative-glycolytic / mostly aerobic	Glycolytic / anaerobic	Glycolytic / anaerobic
Fatigue resistance	High	Fairly high	intermediate	Low
Contraction time	Slow	Moderately fast	Fast	Very fast
Myosin heavy chain	MYH7	MYH2	MYH1	MYH4
Force production	Weak	Moderate	Strong	Very strong
Blood supply	Good	Good	Poor	Poor
Mitochondria	Rich	Rich	Poor	Poor
Myoglobin content	Rich	Rich	Poor	Poor
Oxidative capacity	Very high	High	Low	Low
Glycolytic capacity	Low	Intermediate	High	High
Main fuel storage	Triglycerides	Creatine phosphate, glycogen, triglycerides	Creatine phosphate, glycogen	Creatine phosphate, glycogen

Table 1.1 – Muscle fibre properties in humans and rodents [19, 22]

1.1.5 Skeletal muscle energy metabolism

Further to physical movement, skeletal muscle plays a crucial role in energy metabolism and nutrient storage [26, 27]. As the largest organ by mass, skeletal muscle is the body's major site of glycogen storage and acts as an energy reservoir to sustain systemic energy homeostasis and deal with perturbations following metabolic stresses like physical activity, food intake or fasting by modulating glucose uptake and glycogen breakdown [28, 29]. During metabolic stress, muscle demonstrates high plasticity through its ability to metabolically adapt both acutely and chronically in response to environmental cues, intrinsic hormonal signals and myokines to meet changing energy requirements [30, 31]. Metabolic adaptations include modulating mitochondrial biogenesis and function, myogenesis or atrophy, glucose mobilisation, fuel substrate use, blood flow, fibre-

type composition and fibre size [23, 32]. However, the adaptive response of muscle can be compromised in numerous disease states including diabetes, cancer cachexia and chronic obstructive pulmonary disease (COPD) with muscle wasting and impaired energy homeostasis common [33-35].

The primary fuel source used in muscle to produce ATP is dependent on the type of muscle activity and energy demand. The main fuels stored in muscle tissue are glycogen, creatine phosphate, and triglycerides (figure 1.5) [36, 37]. Creatine phosphate provides a rapid short-term energy source that is metabolised to creatine, whilst donating a phosphate group to ADP in the process [37]. Alternatively, glycogen stores can be broken down to glucose and used to fuel sustained activity [38]. During anaerobic glycolysis a chain of enzymatic reactions generate ATP through the breakdown of glucose to pyruvate [39]. For endurance activities, a much greater supply of energy is required and under aerobic conditions pyruvate enters the mitochondria and is converted to acetyl Coenzyme A (acetyl CoA). Acetyl CoA is oxidised in the Krebs cycle and importantly results in the reduction of NAD^+ to NADH; an essential reducing agent for driving oxidative phosphorylation and leading to larger scale ATP production [39, 40]. Finally, fatty acids can be broken down to provide an alternative source of acetyl CoA and ultimately generate ATP. Triglycerides stored in adipose tissue are broken down by lipolysis to glycerol and free fatty acids. The fatty acids can then be transported to other cells where they react with coenzyme A (CoA) to produce acyl-CoA, which finally undergoes β-oxidation resulting in acetyl-CoA to fuel the Krebs cycle [41].

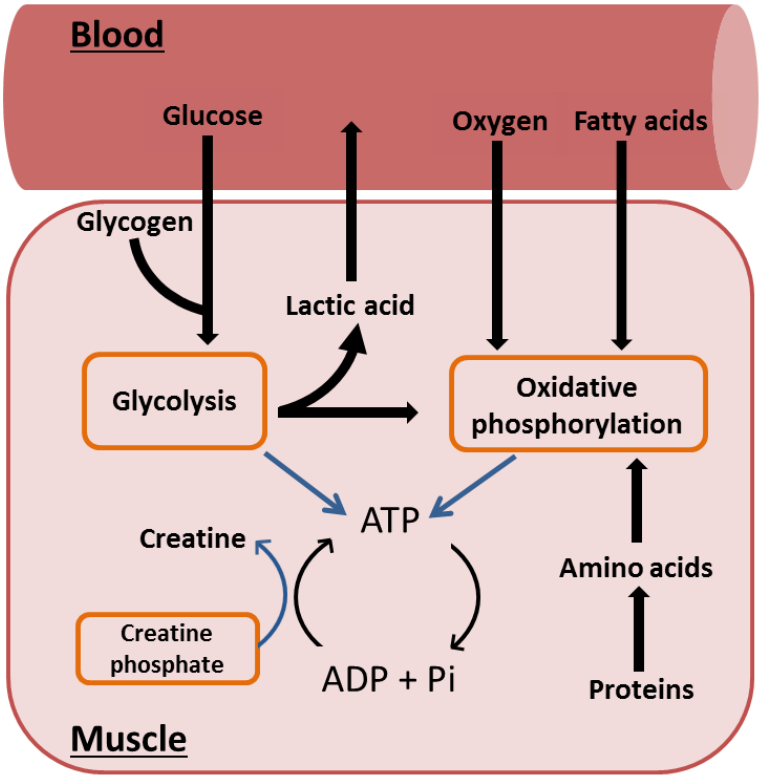

Figure 1.5 The important fuel sources for skeletal muscle energy production

Skeletal muscle acts as a major energy fuel store. For acute activity, it can use creatine phosphate to generate ATP and creatine. Muscle also stores glycogen that can be broken down to glucose and used for glycolysis. For sustained activity, oxidative metabolism is required to produce larger quantities of ATP. In oxygenated conditions, pyruvate from glycolysis can enter the TCA cycle. Fatty acids can be transported through the circulation to the muscle and β-oxidation leads to acetyl-CoA production. During starvation muscle protein can be broken down providing amino acids which can be used to assemble substrates for the TCA cycle (e.g. pyruvate).

Alternatively, when muscle energy stores are depleted (typically in starvation) amino acids from muscle protein itself can be used to generate ATP. Muscle degradation releases amino acids such as alanine for hepatic gluconeogenesis or in some cases (mostly leucine, isoleucine, and valine) in the muscle. This allows the building of substrates for energy production including pyruvate and intermediates of the TCA cycle [42, 43]. However, the use of amino acids from

muscle for energy is limited as excessive breakdown of muscle protein can lead to muscle atrophy if protein degradation exceeds protein synthesis [44].

1.1.6 Metabolic adaptation to exercise

Adaptive changes that manifest in muscle during metabolic stress demonstrate its plasticity in response to scenarios that may otherwise threaten energy homeostasis, including exercise, food consumption and fasting. For example, contracting muscle during exercise leads to a surge in ATP consumption [45]. Thus, widespread metabolic adaptation is necessary for the muscle to meet the increased energy requirements during the bout of exercise as well as improving muscle performance and endurance during repeated bouts of exercise. A large array of genomic, proteomic and metabolic changes are stimulated in skeletal muscle during and following exercise. Contraction induced cues (including posttranslational modifications and changes to metabolite levels) selectively activate transcription factors central to regulating metabolic genes; permitting molecular reprogramming. Some of the many important adaptive response targets include forkhead transcription factor (FOXO1), cyclic AMP response element binding protein (CREB), histone deacetylase (HDAC), Myogenic regulatory factors (MRFs), peroxisome proliferator-activated receptor gamma coactivator-1-alpha (PGC1α), mitochondrial transcription factor A (Tfam), nuclear respiratory factor (NRF) and glucose transporter 4 (GLUT4) [46]. Important targets of metabolic adaptations include energy production pathways (oxidative phosphorylation and carbohydrate metabolism), myogenesis, lipid mobilisation, increased blood flow and mitochondrial biogenesis to support mitochondrial metabolism and ATP generation (figure 1.6). Metabolic reprogramming intends to maximise substrate

delivery and in turn enhance glycolytic activity and/or mitochondrial oxidative capacity; allowing improved performance and resistance to fatigue on repeat [46].

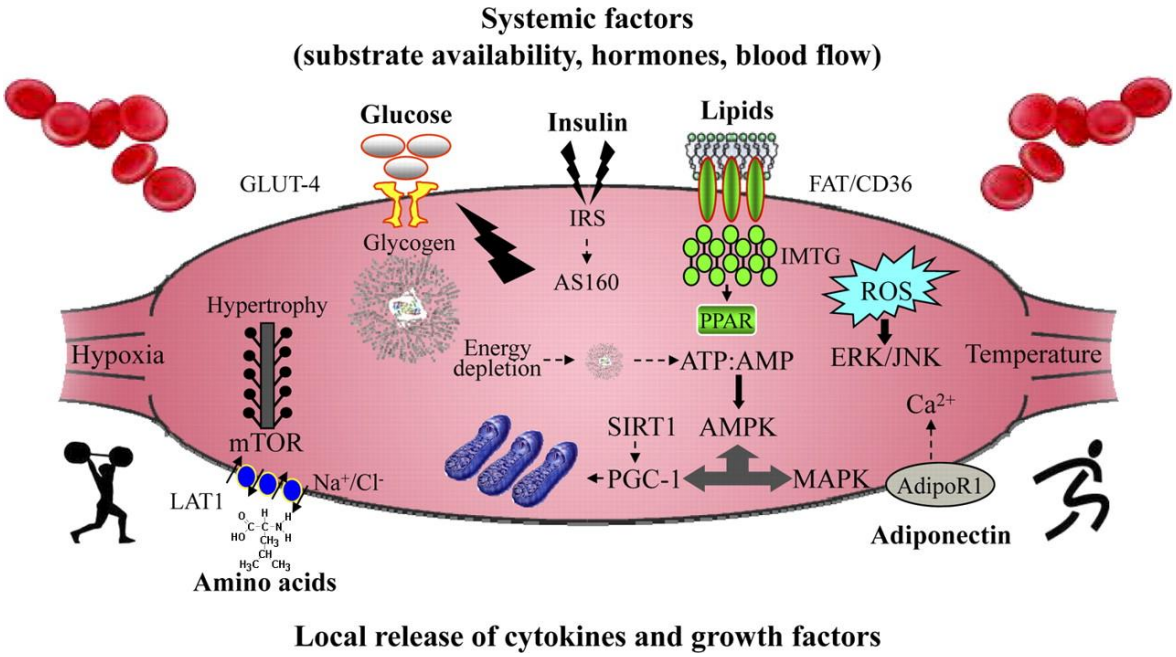

Figure 1.6 Pathways and responses involved in metabolic adaptation

An overview of important pathways targeted during the adaptive response to exercise and the desired outcomes. Metabolic and transcription reprogramming results in both systemic and local adaptations. Systemic changes include increased blood flow and delivery of substrates (lipids, glucose). Local adaptations include the release of growth factors and myokines to act upon cell receptors and induce cellular signalling cascades. Intrinsic changes induced by contacting muscle such as, substrate depletion, hypoxia and lactate accumulation combine with local and systemic signalling to drive metabolic adaptation [30].

The specific adaptations seen in response to exercise are dependent on the type of exercise performed [46]. Table 1.2 demonstrates some of the common skeletal muscle metabolic adaptations following high intensity and endurance exercise. Metabolic adaptation following high intensity exercise mostly leads to muscle hypertrophy with an increase in protein synthesis and muscle strength; whereas

adaptations following endurance activity target oxidative performance through enhanced mitochondrial function [46-48].

	High intensity	Endurance
Muscle mass	**+ + +**	**=**
Mitochondrial biogenesis	**+**	**+ + +**
Myofibrillar protein synthesis	**+ + +**	**+ / =**
Mitochondrial protein synthesis	**= / +**	**+ +**
Contractile force	**+ + +**	**= / –**
Capillarisation	**=**	**+ +**
Endurance capacity	**= / +**	**+ + +**

Table 1.2 – Skeletal muscle metabolic adaptations following exercise ([**+**] is an increase, [**=**] is unchanged and [**–**] is a decrease, **+++** is high, **++** is intermediate, **+** small and **+ / =** is a slight change).

Exercise training also results in adaptations to systemic metabolism including; elevated bone mineral density, increased insulin sensitivity, lower percentage body fat, reduced inflammatory markers and increased basal metabolic rate [49-52]. Together, these systemic and muscle specific adaptations demonstrate the globally beneficial health effects of physical activity and highlights the importance of understanding the key interactions and regulators involved in metabolic adaptation.

1.1.7 Mitochondrial biogenesis and metabolism

Mitochondria are distinct double membraned organelles with their own circular genome at around 16 Kb in size and can divide independently from the cell [53,

54]. They evolved by endosymbiosis from bacteria residing in larger cells and still share some characteristics with bacteria [55]. Mitochondria are known as the 'powerhouses' of cells; providing ATP by oxidative phosphorylation and are therefore abundant in skeletal muscle, particularly in slow-twitch fibres, to ensure energy production meets demand [22, 40]. Mitochondrial biogenesis is a process that results in the growth and division of mitochondria and is essential for maintaining function. Studies have shown disruption to mitochondrial biogenesis during ageing – associated with a reduction in activity of mitochondrial regulatory proteins such as AMP-activated protein kinase (AMPK) – results in reduced mitochondrial function [56]. There are numerous contributory factors regulating mitochondrial biogenesis including physical activity, calorie restriction, oxidative stress, cold temperatures, cell regeneration, cell differentiation, age and disease [57-59]. Mitochondrial biogenesis is normally coordinated in parallel to an increase in mitochondrial size and mass; collectively resulting in enhanced mitochondrial capacity. PGC1α is the principal coordinator of mitochondrial biogenesis, and on activation by deacetylation it activates cohorts of mitochondrial transcription factors, including nuclear respiratory factor (NRF) 1 and 2, uncoupling protein 2 (UCP2) and mitochondrial transcription factor A (TFAM), required for the transcription and replication of mitochondrial DNA [57-59].

As a master regulator of mitochondrial biogenesis, PGC1α is highly modulated by upstream energy sensing proteins such as AMPK [56]. AMPK acts as an energy sensor within the cell to ensure ATP consumption and generation are tightly regulated. When ATP levels drop, such as during exercise, a rise in AMP or ADP leads to the activation of AMPK [31], which coordinates the reprogramming of cellular energy pathways to enhance energy production and inhibit consumption

[60, 61]. Importantly, AMPK can directly phosphorylate PGC1α and upregulate expression of metabolic genes (including GLUT4, Cytochrome C, UCP2 and UCP3) to stimulate mitochondrial biogenesis and ultimately enhance ATP production [62]. Another notable regulator of PGC1α is the NAD^+-dependent enzyme Sirtuin1 (SIRT1), which responds to an increase in NAD^+ levels during metabolic stress and activates PGC1α by deacetylation [31, 63]. Together, these reversible post-translational modifications to PGC1α allow rapid and highly sensitive modulation of mitochondrial biogenesis.

1.2 NAD^+: History and classic functions

The coenzyme NAD^+ is a vital cellular signalling intermediate first identified more than a century ago as a cofactor in yeast fermentation and now widely known for its essential role in energy production [64-66]. It consists of a nicotinamide and an adenine nucleotide joined by respective phosphate groups to form a dinucleotide and exists in both an oxidised (NAD^+) and reduced (NADH) forms (figure 1.7). Oxidised NAD^+ accepts electrons from molecules and is thereby reduced to NADH; this transfer of electrons allows oxidoreductase enzymes to catalyse transhydrogenase reactions. Otto Warburg further determined the importance of NAD^+ as a cofactor and it is now well recognised that NAD(H) in both its oxidised and reduced form is essential to many fundamental cellular processes [67].

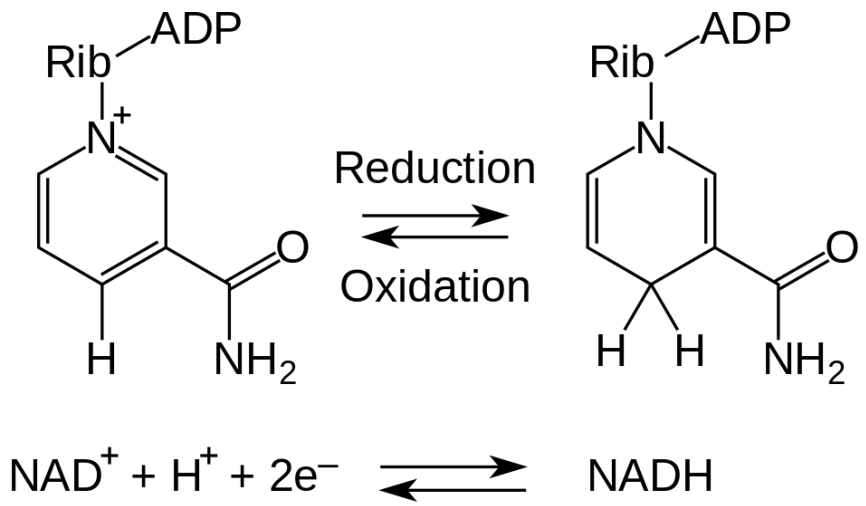

Figure 1.7 NAD(H) as a coenzyme

Reversible hydride transfer by NAD redox reactions. During oxidation NAD^+ accepts electrons and is reduced to NADH. NADH may then act as a reducing agent by donating electrons.

Although not limited to energy production, the vital role of NAD^+ as a redox cofactor for rate limiting enzymes in pathways that generate ATP, such as glycolysis and oxidative phosphorylation, is well demonstrated [68] . NADH can be generated from the reduction of NAD^+ in glycolysis, whereby NAD^+ acts as an essential cofactor for glyceraldehyde-3-phosphate dehydrogenase activity, converting glyceraldehyde-3-phosphate to 1,3-biphosphoglycerate [69]. Under oxidative conditions pyruvate, ultimately produced from glycolysis can be metabolised to acetyl CoA by pyruvate dehydrogenase with NAD^+ concurrently reduced to NADH [70]. Alternatively, fatty acid oxidation and oxidation of ketone bodies can also produce acetyl CoA and both processes also feature enzymes that require NAD^+ as a cofactor (e.g. long-chain 3-hydroxyacyl-CoA dehydrogenase, hydroxyacyl-CoA dehydrogenase and D-β-hydroxybutyrate dehydrogenase) [71, 72]. The TCA cycle hosts further NAD^+ redox enzymes (isocitrate dehydrogenase, α-ketoglutarate dehydrogenase and malate

dehydrogenase) [73]. The reduction of NAD^+ to NADH by these enzymes is essential to drive the electron transport chain (with FAD+ to FADH) by donating electrons to acceptors (figure 1.8) [72]. Depletion of cellular NAD^+ has been shown to impede glycolysis and oxidative phosphorylation, ultimately leading to a loss in cellular ATP and cell death; demonstrating the importance of redox signalling pathways [74-76].

Notably, NAD^+ can also be phosphorylated by NAD kinase (NADK) to $NADP^+$ and similarly this also exists in its reduced form NADPH. NADPH acts as an important reducing agent aiding many anabolic pathways including nucleic acid and lipid biosynthesis [77]. NADPH can be generated by the pentose phosphate pathway through glucose-6-phosphate dehydrogenase and phosphogluconate dehydrogenase redox activity where by ribose-5-phospate can be also produced for nucleotide and nucleic acid synthesis [78, 79]. NADPH also plays an important role is alleviating oxidative stress following an increase in the production of reactive oxygen species by acting as an essential reducing factor for antioxidants such as glutathione that remove hydrogen peroxide, a downstream product of ROS [80].

Beyond its redox role, NAD^+ was later proposed to have additional important functions owing to its high turnover rate with the majority of NAD^+ synthesised later consumed and only a small proportion maintaining the NAD^+ pool [81]. Further evidence was provided when the half-life of NAD^+ in enucleated cell types was extended to 10 hours from an average of ~ 1 hour in nucleated cells [81, 82]. It has since been established that NAD^+ is an important cellular signalling molecule [83-86].

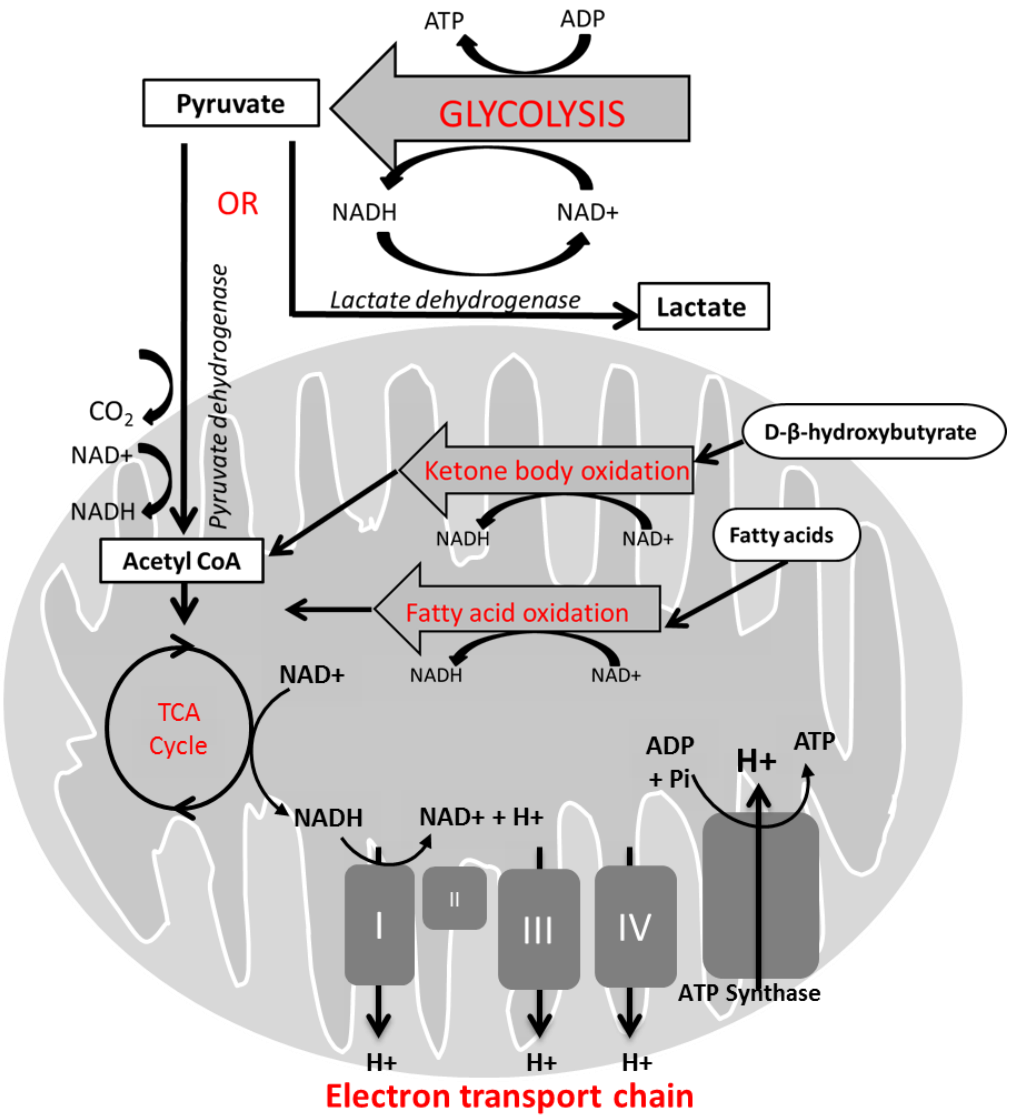

Figure 1.8 NAD^+ as a cofactor in energy production

NAD^+ is an essential cofactor that features in the energy production pathways of glycolysis, fatty acid oxidation, oxidation of ketone bodies, tricarboxylic acid cycle (TCA) and the electron transport chain.

More recently, NAD^+ has been identified as a signalling molecule. During these signalling events, NAD^+ is consumed by numerous enzymes including sirtuins (SIRTs), poly (ADP-ribose) polymerases (PARPs) and cADP-ribose synthases. The discovery of these NAD^+ driven enzymatic reactions has since recognised NAD^+ as an important modulator of metabolism and energy homeostasis as well as DNA repair and calcium signalling [87-90].

More specifically, the new found metabolic regulatory role of NAD^+ is predominantly exerted through its ability to activate SIRTs, NAD^+ 'sensing' proteins, which act downstream to modulate energy metabolism [91]. SIRT activity is NAD^+ dependent; thus to prevent cellular NAD^+ depletion upon consumption by SIRTs, and other NAD^+ signalling enzymes such as PARPs [92], NAD^+ biosynthesis and salvage pathways are critical for replenishing NAD^+ in order to preserve vital signalling processes and support NAD(P)(H) dependent reactions.

Although currently not fully understood due to technical limitations, organelle specific expression of NAD^+ generating and consuming enzymes indicates the presence of distinct subcellular pools of NAD^+ in the mitochondria, nucleus and cytoplasm [93, 94] (figure 1.9). Recent technical advances using an NAD^+ fluorescent biosensor supports this notion and shows that nucleic and cytosolic NAD^+ levels appear interchangeable whereas mitochondrial NAD^+ independently fluctuates [94]. These individual NAD^+ pools allow for tightly regulated and compartment specific NAD/NADH redox reactions and signalling. NAD^+ can pass freely through the pores of the nuclear membrane and thus nuclear NAD^+ is thought to be comparable to cytoplasmic; whereas NAD^+ and NADH are impermeable to the mitochondrial membrane. The size of compartmental NAD^+ pools also differ between tissues, for example cardiac myocytes were previously shown to have a much higher percentage of mitochondrial NAD^+ compared to the cytosolic yet other cell types including astrocytes and hepatocytes have a larger cytosolic pool [95]. These differences are likely to be related to the oxidative capacity and function of the individual cell. Further evidence for a distinct mitochondrial pool was identified by mitochondrial resistance to NAD^+ decline

following pharmacological cellular depletion of NAD^+ [96]; allowing for continued oxidative phosphorylation and protecting from cell death for over 24 hours [96].

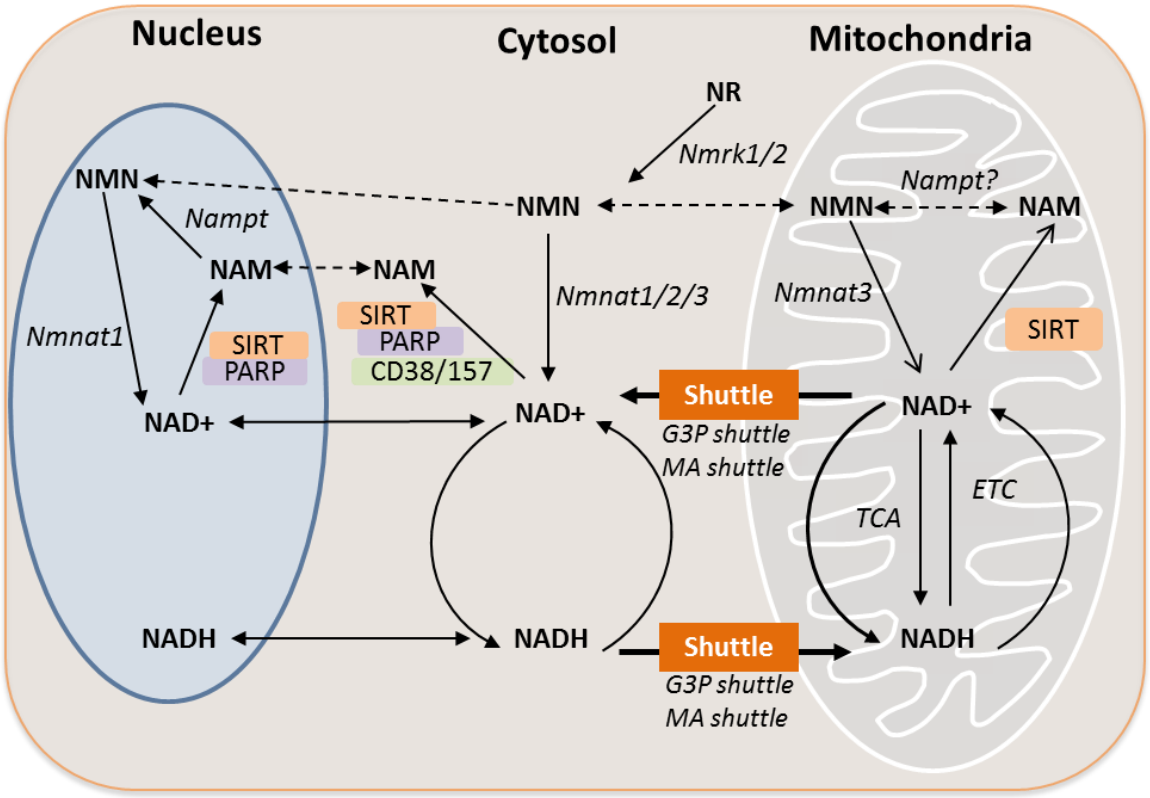

Figure 1.9 Subcellular NAD^+ compartmentation

Graphical representation of different cellular NAD^+ pools and localisation of NAD^+ generating (Nampt, Nmnat, Nmrk) and consuming enzymes (PARPs, SIRTs and CD38/CD157). NAD^+ can freely move through nuclear pores from the cytoplasm; with nucleic and cytosolic levels thought to be comparable. The mitochondrial membrane in impermeable to NAD^+ and NADH and therefore relies on shuttles including glyceraldehyde-3-phosphate (G3P) or malate-aspartate (MA) shuttles to transfer electrons across the mitochondrial membrane. Enzymatic reactions involving the same shuttles leads to NAD^+ generation and replenishes cytosolic NAD^+.

Despite compartmentalisation of NAD^+ pools, and although the mitochondrial membrane is impermeable to NAD^+ and NADH, there is still vital crosstalk between compartments (figure 1.9). For example, pyruvate and NADH derived from glycolysis in the cytosol are important reducing factors for the tricarboxylic acid cycle (TCA) and the electron transport chain (ETC). Electrons from cytosolic

NADH are shuttled into the mitochondria by glyceraldehyde-3-phosphate (G3P) or malate-aspartate shuttles [97] and NAD^+ released into the cytosol. Therefore, cytosolic NAD^+ content is an important determinant of mitochondrial NADH flux; with substantial drops in NAD^+, particularly in cells using glucose as a principal fuel source, leading to a loss of cell viability [97].

1.3 NAD^+ signalling and consumption

Since NAD^+ has been acknowledged for its integral role as a consumed substrate in multiple cellular signalling pathways, understanding the importance and regulation of cellular NAD^+ levels and availability is imperative. NAD^+ consumption during signalling is mostly attributed to the activity of three enzyme families: SIRTS, PARPs and cyclic ADP-ribose synthases [98-100]. The relative amount these enzymes contribute to NAD^+ consumption may have an important influence on the activity of the other enzymes through changes to NAD^+ availability; highlighting the important need to consider crosstalk between these distinct signalling pathways.

1.3.1 Sirtuins

The SIRT proteins are a family of seven NAD^+ dependent deacetylases, known as SIRT1-7, which act as metabolic sensors within the cell [101]. They are homologous to Sir2 in yeast, thought to mediate cellular longevity post calorie restriction [102], and work by reversing acetylated lysine residues on proteins such as histones [103]. However more recent research, standardising for the genetic background of Caenorhabditis elegans and Drosophila melanogaster models through outcrossing, showed that Sir2 overexpression did not impact on lifespan and in fact differences previously seen were explained by alternative genetic

mutations [104]. On activation, the SIRTs can induce metabolic adaptations through the regulation of downstream metabolic transcriptional targets. During SIRT-mediated deacetylation, NAD^+ is consumed and the products nicotinamide (NAM) and O-acetyl-ADP-ribose (OAADPr) are released (figure 1.10) [105, 106]. The seven SIRT homologs are ubiquitously expressed and share a core 275 amino acid sequence attributing to their catalytic activity [107]. The different SIRT enzymes can be further grouped by their organelle specific expression (although expression is not completely compartment exclusive). SIRT1, SIRT6 and SIRT7 are mostly localised in the nuclei and are able to easily access and modulate nuclear transcription factors and chromatin remodelling proteins [108]. SIRT2 is predominantly cytoplasmic and can regulate transcription factors that reside in the cytoplasm when inactive [109]. Finally, SIRT3, SIRT4 and SIRT5 are mainly localised in the mitochondria and are thought to play critical roles sensing the cellular redox state and inducing appropriate metabolic responses [107, 110]. Together the SIRT proteins cover a vast range of cellular processes from cell cycle control to regulation of DNA repair processes [111, 112].

From a metabolic perspective, SIRT1 and SIRT3 have provided the most interest to date [113]. SIRT1 is typically activated during metabolic stress, for example, in response to periods of exercise and fasting, when there is a concurrent increase in NAD^+ levels [84]. SIRT1 works to modulate energy homeostasis by modifying the acetylation status of transcription factors associated with metabolic regulation and mitochondrial biogenesis including the forkhead box class O (FOXO) proteins, peroxisome proliferator-activated receptor γ (PPARγ), and PPAR γ coactivator-1α (PGC-1α) [84, 114, 115]. To illustrate the role of SIRT1 in mice, during fasting there is more than a two fold increase in liver NAD^+ content with an associated

increase in SIRT1 activity leading to deacetylation and activation of PGC1α which promotes gluconeogenesis [116]. Reduction in SIRT1 expression has also been shown to decrease fasting hyperglycaemia and hepatic glucose production through increased acetylation of SIRT1 substrates including PGC1a and FOXO1, implicating SIRT1 activity as a potential regulator of type 2 diabetes and a possible therapeutic target [117, 118].

In skeletal muscle SIRT1 activity is also upregulated with a concomitant increase in AMPK activity; together activating and upregulating the expression of PGC1α to reprogram transcription profiles in favour of mitochondrial fatty acid oxidation [63]. SIRT3 has also been linked to energy homeostasis through regulation of mitochondrial expressed genes. Recent work by Jing et al. in skeletal muscle has shown that through deacetylation of pyruvate dehydrogenase (PDH), which converts pyruvate to Acetyl CoA, SIRT3 can coordinate energy metabolism and acts as a metabolic switch by altering energy substrate choice. Postprandial, SIRT3 activity is increased and therefore it pushes metabolism in favour of glucose metabolism whereas during fasting SIRT3 activity is reduced resulting in hyperacetylation of PDH and a switch to fatty acid metabolism [119].

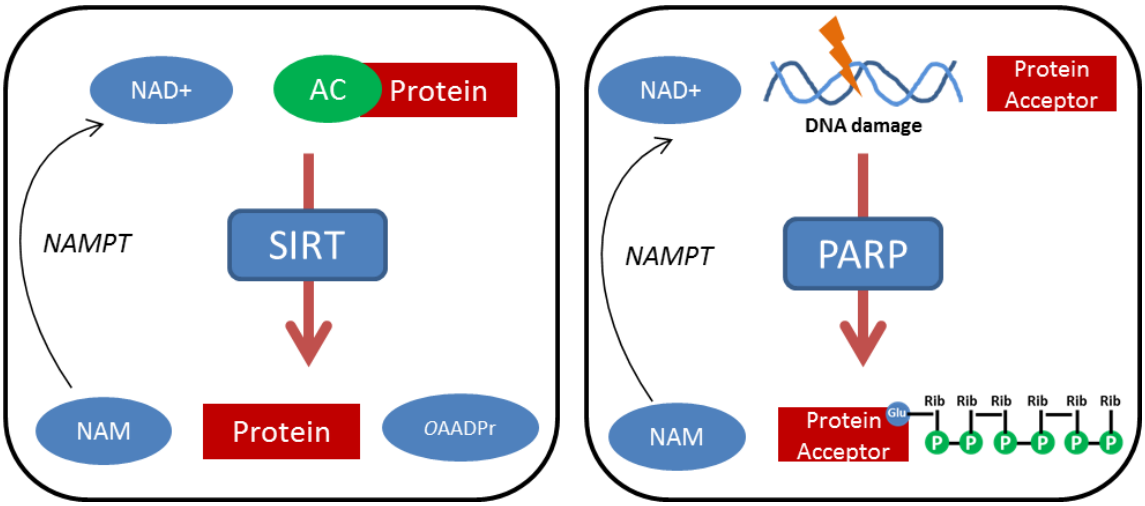

Figure 1.10 Sirtuin and PARP signalling

Sirtuin (SIRT) deacetylation of proteins is an NAD^+ dependent process with nicotinamide (NAM) and oAADPr released (left). PARP signalling is induced by DNA damage and results in poly-ADP-ribosylation of proteins, NAD^+ is consumed by signalling and NAM released (right).

1.3.2 PARP

The PARP family of proteins are ADP-ribosyl transferases. Currently 17 PARPs have been discovered with PARP-1 the best understood. PARP activity leads to post translational modification of proteins by poly-ADP-ribosylation using NAD^+ as a substrate. During this reaction, ADP-ribose groups can be linked to an amino acid receptor with NAM released [120, 121] (figure 1.10). Unlike SIRTs, they are not necessarily dependent on NAD^+ for their activity; they are in fact mostly regulated by binding to breaks in DNA with activity remaining low in the absence of DNA damage [87, 121-123]. Despite this, it is thought that PARPs are the major NAD^+ consumers within the cell and their activity has a substantial impact on cellular NAD^+ availability [92, 124-126]. Inhibition of PARP activity has been shown to increase cellular NAD^+ [92, 127]. This means that sufficient salvage and synthesis of NAD^+ is continuously required to maintain pools and metabolic homeostasis [125].

Although PARPs are involved in a diverse range of processes such as apoptotic and epigenetic signalling, the primary role of PARPs is to maintain DNA integrity within the cell [122]. PARPs are highly responsive to DNA damage, especially DNA strand breaks, and work to induce DNA strand repair by recruitment of proteins and formation of repair complexes [87, 120, 123]. Additionally, a role for PARPs has also been outlined in modulating metabolism. For example, high PARP activity during DNA damage can cause a repression of SIRT activity through NAD^+ consumption [128] whereas inhibition of PARP-1 leads to an increase in SIRT activity and metabolic adaptations including enhanced muscle mitochondrial content and energy expenditure [92]. Moreover, PARP-2 has been identified as a direct repressor of the SIRT1 promoter, with PARP-2 deficiency resulting in an increase of SIRT1 activity through enhanced expression rather than increased NAD^+ availability [129]. The interplay between SIRTs and PARPs and the great influence they exert on their respective enzyme activity demonstrates the importance of continually balancing NAD^+ consumption and biosynthesis to maintain homeostasis.

1.3.3 Cyclic ADP-Ribose Synthases

The highly conserved cADP-ribose synthases, also known as CD38 and CD157, are ectoenzymes that consume NAD^+ and produce second messengers to coordinate numerous processes [130]. For example, they can generate cADP-riboses which act as central modulators of intracellular calcium signalling [98]. Importantly, studies have revealed that CD38 requires a large amount of NAD^+ to generate cADP-ribose with a 100:1 ratio of NAD^+ substrate for every cADP-ribose molecule [131]. Thus, even during low activity, CD38 is a central modulator of cellular NAD^+. Further research by Aksoy et al highlighted this using a CD38 KO

mouse model, which exhibited a 10-20 fold increase in intracellular NAD^+ content and with this they demonstrated enhanced SIRT activity [85, 131].

1.4 NAD^+ Biosynthesis

As previously described in section 1.3, the consumption of NAD^+, as part of numerous signalling pathways, necessitates continuous re-synthesis to maintain cellular NAD^+ levels. The significance of replenishing NAD^+ was first delineated by the disease pellagra. Pellagra is characterised by the triad of symptoms; dermatitis, diarrhoea and dementia caused most commonly by malnutrition – more specifically a deficiency in vitamin B3 NAD^+ precursors. Dietary replacement of NAD^+ precursors can successfully treat pellagra [132, 133]. In mammalian cells, numerous NAD^+ synthesis pathways have since been identified. Without these biosynthesis pathways the high turnover of NAD^+ means cellular levels would deplete within hours and ultimately lead to cell death [134, 135].

1.4.1 De novo synthesis

NAD^+ can be synthesised *de novo,* predominantly from the dietary amino acid L-tryptophan. Briefly, as demonstrated in figure 1.11, biosynthesis begins with the conversion of tryptophan to N-formylkynurenine by the rate limiting enzyme indoleamine 2,3-dioxygenase (IDO) or alternatively tryptophan2,3-dioxygenase (TDO). Following this, 4 enzymatic reactions convert N-formylknurenine to α-amino-β-carboxymuconate-ε-semialdehyde (ACMS) [136]. ACMS can undergo complete oxidation or spontaneous cyclization producing quinolinic acid. Quinolinate phosphoribosyl-transferase (QPRT) catalyses the conversion of quinolinic acid to nicotinic acid mononucleotide (NAMN) which is subsequently converted by the ubiquitously expressed enzyme nicotinamide mononucleotide

adenylyltransferase (NMNAT) to nicotinic acid adenine dinucleotide (NAAD)[136]. Finally NAAD undergoes ATP dependent amidation via glutamine-dependent NAD^+ synthase (NADS) activity to produce NAD^+ [137].

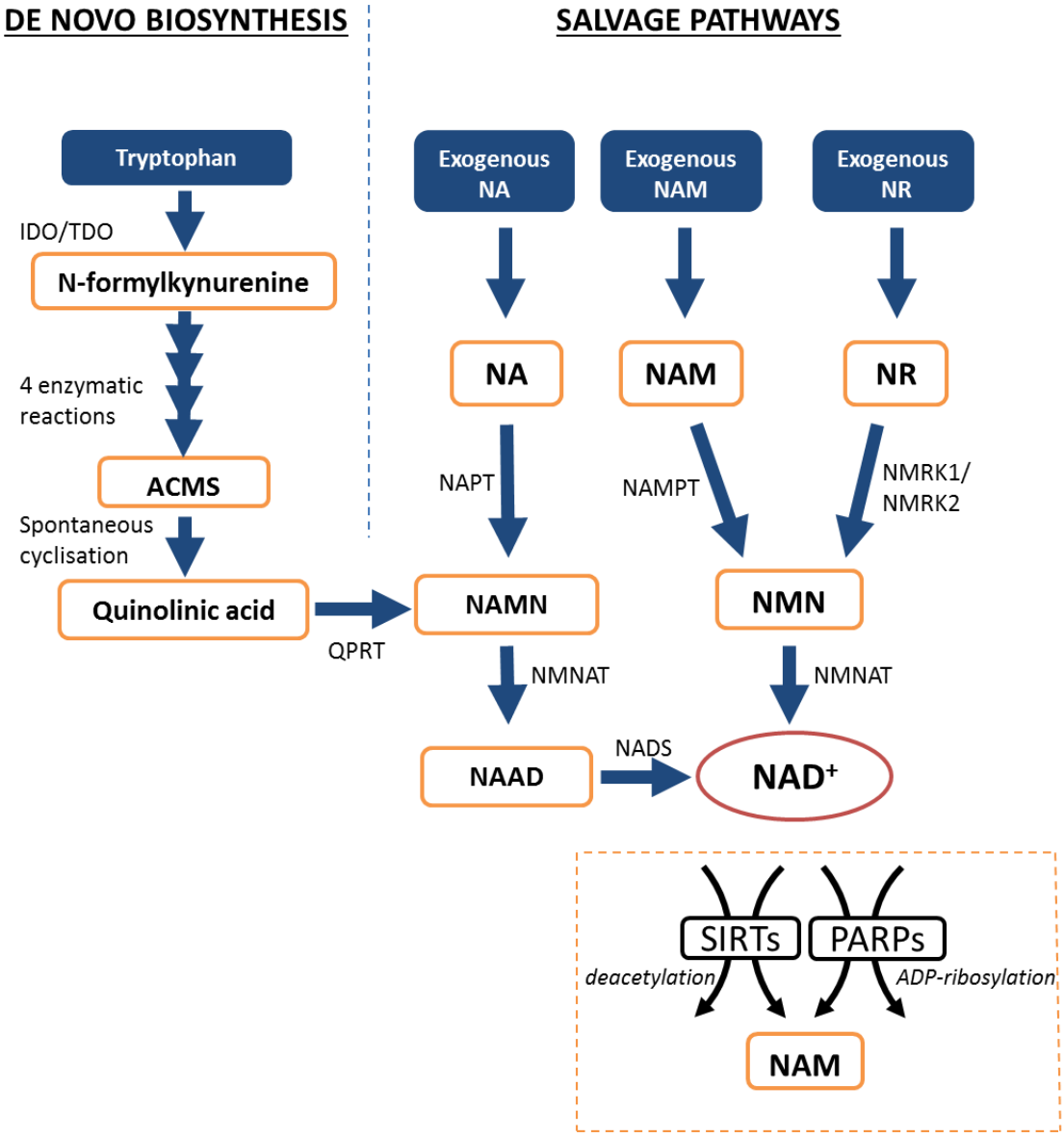

Figure 1.11 NAD^+ biosynthesis pathways

NAD^+ can be generated through multistep de novo synthesis from L-tryptophan or through the salvage of NAD^+ precursors; nicotinic acid (NA), nicotinamide (NAM) and nicotinamide riboside (NR). Replenishment of NAD^+ allows continued signalling by enzymes including SIRTs and PARPs and released NAM can be recycled back to NAD^+.

1.4.2 Vitamin B3 Salvage pathways

Despite *de novo* biosynthesis being a major route to NAD^+ in the liver [138, 139], it is thought that the majority of cellular NAD^+ content in other tissues is attributed to salvage pathways. Illustrated in figure 1.11, these pathways resynthesise NAD^+ from vitamin B3 precursor molecules nicotinic acid (NA), nicotinamide (NAM) and nicotinamide riboside (NR), found in the diet or as consumed NAD^+ metabolites, with similar chemical structures to NAD^+ (figure 1.12) [140-142].

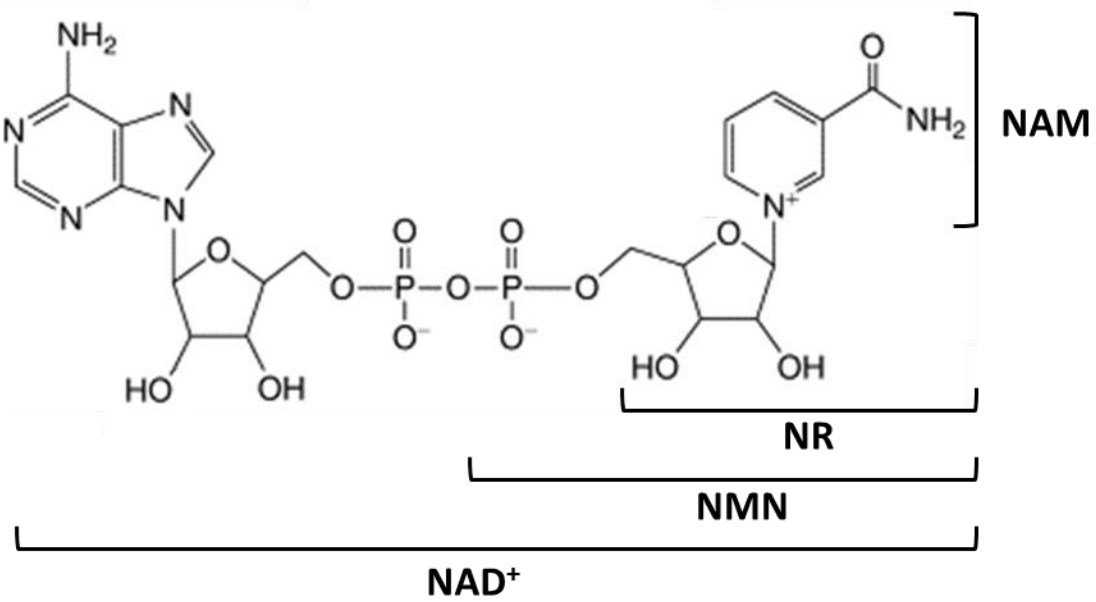

Figure 1.12 Structure of NAD^+ and NAD^+ precursors

NAD^+ and precursors NAM, NR and NMN all share a common nicotinamide moiety (adapted from Bogan et al. 2014) [143].

It is thought that NAM is the preferred NAD^+ precursor over NA; this was illustrated by only transient increases of NAD^+ after intraperitoneal injection with NA as opposed to stable increases following NAM administration [144]. Despite the growing interest in NAD^+ metabolism, particularly since NAD^+ dependent SIRT proteins have been acknowledged for their central metabolic regulatory role [63, 145], it is still unclear how these different biosynthesis and salvage pathways

interact. The relative importance and tissue specificity of the different precursor molecules in NAD^+ replenishment *in vivo* remains unclear.

1.4.3 Preiss – Handler pathway

NA is converted into NA mononucleotide (NAMN) in the Preiss-Handler pathway; the reaction is catalysed by NA phosphoribosyltransferase (NAPT) with 5-phospho-α-D-ribose-1-diphosphate as its substrate [146]. Following this initial step this pathway undergoes a similar route to the *de novo* biosynthesis pathway, where NAMN is converted to NAAD by NMNAT and finally to NAD^+ by NADS [146].

Mammalian, NADS is a homohexameric cytosolic protein that uses co-substrates ATP and glutamine to convert NAAD to NAD^+ and releasing AMP, PPi and glutamic acid in the process [147]. As the final step of both the de novo and Preiss-Handler pathway, NADS activity is rate-limiting for NAD^+ generation by either of these routes. The importance of NADS activity for NAD^+ generation has been shown to be organism and tissue specific. Some bacteria such as *mycobacterium tuberculosis* are dependent on NADS for NAD^+ synthesis, making it a potential antibacterial target, whereas others make NAD^+ independent of NADS [148, 149]. The rate of NADS enzyme activity differs across tissues, with highest levels of activity demonstrated in liver and kidney tissue. Activity is undetectable in lung and skeletal muscle tissues and very low in brain homogenates, indicating NAD^+ production via the de novo and Press-Handler pathways is limited in these tissues [147].

1.4.4 NAMPT salvage pathway

Alternatively, NAM can replenish NAD^+ pools by the nicotinamide phosphoribosyltransferase (NAMPT) pathway [150]. Here, NAMPT acts as the rate-limiting enzyme and catalyses the conversion of NAM and 5'-phosphoribosyl-1-pyrophosphate (PRPP) to nicotinamide mononucleotide (NMN) in an ATP dependent reaction. NMN is then converted to NAD^+ by NMNAT enzyme activity [151]. As NAM is a product of SIRT and PARP mediated NAD^+ signalling, salvage by NAMPT provides a direct NAD^+ recycling mechanism. This pathway also allows for tight regulation of NAD^+ levels with NAMPT expression shown to be regulated by cellular NAD^+ levels and SIRT activity negatively regulated by NAM levels [152].

NAMPT is a dimeric, type II phosphoribosyltransferase [153]. It was initially thought to be a cytokine termed pre-B cell colony enhancing factor (PBEF) [154]; but was later redefined as a hormonal factor, named visfatin, with alleged insulin mimetic effects [155] (now found to be unsupported [156]), before a universal name of NAMPT was assigned. NAMPT is highly conserved from prokaryotes to humans and expressed in almost all the tissues and cells that have been examined highlighting a necessity for NAMPT activity in normal cell function [157]. It exists both intracellularly, predominantly in the cytosol and nucleus, and extracellularly [158, 159]. Intracellular NAMPT activity has proved critical for maintaining cellular NAD^+ and redox pathways through salvage of NAM to NAD^+. Inhibition of enzyme activity with the potent NAMPT inhibitor FK866 leads to a reduction in NAD^+ over time and ultimately leads to cell death [134, 150]. The role of extracellular NAMPT (eNAMPT) is still unclear but activity has been associated with cell pathology whereby cell death results in a release of ATP and PRPP into

the circulation (both normally have low plasma concentrations), which then drive enzyme activity [157, 160]. Proinflammatory responses, such as the induction of inducible nitric oxide synthase, have also been associated with eNAMPT activity in diabetes [161]. Moreover, eNAMPT is also believed to promote macrophage survival whilst muting T-cell responses through non-enzymatic actions in some disease states including chronic lymphocytic leukaemia [162, 163].

1.4.5 NMRK salvage pathway

In addition to these long-established salvage pathways, a new route to NAD^+ has been more recently recognised since the identification of the nicotinamide riboside kinase 1 and 2 (NMRK1 and NMRK2) enzymes. The NMRKs phosphorylate the vitamin B3 nicotinamide riboside (NR) to NMN [164] which is then subsequently converted to NAD^+ by NMNAT1 [142].

Initial identification of the NMRK enzymes stemmed from the finding of NR as a novel NAD^+ precursor with the ability to extend lifespan of yeast via enhanced NAD^+ dependent Sir2 signalling [142]. Although NMRK1 and 2 are close paralogues, both with a high affinity for NR, their substrate specificity differs. NMRK1 has a Km (substrate required for half maximal enzyme rate) for NR of 0.088 mM whereas NMRK2 has a Km of 0.19 mM [164]. Moreover, NMRK1 can use ATP or GTP (guanosine triphosphate) as a substrate to phosphorylate NR to NMN yet NMRK2 exhibits ATP specific activity [164, 165]. There is currently little understanding regarding the roles NMRK1 and 2 play in endogenous NAD^+ biosynthesis – or beyond NAD^+ metabolism – with only recent findings showing that loss of NMRK1 function is not critical to basal NAD^+ signalling [166]. However, in hepatocytes NMRK1 is an essential component for NAD^+ biosynthesis following

exogenous NR and NMN supplementation [166]. Understanding the function of NMRK2 is also of great interest since it was found to be the most upregulated NAD^+ biosynthetic gene (by over 20-fold) following injury to dorsal root ganglion neurons, despite expression normally absent or low in the nervous system [167].

1.4.6 NAD^+ biosynthesis in skeletal muscle

Metabolic profiling of tissue enzyme activity has revealed NADS activity to be negligible in muscle whereas enzyme activity of NMNAT1 through the amidated routes (thus via NAMPT and NMRK) was detected to a much greater extent [147]. This data already indicates that the *de novo* and Preiss-Handler routes to NAD^+ may be limited in skeletal muscle. The NAMPT salvage pathway has previously been demonstrated to be a critical determinant of NAD^+ content across many tissues including liver, skeletal muscle and adipose [76, 168-170] . Conversely, due to the infancy of research surrounding the NMRKs, the extent to which they contribute to the maintenance of skeletal muscle NAD^+ pools is unknown. The NMRKs are highly conserved in all eukaryotes [142] and although NMRK1 is ubiquitously expressed [166], NMRK2 is thought to be specifically expressed in skeletal muscle but has not been well characterised in this regard [171].

NMRK2 and its orthologs have been implicated in coordinating muscle differentiation and improving dystrophic muscle function in zebrafish. Previously Li et al. have defined a role for muscle-specific β1 integrin binding protein (MIBP), a 186 amino acid protein which they believe to be a splice variant of NMRK2, in regulating muscle differentiation where by MIBP expression may repress terminal differentiation in muscle [172]. Furthermore, research in zebrafish has associated Nrk2b, believed to be the zebrafish orthologue of MIBP, with NAD^+ mediated

amelioration of muscular dystrophy through activation of downstream targets such as paxillin [173].

1.5 NAD^+ metabolism in health and disease

The important role NAD^+ plays in metabolic health is now widely acknowledged and can be well demonstrated during exercise. As previously described, physical activity enhances NAD^+ turnover in muscle, results in changes to NAD^+ redox and induces metabolic adaptation [174]. The key regulatory response to exercise that allows these signalling events to occur is the AMPK induction of NAMPT expression [145]. Upregulation of NAMPT leads to an increase in NAD^+ turnover through enhanced recycling of NAM. The consequent rise in NAD^+ allows for an increase in SIRT activity and rapid salvage of NAM to NAD^+ preventing NAM inhibition of SIRTs (figure 1.13) [31, 175].

The perturbations to skeletal muscle NAD^+, NADH and NAD^+/NADH ratio following exercise allow for increased ATP production by glycolysis and oxidative phosphorylation to tightly maintain ATP levels during muscle contraction [145]. Metabolic adaptation by SIRT signalling is equally important for enhancing oxidative capacity, fuel utilisation and improving metabolic performance on repeat activity. Notably, metabolic adaptation and mitochondrial biogenesis can be induced following just a single bout of exercise [176, 177]; demonstrating the acute positive health effects of enhancing NAD^+ signalling.

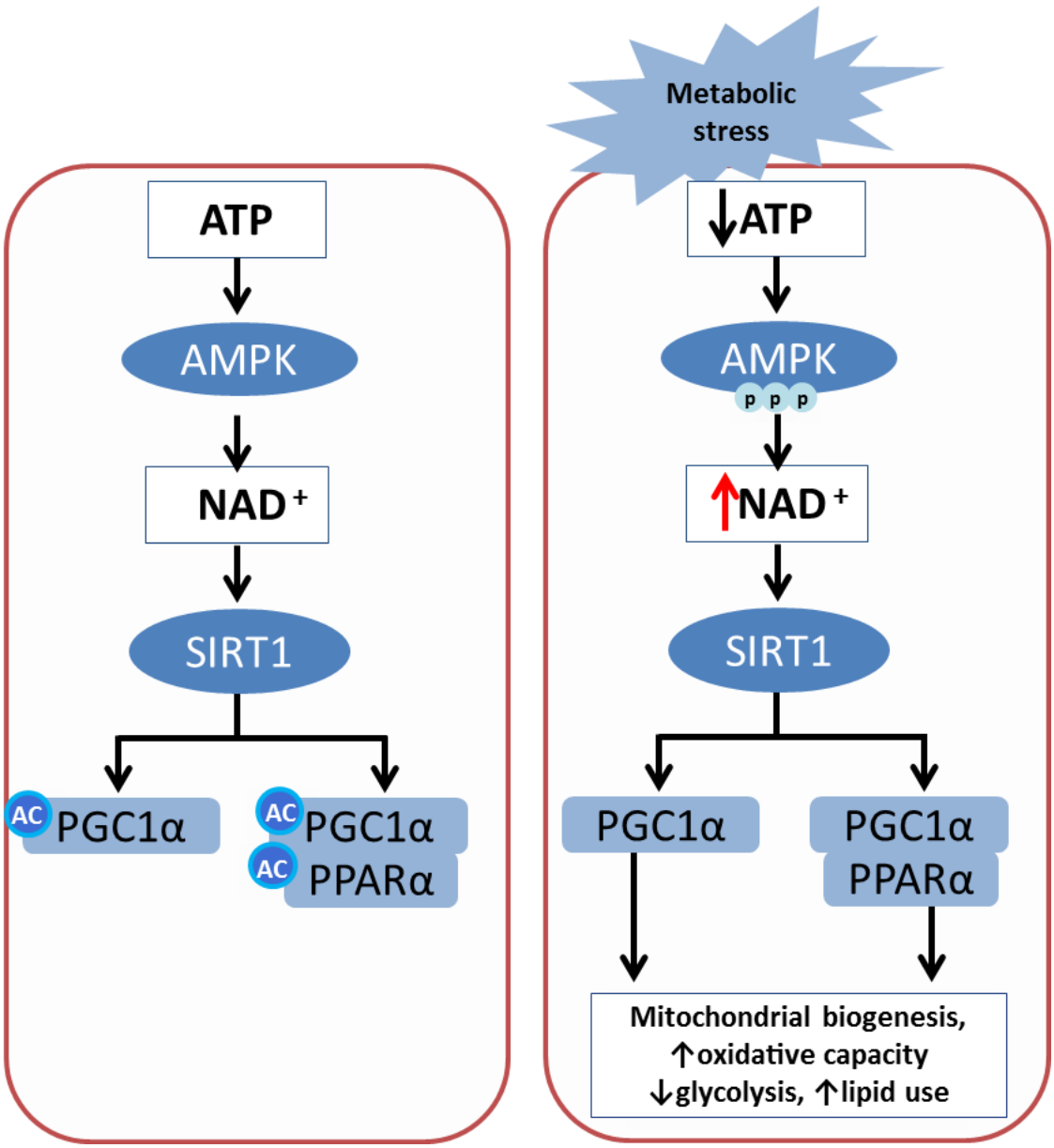

Figure 1.13 Metabolic signalling in skeletal muscle following metabolic stress

Metabolic stresses such as exercise lead to a depletion in available ATP, this stimulates metabolic sensors such as AMPK which can induce a surge in NAD^+ content to drive SIRT activity and reprogram metabolic pathways to replete ATP.

However, NAD^+ signalling can be perturbed in disease and a drop in cellular NAD^+ content has been associated with numerous pathophysiological states, examples of which include diabetes, neuronal degeneration, non-alcoholic fatty liver disease and noise-induced hearing loss [100, 169, 178-180]. In these examples, depleted

NAD^+ levels are thought to be - at least in part - a consequence of hyper-activation of PARPs by oxidative stress induced DNA damage and thereby resulting in excessive NAD^+ consumption [100, 180]. Reduced NAD^+ availability is then associated with a decline in SIRT activity [89].

Importantly, restoration of NAD^+ signalling through repletion of NAD^+ in these diseases has demonstrated positive outcomes. Brown et al. demonstrated that NR supplementation protected against noise-induced hearing loss by restoring NAD^+ levels and SIRT3 activity [179]. Remarkably, studies have also shown NR repletion of NAD^+ improved the metabolic phenotype of high fat diet (HFD) induced diabetes in mice with reduced weight gain, insulin resistance and hepatic steatosis [178]. Alternatively, PARP mutation strategies, to limit excessive NAD^+ consumption during DNA damage, led to increased NAD^+ availability and protection from neurodegeneration in drosophila models of Parkinson's disease [180]. Finally, primary cardiac-myocytes taken from mouse models of heart failure were also shown to be protected from cell death induced by excessive PARP1 mediated NAD^+ consumption following repletion of NAD^+ [128].

1.6 NAD^+ in Ageing and Sarcopenia

More recently there has been a major focus on ageing research due to growing ageing populations and the need to improve health span which continues to lag behind lifespan. During ageing, cells typically have increased levels of DNA damage, a reduction in mitochondrial function and consequently a reduction in cellular ATP turnover [181].

In terms of muscle health and metabolism, a major problem during ageing is sarcopenia – defined as a degenerative loss of muscle mass and function [182].

Sarcopenia characteristically manifests with muscle weakness, loss of strength, frailty and immobility; with a decline in muscle health also negatively impacting on whole body metabolism. Although sarcopenia is mostly associated with ageing, physical inactivity and metabolic diseases also drive muscle loss [183]. It is now thought of as a multifactorial process with several factors involved including nutrition, hormone changes, muscle catabolic imbalance, chronic disease states and inflammation [182-184]. The pathophysiological processes of sarcopenia have shown sex-specific differences with malnutrition thought to be a major reversible factor aside from physical activity [185].

Reduced NAD^+ availability is commonly featured in aged muscle and associated morbidities including insulin resistance, obesity and cardiovascular disease [89, 128, 170, 181, 186]. Physical inactivity drives sarcopenia progression but can also be a resulting outcome due to muscle loss and weakness [183]. With metabolic adaptation and NAD^+ signalling highly regulated by exercise it is difficult to delineate whether a drop in cellular NAD^+ contributes to the progression of sarcopenia or a consequence of muscle wasting and metabolic decline (figure 1.14). Accumulation of reactive oxygen species (ROS) in sarcopenic muscle has been associated with activation of PARP1, providing an initial mechanism for NAD^+ decline and reduced SIRT activity [187]. Additionally, vitamin B3 nutrient availability appears important for NAD^+ signalling and malnutrition is a key factor for driving sarcopenia [185]; thus, nutrient replenishment may be valuable strategy for reversing or impeding sarcopenia progression, particularly when physical activity is limited due to muscle weakness and disability.

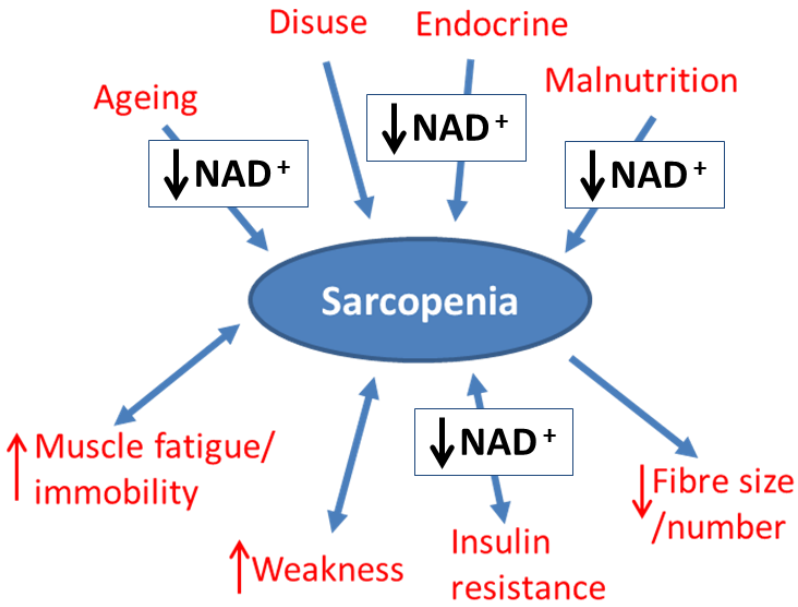

Figure 1.14 Factors associated with sarcopenia

An illustration of the key factors involved in sarcopenia and the consequential outcomes that drive further progression. A potential role for NAD^+ is highlighted by an associated decline with a number of sarcopenic factors.

Since an age-related reduction of NAD^+ availability in some tissues has been identified, the impact of NAD^+ signalling in ageing has been investigated. NAMPT protein expression has been shown to be downregulated in aged rats concomitant with a decline in muscle NAD^+ content [174]. Muscle from exercised aged rats however, displayed increased NAMPT expression and NAD^+ content similar to that of unexercised young rats. This demonstrates some degree of 'reversal' of age-related NAD^+ decline; yet the aged cohort was still unable to upregulate NAMPT to the same extent as young rats following exercise [174]. This highlights the importance of NAD^+ salvage mechanisms in response to exercise and identifies aberrant NAMPT activity as a possible driver of age-related metabolic decline.

1.7 Strategies to boost NAD^+ signalling

The implications of perturbed NAD^+ signalling in disease and ageing clearly demonstrate the criticality of NAD^+ signalling for energy metabolism and beyond. This has driven current research to develop new therapeutic strategies based on restoring NAD^+ levels and metabolic signalling (figure 1.15). PARP inhibitors, to prevent excessive NAD^+ consumption, have been shown to not only increase NAD^+ availability and drive SIRT1 mediated mitochondrial metabolism but also act as effective anti-cancer agents [92, 188]. Alternatively, SIRT activators, such as derivatives of resveratrol and SRT1720, can potently stimulate SIRT1 activity and exert widespread metabolic effects [189-191]. These include; protection from diet induced obesity and insulin resistance through enhanced fatty acid oxidation signalling, improved endothelial function and enhanced mitochondrial content and function [189-191]. Although these strategies have promising therapeutic potential in regards to metabolic disease, more recently there has been a major focus on vitamin B3 supplementation strategies. As naturally bioavailable 'nutraceuticals', that have also been synthetically established, they potentially provide a relatively inexpensive approach with low toxicity and limited side-effects [139, 171, 192].

1.7.1 Vitamin B3 supplementation

From a clinical perspective, NA supplementation is the most therapeutically characterised. The hypolipidemic effects of NA and its derivatives were first described in the 1950's and have since been used to treat hyperlipidaemia and associated cardiovascular diseases. NA supplementation reduces plasma triglycerides and low density lipoprotein (LDL) whilst also elevating circulating high density lipoprotein (HDL) [193, 194]. However, activation of the nicotinic acid receptor GPR109A following NA treatment results in severe cutaneous

vasodilation, known as flushing, in a large majority of patients leading to poor compliance [195]. More recently, short-term clinical studies have shown that the NA derivative acipimox can also enhance mitochondrial respiration in skeletal muscle and elevate ATP content [196]. Importantly, the study also identified unwanted effects with acipimox treatment causing an increase in plasma non-esterified fatty acids (NEFA) and reduced insulin sensitivity [196]. This along with the adverse flushing has limited the use of NA as a nutraceutical to enhance NAD^+ signalling and metabolism in skeletal muscle. Nonetheless, the health benefits demonstrated by NA were a major driving factor towards the ongoing research investigating the therapeutic potential of alternative vitamin B3 NAD^+ precursors.

NAM supplementation as a strategy to boost NAD^+ signalling and energy metabolism is also limited due to the inhibitory effects of NAM on SIRT activity [197]. However, in some cases NAM supplementation may still be useful. For example, during cerebral ischaemia NAD^+ levels diminish, altering the cells bioenergetic state and leading to excitoxicity [198]. Short-term NAM supplementation can both replete cellular NAD^+ and inhibit PARP and SIRT activity to reduce NAD^+ consumption; restoring the bioenergetic state and protecting against excitotoxic shock and neuron death [198].

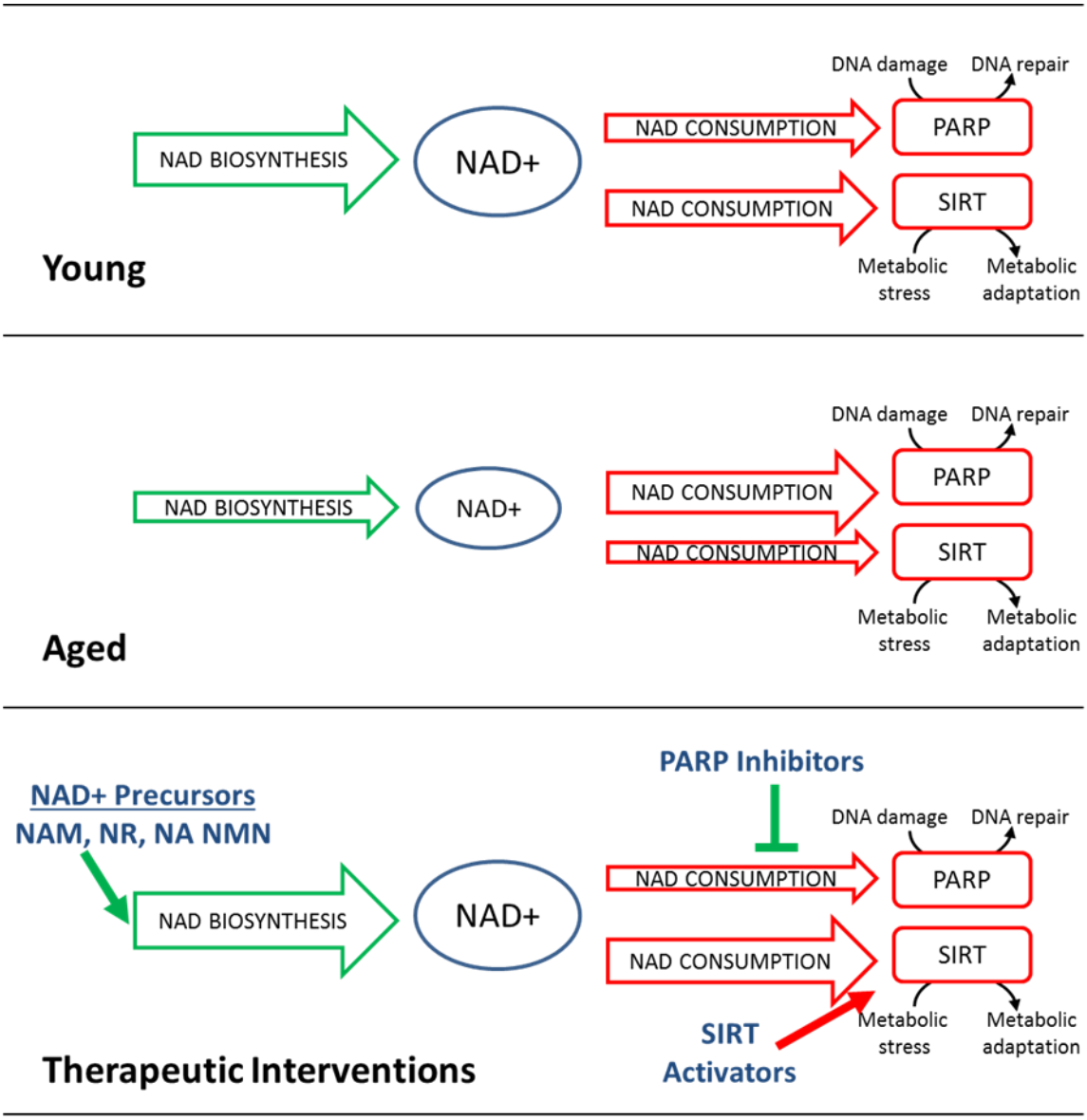

Figure 1.15 Strategies to boost NAD^+ signalling in aged muscle

An illustration of current understanding of basic NAD^+ signalling in young (top) and aged (middle) muscle. Aged muscle exhibits reduced basal NAD^+ availability, thought to be in part due to perturbed NAD^+ biosynthesis and enhanced consumption by PARPs as a response to increases DNA damage. The therapeutic strategies (bottom) that are currently being investigated in human and mouse models of metabolic decline are shown including NAD^+ precursor supplementation, PARP inhibitors and SIRT activating compounds.

Currently NMN and NR supplementation are the most therapeutically promising approaches in regards to metabolic health. Both have been shown to significantly elevate NAD^+ levels without inhibiting SIRT activity or causing flushing through the

activation of the GPR109A receptor [166, 199, 200]. Although limited, human and animal studies have yet to identify major side effects of NR or NMN supplementation [170, 200, 201], however considerably larger cohorts and longer term supplementation is required to establish any harmful effects. Importantly, recent studies have quantified NR and NMN in foods such as milk (NR and NMN) and vegetables (NMN), identifying a possible dietary source for both [192, 202, 203]. Thus the value of NMN and NR supplementation is currently being extensively studied in a wide range of disease contexts.

Short-term NMN supplementation has already shown promise in animal models of obesity, neuropathy and ageing. NMN supplementation (17 days) led to an improved metabolic phenotype of high fat diet (HFD) fed obese mice with enhanced NAD^+ detected in liver and muscle tissue and improved glucose tolerance [200]. In mouse models of Alzheimer's, NMN supplementation (10 days) recovered neuronal NAD^+ levels and mitochondrial respiratory function leading to repletion of ATP, reduced reactive oxygen species and attenuation of neuronal cell death [204, 205]. In studies of age-related pathologies NMN supplementation (8 weeks) could restore vascular function of aged mice through a SIRT1-mediated reduction in oxidative stress [206], and NMN (10-11 days) was able to improve glucose intolerance and lipid profiles of mice with age-induced type 2 diabetes (T2D) [170]. Remarkably, aged mice treated daily with NMN for one week had restored mitochondrial function to the same level as a young mouse through NAD^+-induced SIRT1 dependent signalling [181]. More recently, long term NMN supplementation (1 year) through dietary supplementation has been investigated in mice in terms of ageing. Here NMN was shown to be orally bioavailable and able to alleviate some of the effects associated with age-related metabolic decline

including reduced weight gain associated with ageing, improved insulin sensitivity, enhanced energy expenditure and increased maximal mitochondrial respiration [203].

Equally, NR supplementation has also demonstrated great therapeutic potential across a range of metabolic pathologies [178, 179, 199, 207]. Since the discovery of the NMRK enzymes there has been considerable interest in the importance of the NR salvage pathway to NAD^+. Initial studies in yeast identified that NR salvage was essential for calorie-restriction lifespan extension via NAD^+-dependent Sir2 deacetylase [208]. Numerous positive effects of NR supplementation on mammalian metabolic health were subsequently demonstrated by Canto et al. in HFD fed mice [199]. NR supplementation (for the entire HFD period) increased NAD^+ in key metabolic tissues including muscle and liver; leading to increased SIRT1 and 3 activity detected by deacetylation of FOXO1 and induction of downstream gene expression. NR treated HFD mice exhibited an improved metabolic phenotype with reduced weight gain and fat mass from increased energy expenditure, improved insulin sensitivity and reduced total cholesterol compared to control HFD mice. Furthermore, analysis of muscle tissue identified upregulation of mitochondrial genes and proteins and enhanced oxidative performance [199].

More recent studies have shown NR supplementation to protect against noise induced hearing loss [179], diet-induced T2D [178] (both described in section 1.5), as well as mitochondrial myopathy [207]. In mouse models of progressive adult-onset mitochondrial myopathy, dietary NR treatment (16 weeks) significantly delayed disease progression and protected against mitochondrial structural

abnormalities as well as sustaining mitochondrial biogenesis, mitochondrial DNA copy number and oxidative capacity; all of which deteriorated more rapidly in untreated mice [207]. An alternative model of mitochondrial myopathy characterised by cytochrome c oxidase (COX) deficiency and exercise intolerance also demonstrated the beneficial effects of NR treatment on mitochondrial health in muscle. Here, NR supplementation (4 weeks) enhanced skeletal muscle NAD^+ and upregulated SIRT1 activity. In addition, treated mice displayed enhanced expression of mitochondrial oxidative phosphorylation genes and proteins, upregulated mitochondrial respiratory chain enzyme activities and improved endurance exercise performance [99].

Despite the large amounts of evidence supporting the notion that increasing NAD+ levels may be beneficial in a range of disease settings, there may be some scenarios where NAD+ supplementation may be potentially detrimental. For example, studies have shown a reduction of NAD+ via inhibition of NAMPT may be beneficial under some circumstances including tumorigenesis and autoimmune disease. In terms of cancer, studies have shown reduction of NAD+ to limit glycolytic flux, ATP levels and inhibition of further cancer cell or tumour growth [74, 75, 209-211]. Furthermore, upregulation of NAMPT has been identified in patients with inflammatory diseases such as rheumatoid arthritis [212]. Inhibition of NAMPT has been shown to have anti-inflammatory effects, with reduced circulating TNFα, decreased NAD+ in inflammatory cells and a reduction in ROS [213, 214].

Clinical studies involving vitamin B3 supplementation remain in their infancy; but the first controlled human study of NR supplementation determined that oral delivery could significantly elevate peripheral blood mononuclear cell (PBMC)

NAD^+ [201]. Although no major adverse effects were reported, this was a short-term study based on a small cohort of 12 healthy subjects and therefore larger scale investigations are necessary to determine potential adverse events.

Together these examples demonstrate the potential of vitamin B3 supplementation as a therapeutic strategy for treating metabolic diseases. However, there are still large knowledge gaps to be addressed surrounding vitamin B3s in order to determine their true potential as nutraceuticals. These include tissue specific substrate preference, substrate delivery to the target tissue, substrate stability and dose. Previously studies, particularly with NMN supplementation, have often used Intraperitoneal (I.P) injections over oral supplementation due to concerns with long-term stability in food and water, uncertainty of stability in the gut and the use of large doses [170, 181, 200]. Although, NR has been shown to be orally bioavailable in humans (and mice) [201], questions remain regarding whether NR can bypass breakdown by the bacteria of the gut and be delivered to target tissues in sufficient quantities.

1.8 Project rationale

The importance of NAD^+ as a signalling molecule has now been well established and outlined in this chapter. Its central role in regulating important processes such as energy metabolism, DNA repair and calcium signalling has put NAD^+ and its metabolism into the spotlight in many research fields [32, 66, 86]. Understanding how NAD^+ and its metabolites are generated, their interactions and downstream signalling is now critical to establish new therapeutic strategies scoping from metabolism to cancer. Extensive studies, many that have been discussed, have already begun to demonstrate the beneficial potential of enhancing NAD^+

availability across different tissues and diseases yet the underlying signalling mechanisms are still unclear. A better understanding of how NAD^+ is generated and metabolised, and how changes to this impact on signalling in tissues and pathophysiological states is essential. This knowledge will help elucidate whether 'boosting' NAD metabolism can provide beneficial health outcomes and, if so, how can these beneficial outcomes be maximised.

This project focusses on understanding the importance of NAD^+ biosynthetic pathways in regulating energy metabolism specifically in skeletal muscle. A demonstration of the potential metabolic impact that enhancing NAD^+ availability and signalling may have on ageing muscle health is demonstrated in figure 1.16. Despite increasing interest in vitamin B3 NAD^+ precursor supplementation as a novel strategy to enhance NAD^+ and improve metabolism, the pathways and precursors important to skeletal muscle NAD^+ metabolism remain ill-defined. Thus, defining these pathways will not only provide a better insight to muscle specific NAD^+ signalling pathways but also delineate the best therapeutic targets.

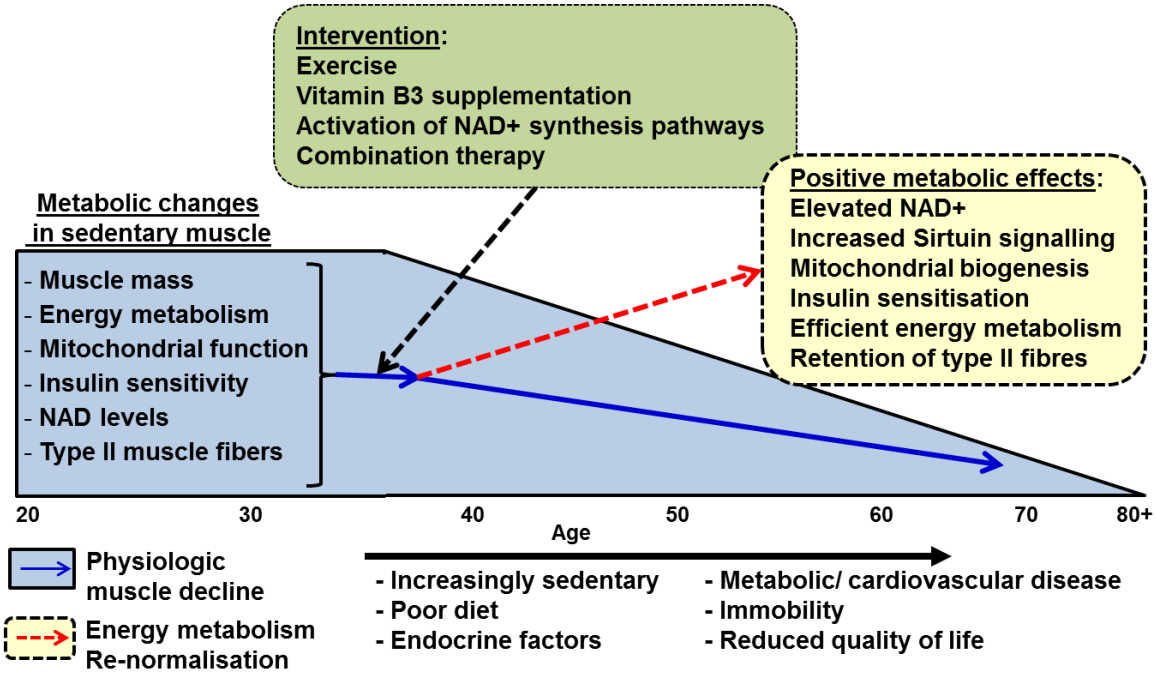

Figure 1.16 Time line of metabolic muscle health

An outline of physiological changes that contribute to muscle decline during ageing (blue box). Interventions that may protect against metabolic decline (green) and the positive metabolic outcomes these interventions may induce (orange).

1.9 Hypothesis

NAD^+ availability is a central determinant of skeletal muscle health and during metabolic decline NAD^+ levels decrease. Driving NAD^+ biosynthesis enzyme activity through vitamin B3 precursor supplementation can enhance NAD^+ availability and negate the effects of metabolic decline in skeletal muscle.

1.10 Project Aims

To characterise the important NAD^+ biosynthesis and salvage pathways for NAD^+ turnover in skeletal muscle (Chapter 3).

Using *in vitro* models of skeletal muscle, investigate the therapeutic potential of the different vitamin B3 precursors in muscle and determine the effects of supplementation on cellular NAD^+ metabolism and downstream signalling (Chapter 3).

Establish the effects of NAD^+ biosynthesis enzyme depletion on NAD^+ metabolism and NAD^+ related cellular signalling through knockout mouse models and chemical enzyme inhibition (Chapter 4).

Determine the effects of NMRK2 deficiency on energy homeostasis *in vivo* using NMRK2 knock out (NMRK2KO) mouse models (Chapter 5).

Chapter 2 Materials and Methods

Unless stated otherwise, all reagents were obtained from Sigma-Aldrich Chemical Company (Poole, Dorset, UK) and all cell culture plasticware was obtained from Corning (Artington, Surrey, UK).

2.1 C2C12 cell line growth and maintenance

All tissue culture was performed under sterile conditions in a Class I biological safety cabinet (Holten LaminAir) using sterile tissue culture flasks and reagents. All cells were incubated at 37 ˚C in 5% CO_2/95% air.

2.1.1 C2C12 cell line

The murine C2C12 myoblast cell line was purchased from the European Collection of Cell Cultures (Salisbury, UK). The cell line is a well-recognised skeletal muscle cell model, sub-cloned from serially passaged C2 myoblasts originally isolated from thigh muscles of C3H mice 70 hours after a crush injury [215, 216]. Following serum removal C2C12 myoblasts can rapidly differentiate into contractile myotubes and exhibit comparable expression of muscle proteins to normal muscle cells [217].

2.1.2 Proliferation

C2C12 cells were cultured in 75 cm^3 tissue culture flasks in growth media (GM) - Dulbecco's modified Eagle's medium (DMEM) supplemented with 10% (v/v) fetal calf serum (FCS), 2 mM L-glutamine and 1% (v/v) penicillin/streptomycin (P/S) and 4.5 g/L glucose. Before reaching 60-70% confluence cells were split by removing media and washing with sterile phosphate buffered saline (PBS), 1 ml of TrypLE™ Express trypsin enzyme (Gibco™, UK) was added to the flask and incubated for 5 minutes at 37 ˚C. Fresh DMEM was added to detached cells and a proportion of cells were added to a new flask or alternatively, for experiments,

cells were seeded into 6 or 12-well tissue culture plates at the desired density. GM was replaced every 48 hours.

2.1.3 Differentiation

At 70-80% confluence C2C12 myoblasts were induced to begin differentiating by replacing GM with DMEM supplemented with 5% (v/v) horse serum (HS). Over a period of days C2C12 myoblasts begin to fuse and extend into multinucleated myotubes as illustrated in figure 2.1. Differentiation media was replaced every 48 hours.

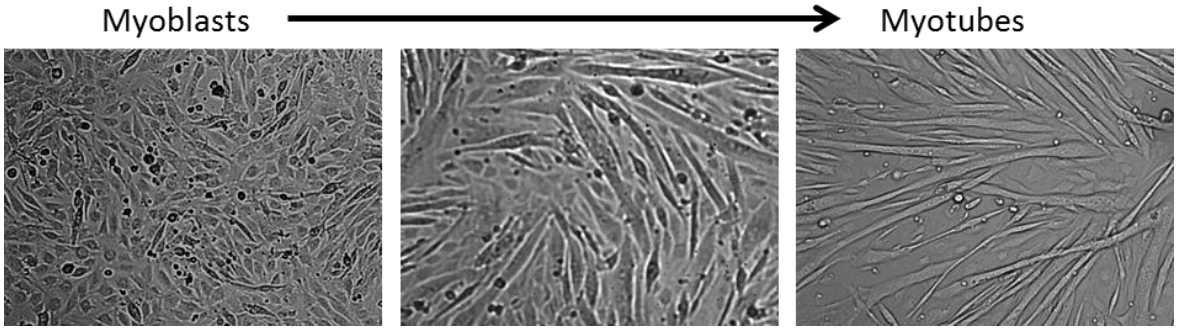

Figure 2.1 C2C12 differentiation

C2C12 myoblasts (left) are induced to differentiate with low serum media, myoblasts begin to fuse with surrounding myoblasts (centre) and finally fully extend into multinucleated myotubes (right).

2.1.4 Cryopreservation

Cryopreservation of C2C12 cells allowed for long term storage and prevented high cell passage numbers. C2C12s were detached from 75 cm^3 flasks using trypsin (described in 2.1.2), transferred to a falcon tube and pelleted by centrifugation. Supernatant was removed and the cells were re-suspended in 10 ml of freezing media - GM supplemented with 20% (v/v) FCS and 5% (v/v) DMSO. The re-suspended cells were aliquoted into 1 ml cryotubes, placed in a pre-cooled Mr

Frosty™ freezing container (Sigma, UK) overnight at -80°C and then stored at -160˚C in liquid nitrogen tanks.

To start new C2C12 cultures from the cryopreserved cells, the cells were quickly thawed in a water bath at 37˚C and added to 10 ml of DMEM. Cells were pelleted by centrifugation and freezing media was replaced with fresh growth media.

2.2 Primary muscle cell isolation and culture

Primary myotubes were cultured from mice by isolating satellite cells from single muscle fibres following an adapted protocol by Rosenblatt et al [218]. Primary cultures provided a more physiologically representative model of muscle and allowed for longer differentiation periods to ensure full myotube formation before treatment. C2C12 myotubes begin to detach once fully differentiated making 24-72 hour treatments post differentiation difficult. In addition, isolating primary myotubes from mouse models allowed direct *in vitro* analysis of genetic interventions. All cells were incubated at 37 ˚C in 5% CO_2/95% air.

2.2.1 Primary murine satellite cell isolation

Gastrocnemius, extensor digitorum longus (EDL), tibialis anterior (TA) or soleus (Sol) muscles were dissected from 10-12 week old mice and digested for 2 hours in DMEM with 0.2% (w/v) type I collagenase at 37°C. The digested muscles were washed and then placed in fresh DMEM in horse serum (HS) coated cell culture plates to equilibrate for 1 hour at 37°C. The muscles were moved into adjacent wells with fresh DMEM and using serum-coated glass pipettes, media was expelled vigorously onto the muscle to allow single myofibres to detach. Cell culture plates were pre-coated in Matrigel (BD biosciences) and left to set for 3 hours in the incubator. Once set, plating media was added, consisting of DMEM

supplemented with 30 % (v/v) FCS, 10% (v/v) HS, 1% (v/v) P/S, 2mM L-glutamine, 1% (v/v) Chick embryo extract (CEE) (Seralab, UK) and 10 ng/ml of fibroblast growth factor-basic (bFGF) (Peprotech, UK), and single myofibres were transferred into the wells and left for 72 hours at 37°C to allow satellite cells to migrate from the myofibres.

2.2.2 Proliferation

Following satellite cell migration, plating media was replaced with proliferation media (DMEM with 10% (v/v) HS, 1% (v/v) P/S and 0.5% (v/v) CEE). Proliferation media was replaced every 48 hours until satellite cell derived myoblasts were around 70% confluent.

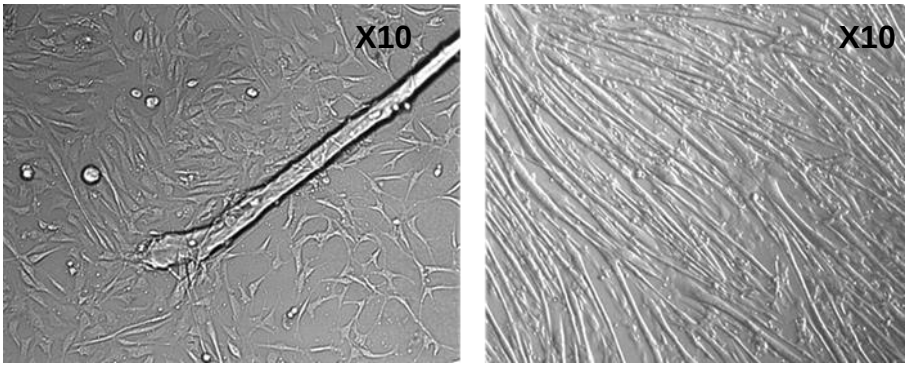

Figure 2.2 Primary myotube differentiation
Satellite cells migrate from isolated myofibres and on activation become proliferating myoblasts (left). Primary myoblasts are induced to differentiate with low serum media, where myotubes fuse and extend into multinucleated myotubes (right).

2.2.3 Differentiation

Differentiation of primary myoblasts was initiated once the cells reached around 70% confluence. Proliferation media was changed to differentiation media consisting of DMEM supplemented with 2% (v/v) HS, 0.5% (v/v) CEE and 1% (v/v)

P/S. Cells were left to differentiate until they formed fully fused and elongated tubes with fresh differentiation media applied every 48 hours (figure 2.2).

2.3 C2C12 and primary myotube treatments

Unless otherwise specified, following 5 (C2C12) or 6 (primary muscle) days of differentiation myotubes were treated with 100 nM FK866 for 24, 48 or 72 hours. Myotubes were also supplemented with vitamin B3 NAD^+ precursors, including NR (ChromaDex, USA), NAM, NMN and nicotinic acid riboside (NaR) at 0.5 mM unless otherwise stated (0.5 mM is a standard dose used in literature and NR is thought to give a maximal NAD^+ response in C2C12s at this concentration [199]). All experiments were performed with vehicle controls (DMSO for FK866 (0.001% (v/v) final volume) and sterile water for vitamin B3 experiments.

2.4 siRNA transfections

Transfecting cells with siRNA enabled transient silencing of target genes *in vitro*. Primary myotubes seeded in 6 well plates were grown to confluence. On day 3 and 5 of differentiation 0.5 µg/µl Nmrk1 siRNA (MSS212930, Invitrogen, UK) or negative (scrambled) siRNA medium GC duplex control (Invitrogen, UK) was added to a final volume of 250 µl of OptiMem per sample whilst, in a separate tube, 4 µl of Lipofectamine 2000 was added to 246 µl of OptiMem. Each tube was incubated at room temperature (RT) for 5 minutes and then mixed gently together and incubated for a further 30 minutes at RT. Cells were washed twice with sterile PBS and 1 ml of antibiotic and serum free DMEM was added to cells. Finally, 500 µl of transfection solution was added to each well and left overnight. Media was then changed back to normal differentiation media until cells were harvested.

2.5 Polymerase chain reaction (PCR)

Conventional PCR is used to amplify deoxyribonucleic acid (DNA). Double stranded DNA is denatured to single strands at 95°C, and at a reduced temperature ~ 60°C (primer dependent), primers complimentary to the gene of interest anneal to the template DNA and at an increased temperature (72°C) the oligonucleotides can be extended by Taq DNA polymerase activity.

DNA samples were amplified using 2x BioMix Red (Bioline, UK) and the relevant primers listed in appendix A. 19 µl of the PCR mastermix, described in table 2.1, was added to a PCR Eppendorf tube with 1 µl of DNA and samples were then placed into a thermocycler set to 3 minutes at 95°C, then 35 cycles of [30 seconds 95°C, 30 seconds 60°C and 30 seconds 72°C] followed by 3 minutes at 72 °C and left indefinitely at 4 °C. Samples were assessed qualitatively by electrophoresis at 100 V using 1.8% agarose gels in TBE buffer (89 mM Tris (pH 7.6), 89 mM boric acid and 2 mM EDTA) supplemented with 10,000x GelRed nucleic acid gel stain (Biotium, USA). Separated bands were visualised using a G Box Syngene UV transilluminator (Syngene, UK). Fragments were identified by size by comparing to a 100 base pair DNA ladder (New England Biolabs, UK).

	Per sample (µl)
2 x BioMix Red	10
Primers	0.5
Nuclease free water (NFW)	9 – (0.5 * No. of primers)

Table 2.1 – PCR mastermix

2.6 Ribonucleic acid (RNA) extraction and analysis

RNA was extracted and prepared to complimentary DNA (cDNA) from tissues and cells for the analysis of cellular messenger RNA (mRNA) levels as a measurement of gene expression.

2.6.1 RNA extraction

Cells were harvested in 0.5 ml of TRIzol (Invitrogen, UK) per well, cells were scraped from the well surface, pipetted up and down to maximise lysis and transferred to an Eppendorf tube. For tissues, samples were harvested in 1 ml of TRIzol and manually homogenised. Once in TRIzol, all samples were left at room temperature for 5 minutes and from this point both cell and tissue samples were treated the same with all concurrent reagent volumes described per 1 ml of TRIzol. 200 µl of chloroform was added to samples. Samples were briefly vortexed and then incubated for 5 minutes at room temperature. Samples were centrifuged at 4°C at 12,000 revolutions per minute (rpm) for 5 minutes and the top aqueous fraction of each sample was transferred to a new Eppendorf tube. 500 µl of isopropanol (propan-2-ol) was then added to each sample and tubes were then inverted 5 times to gently mix before leaving samples to precipitate at -20˚C for 30 minutes. Samples were centrifuged at 4°C for 10 minutes at 12,000 rpm to pellet RNA and supernatant was discarded. Pellets were washed by resuspension in 1 ml of 70% (v/v) ethanol and pelleted again by centrifugation at 4°C for 10 minutes at 12,000 rpm and the ethanol was removed. Samples were left at room temperature for 5 minutes to dry and resuspended in 30 µl of nuclease free water (NFW). RNA samples were stored at -80˚C and thawed on ice before use.

2.6.2 RNA sample quantification

RNA concentration was determined using the NanoDrop (ND, Labtech international). 1 µl of NFW was applied to the NanoDrop sample detection arm and measured to use as a blank sample. The detection arm was cleaned and 1 µl of RNA sample was added to the detector and measured. RNA with a 260/280 nm ratio between 1.7 - 2 was deemed of sufficient quality. RNA quality was confirmed by running samples in 6x DNA loading buffer (30% (v/v) glycerol, 0.25% (w/v) bromophenol blue and 0.25% (w/v) xylene cyanol) on a 1.8% agarose gel. Two clear bands of ribosomal 28 and 18 subunits (28S and 18S) can be visualised following the same process as in section 2.5 with smearing of bands suggesting RNA degradation.

2.6.3 Reverse transcription (RT)

Reverse transcription (RT) converts single stranded RNA to more stable double stranded cDNA for amplification and analysis. RNA samples were made up to a 1 µg concentration in NFW with a final volume of 10 µl per sample. Using the High capacity cDNA reverse transcription kit (Applied Biosystems, USA) a RT master mix was made with the reagent quantities listed in table 2.2. 10 µl of the RT master mix was added to each 10 µl RNA sample (1 µg) and samples were placed in the thermal cycler set to: 10 minutes at 25°C, 120 minutes at 37°C, 5 minutes at 85°C and then continuously at 4°C. Following RT cDNA was stored at 4°C.

	Per sample (µl)
RT buffer	2
Random primers	2
MultiScribe® Reverse Transcriptase	1
RNase inhibitor	1
Deoxynucleotide (dNTP) mix	0.8
Nuclease free water	3.2

Table 2.2 – High capacity cDNA reverse transcription master mix

2.6.4 Real-time PCR (qPCR)

Real-time PCR (qPCR) allows highly sensitive quantification of target genes using TaqMan probes with complimentary 5'-3' regions to the gene of interest. The probes consist of a fluorophore and quencher attached to 5' and 3' ends respectively. Primer hybridisation and extension of target DNA leads to cleavage of the probe by Taq polymerase 5' to 3' exonuclease activity. This releases the fluorophore from the quencher and results in fluorescence. Fluorescence is proportional to the amount of DNA template in the sample and the number of amplifications for the fluorescent signal to reach the threshold is given as cycle threshold (Ct) values. TaqMan primers of interest (Appendix B) (Life Technologies, UK) were thawed on ice and protected from light. A separate master mix for each primer probe was made as follows - 3.5 µl NFW, 0.5 µl TaqMan primer probe and 5 µl 2x qPCR master mix (Life Technologies, UK) – per sample. 1 µl of cDNA sample was added to a well of a 96 or 384 well PCR plate followed by 9 µl of the gene probe master mix. All samples were run in duplicate or triplicate. Plates were sealed with film and spun briefly before they were loaded onto the ABI 7500 Real-

time-PCR machine using the pre-set PCR program settings: 95°C for 10 minutes then 40 cycles of 95°C for 15 seconds and 60°C for 1 minute. Data were collected as Ct values (figure 2.3) and normalised with the housekeeping gene 18s rRNA (VIC) (Life Technologies, UK) by subtraction of the samples 18s Ct value from the gene of interest Ct value to give deltaCt (dCt) values [219].

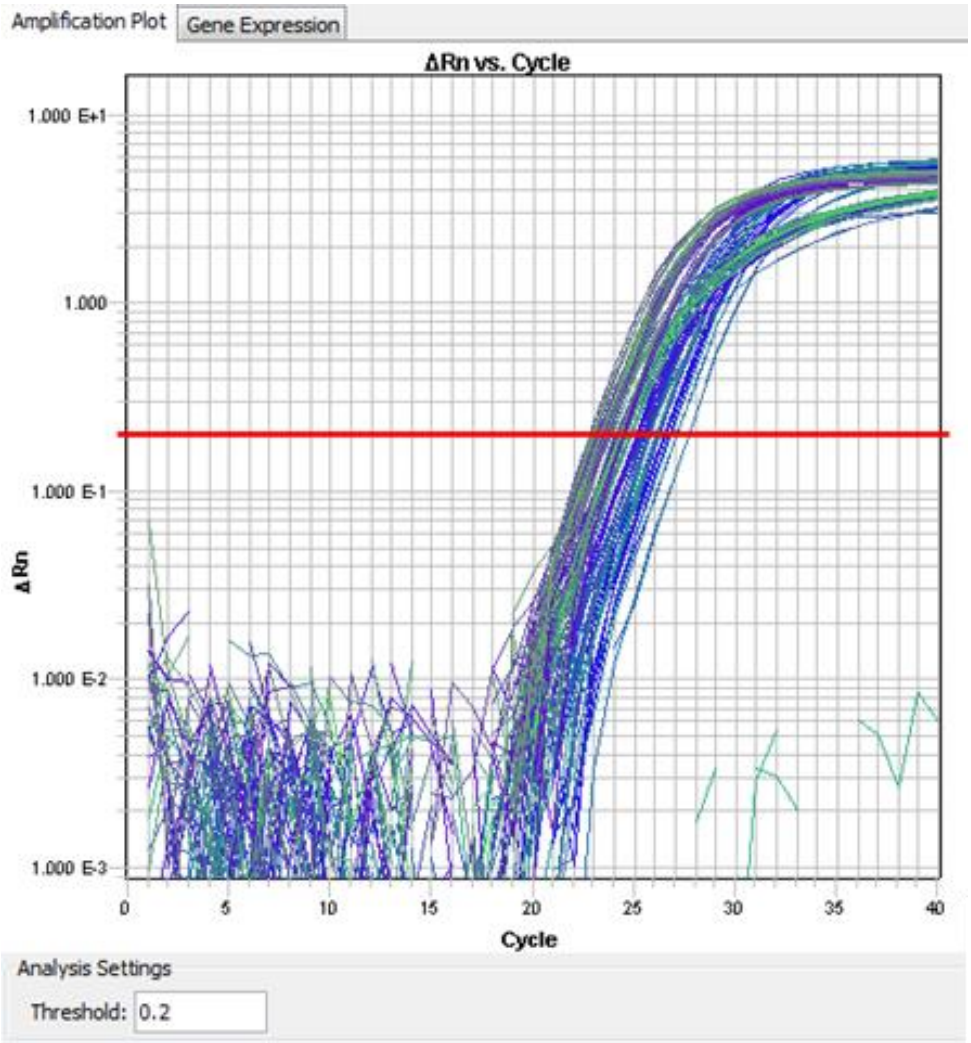

Figure 2.3 Real-time PCR amplification plot

An example amplification plot of samples analysed by qPCR, with data given as the cycle number that the signal reaches the set cycle threshold at a linear part of the curve.

2.7 Protein analysis

Protein, extracted from both cells and tissue, was quantified and analysed by immunoblotting to assess cellular protein expression.

2.7.1 Protein extraction

For cells, media was removed from wells and cells were washed with ice cold PBS before adding 75 µl of radioimmunoprecipitation assay (RIPA) lysis and extraction buffer (50 mM Trizma hydrochloride (Tris HCl) [pH 8], 150 mM sodium chloride (NaCl), 1% (w/v) Nonidet P-40 (NP-40), 0.5% (w/v) sodium deoxycholate 0.1% (w/v) sodium dodecyl sulfate (SDS), 1 mM ethylenediaminetetraacetic acid (EDTA)). Each 10 ml RIPA stock was supplemented with 100 µl of phosphatase inhibitor, 1 Pierce protease inhibitor tablet (Life Technologies, UK) and, to inhibit histone deacetylase (HDAC) enzymes, 10 mM nicotinamide and 1 µM of trichostatin A (TSA). Using a scraper cells were removed from the well surface in RIPA and pipetted up and down to maximise lysis. Lysates were transferred to Eppendorf tubes on ice and underwent two freeze thaw cycles to further enhance lysis. Samples were centrifuged at 12000 rpm for 10 minutes to pellet debris and the supernatant was transferred to a new Eppendorf. For tissues, previously snap frozen tissues were placed immediately into 150 µl of ice cold RIPA buffer and manually homogenised. Samples were also freeze thawed twice and followed the same extraction process as cell lysates from this point.

2.7.2 Quantification

The Bio-Rad DC^{TM} protein assay kit was used to measure protein lysate concentration. 5 µl of protein samples, and serially diluted bovine serum albumin (BSA) protein standards (of known concentrations in RIPA), were added to a 96

well plate in duplicate. 200 µl of Bio-Rad protein assay reagent B was added to each well followed by 25 µl of Bio-Rad protein assay reagent A (supplemented with 20 µl of reagent S per 1 ml of reagent A). Samples were incubated at room temperature for 5 minutes and then plates were read using the Victor3 1420 multilabel plate reader (PerkinElmer, USA) at 595 nm. Standards were plotted on a scatter graph and sample concentrations were extrapolated from the standard curve (see figure 2.4 for an example standard curve).

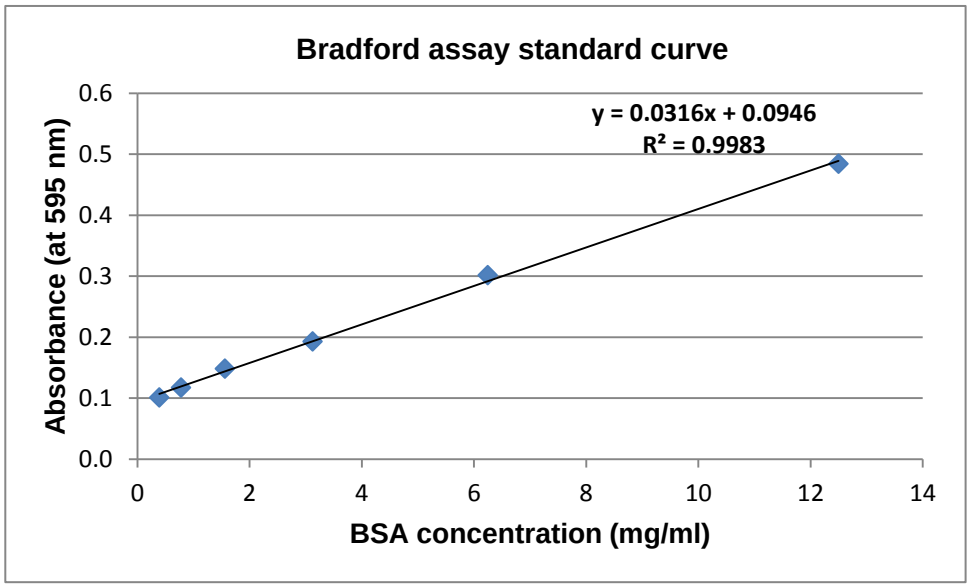

Figure 2.4 BSA standard curve

Following the Bradford assay a BSA standard curve was plotted using the absorbance of BSA at known concentrations. The concentration of samples was then determined by extrapolating absorbance values to the standard curve.

2.7.3 Immunoblotting

Sodium dodecyl sulphate - polyacrylamide gel electrophoresis (SDS-PAGE) was used to separate proteins based on their molecular weight. 10% (v/v) acrylamide gels were made in Bio-Rad SDS-PAGE apparatus using ProtoGel reagents (national diagnostics, UK). Firstly, 10 ml resolving gels were made (3.33 ml of 30% acrylamide, 2.5 ml of 4x resolving buffer, 0.5 ml 1.5% (w/v) ammonium persulfate,

3.67 ml distilled water and 10 µl tetramethylethylenediamine (TEMED)) and poured into the gel apparatus and left until set. Following this, stacking gels were made (0.6 ml of 30% acrylamide, 1.25 ml of stacking buffer, 0.2 ml 1.5% (w/v) ammonium persulfate, 2.6 ml distilled water and 15 µl TEMED) and poured on top of set resolving gel. 10 well combs were added to the top of the stacking gel and then left to set. Once set gels were transferred into Bio-Rad SDS-PAGE tanks and running buffer (0.1 M Tris [pH 7.4], 0.1 M glycine and 0.1% (w/v) SDS) was added.

Protein samples were made up to 20 µg/µl in distilled water and 2x Laemmli sample buffer (4% SDS, 20% glycerol, 10% 2-mercaptoethanol, 0.004% bromophenol blue and 0.125 M Tris HCl [pH approx. 6.8]) was added in a 1:1 ratio. Samples were boiled for 3-5 minutes before loading.

Combs were removed from the gels, wells were washed with running buffer and 5 µl of PAGE-Ruler plus prestained protein ladder was added to the first well to mark specific molecular weights. Then protein samples were added to the remaining wells. The Bio-Rad tank was filled with running buffer and the gels were electrophoresed at 120 V for 1.5 hours or until the dye front reached the end of the gel. Gels were removed and transferred onto nitrocellulose membranes using the iBlot (Invitrogen, UK). Ponceau S stain was added to membranes to confirm even transfer and then membranes were washed briefly in PBS. Membranes were blocked in 5% (w/v) milk or 5% (w/v) BSA in PBS with 0.1% (v/v) Tween (PBS-T) for 1 hour rocking at room temperature. Membranes were briefly washed in PBS-T and then primary antibody (in 5% milk or BSA in PBS-T) was added to membranes and left rocking overnight at 4°C. Membranes were washed in PBS-T for 5 minutes 3 times and then secondary antibody (in 5% milk or BSA in PBS-T)

was added to membranes for 1-2 hours rocking at room temperature (see Appendix C for antibody details). Membranes were washed for 15 minutes 4 times in PBS-T and then 1 ml of electrochemiluminescence (ECL) luminance substrate (Bio-Rad, UK) was added to each membrane and left at room temperature for 5 minutes. Membranes were placed into a developing cassette and covered with seran wrap; then in darkness a blue-x-ray film (GE Healthcare Life Sciences, UK) was placed in the cassette and left for the required exposure time. Films were removed and developed in the Xograph compact X4 developer (Xograph healthcare, UK).

2.8 NAD^+ measurements

2.8.1 NAD^+ cycling assay

To measure cellular NAD/NADH content we used reagents provided in the NAD/NADH quantification colorimetric kit (BioVision, USA). NAD cycling enzyme activity results in sample colour intensity proportional to the amount of NAD/NADH present; providing both specific and sensitive detection.

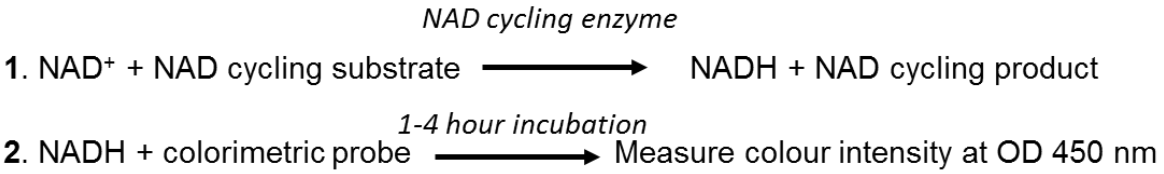

Figure 2.5 NAD/NADH assay principals

The two key steps to detect NADH using the NAD/NADH colorimetric cycling assay. Step 1 converts all of the sample NAD^+ to NADH and step 2 involves the addition of a colorimetric probe to develop colour intensity proportional to NADH content

Samples were kept on ice unless otherwise stated. Cells were differentiated in 12 well plates for 6 days and washed twice with ice cold PBS. 400 µl of extraction buffer was added to each well, cells were scraped from the well surface and transferred to an Eppendorf tube. Cells were freeze thawed twice on dry ice to maximise lysis and vortexed for 10 seconds. Samples were centrifuged at 14000 rpm to pellet debris and supernatant was split between two new tubes (200 µl in each), labelled as total NAD and NADH. The NADH samples were then heated for 30 minutes at 60˚C to allow NAD^+ decomposition. 50 µl of each sample was added to a 96 well plate in duplicate. In addition, a set of NADH standards of known concentrations (0-100 pmol) were also set up in duplicate and made up to 50 µl in extraction buffer. A mix of NAD cycling enzyme in NAD cycling buffer was made with 2 µl enzyme and 98 µl buffer per sample. 100 µl of the mix was added to each well and plates were mixed gently and left to incubate at room temperature for 5 minutes. 10 µl of NADH developer was then added to each well and the plate was left for 1 – 4 hours at room temperature for the cycling reaction to take place (reaction principals represented in figure 2.5).

Plates were read using Victor3 1420 multilabel plate reader (PerkinElmer, USA) at optical density (OD) 450 nm. Using the known standard values a standard curve was plotted (demonstrated in figure 2.6) and sample concentrations were extrapolated. NAD^+ content was determined by subtraction of NADH from total NAD.

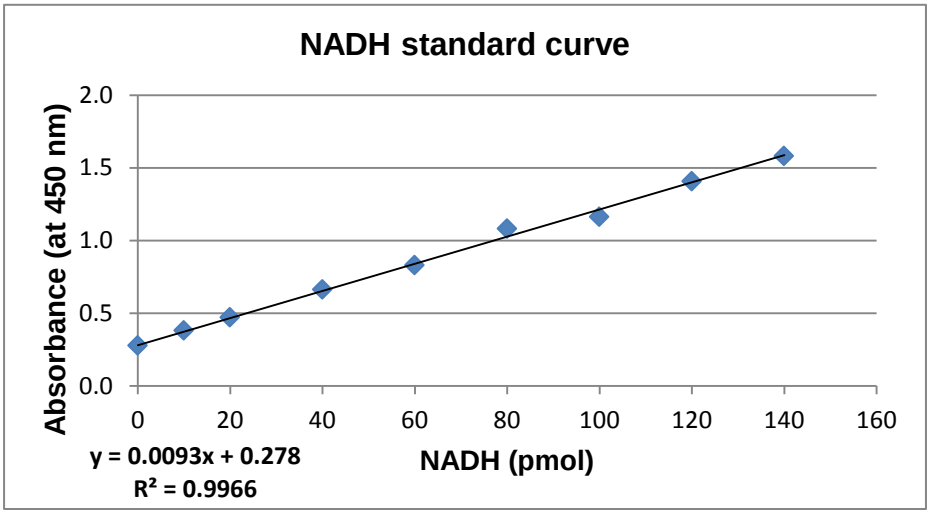

Figure 2.6 NAD/NADH cycling assay standard curve

Following the NAD/NADH cycling assay an NADH standard curve was plotted using the absorbance of NADH at known concentrations. Sample concentrations were determined by extrapolating absorbance values to the standard curve.

2.8.2 High performance liquid chromatography (HPLC) NAD^+ measurement

HPLC was used as an alternative technique to measure NAD^+ content in tissues. Tissue samples were analysed by Dr Antje Garten at the University of Leipzig using their established HPLC protocol [220]. Frozen muscle tissue was pulverized and then extracted in 1 M perchloric acid. Samples were neutralized in 3 M potassium carbonate on ice and centrifuged at 13,000 rpm for 10 minutes at 4°C. The supernatant was filtered and loaded onto the column. HPLC analysis was performed with the Chromaster Purospher STAR RP-18 endcapped 3 mm Hibar RT 150-3 HPLC column (Merck). To measure NAD^+, the HPLC was run at a flow rate of 0.4 ml/min with 100% buffer A (50 mM dipotassium phosphate, pH 7.0) from 0–5 min, a linear gradient to 95% Buffer A/5% Buffer B (100% methanol) from 5–6 min, 95% Buffer A/5% Buffer B from 6–11 min, a linear gradient to 85% Buffer A/15% Buffer B from 11–12 min, 85% Buffer A/15% Buffer B from 12–16 min, and a linear gradient to 100% Buffer A from 16–17 min. NAD^+ was eluted as

a sharp peak at 15 min and quantitated by peak area relative to a standard curve and normalised to tissue weight.

2.9 Cell viability

Cellular viability and apoptotic activity were both determined using the ApoLive-Glo^{TM} Multiplex assay (Promega, USA). As the aim of this experiment was to determine cell viability upon changing NAD^+ content this assay was specifically chosen because the reactions are not NAD^+ dependent.

Cells were seeded into 96 well plates at a density of 15,000 per well and differentiated for 6 days, before cells were treated with the relevant compounds for 24, 48 or 72 hours with a final well volume of 100 µl. Hydrogen peroxide (1 mM and 100 µM) and ionomycin (100 µM) were added as controls to induce cell death. Firstly, cell viability was measured; 10 µl of glycyl-phenylalanyl-amino fluorocoumarin (GF-AFC) substrate – cleaved by protease activity limited to viable cells - was added to 2 ml of assay buffer provided to make viability reagent. Then 20 µl of the reagent was added to each well and the plate was mixed using an orbital shaker at 300 rpm for 30 seconds. The plate was incubated for 30 minutes at 37°C. Fluorescence was measured at $400_{EX}/505_{EM}$ with the signal proportional to the number of viable cells (see step 1 figure 2.7 for viability reaction).

Secondly, induction of apoptosis in cells was determined by measuring the activity of the apoptotic marker caspase-3/7. 100 µl of the Caspase-Glo® was added to each well and mixed using an orbital shaker at 300 rpm for 30 seconds. The plate was incubated for 30 minutes at room temperature and then luminescence was measured with an increase in signal proportional to caspase-3/7 activity (step 2 figure 2.7).

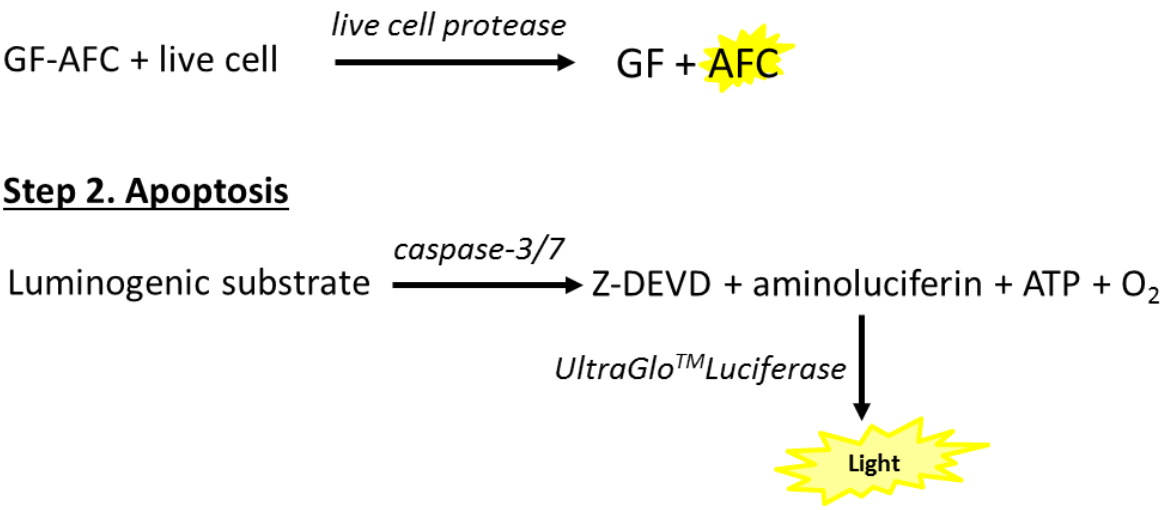

Figure 2.7 Cell viability and apoptosis assay

Key principals of the ApoLive- Glo™ Multiplex assay (Promega). Cell viability (step 1) can be determined by addition of the glycyl-phenylalanyl-amino fluorocoumarin (GF-AFC) substrate which can cross cell membranes and can be cleaved by live cell protease activity to release fluorescent AFC (live cell protease is inactive in membrane compromised cells). Cellular apoptotic activity (step 2) can be determined by caspase-3/7 activity. Luminogenic substrate is added to cells and upon caspase-3/7 activity aminoluciferin is released, which is a substrate for the UltraGlo™ luciferase enzyme and ultimately leads to production of light.

2.10 Bioinformatics

Online bioinformatic databases were used to investigate protein and nucleotide sequences of genes of interest. To maximise reliability numerous sequence database sites were used including PubMed (https://www.ncbi.nlm.nih.gov/gene), Ensembl (http://www.ensembl.org/index.html) and Z-Fin (https://zfin.org) and cross examined. Sequences were aligned using multiple sequence alignment software ClustalW2 (http://www.ebi.ac.uk/Tools/msa/clustalw2/) using on an adaption to the Myers and Miller alignment algorithm and scored on sequence similarity (using the Gonnet PAM 250 matrix) [221, 222].

2.11 Respirometry

Respirometry can be used to provide insight into mitochondrial function. Technology has been developed using oxygen sensors to measure oxygen flux in cells and tissue. Oxidative capacity can be inferred by assessing changes in oxygen over time. Seahorse Extracellular flux (XF) analysis provides a high throughput technique in response to different cellular stressors or treatments whereas Oroboros technology provides a high resolution analysis.

2.11.1 Seahorse Extracellular flux (XF) analyser

Primary and C2C12 myoblasts were seeded at 25,000 cells/well density in 24 well XF cell culture microplates (wells were equivalent size to those in a standard 96 well plate). Prior to the assay an XF sensor cartridge was hydrated overnight in XF calibrant (Agilent Technologies, USA) at 37˚C in a non CO_2 incubator. Upon 6 days of differentiation cells were analysed using the XF Cell Mito Stress Test kit on the Seahorse XF analyser following the Seahorse Bioscience user guide (Agilent Technologies, USA). Assay medium was prepared by supplementing XF base medium with 1 mM pyruvate, 2 mM glutamine and 10 mM glucose at pH 7.4. Stock solutions of the compounds from the XF cell mitochondrial stress test kit were made by resuspending each compound – oligomycin, carbonyl cyanide-4 (trifluoromethoxy) phenylhydrazone (FCCP) and rotenone/antimycin A – in assay medium to concentrations of 100 µM, 100 µM and 50 µM respectively. Each test compound was made up to its final concentration in 3 ml of assay medium (oligomycin (2.5 µM), FCCP (5 µM) and rotenone/antimycin A (1 µM)) and 25ul of each added to sensor cartridge ports A (oligomycin), B (FCCP) and C (rotenone/antimycin A). Following this, cell media from microplates was changed

to Seahorse assay media and incubated for 1 hour at 37˚C in a non-CO2 incubator. The plate was then loaded onto the XF analyser and the assay was run following the software instructions. During the run, each compound from the mitochondrial stress kit was subsequently released from its respective cartridge following a pre-set programme, table 2.3 and figure 2.8 demonstrate the order the compounds were released and the intended effect on mitochondrial respiration measured by oxygen consumption rate (OCR).

Compound	**Mitochondrial ETC target**	**Effect**
Oligomycin	ATP Synthase (complex V)	Inhibition of ATP synthase and decrease OCR – indicating the cells ATP production to meet energy demand of the cells
FCCP	Inner membrane	Uncoupler to give maximum OCR of the cells – providing the maximal respiratory capacity of the cell
Rotenone/ antimycin A	Complex I and III respectively	Inhibit complexes and decrease OCR- by shutting off mitochondrial ATP production

Table 2.3 – Mitochondrial stress kit components – listed in order of loading with a description of intended effect on mitochondrial electron transport chain (ETC) [223].

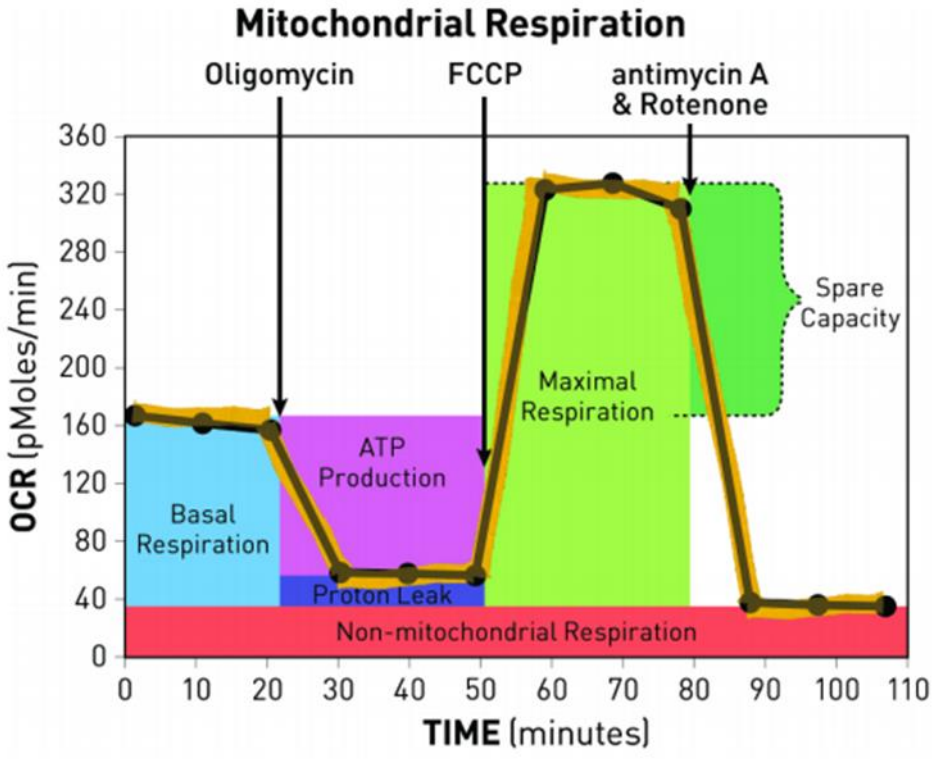

Figure 2.8 Seahorse Bioscience XF Cell Mito Stress Test profile

Graphical representation by Seahorse Biosciences (Agilent Technologies, USA), of mitochondrial respiration (measured by cellular OCR) over time with the XF Cell Mito Stress Test kit components oligomycin, FCCP and antimycin A and rotenone [223].

2.11.2 High resolution respirometry - Oroboros

Excised muscles were placed in 2 ml of ice cold biopsy preservation solution (BIOPS) buffer (10 mM Ca-EGTA buffer, 0.1 µM free calcium, 20 mM imidazole, 20 mM taurine, 50 mM K-MES, 0.5 mM dithiothreitol (DTT), 6.56 mM magnesium chloride ($MgCl_2$), 5.77 mM ATP, 15 mM phosphocreatine, pH 7.1) and kept on ice. The muscles were transferred into a petri dish with 2 ml BIOPS buffer and using forceps and a dissecting microscope muscle fibres were separated into clusters with care taken not to tear fibres and damage mitochondrial membranes. Fibre clusters were transferred into new ice cold BIOPS buffer and 20 µl of saponin stock solution (at 5 mg / ml of BIOPS) was added and fibres were incubated –

shaking at 4 °C – for 30 mins to permeabilise. Fibres were then removed from the BIOPS and dried out on filter paper before 5 mg of fibres were weighed out and transferred into 2 ml of ice cold mitochondrial respiration medium (MiRO5) (0.5 mM EGTA, 3 mM $MgCl_2$-hexahydrate ($MgCl_2 \cdot 6\ H_2O$), 60 mM lactobionic acid, 20 mM taurine, 10 mM potassium dihydrogen phosphate (KH_2PO_4), 20 mM 4-(2-hydroxyethyl)-1-piperazineethanesulfonic acid (HEPES), 110 mM D-Sucrose and 1 g/l BSA, essentially fatty acid free) at pH 7.1. The suspended fibres were then transferred into the pre-cleaned and calibrated Oroboros respirometer chambers.

Once airflow stabilised a succession of substrates were added after 5 minutes of stable signal from the previous substrate. Using a Hamilton syringe substrates were added in the following order and concentrations; 0.5 mM malate, 55 µM palmitoyl carnitine (for fatty acid oxidation), 10 mM glutamate, 5 mM ADP, 10 µM cytochrome *c* (to check mitochondrial integrity), 10 mM succinate, 0.5 µM FCCP (for maximal respiration), 0.5 µM rotenone and finally 2.5 µM antimycin A (to Inhibit mitochondrial respiration). Oxygen flux is measured following addition of each substrate to the myofibres, with a representative oxyograph trace demonstrated in figure 2.9.

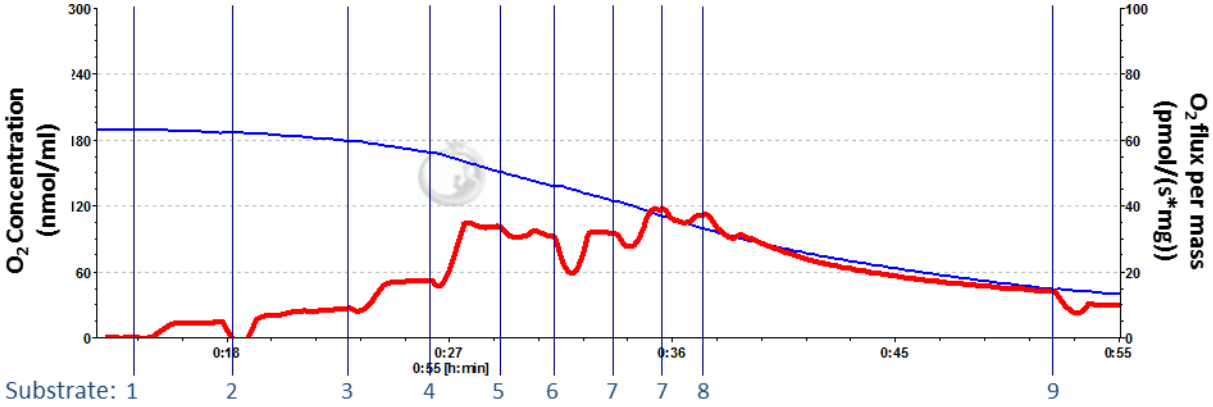

1. Malate, complex I linked substrate
2. Palmitoyl-carnitine, substrate for fatty acid oxidation, via electron-transferring flavoprotein complex
3. Glutamate, complex I linked susbtrate
4. ADP, to measure oxygen flux during oxidative phosphorylation
5. Cytochrome C, to test mitochondrial membrane integrity
6. Succinate, complex II linked substrate
7. FCCP, in sequential steps for optimal uncoupler concentration without destroying the membrane, to assess maximal capacity of electron transport chain (ETC)
8. Rotenone, inhibitor of complex I, to assess complex II-linked maximal capacity of ETC
9. Antimycin A, inhibitor of complex III, to measure residual oxygen consumption

Figure 2.9 Oroboros respirometry trace

A representative Oroboros high resolution respirometry trace of myofibres treated sequentially with the substrates listed (added at each vertical blue line on the trace). Chamber oxygen is concentration is represented by the blue line and oxygen flux represented in red.

2.12 Metabolomics

Metabolomic techniques can detect and quantify metabolites. Methods can be specifically targeted to metabolites of interest – and with the addition of internal standards can provide accurate quantification – or methods can be untargeted in order to identify new metabolites of interest for further analysis.

2.12.1 Primary muscle cell treatments for targeted metabolomics

Primary myotubes were differentiated for 6 days in 175 cm^3 flasks and cultures were either untreated or treated for 24 hours with 0.5 mM NR, 100 nM FK866 or both 0.5 mM NR and 100 nM FK866. Media was expelled and the myotubes were

washed once with ice-cold PBS. Myotubes were then detached from the surface using a cell scrapper in 3 ml of PBS and transferred in equal amounts into two new Eppendorf tubes for separate acid (A) and alkaline (B) extractions. Cells were pelleted by centrifugation at 4°C, supernatant was removed and pellets were stored at -80°C until extraction.

2.12.2 Extraction procedure for primary muscle cells liquid chromatography- mass spectrometry (LC-MS) - based metabolomics

Cell pellets were kept on dry ice and 20 µl of internal standard (IS) A or B diluted 1 in 20 in LC-MS grade water was added to each sample. IS A (^{13}C yeast extract) was used for the acid extraction and IS B (^{18}O nicotinamide riboside (NR), ^{18}O nicotinamide (Nam), D_4 nicotinic acid (NA), D_3, ^{18}O MeNam solution (60 µM of heavy NR, Nam, and MeNam and 240 µM of heavy NA)) was added to alkaline extractions. 300 µl of buffered ethanol (75 % ethanol: 25 % 10 mM HEPES pH 7.1) pre-heated to 80°C was added to each sample and samples were placed on the pre-heated Eppendorf Thermomixer at 80°C for 3 minutes shaking at 1050 rpm. Samples were then sonicated for 30 seconds in a bath sonicator (VWR, USA) and placed on ice. Samples were centrifuged for 10 minutes at 4°C at maximum speed and the supernatant was then transferred to a new Eppendorf tube. Both the pellet and supernatant (extract) were dried using a speed vacuum. Dried pellets were weighed and discarded and the dried extract was resuspended in 40 µl of the appropriate buffer (LC-MS grade water for acid extract and 10 mM ammonium acetate for alkaline extract). Extracts were then centrifuged at maximum speed for 10 minutes at 4°C and the supernatant was transferred to fresh Waters Polypropylene 0.3 ml plastic screw-top vials and analysed by LC-MS/MS using the ACQUITY UPLC H-class system (Waters, USA). Acidic and

alkaline separation gradients are listed in table 2.4. Acidic solvent A was 10 mM ammonium acetate and 0.1% formic acid and solvent B was 0.1% formic acid in acetonitrile. Alkaline solvent A was 7.5 mM ammonium acetate and 0.05% (v/v) ammonium hydroxide and solvent B was 0.05% (v/v) ammonium hydroxide in acetonitrile). Detection parameters for each metabolite are provided in appendix D (as described by Trammell et al. [224]) and representative LC-MS raw data for NAD^+ detection is displayed in figure 2.10.

Acidic separation gradient.				**Alkaline separation gradient.**		
Time (min)	Solvent B (%)	Column Volumes		Time (min)	Solvent B (%)	Column Volumes
0	5	-		0	5	-
1.8	5	1		1.8	5	1.8
11.2	35.9	5.4		14	54	12.4
11.3	90	-		14.1	90	-
13.3	90	1.2		17.1	90	3
13.4	5	-		17.2	5	-
23.4	5	5.8		32.2	5	15.3

Table 2.4 – LC-MS acidic and alkaline separation gradients

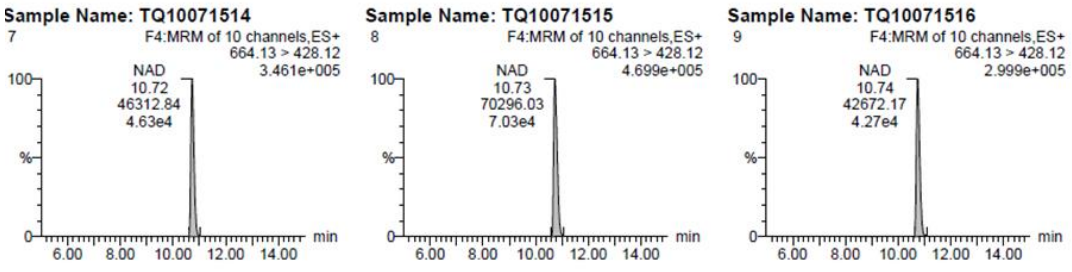

Compound name: NAD
Correlation coefficient: r = 0.996987, r^2 = 0.993982
Calibration curve: 0.000310839 * x + -0.00116855
Response type: Internal Std (Ref 27), Area * (IS Conc. / IS Area)
Curve type: Linear, Origin: Exclude, Weighting: 1/x^2, Axis trans: None

	# Name	Type	Std. Conc	RT	Area	IS Area	Response	Detecti...	pmol
10	10 TQ10071514	Analyte		10.72	46312.836	24954.301	1.856	bd	5974.4
11	11 TQ10071515	Analyte		10.73	70296.031	23784.393	2.956	bb	9512.1
12	12 TQ10071516	Analyte		10.74	42672.168	24607.195	1.734	bb	5582.6

Figure 2.10 Representative LC-MS raw data

Exemplary data for detection of NAD^+ using quantitative LC-MS. With traces from 3 samples showing clear NAD^+ peaks and resulting data tabulated below.

2.12.3 Tissue pulverisation and weighing

Samples were kept frozen in liquid nitrogen. Liquid nitrogen was added to a polystyrene insulated box and all the equipment – Bessman Pulveriser, tweezers and spatulas – was submerged in liquid nitrogen and left until fully cooled. Cryo-protective gloves were worn and the cooled pulveriser base was placed on foil, frozen tissue was immediately placed into the pulveriser base. The pulveriser pin was then placed into the base and pounded with a hammer until the tissue was powdered. The pin was removed and using a cooled spatula powdered tissue was transferred back into the cooled cryotube. The pulveriser was then cleaned with a Kimwipe (Kimtech, US) and placed back into the liquid nitrogen.

For weighing, Eppendorf's were pre-cooled on a rack in liquid nitrogen. A cooled tube was placed on the balance and 10-20 mg of frozen pulverised tissue was transferred using a cooled spatula, the exact weight was recorded, and immediately returned to the pre-cooled rack.

2.12.4 Muscle tissue extraction for targeted metabolomics

Pulverised muscle samples were placed on dry ice and a stock of 1 in 300 diluted IS A or B in LC-MS grade water was prepared to give 300 µl of IS per sample. Dry ice was added to a beaker of acetone to make a water bath at -4°C. Before starting the Branson sonifier was washed in a 50:50 water and methanol solution. Then 0.2 ml of ice cold LC-MS grade methanol was added to a sample, which was immediately returned to ice, before adding 300 µl of either IS A or B stock solution. Using a buoyancy aid the sample was then placed in the acetone water bath and sonicated for 20 seconds (with duty cycle set at 40% and output control at 4) and placed back on ice. This was repeated for all samples one at a time. Then all the

samples were placed on the Eppendorf Thermomixer pre-heated to 85°C for 5 minutes shaking at 1050 rpm. Samples were returned to ice for 5 minutes – an essential step to help preserve some metabolites – before they were centrifuged for 10 minutes at 4°C at maximum speed. The supernatant was transferred to a new Eppendorf tube. Both the pellet and supernatant (extract) were dried using a speed vacuum. Dried pellets were weighed and discarded and the dried extract was resuspended in 40 µl of the appropriate buffer (LC-MS grade water for acid extract and 10 mM ammonium acetate for alkaline extract). Extracts were then centrifuged at maximum speed for 3 minutes at 4°C and the supernatant was transferred to fresh Waters Polypropylene 0.3 ml plastic screw-top vials and analysed by LC-MS/MS using the ACQUITY UPLC H-class system (Waters, USA). Acidic and alkaline separation gradients are listed in table 2.4. Detection parameters for each metabolite are provided in appendix D (as described by Trammell et al. [224]) and representative LC-MS raw data for NAD^+ detection is displayed in figure 2.10.

2.13 Mouse investigations

All experiments and procedures involving animals were approved by and performed under British Home Office Guidance (Animals Scientific Procedures) Act 1986

2.13.1 Nmrk2 KO mouse

NMRK2KO mice were acquired from The Nmrk2 KO mutant allele was generated through the Knockout Mouse Phenotyping Program (KOMP2) on a C57BL/6N background. A ZEN-UB1 Velocigene cassette (beta-galactosidase coding sequence from E. coli lacZ gene; polyadenylation

signal; loxP site; promoter from the human ubiquitin C gene; neomycin phosphotransferase;polyadenylation signal; loxP site) was inserted through homologous recombination into the gene in place of all coding exons inhibiting transcription (figure 2.11). The construct was introduced into embryonic stem (ES) cells, and successfully targeted cells were injected into blastocysts and implanted into B6(Cg)-*Tyr*$^{c-2J}$/J mice. After breeding, male chimeras containing the KO cassette were identified and bred with C57BL/6NJ females. The neo cassette and the cre-expressing transgene were removed following further breeding of offspring [225]. On receipt of heterozygous male and female mice, genotyping was conducted to confirm heterozygosity of the Nmrk2 gene.

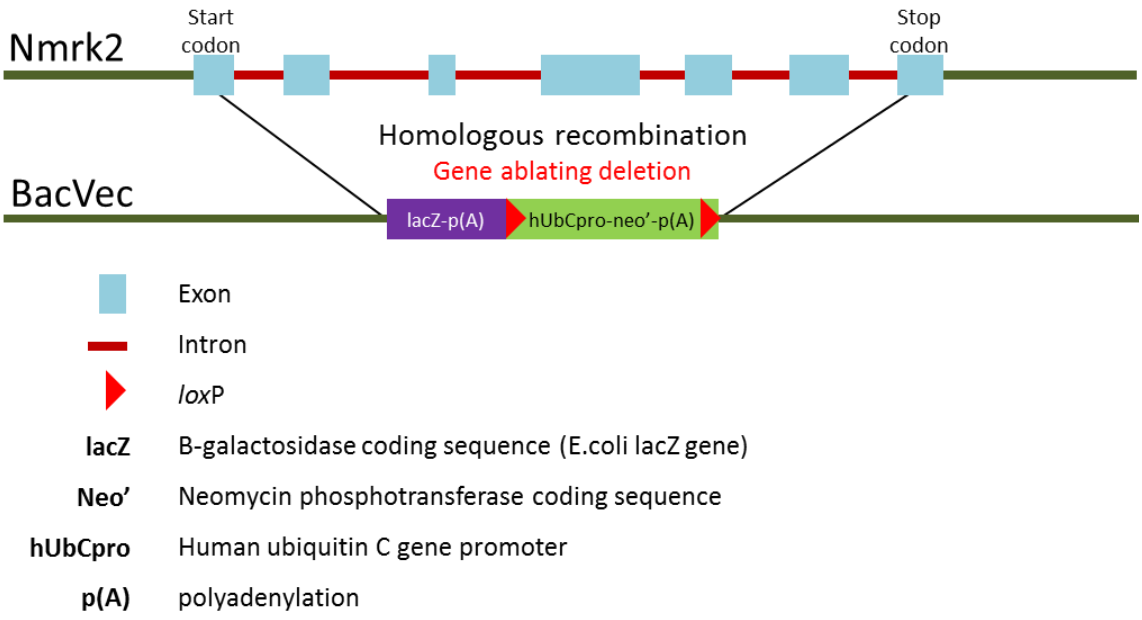

Figure 2.11 NMRK2 KO mouse construct map

An illustration of a full insertional cassette gene ablation of the Nmrk2 gene through homologous recombination with a neomycin cassette.

2.13.2 Genotyping

Tail or ear clippings from mice were digested by adding DNA extraction buffer (75 µl of 25 mM sodium hydroxide (NaOH) and 0.2 mM EDTA) and heated for 1 hour at 98°C. Temperature was reduced to 15°C and 75 µl of 40 mM Tris-HCl (pH 5.5) was added. Samples were briefly centrifuged at 4000 rpm to pellet debris. 1 µl of extracted DNA was then aliquoted for PCR. PCR samples were made to a final volume of 20 µl using a mastermix with 2x BioMix Red (Bioline, UK) and the primers listed in table 2.5, as described in section (2.5). Samples were placed in the PCR thermocycler set to 5 minutes at 95 °C then 35 cycles of [30 seconds 95 °C, 30 seconds 60 °C and 30 seconds 72 °C] followed by 5 minutes at 72 °C and left indefinitely at 4°C and analysed by electrophoresis on 1.8% agarose gels (figure 2.12) (see section 2.5).

Primer sequence	
CGG TCG CTA CCA TTA CCA GT	Mutant forward
GGG ACA TGC CCT CCT ATG TA	Mutant Reverse
CCA AAT AGC AGT CGG AGA GG	Wild type Forward
GCA AAC TTG TGT GGA TCC TTC	Wild type Reverse

Table 2.5 – Wild type (WT) and mutant Nmrk2 primers

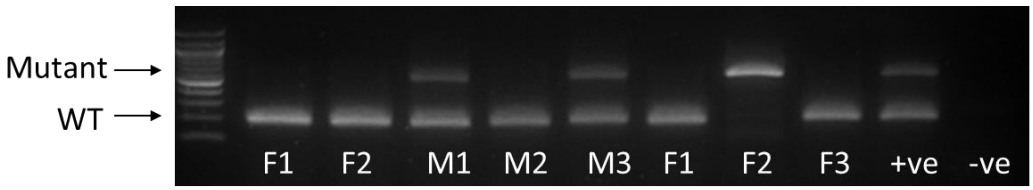

Figure 2.12 Nmrk2 genotyping

An example image from Nmrk2 genotyping with lower WT band and upper mutant band. A Nmrk2 heterozygous positive (+ve) control was used.

2.13.3 Animal breeding and care

Heterozygous breeding of the Nmrk2 KO mouse (NMRK2KO) line was employed to provide litter matched WT and NMRK2KO offspring for studies. Animals were all kept in an enriched pathogen–free environment at 21-23°C with 12 hour light/dark cycles. Unless otherwise stated standard chow and water was available *ad libitum*.

2.13.4 Glucose tolerance test (GTT)

GTTs were performed following 6 hours of food restriction with water remaining *ad libitum*. Mice were placed into restrainers, analgesic cream was applied to the tail and using a scalpel a small incision was made to the tail's lateral superficial vessel. A drop of blood from the incision was collected on Accu-Chek blood glucose strips (Boots, UK) and read using a glucometer to provide a baseline blood glucose reading. Following this glucose (2g/kg) was administered by I.P injection into the lower left quadrant of the abdomen and blood glucose was measured by taking a drop of blood from the original tail incision at 15, 30, 60, 90 and 120 minutes post glucose administration. Animals were monitored during and following the procedure for any signs of unexpected stress.

2.13.5 Fasting

Mice were single housed in clean cages with no access to food for 16 hours (overnight) before tissue collection. Mice had normal access to water and were kept in normal housing conditions.

2.13.6 High fat diet (HFD)

From 10 weeks of age, mice were fed a commercially available High fat chow (Brogaarden, Denmark), composed of 60% Kcal fat, for 16 weeks. The mice were weighed before starting the HFD and once a week until the end of the diet.

2.13.7 *In vivo* metabolic phenotyping

The PhenoMaster (TSE systems, Germany) system was used to collect indirect-calorimetry data *in vivo*. The 8 house system measures the exchange of O_2 and CO_2 to give the respiratory exchange ratio (RER) and predicted heat production, as well as measuring food and drink intake. Mice were weighed and placed into the PhenoMaster with their original litter mates and in their original cages for 24 hours to acclimate to the new environment. Following this, the mice were separated and housed individually for 72 hours within the PhenoMaster. The first 24 hours allowed the mice to adapt to isolation from litter mates, and then metabolic data was collected during the final 48 hours. Body weight, food and drink intake was monitored throughout, an example metabolic trace is provided in figure 2.13.

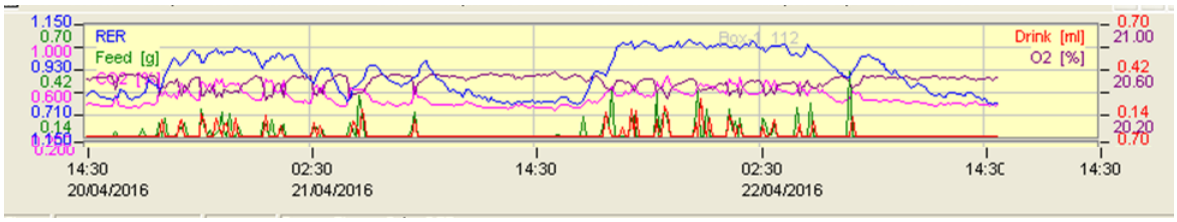

Figure 2.13 PhenoMaster *in vivo* metabolic trace

An example trace from a mouse placed in a PhenoMaster metabolic house. RER (blue), drink (red), feed (green), O_2 (purple) and CO_2 (pink) are some of the key parameters that can be tracked over 72 hours.

2.13.8 Treadmill exercise

To assess performance and metabolic adaptation of skeletal muscle following exercise a six lane mouse treadmill (TSE systems, Germany) was used for endurance exercise. Mice were acclimatised to the treadmill apparatus by initially placing them into lanes and giving them the opportunity to become familiar with the new environment. After this the treadmill was switched on and the treadmill speed and duration was gradually increased over a two-week period until mice were running for one hour at the full protocol speed of 0.2 m/s at a 15% incline. Following acclimatisation, mice were exercised for six weeks at 10am for one hour, three times a week at a speed of 0.2 m/s and 15% incline. Upon stopping at the end of the treadmill during the exercise, mice were encouraged to re-join the treadmill and were briefly blown with air if they failed to re-join the treadmill (up to a maximum of three times).

2.13.9 Animal sacrifice and tissue collection

Mice were sacrificed by schedule one cervical dislocation at 10 am to minimise circadian influence and, following cessation of circulation, tissues were excised immediately with muscle tissue prioritised to reduce acute signalling changes and metabolite degradation. Tissues were then either snap frozen in liquid nitrogen or placed in the required buffer or fixing agent for further analysis.

2.14 Muscle fibre typing

Using antibodies specific to the different myosin heavy chain (MHC) subunits expressed in muscle it was possible to count the different fibres and estimate the fibre type composition of individual muscles.

For fibre typing, muscles were specially snap frozen in isopentane, converting water within the tissue to small ice crystals and allowing effective cryostat sectioning. A beaker containing isopentane was lowered into liquid nitrogen and left until it was mostly frozen, leaving a small liquid pool in the centre of the beaker for tissues to freeze. Small cork discs were prepared with pins placed perpendicular and a drop of optimal cutting temperature compound (OCT) placed on the disc at the base of the pins. Muscle was excised carefully and intact to prevent structural damage and placed perpendicular to the cork disc alongside the pin. The cork disk was quickly lowered into the isopentane pool and left for 15-20 seconds to ensure the muscle was fully frozen. On removal, the disks containing the tissue were immediately wrapped in foil and placed on dry ice taking care to prevent tissue thawing or damage and stored at -80°C.

The frozen tissue was then analysed by Dr Gabriela Da Silva Xavier at Imperial College London using their established immunofluorescence staining protocol. Tissues were cut into 10 µm sections using a cryostat, mounted onto Superfrost slides and air dried for 10 minutes. Sections were washed 3 times for 5 minutes in PBS-T and blocked of 60 minutes in 10% goat serum in PBS-T. Sections were then stained using primary antibodies for different myosin heavy chain subunits (grouped into cocktails- see table 2.6) for 2 hours, Sections were washed in PBS-T 3 times for 5 minutes and secondary immunofluorescent antibodies, all outlined in table 2.6, were then added for 60 minutes. Sections were formalin fixed and washed in PBS for 5 minutes before coverslips were mounted with Vectashield hard setting (Vector laboratories, USA). Using a Zeiss Axio Observer inverted microscope (Carl Zeiss, Germany) – set up with Green (470 nm LED; Excitation 472/30; Emission 520/35), Red (540 - 580 nm LED; Excitation 534/20; Emission

572/28), Far Red (625 nm LED; Excitation 631/22; Emission 688/20) and Hammamatsu Flash4 camera – the entire section was imaged. Fibres were counted across the whole section manually using Image J (Fiji) software and recorded as positive for each fibre expressing the relevant visible colour.

Cocktail	Primary antibodies	MHC Reactivity	Secondary antibodies
Cocktail 1a	BA-F8 (1:50)	MHC I	IgG AF 647 (1:500) - Blue
	BF-F3 (1:100)	MHC IIb	IgM AF 555 (1:500) - Red
Cocktail 1b	SC-71 (1:600)	MHC IIa	IgG AF 488 (1:500) - Green
	BF-F3 (1:100)	MHC IIb	IgM AF 555 (1:500) - Red
Cocktail 2	SC-71 (1:600)	MHC IIa	IgG AF 488 (1:500) - Green
	6H1	MHC IIx	IgM AF 555 (1:500) - Red

Table 2.6 – Primary and secondary antibodies used for muscle fibre-typing

2.15 Statistical analysis

Statistical analysis was conducted using GraphPad Prism6 software (GraphPad software, USA). Unpaired Student t-test analysis was used when comparing single treatments or groups to a control. One way ANOVA was used for the comparison of multiple treatments, groups or times and two-way ANOVA was used for comparison of multiple groups over time. Statistical analysis of qPCR data was conducted using deltaCT values after normalisation with housekeeping gene 18s. ‘n’ numbers for each experiment are noted in the related figure legend. Key: * = P<0.05, ** = P<0.01, *** = P<0.001

Chapter 3 Characterisation of NAD^+ biosynthesis and salvage pathways in skeletal muscle.

(For targeted NAD^+ metabolomics LC-MS training and facilities were provided by Prof Charles Brenner at the University of Iowa and conducted during a one month lab placement)

3.1 Introduction

Skeletal muscle plays a central role in whole body metabolism and accounts for approximately 30% of an adult's total energy metabolism at rest [46]. Importantly, skeletal muscle also acts a major reservoir of nutrient reserves (such as glycogen and amino acids) that can be used upon changes to energy demand [26]. The complex mechanisms involved in skeletal muscle metabolic adaptation in response to energy stress cues are still undefined. Further understanding of these mechanisms is essential to determine novel molecular targets, which may play a central role in skeletal muscle metabolic decline, for therapeutic intervention.

3.1.1 NAD^+ signalling in skeletal muscle metabolism

Since the discovery of NAD^+ dependent sirtuin (SIRT) proteins, NAD^+ has risen to prominence as a key regulator of cellular metabolism and mitochondrial function. During SIRT signalling NAD^+ is consumed [90, 99] and therefore necessitates NAD^+ re-synthesis to replenish and maintain cellular NAD^+ content for continued signalling and unperturbed redox homeostasis. Numerous NAD^+ biosynthesis pathways have been identified in mammalian cells [142, 146, 226, 227]; yet it is still unknown how these biosynthesis pathways interact. The relative importance of the different NAD^+ biosynthesis pathways and tissue specificity remains poorly understood. As metabolic decline can be both causal and consequential of muscle decline, this chapter aims to identify NAD^+ biosynthesis pathways in skeletal muscle and define their relative importance to NAD^+ metabolism and energy homeostasis.

3.1.2 NAD^+ salvage pathways

NAD^+ can be replenished from NAD^+ precursors tryptophan, nicotinic acid (NA), nicotinamide (NAM) and nicotinamide riboside (NR) through a number of known biosynthesis pathways (outlined in figure 3.1 and section 1.4). These biosynthesis pathways can be grouped into two distinct routes described as “amidated” or “deamidated” [147]. De novo synthesis from tryptophan and NA salvage are metabolised through multi-enzyme pathways which converge with NADsynthase1 (NADS) – the final rate limiting “amidation” enzyme [146]. NAM and NR follow the “amidated” route and are metabolised to the intermediate nicotinamide mononucleotide (NMN) by the enzymes NAM-phosphoribosyltransferase (NAMPT) and nicotinamide riboside kinase (NMRK) respectively and finally NMN is converted to NAD^+ via NMN-adenylyltransferase (NMNAT) [142, 147, 150].

3.1.3 NAD^+ biosynthesis tissue specificity

Despite *de novo* biosynthesis acting as the preferred route of NAD^+ biosynthesis in the liver [138, 139], in other tissues it is thought that the majority of cellular NAD^+ is attributed to salvage pathways [147]; which resynthesise NAD^+ from precursor molecules (NA, NAM and NR) found in the diet or as consumed NAD^+ metabolites [140-142] (figure 3.1) . NAM is thought to be the preferred over NA in most tissues; illustrated by only transient increases in NAD^+ after intraperitoneal (IP) injection with NA as opposed to stable increases following NAM administration [144]. The extent to which NMRK-mediated salvage contributes to the maintenance of skeletal muscle NAD^+ pools is unknown. Unlike NAMPT and NMRK1, which are ubiquitously expressed [166, 228], NMRK2 is suggested to be skeletal muscle specific but has not been well characterised in this regard [171].

This chapter aims to establish the key NAD^+ biosynthesis and salvage genes involved in skeletal muscle NAD^+ maintenance. Skeletal muscle microarray data will be analysed to identify important muscle specific NAD^+ biosynthesis genes. Further investigation of these genes will help elucidate their relative importance in skeletal muscle NAD^+ metabolism and energy homeostasis.

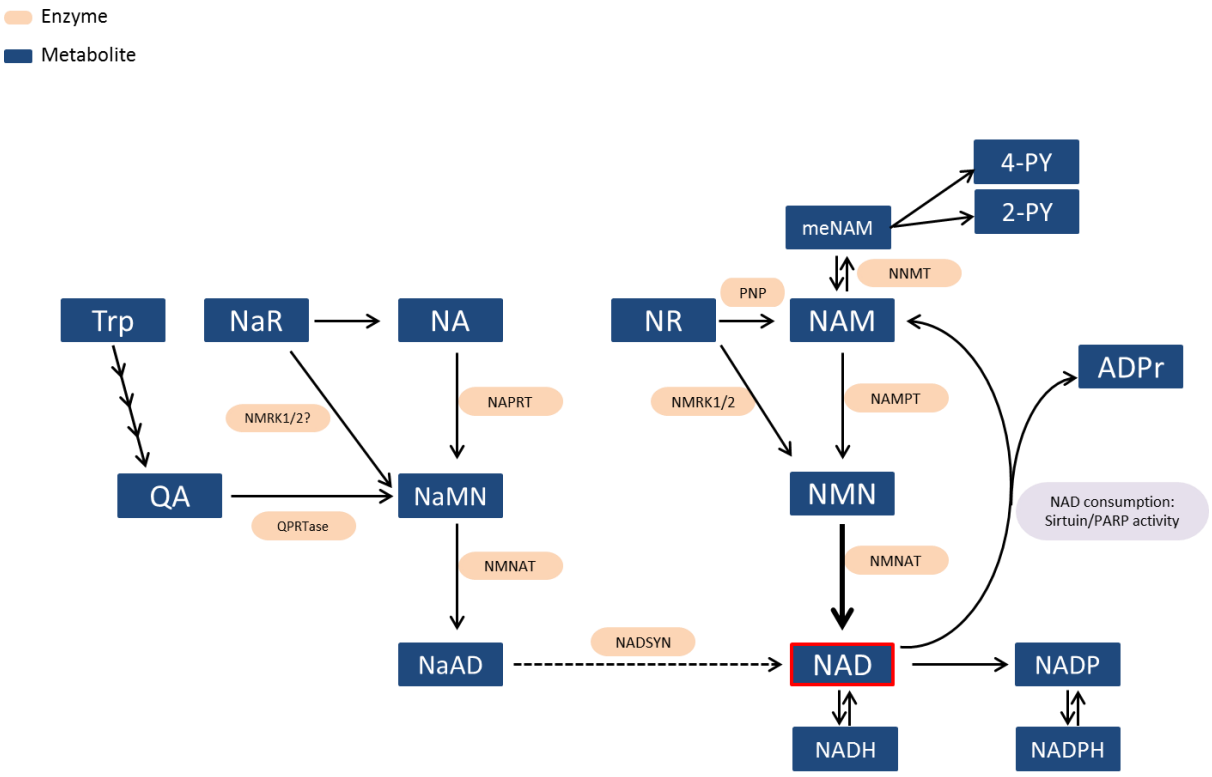

Figure 3.1 NAD^+ de novo synthesis and salvage pathways

A global illustration of the metabolites (blue) and enzymes (pink) involved in mammalian NAD^+ biosynthesis and salvage pathways.

3.2 Materials and Methods

3.2.1 C2C12 and Primary cell culture

Tissue culture was performed under sterile conditions and all cells were incubated at 37 ˚C in 5% CO_2/95% air. All culture media was refreshed every 48 hours.

C2C12 cells were maintained in 75 cm^3 tissue culture flasks in growth media (GM) - Dulbecco's modified Eagle's medium (DMEM) supplemented with 10% (v/v) foetal calf serum (FCS), 2 mM L-glutamine and 1% (v/v) penicillin/streptomycin (P/S) and 4.5 g/L glucose. For experiments, cells were seeded into 6 or 12 well plates at 60-70% confluence and left to incubate overnight. Cells were differentiated by replacing GM with differentiation media – DMEM supplemented with 5% (v/v) horse serum (HS).

Primary muscle cells were grown from isolated satellite cells, as described in section 2.2, in proliferation media (DMEM with 10% (v/v) HS, 1% (v/v) P/S and 0.5% (v/v) CEE). At 70% confluence media was changed to differentiation media (DMEM supplemented with 2% (v/v) HS, 0.5% (v/v) CEE and 1% (v/v) P/S).

3.2.2 Vitamin B3 supplementation

Unless otherwise specified, C2C12 and primary myotubes were supplemented in serum free media with NR, NAM, NaR and NMN at 0.5 mM for 24 hours with or without 100 nM FK866 (DMSO was used as a vehicle control at 0.001% (v/v) of final amount).

3.2.3 RNA Extraction

TRIzol reagent (Invitrogen, UK) was directly added to cells or to 20 mg of frozen tissue. Samples were homogenised and RNA was then extracted following the

TRIzol extraction method outlined in section 2.6. RNA concentration and quality was quantified using the NanoDrop (section 2.6).

3.2.4 Reverse transcription (RT)

1 µg of RNA sample was made in NFW with a final volume of 10 µl per sample. Using the High capacity cDNA reverse transcription kit (Applied Biosystems, USA) a RT master mix was made using the reagents listed in table 2.2. 10 µl of the mastermix was added to each RNA sample and samples were placed in the thermal cycler set to: 10 minutes at 25˚C, 120 minutes at 37˚C, 5 minutes at 85˚C and then continuously at 4˚C. Following RT cDNA was stored at 4˚C.

3.2.5 PCR

DNA was amplified using the 2x BioMix Red (Bioline) following manufacturer's instructions and using the primers listed in appendix A. Samples were placed in the PCR machine set to 5 minutes at 95 °C then 35 cycles of [30 seconds 95 °C, 30 seconds 60 °C and 30 seconds 72 °C] followed by 5 minutes at 72 °C and left indefinitely at 4 °C. Samples were analysed by electrophoresis on 1.8% Agarose gels.

3.2.6 Real-time PCR (qPCR)

For each TaqMan primer probe (Applied Biosystems, USA) a master mix was made as follows - 3.5 µl NFW, 0.5 µl gene primer probe and 5 µl 2x qPCR master mix (Applied Biosystems, USA) – per sample. 1 µl each cDNA sample was added to a well of a PCR plate followed by 9 µl of the gene probe master mix. All samples were run in duplicate or triplicate. Plates were sealed and spun briefly before they were loaded onto the ABI 7500 Real-time-PCR as described in section 2.6.4.

3.2.7 Bioinformatics

Bioinformatic analysis was conducted using online resources. Sequence alignment was performed using the software ClustalW2 and alignments were then scored based on sequence similarity.

3.2.8 Immunoblotting

10% (v/v) acrylamide gels were made using ProtoGel reagents (national diagnostics, UK) in Bio-Rad SDS-PAGE apparatus as described in section 2.7.

Protein samples were made up to 20 µg/µl in distilled water and 2x Laemmli sample buffer was added in a 1:1 ratio. Samples were boiled for 5 minutes before loading. Samples were loaded into the wells and gels were electrophoresed at 120 V for 1.5 hours or until the dye front reached the end of the gel. Gels were removed and transferred onto nitrocellulose membranes using the iBlot (Invitrogen, UK). Membranes were blocked and probed with primary and secondary antibodies as described in section 2.7 In darkness, (GE Healthcare Life Sciences, UK) was applied to the membrane following ECL treatment and then processed using the Xograph compact X4 developer (Xograph healthcare, UK).

3.2.9 Targeted NAD^+ metabolomics

Primary myotubes or tissue samples were extracted in ice cold LC-MS grade methanol. 300 µl of internal standard (diluted 1:300 in LC-MS grade water) was added and samples were sonicated for 20 seconds at -4°C. Then the samples were incubated at 85˚C for 5 minutes, shaking at 1050 rpm. Samples were returned to ice for 5 minutes and centrifuged. Supernatant was transferred to a new tube and dried using a speed vacuum. Dried extract was resuspended in 40 µl of either LC-MS grade water for acid extract or 10 mM ammonium acetate for

alkaline extract. Following a brief centrifugation, supernatants were transferred into Waters Polypropylene 0.3 ml plastic screw-top vials and analysed by LC-MS/MS using the ACQUITY UPLC H-class system as described in section (2.12.2).

3.2.10 NAD^+ cycling assay

NAD^+ was extracted from C2C12 and primary myotubes and quantified using the NAD/NADH quantification colorimetric kit (BioVision, UK) as described in section 2.8.1.

3.2.11 Respirometry

The Seahorse extracellular flux (XF) mitochondrial stress kit was used to measure cellular oxygen consumption. Differentiated C2C12 and primary myotubes were treated and analysed on the Seahorse XF analyser following the Seahorse Bioscience user guide (Agilent Technologies, USA).

3.2.12 Cell viability

C2C12 myotubes were differentiated and treated in a 96 well plate. Cell viability and apoptosis was assessed using the ApoLive-Glo™ multiplex assay (Promega) according to the section 2.9.

3.2.13 Statistics

Prism 6 (GraphPad) was used for statistical analysis with data presented as mean± SEM and P values <0.05 determined significant. Mean ΔCt values from the qPCR data was analysed using unpaired t-tests and One way ANOVA analysis for time course data. 'n' numbers for each experiment are noted in the related figure legend. Key: * = P<0.05, ** = P<0.01, *** = P<0.001

3.3 Results

Since NAD^+ was established as a key signalling molecule in energy metabolism, there has been a spike in research investigating NAD^+ dynamics and re-synthesis pathways in metabolically important tissues and pathological states [66, 86, 145]. Yet, despite this growing interest and the clear therapeutic potential of enhancing NAD^+ availability, NAD^+ biosynthesis and salvage pathways remain ill-defined in skeletal muscle.

3.3.1 NAD^+ metabolism in aged skeletal muscle

During ageing skeletal muscle typically becomes sarcopenic and manifests with progressively reduced muscle mass and function [182]. Perturbed NAD^+ metabolism has previously been associated with ageing in mice and rats [89, 174, 229]. To further investigate changes to NAD^+ in aged skeletal muscle, targeted LC-MS metabolomics was used to provide a global view of the NAD^+ metabolome. Tissue from young (up to 6 months) and aged (27-33 months) mice was acquired from the Shared Ageing Research Models (ShARM) tissue bank (Sheffield, UK) and analysis determined that the NAD^+ metabolome was indeed changed. Total NAD(H) was significantly lower in aged skeletal muscle, corroborating with current published datasets in rats and mice [89, 174, 187]. The NAD^+ signalling metabolite ADPr, released following NAD^+ consumption, and ATP were both also significantly reduced in the aged skeletal muscle (figure 3.2). Other metabolites tested (including NAM, NADP, ADP, meNAM and NMN) were not significantly different. These findings show some degree of disruption to NAD^+ signalling and energy metabolism in aged muscle that are likely to be directly associated with metabolic decline.

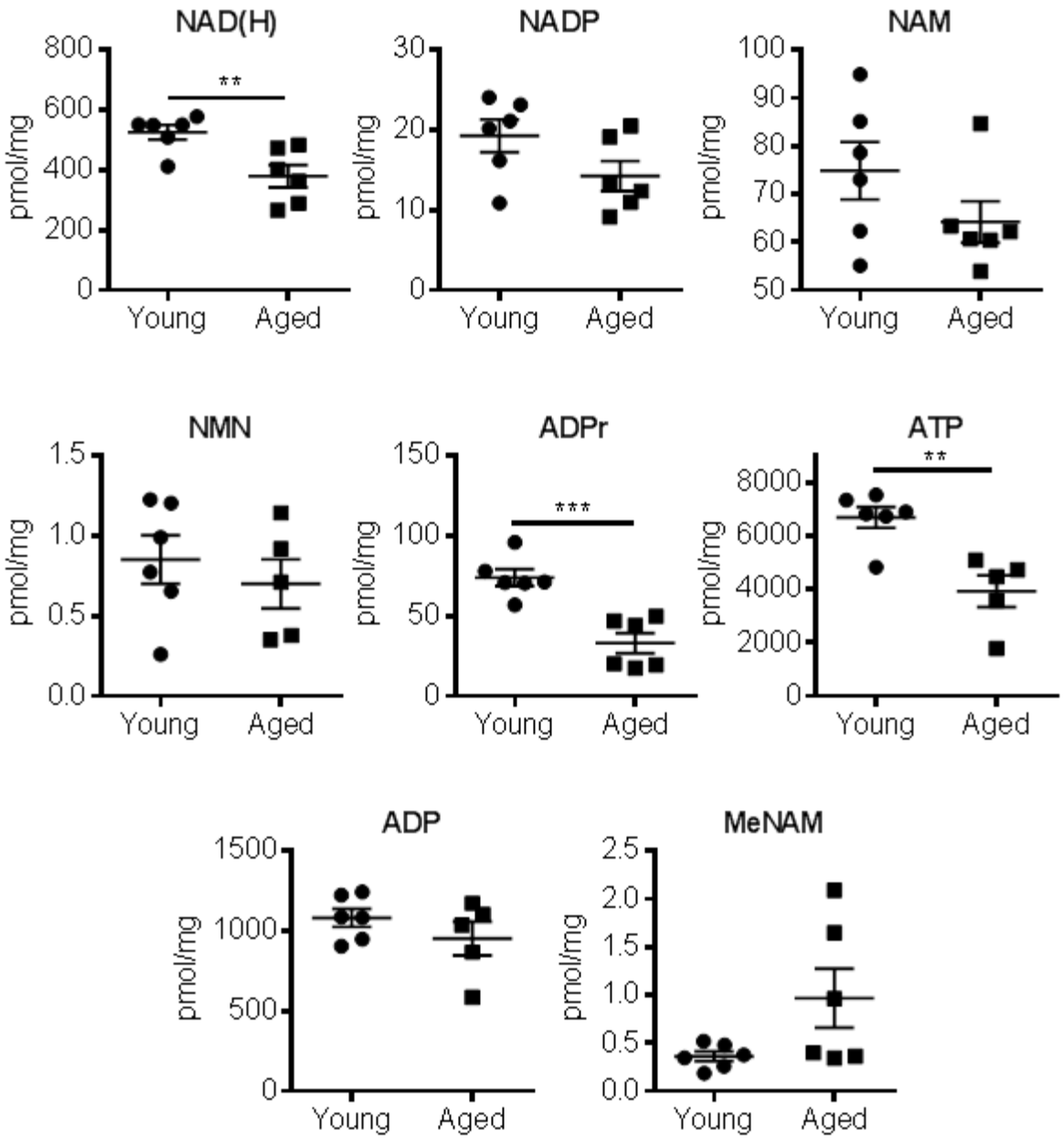

Figure 3.2 NAD$^+$ metabolomics of young and aged mouse skeletal muscle

Quantitative LC-MS analysis of total NAD(H) and related metabolites in skeletal muscle from young (less than 6 months) and aged (over 2 years) mice. Tissue was acquired from the ShARM tissue bank (Sheffield, UK), n=6. Statistical significance was determined by unpaired student t-test (* $p<0.05$, **$p<0.01$, ***$p<0.001$).

3.3.2 Identification of skeletal muscle NAD^+ biosynthesis pathways

With a decline in NAD^+ metabolism seen during ageing a better understanding of NAD^+ biosynthesis in skeletal muscle is necessary to establish the best targets for therapeutic intervention. To initially identify NAD^+ biosynthesis genes expressed in skeletal muscle, previous microarray data [230] was analysed; providing the relative mRNA expression of NAD^+ biosynthesis genes in TA and soleus skeletal muscle. The heat map presented in figure 3.3A identifies the three main NAD^+ biosynthesis genes expressed in both TA and soleus muscle namely; Nmrk2, Nampt and Nmnat1. Interestingly, Nmrk2 expression was found to be predominant and expressed in a muscle fibre type specific manner with a higher expression in fast twitch TA muscle compared to soleus muscle.

Follow up real-time PCR analysis of TA and soleus mRNA expression confirmed that Nmrk2, Nampt and Nmnat1 were the most predominantly expressed NAD^+ biosynthesis genes in skeletal muscle with comparatively low expression of Nmrk1 and NADsyn1 (figure 3.3B). As the expression of Nmrk1 and NADsyn1 - the key and final rate-limiting enzyme in both NAD^+ de novo synthesis and the Preiss-Handler salvage pathway [231] - were negligible in skeletal muscle this data suggests that the NMRK2 and NAMPT pathways may be the most important for maintaining NAD^+ availability in muscle.

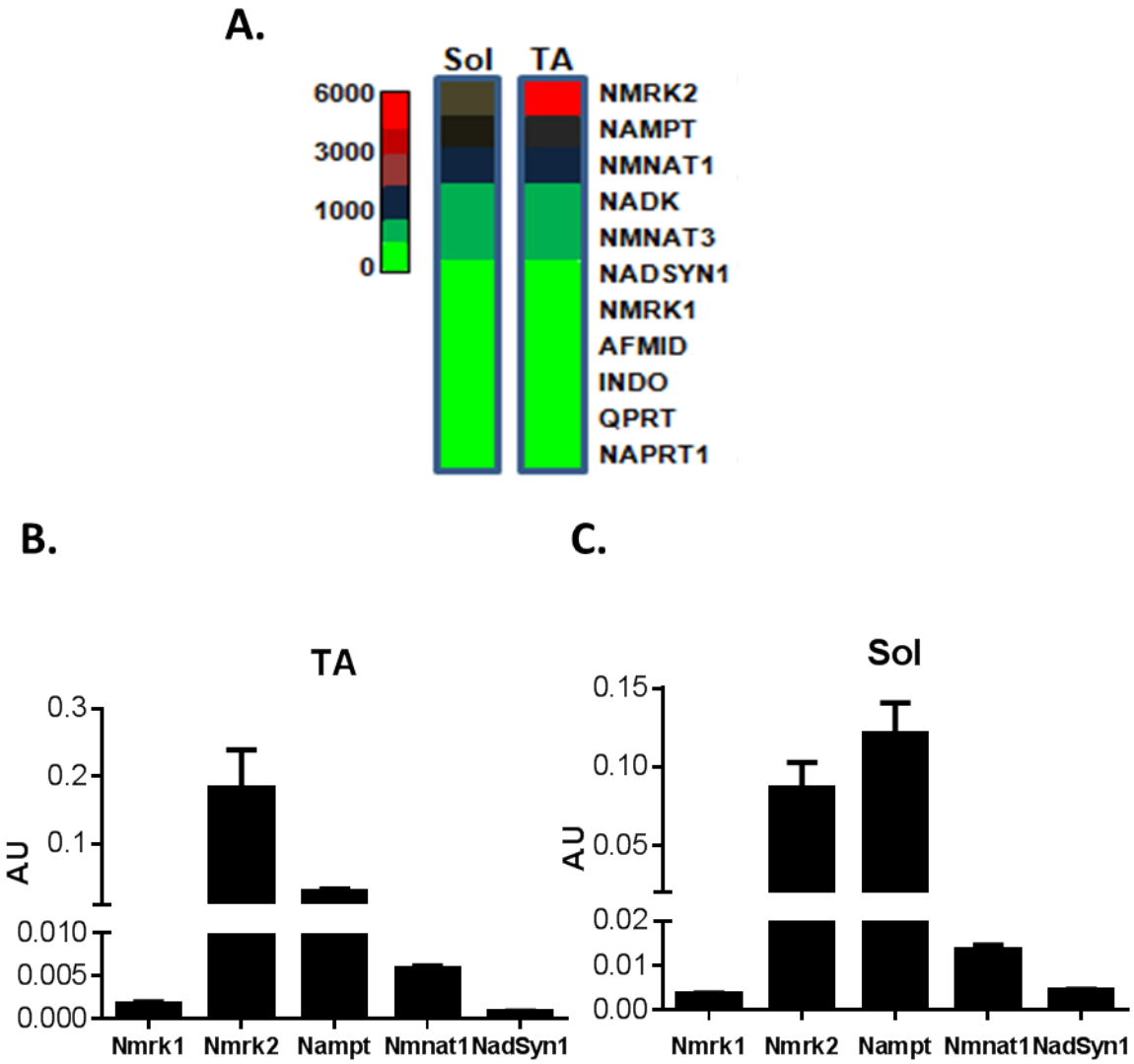

Figure 3.3 Expression of rate-limiting NAD^+ biosynthesis genes in skeletal muscle

(A) Previous microarray data from tibialis anterior (TA) and soleus (SOL) skeletal muscle by Lavery et al. [230] was used to identify the expression of NAD^+ biosynthesis genes. Follow up qPCR analysis of rate-limiting genes from NAD^+ biosynthesis pathways in (B) TA and (C) soleus muscle. Data is presented as mean A.U values ± SEM, n=4.

To determine their tissue specificity, the expression of the key rate-limiting NAD^+ biosynthesis enzymes - Nampt, NADsyn1, Nmrk1, Nmrk2 and Nmnat1 – from each of the identified pathways illustrated in figure 3.1– was assessed in a range of metabolically important tissues including; skeletal muscle (quadriceps, TA,

soleus and diaphragm), heart, liver, kidney, white adipose (gonadal) and brain tissue. Analysis of mRNA expression by qPCR, identified predominant Nmrk1 expression in kidney tissue (figure 3.4A). Expression of Nmrk2, the paralogue to Nmrk1, was found to be highly skeletal muscle specific, with some expression in cardiac muscle and white adipose tissue (figure 3.4B). In comparison Nampt mRNA was ubiquitously expressed across all the tissues analysed (figure 3.4C) with slightly lower expression in liver tissue. NADsyn1 was predominantly expressed in liver and kidney tissue suggesting that de novo NAD^+ biosynthesis and NA salvage is limited to these metabolic tissues (figure 3.4D). Conversely, NMNAT1, the final enzyme common to all the NAD^+ biosynthesis pathways, was universally expressed (Figure 3.4E).

Immunoblot analysis of NMRK1, NMRK2 and NAMPT across the same metabolic tissues supported these findings (Figure 3.4F). Protein expression of NMRK2 was muscle specific, whereas NAMPT was ubiquitously expressed and NMRK1 expression was predominant in liver and kidney tissue. This data further supports the suggestion that NMRK2 and NAMPT are the main enzymes for skeletal muscle NAD^+ biosynthesis with the alternative biosynthesis pathways potentially having more distinct roles in other tissues [76, 147]. Moreover, the predominant expression of NMRK2 in skeletal muscle identifies a unique role for NMRK2, specific to skeletal muscle cell regulation, compared to NAMPT which is ubiquitously expressed and potentially playing a more global role in NAD^+ resynthesis.

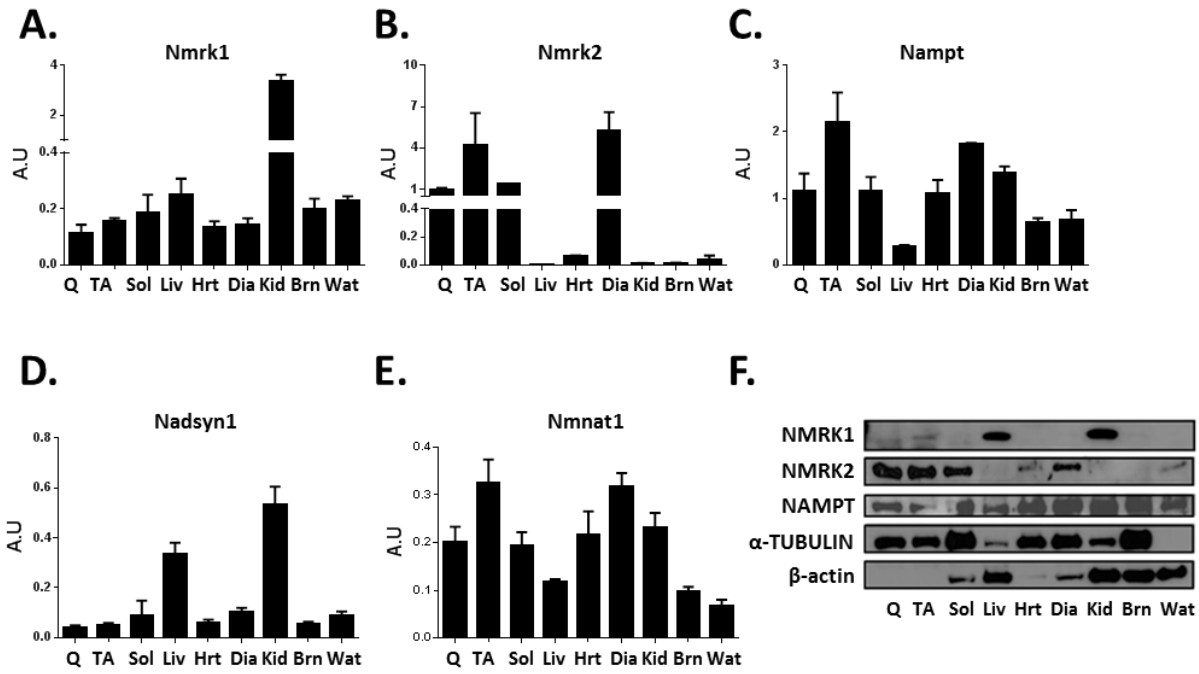

Figure 3.4 NAD$^+$ biosynthesis gene expression across metabolic tissues

Real-time PCR analysis of key rate-limiting NAD$^+$ biosynthesis genes – Nmrk1 (A), Nmrk2 (B), Nampt (C), Nadsyn1 (D) and Nmnat1 (E) – in metabolic tissues including quadriceps (Q), tibialis anterior (TA), soleus (Sol), liver (Liv), heart (Hrt), diaphragm (Dia), kidney (Kid), brain (Brn) and gonadal white adipose tissue (Wat) (all n=3). (F) Protein expression of NAD$^+$ biosynthesis enzymes identified in muscle tissue – NMRK1, NMRK2 and NAMPT – were examined by immunoblot analysis across the same metabolic tissues (representative of n=2). Real-time data is presented as mean A.U values ± SEM.

Muscle gene expression profiles change considerably over muscle cell differentiation [232], and with this it is likely that there would be a shift in energy metabolism when muscle cells differentiate into fused myotubes from proliferating myoblasts. As the C2C12 muscle cell line and primary muscle cultures are used in this project to investigate NAD$^+$ regulation and metabolism *in vitro*, understanding differential expression patterns of biosynthesis genes over muscle differentiation and development is important. Using PCR and immunoblot analysis, mRNA and protein expression of NAMPT, NMRK1 and NMRK2 was examined over an eight day C2C12 muscle cell differentiation time course. Figure 3.5A and B demonstrate

that Nampt mRNA and protein is constitutively expressed in C2C12 cells throughout muscle differentiation. In contrast, Nmrk2 mRNA and protein expression is switched on. In unspecialised C2C12 myoblasts (day 0) Nmrk2 expression is negligible, then by day 2 of differentiation Nmrk2 expression is significantly upregulated and then peaks at day 4 before plateauing when fully differentiated into myotubes at days 6-8 (figure 3.5A-C). Nmrk1 mRNA expression remained constant throughout C2C12 differentiation, with protein expression exhibiting a similar pattern (figure 3.5A and B).

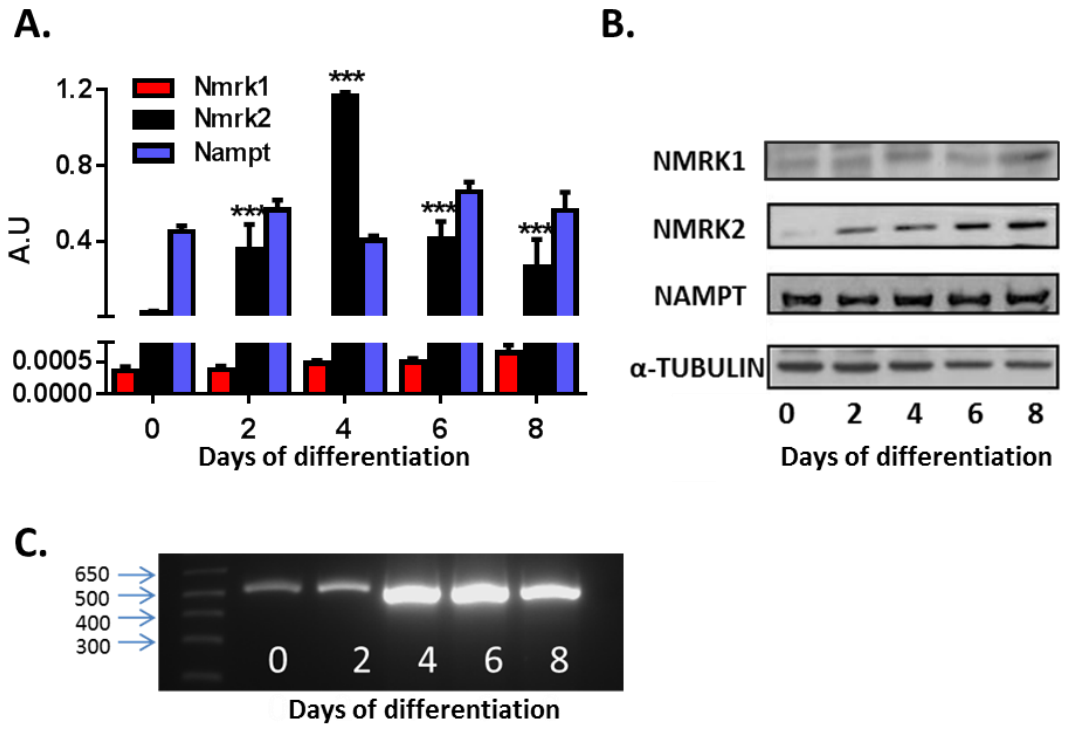

Figure 3.5 NAD^+ biosynthesis enzyme expression over C2C12 myotube differentiation

(A) mRNA and (B) protein expression of Nmrk1, Nmrk2 and Nampt over 8 day C2C12 myotube differentiation and (C) qualitative PCR analysis of Nmrk2. mRNA data is presented as mean ± SEM A.U values (n=3) and statistical significance was determined by one-way ANOVA with Dunnet's multiple comparisons test (* $p<0.05$, ** $p<0.01$, *** $p<0.001$). Immunoblot and qualitative PCR analysis are representative of n=2.

3.3.3 Nmrk2 orthologue differentiation and sequence alignment

In contrast to the results presented here, previous literature has identified alternative differentiation patterns for Nrmk2. Li et al. (1999) showed that muscle-specific beta 1 Integrin binding protein (MIBP), an apparent pseudonym for Nmrk2, was downregulated over differentiation in C2C12 myotubes with overexpression of Nmrk2 preventing terminal differentiation [172].

These differential findings were therefore further investigated using zebrafish as an alternative model. Due to a second genome duplication zebrafish have 4 paralogous genes to Nmrk2 namely, nmrk1, nmrk2, mibp and mibp2 [233]. Initially, expression of the different zebrafish nmrk2 orthologues was examined over embryonic development to potentially identify alternative expression patterns of paralogous genes. Figure 3.6A illustrates the mRNA expression of the four zebrafish Nmrk paralogues over embryo development. Here, differential expression patterns of the 4 genes are shown with mibp and mibp2 constitutively expressed, nmrk2 expression switched on and nmrk1 downregulated.

In addition, sequence alignment of mouse and zebrafish nmrk2 to the alternative zebrafish orthologues identified some sequence divergence although large portions of the sequences remained well conserved. In zebrafish nmrk2 was most closely conserved with mibp at 78.28%. Notably, the mouse Nmrk2 sequence was most conserved with zebrafish nmrk2 at 65.64%. Mouse Nmrk2 was also closely conserved with mibp and mibp2; further investigation of the sequences is required to identify the importance of the sites where the sequences are different and to determine the impact of this on protein structure and function. From these findings, the most likely explanation for the differences in expression patterns seen here to

those previously published is that different proteins were detected. This is supported by the sequence provided by Li et al. for MIBP which was 186 amino acids in length compared to the 195 amino acid sequence that has been determined for NMRK2 [172].

A.

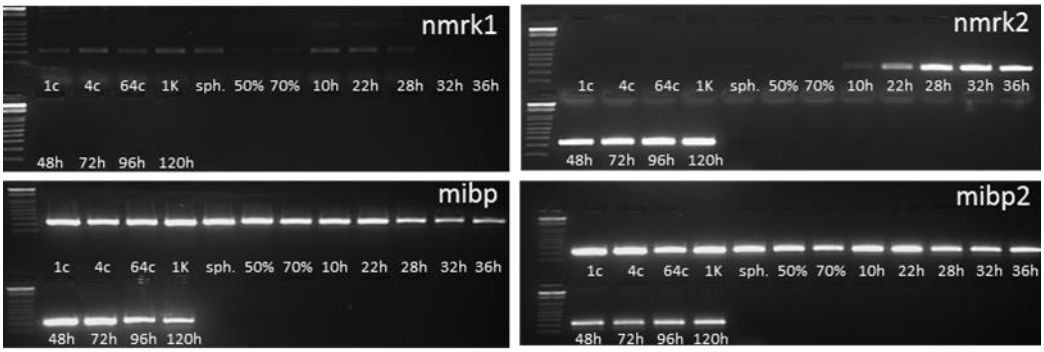

B.

Gene 1	Gene 2	Score (%)
Mm_Nmrk2	Dre_nmrk2	65.64
Mm_Nmrk2	Dre_mibp	63.08
Mm_Nmrk2	Dre_mibp2	62.05
Mm_Nmrk2	Dre_nmrk1	47.18
Dre_nmrk2	Dre_mibp	78.28
Dre_nmrk2	Dre_mibp2	68.69
Dre_nmrk2	Dre_nmrk1	45.96

Figure 3.6 Zebrafish nmrk2 orthologue gene expression and sequence comparison

A. mRNA expression of the 4 zebrafish Nmrk2 paralogues – nmrk1, nmrk2, mibp and mibp2 – over zebrafish embryonic development. With time points of 1 cell (1C), 4C, 64C, 1000 cells (1K), sphere (sph.), 50% epiboly, 70% epiboly, 10 hour post fertilisation (hpf), 22 hpf, 28 hpf, 32 hpf, 36 hpf, 48 hpf, 72 hpf, 96 hpf and 120 hpf. B. Sequence alignment scores determined using ClustalW2 of mouse (Mm) and zebrafish (Dre) Nmrk2 orthologous/paralogous genes with the score given as a percentage of sequence similarity.

Remarkably, this data also demonstrates that the expression of zebrafish nmrk2 is switched on at between 10-18 hours post fertilisation (figure 3.6A), which coincides with the time of initial muscle development and twitching in developing zebrafish embryos [234]. This supports the findings in C2C12 cells (figure 3.5) and suggests a conserved tissue specific role for nmrk2 in muscle development and differentiation across species.

3.3.4 NR supplementation can enhance myotube NAD^+ availability.

To further understand the role of NMRK2 in skeletal muscle NAD^+ salvage, C2C12 and primary muscle cells were supplemented with its primary substrate NR for 24 hours. NR supplementation significantly enhanced both C2C12 and primary myotube NAD^+ content with primary muscle cells more responsive (~25% increase versus >100% increase following 0.5 mM NR) (figure 3.7A and B respectively). Figure 3.7B shows that NR enhances NAD^+ in a dose dependent manner with levels exceeding double that of the control after 0.5 mM NR supplementation in primary myotubes. Nmrk2 mRNA expression consistently trends upwards following NR treatment yet expression of metabolic signalling genes including; Pdk4, Pparα, Sirt1 and Sirt3, were unchanged. Tfam, Ucp2 and Nrf1 are important genes involved in mitochondrial biogenesis and are often upregulated in response to metabolic stress [115, 235]; NR treatment did not alter the expression of these mitochondrial biogenesis markers (figure 3.7C). Concordantly, figure 3.7D illustrates that myotube NR treatment did not alter the expression of key mitochondrial complex proteins. Furthermore, despite an increase in NAD^+ levels, supplementation of C2C12 myotubes with 0.5 mM NR did not alter basal or maximal oxygen consumption rate (figure 3.7E), indicating that an increase in NAD^+ availability does not necessarily lead to enhanced oxidative metabolism.

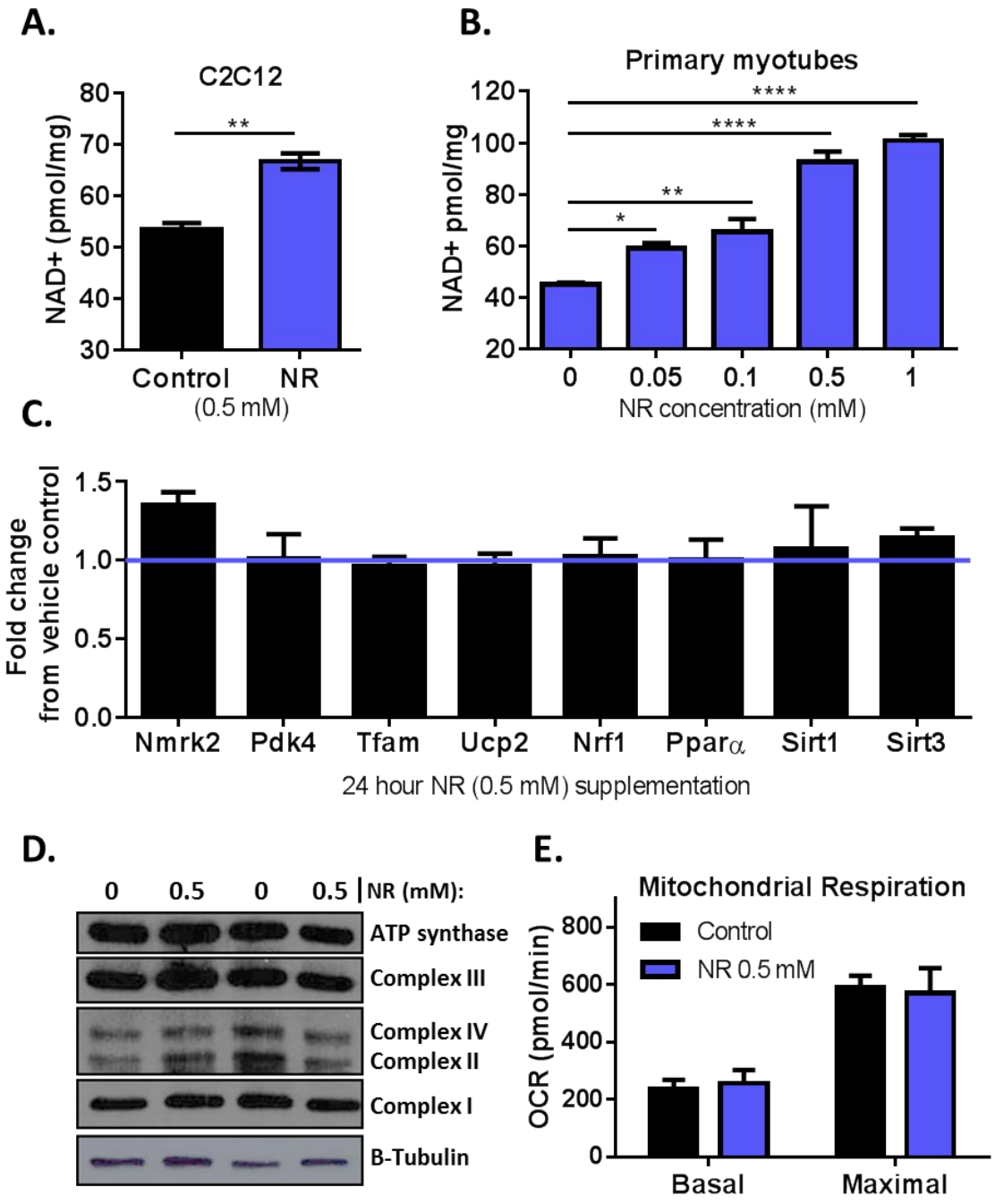

Figure 3.7 Effects of NR supplementation on C2C12 and primary myotubes

NAD^+ content of (A) C2C12 and (B) primary myotubes following 24 hour NR supplementation (0.5 mM and 0.05 -1 mM respectively). (C) Corresponding mRNA expression of Nmrk2 and key metabolic genes previously shown to be regulated by NAD^+ signalling. (D) Immunoblot analysis of mitochondrial complex proteins and (E) corresponding basal and maximal (uncoupled) mitochondrial respiration of C2C12 myotubes following 24 hour 0.5 mM NR treatment. All values presented as mean± SEM, n=3, statistical significance was determined by unpaired t-test (A) and one-way ANOVA with Dunnet's multiple comparisons test (B) (* $p<0.05$, **$p<0.01$, ***$p<0.001$).

3.3.5 The relative contribution of NAMPT and NMRK salvage pathways to NAD^+ availability

Data presented in figures 3.3 and 3.4, and previously published enzyme activity data [147], indicates that the NAMPT and NMRK2 salvage pathways outlined in figure 3.8A are the main routes to NAD^+ in skeletal muscle. To initially investigate the relative importance of NMRK2 and NAMPT for maintaining skeletal muscle NAD^+ availability, the NAD^+ boosting ability of different NAD^+ precursors (NR, NaR, NAM and NMN) was assessed. Interestingly, figure 3.8B shows that exogenous supplementation of 0.5 mM NR and NMN significantly boosts NAD^+ in primary myotubes to a similar level. Yet, 0.5 mM NAM supplementation is much less effective with a 10 fold dose increase required to significantly increase NAD^+. NaR is an alternative substrate for NMRK 1 and 2 that requires NADsyn activity as a rate limiting step to NAD^+ was used as a control [236], and did not lead to an increase in NAD^+ following supplementation at 0.5 mM.

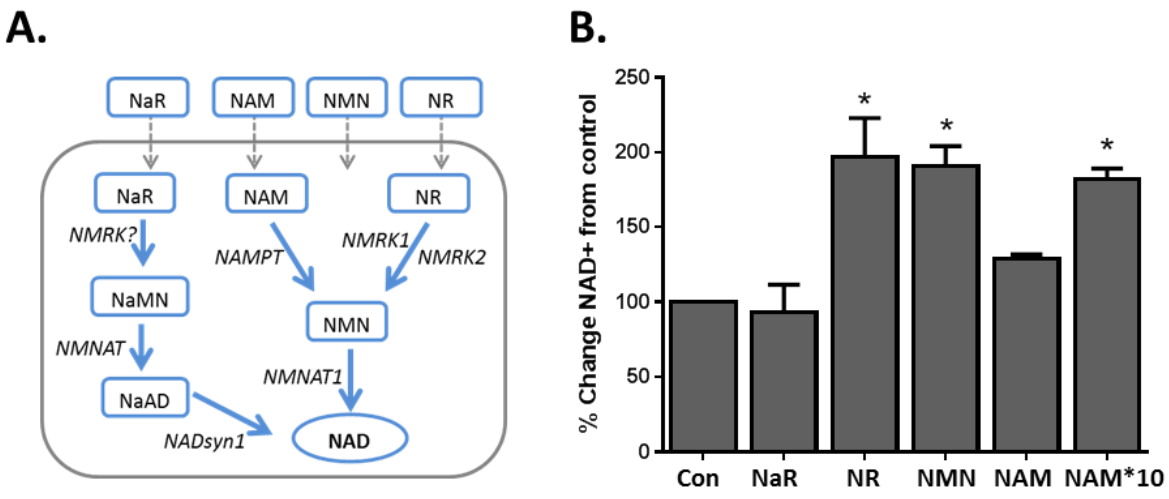

Figure 3.8 Cellular NAD^+ following precursor supplementation
(A) Exogenous NAD^+ precursor strategies to increasing NAD^+ biosynthesis. (B) Primary myotube NAD^+ content following 24 hour precursor supplementation at 0.5 mM (except NAM*10 = 5 mM.) compared to vehicle treated control (Con). Data presented as mean ± SEM, n=4, significance determined by one-way ANOVA with Dunnet's multiple comparisons test (* $p<0.05$).

NAMPT has been previously described as a vital component for NAD^+ turnover in tissues including skeletal muscle [150, 174, 227]; thus NAD^+ levels and precursor salvage was examined in myotubes with and without the NAMPT inhibitor FK866. FK866 is a potent pharmacological inhibitor of NAMPT and, although technically a competitive inhibitor, it's much greater affinity for the enzyme active site compared to NAM means its action is classed as non-competitive [134]. Following 24 hours of FK866 (100 nM) treatment, NAD^+ levels in the control myotubes are significantly depleted (by over 70%) indicating that NAMPT is indeed essential for basal NAD^+ turnover in skeletal muscle (figure 3.9). In addition, both NR and NMN can boost cellular NAD^+ after FK866 treatment, to the same extent as without, highlighting that they are both metabolised independent of NAMPT. As expected, NAM supplementation was unable to recover NAD^+ depletion following NAMPT inhibition (figure 3.9).

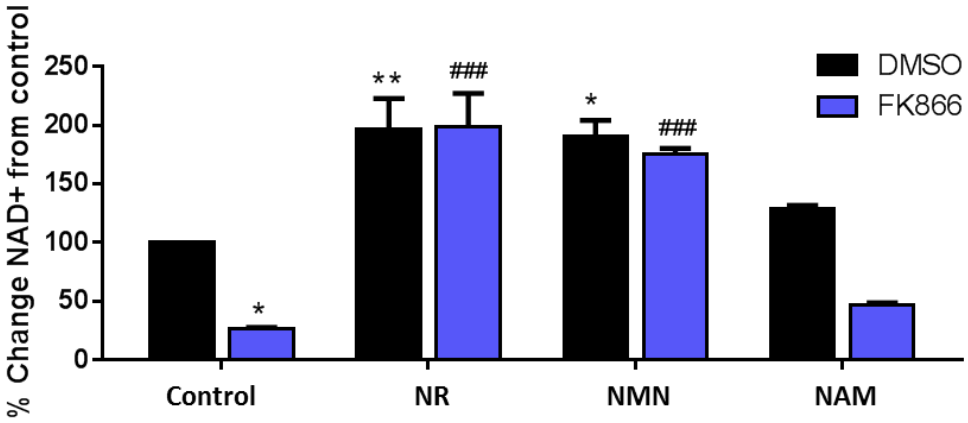

Figure 3.9 Cellular NAD^+ following NAMPT inhibition

Cellular NAD^+ content following 24 hour primary myotube treatment with NAMPT inhibitor FK866 (100 nM) compared to DMSO only control, with and without 0.5 mM NAD^+ precursor supplementation. Data presented as mean ± SEM, n=4, significance determined by one-way ANOVA with Dunnet's multiple comparisons test (with [*****] significant to DMSO control (*p<0.05, **p<0.01) and [#] significant to FK866 control (###p<0.001).

	Control	NR	FK866	FK866 + NR
NAD(H) (pmol/mg)	790.2 ± 54.3	1968.1 ± 518.1*†	253.8 ± 25.7	1564.4 ± 207.6†
NR (pmol/mg)	4.9 ± 0.6	73.6 ± 9.5*†	9.9 ± 2.0	112.1 ± 11.2*†
NAM (pmol/mg)	834.2 ± 29.8	1064.2 ± 172.4†	354.1 ± 43.3*	973.1 ± 75.8†
NMN (pmol/mg)	ND	107.9 ± 26.5*†	3.8 ± 0.7	79.6 ± 12.1*†
NA (pmol/mg)	ND	ND	ND	ND
NaR (pmol/mg)	ND	1.7 ± 0.2*†	0.1 ± 0.1	1.9 ± 0.2*†
NADP(H) (pmol/mg)	90.5 ± 3.1	186.4 ± 62.1	55.1 ± 23.5	98.4 ± 20.1
ADPr (pmol/mg)	535.3 ± 198.4	400.2 ± 54.1	326.6 ± 86	537.5 ± 104.3

Table 3.1 – Targeted LC-MS NAD^+ metabolome of primary myotubes with treated with NR (0.5 mM) and/or FK866 (100 nM). Data presented as mean ± SEM, n=3, and significance determined by one-way ANOVA with Tukey's multiple comparisons test (* significant to control, † significant to FK866 treatment ($p<0.05$).

NAD^+ metabolism is a multilevel signalling process involving a range of metabolites; therefore NAD^+ measurements can be limited when investigating the impact on wider NAD^+ metabolism. To gain further insight into the potential of NR supplementation beyond enhanced NAD^+, LC-MS based targeted NAD^+ metabolomics was employed. This approach enabled the assessment of a range of NAD^+ related metabolites providing a snapshot of the NAD^+ metabolome in response to NR treatment. Table 3.1 shows quantitative levels of key NAD^+ metabolites in primary myotubes treated with FK866 and NR. As expected, NAD(H) levels significantly increased following NR supplementation, and importantly a large increase in cellular NR from control cells was detected 24 hours following cell treatments. NMN levels were also significantly increased following NR treatment. Interestingly, metabolites of NAD^+ signalling NAM and ADPr were not altered by NR treatment but levels were reduced following FK866 NAD^+ depletion; suggesting NAD^+ availability is only rate limiting to NAD^+ signalling below normal levels (table 3.1). NA and other metabolites from the

Preiss handler and de novo NAD^+ biosynthesis pathways (not shown) were undetected in the primary myotubes.

As NAD^+ is a vital co-factor for energy production, the wider cellular impact of depleting NAD^+ was determined. Using C2C12 myotubes, mitochondrial respiration was assessed by myotube oxygen consumption rate (OCR). NAD^+ depletion by FK866 resulted in a significant reduction to myotube OCR (figure 3.10A). This effect may be attributed to limited NAD^+ for energy production but potentially there is likely to be some degree of cell death induced from NAD^+ depletion. Mitochondrial function was recovered by replenishing NAD^+ with NR concomitantly with FK866 or for the final 24 hours of 72 hour FK866 treatment (figure 3.10A). This reinforces the criticality of NAD^+ for energy production but also shows cell viability at least 48 hours post FK866 treatment.

To confirm the effect of FK866 on NAD^+ content (at 24 hours) is not just a direct result of cell death, cell viability and apoptosis was assessed. For up to 48 hours post FK866 treatment the number of viable cells were unchanged despite NAD^+ depletion from 24 hours. Cell viability appears to decline between 48 and 72 hours (figure 3.10B and C). A concomitant increase in apoptotic cells was also detected between 48 and 72 hours post FK866 treatment (figure 3.10B and D). This shows that myotubes can adapt to withstand low levels of NAD^+ for an extended period of time before cell death. Interestingly NR supplementation, even after 48 hours, completely prevented these events (figure 3.10 B-D). NAM was also added for the final 24 hours of 72 hour FK866 treatment and, expectedly, it was unable to recover apoptotic signalling and thereby demonstrated successful inhibition of NAMPT. Ionomycin and hydrogen peroxide (H_2O_2) were used as controls to induce cell death by necrosis (figure 3.10C and D).

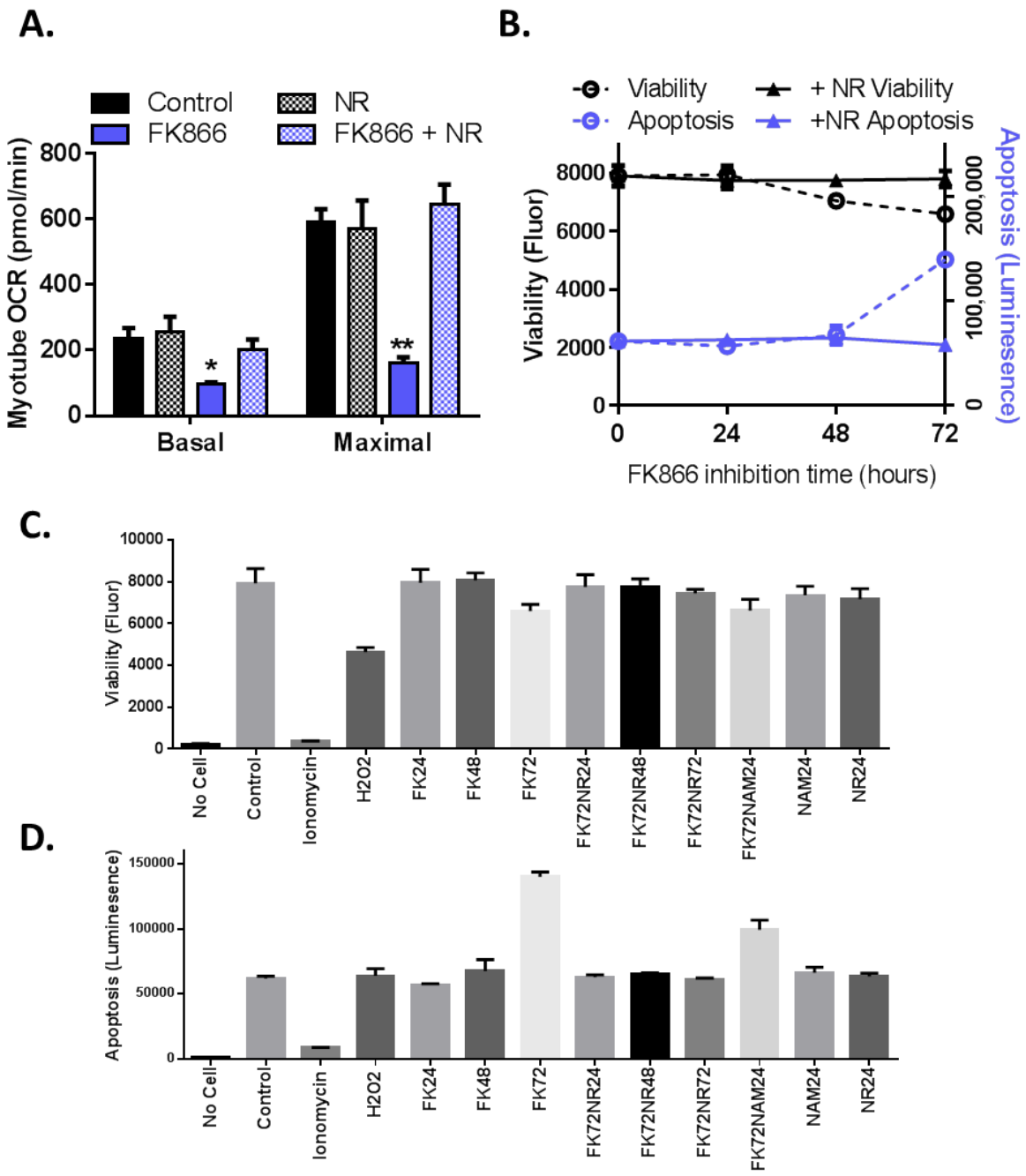

Figure 3.10 NR can rescue the effects of NAMPT inhibition on cell function

(A) Primary myotube oxygen consumption rate (OCR) as a function of basal and maximal mitochondrial respiration following 72 hour FK866 (100 nM) treatment to inhibit NAMPT with or without 24 hour NR supplementation (n=3). (B) Cellular viability and apoptosis markers activity over 72 hour FK866 (100 nM) treatment with (solid line) and without (dashed line) 0.5 mM NR supplementation. (C) Cell viability and (D) apoptosis marker activity with controls, ionomycin (100 µM), H_2O_2 (100 µM), FK866 (FK) (100 nM), NAM and NR (0.5 mM) for the time listed in hours (n=1, experiment quadruplet replicates). Data presented as mean ± SEM and significance determined by one-way ANOVA with Dunnet's multiple comparisons test (* $p<0.05$, ** $p<0.01$).

These data show that NAMPT recycling of NAM is crucial for basal NAD^+ biosynthesis in skeletal muscle, with NAD^+ depletion, mitochondrial decline and cell death a consequence of NAMPT inhibition. Interestingly, NR supplementation can completely rescue this effect, most likely through NMRK-mediated NAD^+ salvage; suggesting that although NMRK activity is independently capable of maintaining cellular NAD^+, NR availability may restrict this alternative pathway under basal conditions.

3.3.6 Fast-twitch and slow-twitch muscle types exhibit different NAD^+ biogenesis profiles

It is well established that muscle tissue is heterogeneous in terms of fibre type composition; with slow to fast twitch fibre composition reflective of the oxidative vs glycolytic capacity of the muscle [20]. Data from the initial tissue screening of Nmrk2 indicated possible fibre-type specific expression. Further immunoblot and real-time qPCR analysis of different muscle beds also corroborated with the microarray data, demonstrating protein and mRNA expression levels were significantly enriched in fast-twitch TA tissue compared to slow-twitch soleus muscle.

Differential expression of Nmrk2 between TA and Soleus muscle (figures 3.3 and 3.4) demonstrates integral differences between different muscle beds. Skeletal muscle structure and composition is vastly dependent on the physiological requirement of the muscle and therefore large differences to metabolism and signalling in different muscle types is unsurprising [237, 238]. Consequently, characterisation of skeletal muscle NAD^+ signalling must also account for muscle fibre-type specificity.

Analysis of total NAD^+ content in different muscle beds showed significantly higher levels per mg of tissue in soleus muscle compared to TA (figure 3.11A), supporting the increased oxidative requirements of the tissue. However, in myotubes originating from TA and soleus muscle, basal NAD^+ levels were similar and 24 hour NR supplementation enhanced NAD^+ to the same degree (figure 3.11B). NADH levels appeared elevated in soleus derived myotubes; thus, lowering the NAD/NADH ratio (figure 3.11C and D).

The oxygen consumption rate of primary myotubes from TA and soleus muscle was additionally examined as a measure of mitochondrial function. As expected, soleus derived myotubes exhibited higher rates of oxygen consumption, indicating a higher oxidative capacity compared to TA derived myotubes. Following 24 hour NR supplementation (0.5 mM), the oxygen consumption rate significantly increased in soleus derived myotubes (figure 3.11E). Expression of key mitochondrial complex proteins was analysed and identified a differential expression with TA exhibiting higher levels of proteins in complex III, IV and ATP synthase and soleus muscle having a higher expression of proteins from complex I (figure 3.11F). Together these data identify important integral differences between different muscle beds in NAD^+ metabolism which may be attributed to their distinct oxidative and glycolytic metabolic functions.

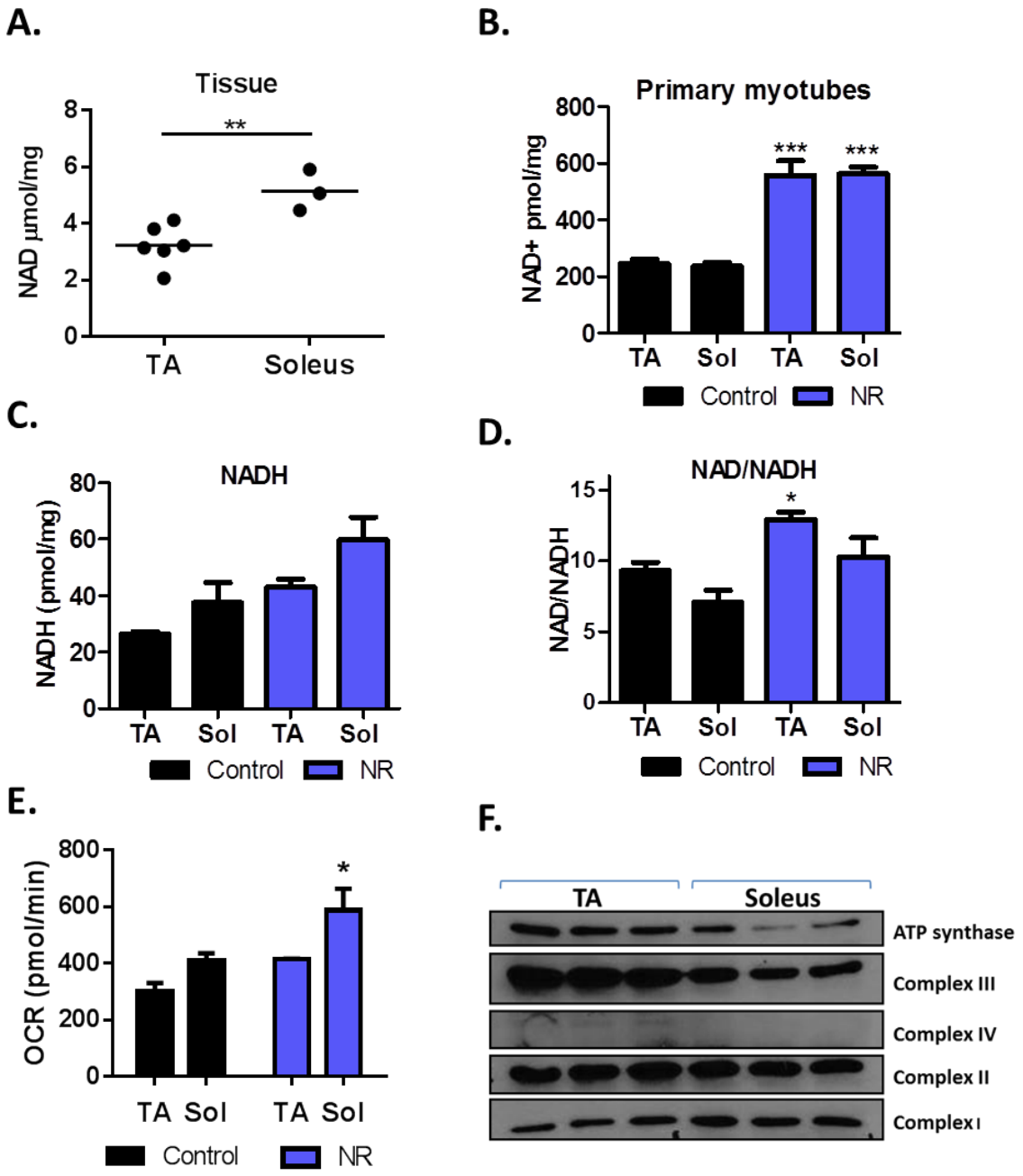

Figure 3.11 Comparison of NAD$^+$ metabolism in TA and soleus muscle beds

(A) NAD$^+$ content of mouse TA and Soleus muscle tissue. (B) NAD$^+$, (C) NADH and (D) NAD/NADH content of primary myotubes from TA and soleus muscle treated with 0.5 mM NR or vehicle control (n=6). (E) Basal mitochondrial respiration of myotubes from TA and soleus muscle treated for 24 hours with 0.5 mM NR or vehicle control (n=4). (F) Immunoblot analysis of key mitochondrial complexes in TA and soleus tissue. Data is presented as mean ± SEM for significance was determined by unpaired T-test (A) and one-way ANOVA (B-E) (* p<0.05, **p<0.01, ***p<0.001).

3.4 Discussion

The interplay between NAD^+ signalling and energy metabolism acts as an essential homeostatic mechanism that when disrupted can be detrimental to metabolic health [76, 89, 227]. Skeletal muscle has long been known as a major site of energy metabolism and nutrient storage [26, 239]. Vast changes to energy demand in muscle, particularly in response to physical activity, requires robust yet dynamic signalling events to maintain energy homeostasis [26]. Aged mouse muscle examined here exhibited a declined NAD^+ metabolome compared to muscle of young mice. With mounting evidence associating NAD^+ availability and metabolic health it is important to identify the critical pathways in skeletal muscle to NAD^+ metabolism [89, 169, 174, 199].

Metabolic enzyme profiling of mouse tissue determined that the amidated route to NAD^+ predominated in all tissues with NMNAT1 activity high and non rate-limiting, except in the blood [147]. The deamidated route was determined to be minor in all tissues, with NADS highest absolute activity in the liver and small intestine and notably undetectable levels in skeletal muscle [147]. This chapter aimed to further characterise the pathways central to NAD^+ biosynthesis in skeletal muscle which until now has been relatively undefined. Here, following analysis of the NAD^+ biosynthesis genes, three enzymes were identified to be predominantly expressed in skeletal muscle namely NMRK2, NAMPT and NMNAT1. From this it was determined that the NMRK and NAMPT pathways (illustrated in figure 3.1), both of which have NMNAT1 activity downstream, are the main routes to NAD^+ biosynthesis in skeletal muscle. NAD^+ salvage via NAMPT has been much more characterised than salvage via the more recently identified NMRK enzymes [157, 227, 240]. NAMPT is ubiquitously expressed and considered essential in most

tissues for NAD^+ regeneration [153, 158]. The data in this chapter shows that NMRK2, however, is highly muscle specific and is the most predominantly expressed NAD^+ biosynthesis enzyme in skeletal muscle with expression favoured in fast-twitch TA muscle. This conserved expression of NMRK2 in muscle across species suggests an important role that has yet to be established.

Moreover, the fast twitch fibre-type specificity of NMRK2 raises more questions about its importance in muscle metabolism. A higher expression in glycolytic muscles, like the TA, may be an important cellular redundancy mechanism to meet extreme changes to energy demand during high intensity exercise to allow muscles to maintain energy homeostasis and effectively induce metabolic adaptation. Soleus derived myotubes did appear to rely more on oxidative metabolism compared to typically glycolytic TA myotubes, yet interestingly NAD^+ levels in soleus and TA myotubes were similar. As soleus muscle fibres are predominantly considered oxidative the soleus derived myotubes may have been expected to have a higher NAD^+ content. The soleus myotubes did however have higher NADH levels and thus the TA and soleus myotubes had different NAD/NADH ratios. The importance of NAD^+ content versus the NAD/NADH ratio has been debated for many years with no conclusive answer [241], so although NAD^+ levels appear consistent the shift in the NAD/NADH ratio may be an important characteristic of their different metabolic activity. Notably, soleus tissue NAD^+ levels were significantly higher than in TA tissue. The differences between tissue and primary myotubes NAD^+ content highlights that although *in vitro* models are extremely useful for investigating and manipulating specific cellular systems there are still limitations. Therefore, it is necessary to accept the metabolic status

of a closed cellular system will not directly reflect a snapshot of *in vivo* metabolism, which is heavily dependent on multi-organ interplay [26].

Further investigation of NMRK2 in skeletal muscle showed that supplementation with its primary substrate, the vitamin B3 precursor NR, could indeed enhance NAD^+ content in C2C12 and primary myotubes. Although supplementation with NR did not appear to alter downstream metabolic signalling in the myotubes, this data shows the ability of muscle cells to respond to changes in substrate availability and adapt cellular NAD^+ levels, which may prove a vital process in muscle to react to metabolic stress and maintain energy homeostasis. In addition, the ability of NR to boost muscle cell NAD^+ content provides great therapeutic promise as an alternative vitamin B3 supplement to nicotinic acid (NA) which, firstly, is not likely to play an important role in muscle NAD^+ biosynthesis and secondly, patient compliance is poor due to adverse flushing effects [195]. Extensive studies looking at NA (or NA derivatives) supplementation in humans has demonstrated numerous health benefits including lowering of total cholesterol and triglycerides [193, 194].This further cements a novel niche for NR, which does not activate the GPR109A receptor and induce flushing, in promoting metabolic health [199].

It is not necessarily surprising that in the C2C12 and primary cell models the significant increase in NAD^+ does not induce metabolic adaptation as these cells are not under metabolic stress and normal 'healthy' cells can already adequately modulate NAD^+ metabolism and signalling. Most studies to date that have demonstrated the beneficial effects of boosting NAD^+ have been in models of metabolic stress or pathophysiology where NAD^+ homeostasis is perturbed [178,

179, 199, 206, 207, 229, 242]. Previously, a study using a muscle specific NAMPT overexpressing mouse model showed that a 50% increase in NAD^+ could not stimulate mitochondrial biogenesis or enhance mitochondrial metabolism in skeletal muscle of young mice, with metabolic differences only apparent upon ageing [76, 240]. Our results show that when NAD^+ is enhanced through NR supplementation NAM and ADPr levels are unchanged, whereas following NAD^+ depletion there is a decrease (table 3.1). As NAM and ADPr are metabolites of NAD^+ signalling (both produced from SIRT-based NAD^+ consumption) [119] this indicates that, although a reduction to NAD^+ can limit NAD^+ signalling and ultimately hinder mitochondrial metabolism, basal NAD^+ content alone is not limiting to NAD^+ signalling.

Interestingly, in the TA and soleus derived primary myotubes there was an induction of mitochondrial respiration following NR treatment unlike in C2C12 myotubes. These differences may be attributed to the fact that the metabolic capacity of an immortalised cell line like C2C12 is very likely to be different to that of primary myotubes with C2C12 cells potentially relying on more glycolytic metabolism particularly in high glucose conditions [243]. In addition, figure 3.7 highlights that NR supplementation boosts NAD^+ by a smaller degree in C2C12 myotubes compared to primary myotubes; this further demonstrates basal metabolic differences between the two cellular models and it may be that this smaller NAD^+ increase in C2C12 cells is not sufficient to drive mitochondrial respiration.

The findings here confirm previous studies that identified intracellular recycling of NAM by NAMPT as a critical process for basal NAD^+ turnover in skeletal muscle

[76, 227, 244]. Inhibiting NAMPT activity significantly depleted NAD^+, mitochondrial respiration and induced apoptosis. Together these data indicate that basally NMRK2 is unable to act as a redundancy pathway to maintain adequate NAD^+ in response to NAMPT inhibition. As exogenous NR delivery can significantly enhance NAD^+ levels even whilst NAMPT activity is blocked, as well as recover all the associated effects of NAD^+ depletion, this suggests that basal NAD^+ salvage via NMRK2 is limited by NR availability rather than enzyme activity. This idea is further supported by LC-MS analysis of primary myotubes that showed relatively low NR levels in control cells and a significant rise 24 hours following NR supplementation with a concomitant increase in NAD^+.

The idea that NMRK2 activity is restricted by NR availability may make NMRK2 even more valuable as a therapeutic target for boosting NAD^+ metabolism particularly in comparison to NAMPT. For example, blocking the NAMPT salvage pathway has profound consequences on the metabolic health of the cell yet NAM supplementation is unable to replicate the NAD^+ booting effects of NR. This may be attributed to a low maximal rate limit for NAMPT, instability of NAM, insufficient cellular uptake or feedback inhibition of NAMPT. The latter of these has been postulated from evidence of post translational regulation of NAMPT activity in response to NAD^+ availability suggesting NAMPT activity is regulated by its ultimate product in order to tightly maintain NAD^+ levels [135, 244]. Studies have also shown that high levels of NAM are inhibitory to SIRT activity, again providing another mechanism for controlling NAD^+ consumption via the NAMPT salvage pathway [152]. So, despite the NAMPT pathway being crucial for maintaining NAD^+ turnover in healthy muscle it may be a poor target for enhancing NAD^+ in metabolically perturbed muscle.

It is essential to note that NAD^+ turnover and metabolic flux is continuously regulated and highly adaptive to countless stimuli including, physical activity, energy source and availability, circadian clock and pathophysiology [32, 89, 169, 200, 245]. Thus, although snapshots of NAD^+ metabolites and signalling in tissues and cells is extremely informative, it is still very difficult to gain conclusive insight into NAD^+ metabolism.

Chapter 4 Investigating the relative importance of NAD^+ biosynthesis genes in skeletal muscle NAD^+ metabolism, *in vitro*.

(NMRK1KO and DKO mice were provided by Dr Carles Canto at the Nestlé Institute of Health Sciences and experiments involving these mice were performed during a one month lab placement)

4.1 Introduction

NAD^+ consumption is prominent in contracting muscle, due to enhanced SIRT activity to meet cellular energy demands [227], thus replenishment of NAD^+ through biosynthesis and salvage pathways is a vital process. Previously, Nampt and Nmrk2 were identified as the key NAD^+ biosynthesis genes in muscle suggesting that muscle relies on NAM and NR salvage to maintain NAD^+ pools. Further research into the relative contribution of these pathways to re-synthesise NAD^+ in resting skeletal muscle, and in response to metabolic stresses such as exercise, is required.

4.1.1 Rationale for boosting cellular NAD^+

Pharmacological inhibition of poly(ADP-Ribose polymerases (PARPs), alternative NAD^+ consumers, in skeletal muscle can boost NAD^+ levels and enhance mitochondrial function and oxidative metabolism [246] through increased SIRT1 activity. Furthermore, increasing NAD^+ through microRNA-149 (miR149) inhibition of PARP-2 specifically in skeletal muscle can enhance mitochondrial biogenesis though activation of PGC-1α by increased SIRT1 expression and activity [127].

In addition, research by Kim et al. showed that NAMPT can regulate mitochondrial biogenesis through NAD^+ following exercise simulation by electrical stimulation (ES) of primary skeletal muscle fibres. They demonstrate that the increase in NAD^+, SIRT signalling and markers of mitochondrial biogenesis induced by ES was inhibited following pharmacological inhibition of NAMPT with FK866 [227].

4.1.2 Precursor supplementation to drive NAD^+ metabolism

This latest research demonstrates the vast potential benefits associated with boosting NAD^+ and the necessity to establish novel methods to do so that are safe and translatable to humans.

Previously, the positive effects of boosting NAD^+ metabolism through precursor supplementation have been established. For example, NA supplementation has been previously used to treat hypercholesterolemia [247]. In humans, the NA derivative acipimox has already shown promising potential for the use of NAD^+ precursors as a new therapeutic strategy for improving the mitochondrial function of skeletal muscle. Treatment with acipimox increased mitochondrial respiration, enhanced expression of genes involved in the Krebs cycle and electron transport chain and increased ATP content [196]. Despite the clear therapeutic benefit, the use of NA and acipimox is limited by adverse flushing effects, through activation of the GPR109A receptor, leading to poor compliance [196].

The positive effects of boosting NAD^+ has created a new therapeutic niche for vitamin B3 supplementation; necessitating the need to examine the potential of supplementation with alternative NAD^+ precursors that do not cause adverse effects. NAM supplementation is limited due to its inhibitory effect on SIRT activity, but the natural availability of NR in the diet and its ability to increase NAD^+ content in cells makes it an ideal new therapeutic approach to treat metabolic related diseases [142, 152, 166, 192].

Canto et al. (2012) showed that NR fed mice had increased levels of NAD^+ and enhanced SIRT1 and SIRT3 activity. High fat diet mice treated with NR had reduced fat mass from enhanced energy expenditure, improved insulin sensitivity

and enhanced skeletal muscle oxidative performance [199]. More recently, Khan et al. showed that NR supplemented transgenic mice manifesting with mitochondrial myopathy effectively delayed progression of both early and late stage mitochondrial disease. NR treated mice showed boosted NAD^+ levels, mitochondrial biogenesis and induction of the unfolded protein response [207].

4.1.3 Manipulations of skeletal muscle NAD^+ metabolism.

Gaining a better understanding of skeletal muscle NAD^+ biosynthesis pathways can help target specific pathways with interventions, such as precursor supplementation, to boost NAD^+ pools and drive energy metabolism. This chapter will focus on the manipulation of key regulators of NAD^+ metabolism in skeletal muscle to elucidate novel targets for enhancing NAD^+ signalling and induce similar metabolic responses to those seen following exercise [32]. Pharmacological and genetic approaches will be used to inhibit and knock-out key skeletal muscle NAD^+ biosynthesis genes (figure 4.1), Nampt and Nmrk2, previously identified – in section 3.3 – and determine their relative importance for skeletal muscle NAD^+ turnover during basal metabolism. Additionally, strategies to boost skeletal muscle NAD^+ content through targeted nutrient supplementation of NAD^+ precursors will be examined.

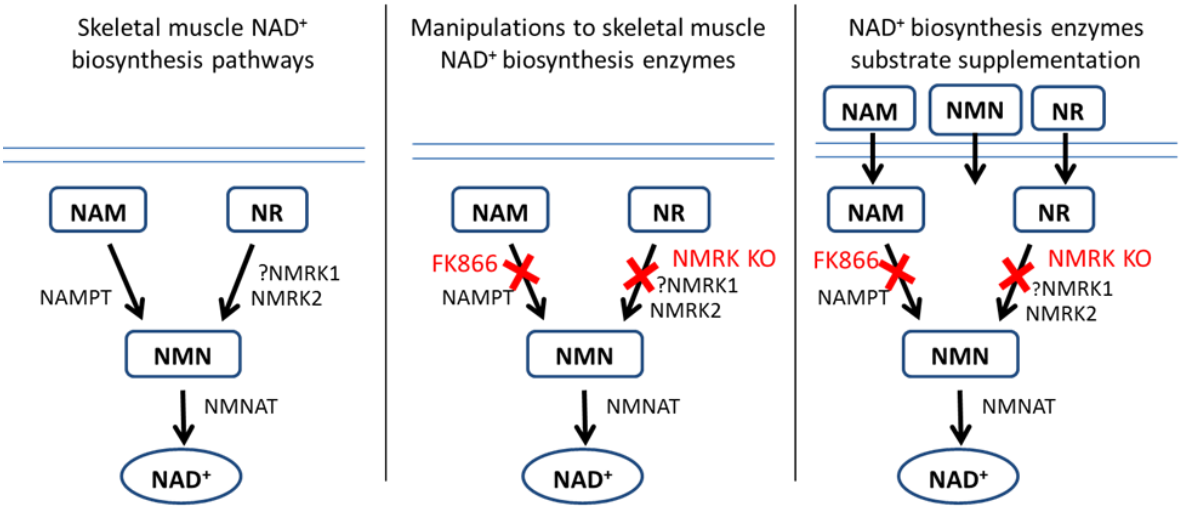

Figure 4.1 Skeletal muscle NAD$^+$ biosynthesis manipulations

An outline of the main NAD$^+$ biosynthesis pathways proposed to be important in skeletal muscle (left). Pharmacological and genetic manipulations (red) to be employed in this chapter (centre) and supplementation of substrates for the key NAD$^+$ biosynthesis enzymes (right).

4.2 Materials and Methods

4.2.1 Generation of NMRK loss of function mice

NMRK2KO mice were acquired from the Jackson Laboratory. The Nmrk2 KO mutant allele was generated through the Knockout Mouse Phenotyping Program (KOMP2) on a C57BL/6N background. A ZEN-UB1 Velocigene cassette (beta-galactosidase coding sequence from E. coli lacZ gene; polyadenylation signal; loxP site; promoter from the human ubiquitin C gene; neomycin phosphotransferase;polyadenylation signal; loxP site) was inserted through homologous recombination into the gene in place of all coding exons inhibiting transcription.

NMRK1KO mice were provided by Carles Canto and generated on a C57BL/6NTac background by Taconic Biosciences, as described by Ratajczak et al. 2016, resulting in recombination of exons 3 to 7 and complete loss of NMRK1 protein.

4.2.2 Genotyping

DNA from digested ear and tail clips was amplified using the 2x BioMix Red (Bioline, UK) and the primers listed in appendix A. Samples were placed in a PCR thermocycler - set to 5 minutes at 95 °C then 35 cycles of [30 seconds 95 °C, 30 seconds 60 °C and 30 seconds 72 °C] followed by 5 minutes at 72 °C and left indefinitely at 4 °C - and analysed by electrophoresis on 1.8% Agarose gels.

4.2.3 Primary muscle culture

Gastrocnemius tissue was excised from hind limbs of mice and digested in DMEM with 0.2% collagenase and isolated myofibres were placed in tissue culture plates

(section 2.2). Following satellite cell migration media was replaced with proliferation media (DMEM with 10% (v/v) HS, 1% (v/v) P/S and 0.5% (v/v) CEE). Upon 70-80% confluence media was replaced with Differentiation media (DMEM supplemented with 2% (v/v) HS, 0.5% (v/v) CEE and 1% (v/v) P/S) and cells were differentiated for 6 days.

4.2.4 Cell treatments

Cells were treated in serum free media with 100 nM FK866 or DMSO as a vehicle control for 24, 48 or 72 hours. Cells were supplemented with 0.5 mM NR, 0.5 or 5 mM NAM and 0.5 mM NMN for 24 hours.

4.2.5 siRNA transfections – Nmrk1 knockdown

Primary myotubes were transfected overnight in antibiotic and serum free DMEM on days 3 and 5 of differentiation. 0.5 µg/µl Nmrk1 siRNA (MSS212930, Invitrogen, UK) was transfected using OptiMem and Lipofectamine 2000 (section 2.4). Following transfections, media was replaced with normal differentiation media until cells were harvested.

4.2.6 RNA extraction

RNA was extracted from tissue and cells using TRIzol reagent (Invitrogen, UK). RNA quality was determined by visualisation on a 1.5% agarose gel and quantified using a nanodrop. Reverse transcription was conducted using 1 µg RNA (see section 2.6).

4.2.7 qPCR

qPCR was performed in a 384-well plate in single-plex format using Assay on Demand primers and probes (Applied Biosystems, UK) (section 2.6.4). The real-

time PCR reaction was performed under the following conditions: 95^{o}C for 10 minutes then 40 cycles of 95^{o}C for 15 seconds and 60^{o}C for 1 minute using an ABI7500 system. Data were collected as Ct values and used to obtain deltaCt (dCt) values.

4.2.8 Western Blotting

Protein lysates were extracted from tissues in RIPA buffer. Total protein concentration was quantified by Bio-Rad assay. Total proteins (20 µg) were resolved on 12% SDS-PAGE gels and transferred onto nitrocellulose membranes. Membranes were blocked in 5% BSA and Primary antibodies were then added and incubated overnight. Membranes were washed and secondary antibodies conjugated with HRP were added at a dilution of 1/10,000. Membranes were washed and bands visualised using ECL detection system (GE Healthcare, UK) (as described in section 2.7)

4.2.9 NAD^+ measurements

NAD^+ was extracted from primary myotubes and muscle tissue and quantified using the NAD/NADH quantification colorimetric kit (BioVision, UK) as described in section 2.8.1.

4.2.10 Targeted NAD^+ metabolomics

20 mg of pulverised tissue samples were extracted in ice cold LC-MS grade methanol. 300 µl of internal standard (diluted 1:300 in LC-MS grade water) was added and samples were sonicated for 20 seconds at -4°C. Then the samples were incubated at 85˚C for 5 minutes, shaking at 1050 rpm. Samples were returned to ice for 5 minutes and centrifuged. Supernatant was transferred to a new tube and dried using a speed vacuum. Dried extract was resuspended in 40

µl of the appropriate buffer (LC-MS grade water for acid extract and 10 mM ammonium acetate for alkaline extract). Extracts were briefly centrifuged and the supernatant was transferred to a Waters Polypropylene 0.3 ml plastic screw-top vial and analysed by LC-MS/MS using the ACQUITY UPLC H-class system (section 2.12.4).

4.2.11 Respirometry

Primary myotubes were differentiated for 6 days. Following treatment with the relevant compounds, respiratory output (by oxygen consumption rate) of myotubes in Seahorse XF-Assay media (Agilent Technologies, USA) was assessed by Seahorse extracellular flux analysis, as described in section 2.11.1, following the Seahorse user guide.

4.2.12 Statistical analysis

Unpaired Students T-test or ANOVA statistical comparisons were made using GraphPad Software Inc. Prism version 6. Data are presented as mean ±SEM with statistical significance determined as *= $P<0.05$, **=$P<0.01$, ***=$P<0.001$. Statistical analysis of real-time PCR data was determined using dCt values.

4.3 Results

In chapter 3, the NAMPT and NMRK NAD^+ biosynthesis pathways were indicated to be the main routes to NAD^+ in skeletal muscle. This chapter focusses on genetic and pharmacological interventions to examine the relative importance of these pathways and identify potential pathway redundancy when these pathways are compromised.

4.3.1 Validation of NMRK2KO mouse model

The importance of NAMPT in muscle NAD^+ salvage has been previously described [76, 227]. However, the role of NMRKs in skeletal muscle NAD^+ salvage and particularly the muscle specific importance of NMRK2 is yet to be defined. Thus, to further investigate the muscle specific role of NMRK2, a global loss of function mouse model was employed. Heterozygous (HET) NMRK2KO mice received from the Jackson Laboratory were genotyped by PCR to confirm heterozygosity. Primers designed for genotyping generated DNA fragments sized at approximately 197 base pairs (bp) for WT mice and 500 bp for NMRK2KO mice. Figure 4.2 shows an agarose gel of DNA extracted from ear clippings of the six original HET mice with a negative and positive WT control as an example of successful genotyping. A single lower WT band and an upper mutant band can be visualised to confirm all the mice as HETs. Following confirmation of Nmrk2 heterozygosity, a breeding program was established and all subsequent litters were genotyped immediately after weaning and retyped following tissue collection.

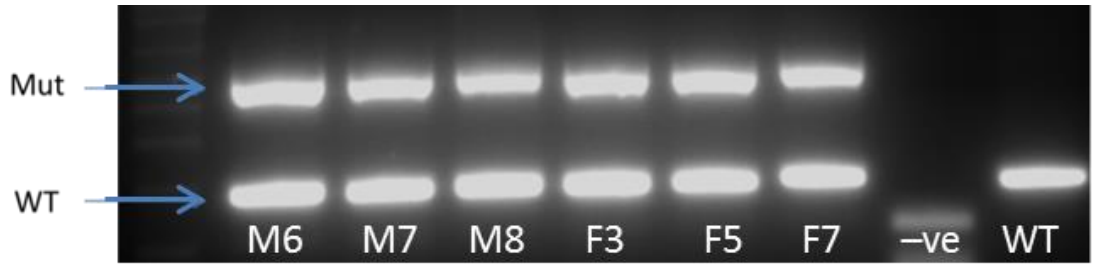

Figure 4.2 PCR analysis of NMRK2 genotype

DNA digested from heterozygous NMRK2 mice was analysed by generic PCR with a negative and WT control. WT (197 bp) and mutant (500 bp) bands were identified as expected.

To validate genotype identification of the Nmrk2 HET, KO and WT mice, harvested tissues from each mouse were examined for the presence or absence of Nmrk2 expression. qPCR analysis in figure 4.3A demonstrates the presence of Nmrk2 mRNA in WT quadriceps and cardiac tissue and the complete absence of gene expression in the respective NMRK2KO mouse tissues. Qualitative PCR analysis was also run on an agarose gel to further validate the loss of Nmrk2 in KO tissues. Figure 4.3B demonstrates Nmrk2 expression in quadriceps tissue from WT, HET and KO mice, with bands clearly detected in WT and HET tissue and no bands in KO muscle - the gene G6pt was detected in all tissues and used as a PCR reaction and loading control. Finally, protein expression was assessed to confirm loss of NMRK2 protein expression in KO mice. Immunoblot analysis of NMRK2 showed loss of protein expression across a range of muscle tissues in NMRK2KO mice. Liver tissue that was previously identified to not express Nmrk2 was used as a control, unfortunately, most likely due to non-specific protein expression bands were seen in a similar region to NMRK2 in KO liver tissue but Nmrk2 mRNA was completely undetectable in both WT and KO tissue (figure 4.3C).

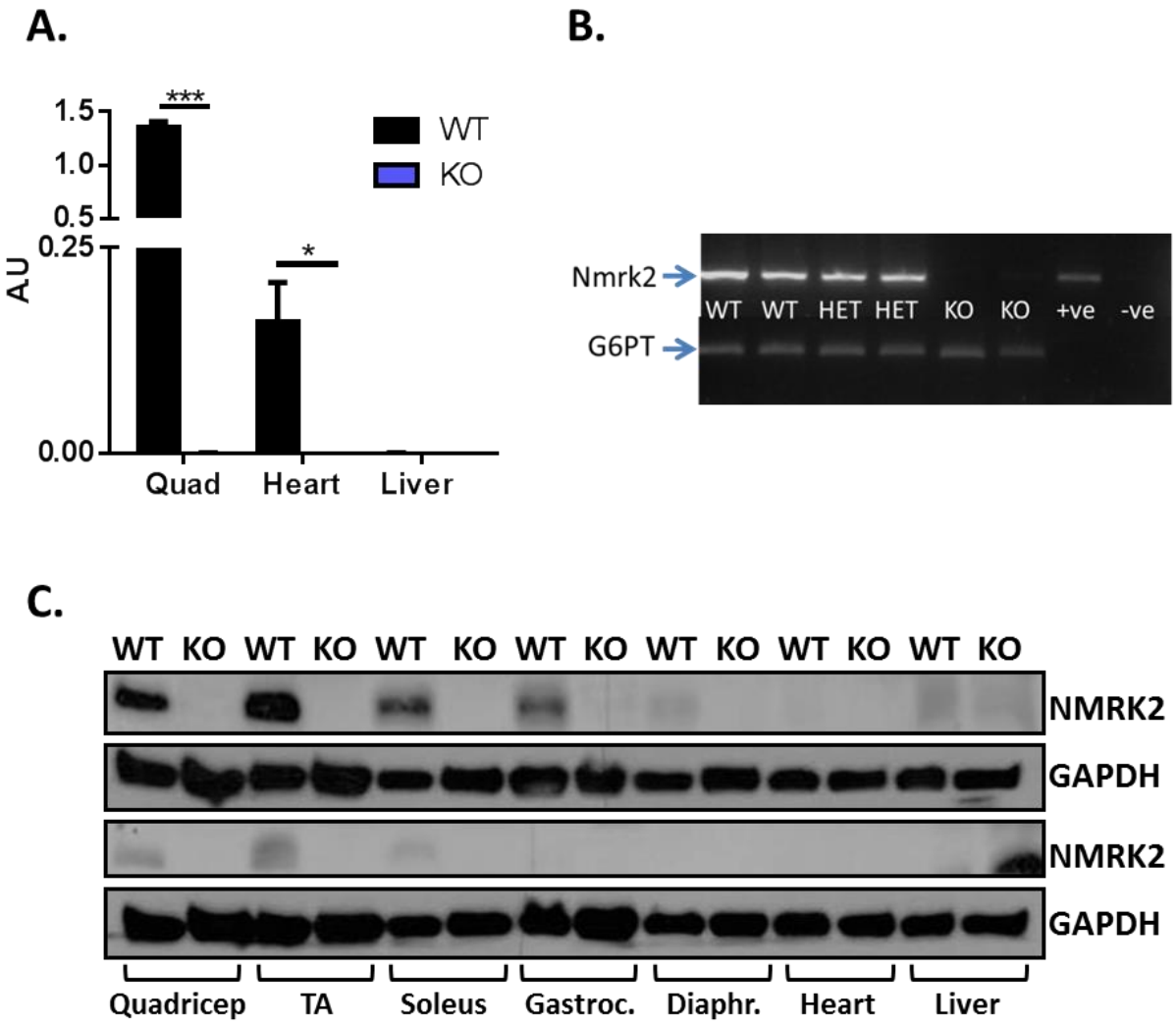

Figure 4.3 Validation of NMRK2KO mouse model

(A) Quantitative real-time PCR analysis of Nmrk2 mRNA expression in quadriceps (quad), heart and liver tissue from WT and NMRK2KO mice (n=3). (B) Qualitative PCR analysis of Nmrk2 mRNA (with G6PT as a loading control) in quadriceps muscle from WT, heterozygous (HET) and NMRK2KO mice. (C) Immunoblot analysis of NMRK2 protein expression in skeletal muscle beds (quadriceps, TA, soleus, gastrocnemius (gastroc) and diaphragm (diaphr), heart and liver tissue from WT and NMRK2KO mice. Real-time PCR A.U values presented as mean ± SEM and significance determined by unpaired t-test.(* $p<0.05$, ***$p<0.001$).

4.3.2 NMRK2KO mouse characterisation

Following initial confirmation of Nmrk2 loss of function basic characterisation was conducted as there is currently no published data available on mammalian Nmrk2 KO models. NMRK2KO mice were fully viable and offspring genotype ratios closely followed Mendelian genetics. The mice appeared healthy and behaved 'normally' with no obvious physical differences *in vivo* between WT and KO mice. There was no difference between the average body weight of WT and KO mice and further examination of different muscle beds (quadriceps, TA, soleus and heart) showed that muscle weight in KO mice was similar to WT (figure 4.4A and B respectively). This initial macroscopic phenotyping of NMRK2KO mice highlights that the loss of NMRK2 function does not severely impair muscle development or systemic metabolism in young mice.

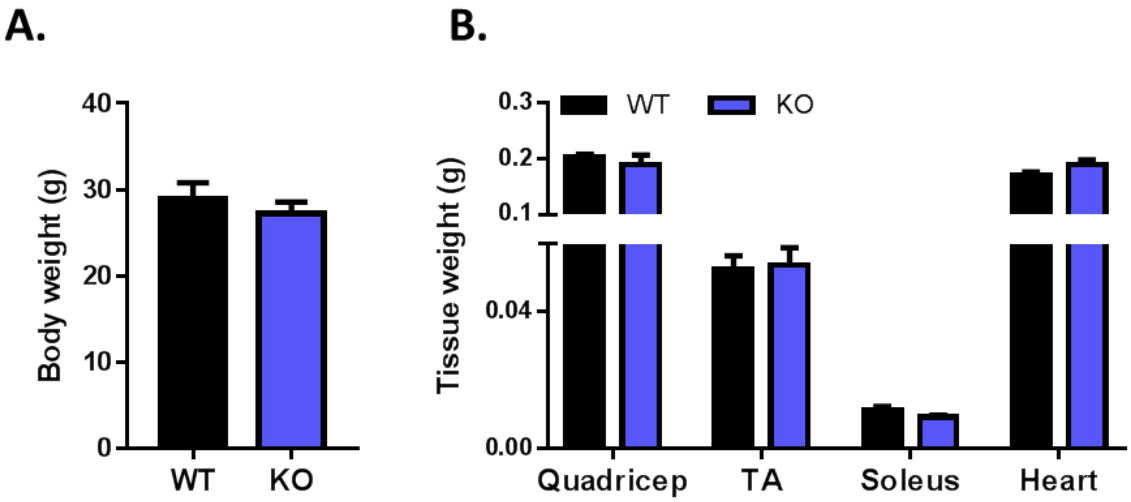

Figure 4.4 Body weight and muscle bed weights of WT and NMRK2KO mice

(A) Whole body weight and (B) skeletal (quadriceps, TA and soleus) and cardiac (heart) muscle weight from 12 week old WT and NMRK2KO males. All data presented as mean ± SEM (n=4).

4.3.3 NAD^+ signalling mechanisms in WT and NMRK2KO muscle

To further understand the role of NMRK2 in skeletal muscle NAD^+ salvage, the effect of Nmrk2 gene deletion on NAD^+ metabolism was investigated. Firstly, tissue harvested from 10 week old WT and KO mice was examined for changes to NAD^+ salvage and signalling pathways. The data confirmed the loss of Nmrk2 mRNA expression in TA and soleus tissue. mRNA expression of NAD^+ salvage genes in tibialis anterior (TA) and soleus tissue (figure 4.5 A and B, respectively) showed mostly unperturbed expression with exception to a slight, yet significant, upregulation of Nmrk1 in the TA. With Nmrk2 expression predominant in TA tissue compared to soleus, this upregulation may be a result of redundancy signalling.

Moreover, additional genes involved in NAD^+ signalling pathways were also examined. These genes included purine nucleoside phosphorylase (Pnp) that can metabolise NR to NAM [248], nicotinamide N-methyltransferase (Nnmt1), which can add a methyl group to NAM [249] and prevent NAM salvage and equilibrative nucleoside transporters (ENT, NT5E) are believed to shuttle NR into the cell [136, 166], as well as NAD^+ consumers CD157 – an ADP-Ribosyl cyclase – and Parp1 [98, 126, 250]. Again, NMRK2KO TA muscle exhibited more profound changes to expression compared to soleus tissue, with significant increases in expression of the genes PNP and CD157. In soleus tissue CD157 was significantly upregulated (~1.5 fold) but to a lesser extent than in TA (~4 fold) (figure 4.5C and D).

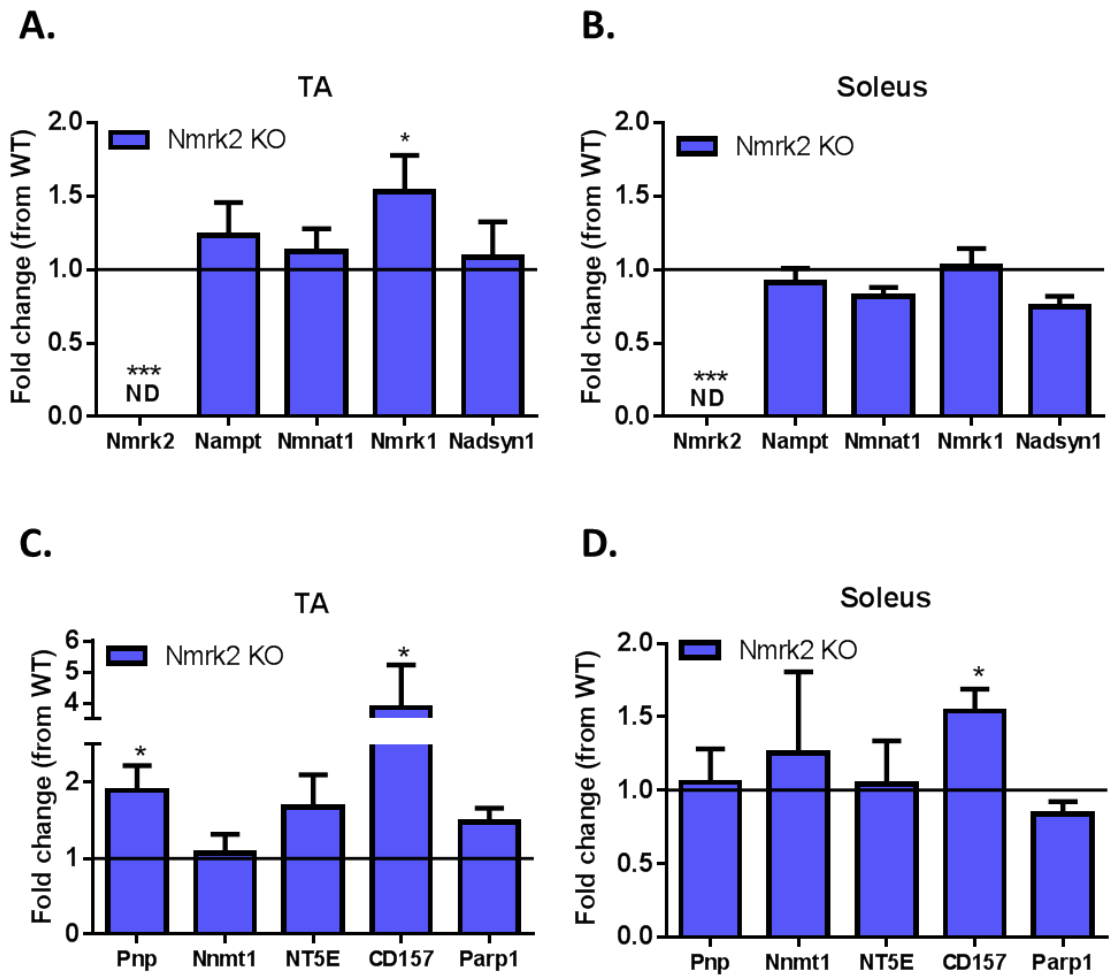

Figure 4.5 NAD$^+$ gene expression profiling in NMRK2KO skeletal muscle

Real-time PCR analysis of NAD$^+$ biosynthesis genes in NMRK2KO (A) TA and (B) soleus skeletal muscle compared to WT. Real-time PCR analysis of key NAD$^+$ signalling genes in NMRK2KO (C) TA and (D) soleus skeletal muscle compared to WT. All tissues were from age-matched NMRK2KO males and analysis fold change of ΔCT compared to WT controls (presented as solid line at y=1), n=4. Statistical significance was determined by unpaired t-test (*p<0.05, **p<0.01, ***p<0.001).

The direct effect of loss of NMRK2 function on basal NAD$^+$ levels was also determined in muscle tissue using a number of different methods. Firstly, using the NAD$^+$ colorimetric assay cellular NAD$^+$, NADH and the NAD/NADH ratio was quantified in TA muscle tissue. There was no difference in NAD$^+$ content detected in NMRK2KO tissue compared to WT (figure 4.6A). Due to the high turnover and quick degradation of NAD$^+$ there can be difficulties in quenching metabolites and

accurately measuring NAD^+, particularly in tissues. Thus, to confirm these findings alternative methods to measure NAD^+ in tissue were employed. HPLC analysis of NAD^+ content in TA muscle showed there was no significant difference in NAD^+ levels; however, there was a potential downward trend in NMRK2KO TA muscle compared to WT (figure 4.6B).

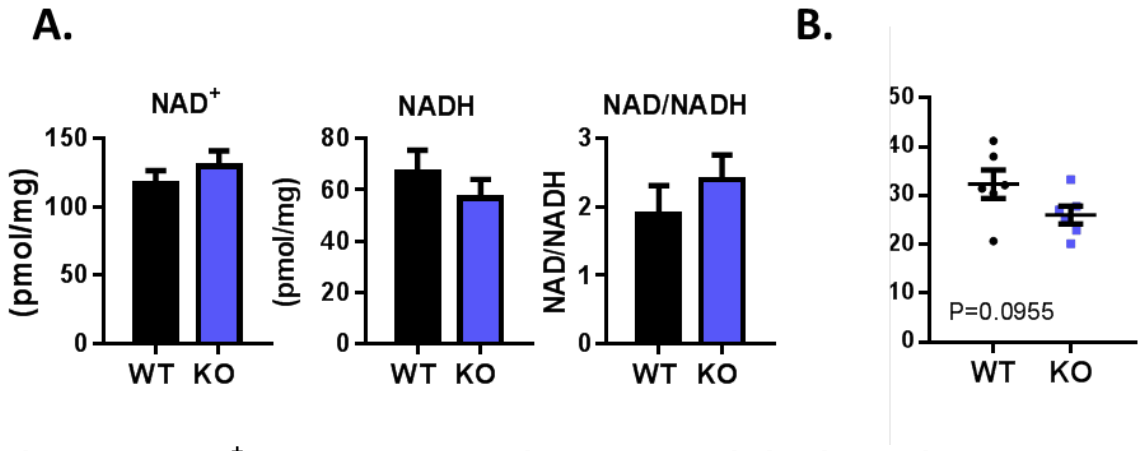

Figure 4.6 NAD^+ content of WT and NMRK2KO skeletal muscle

(A) Colorimetric analysis of NAD^+, NADH and NAD/NADH in TA skeletal muscle from WT and NMRK2KO mice (n=4). (B) HPLC analysis of NAD^+ in WT and NMRK2KO TA skeletal muscle (n=6). All tissues were from age-matched male mice and data presented as mean ± SEM.

Although NAD^+ levels in NMRK2KO muscle tissue were not found to be significantly changed from WT, the complexity of NAD^+ signalling and the high rate of turnover means NAD^+ levels alone do not necessarily uncover perturbations to NAD^+ signalling and metabolism. Therefore, LC-MS-based targeted NAD^+ metabolomics was employed to provide a more global quantification of NAD^+ and its related metabolites. In quadriceps tissue, there was no difference in NAD^+ content following loss of NMRK2 function. Other important NAD^+-related metabolites including NADP, NAM, NR, meNAM and ADPr were also not significantly different. Although both NA and NMN levels are low in comparison to

other metabolites, NA content was significantly reduced and NMN elevated in NMRK2KO mice (figure 4.7).

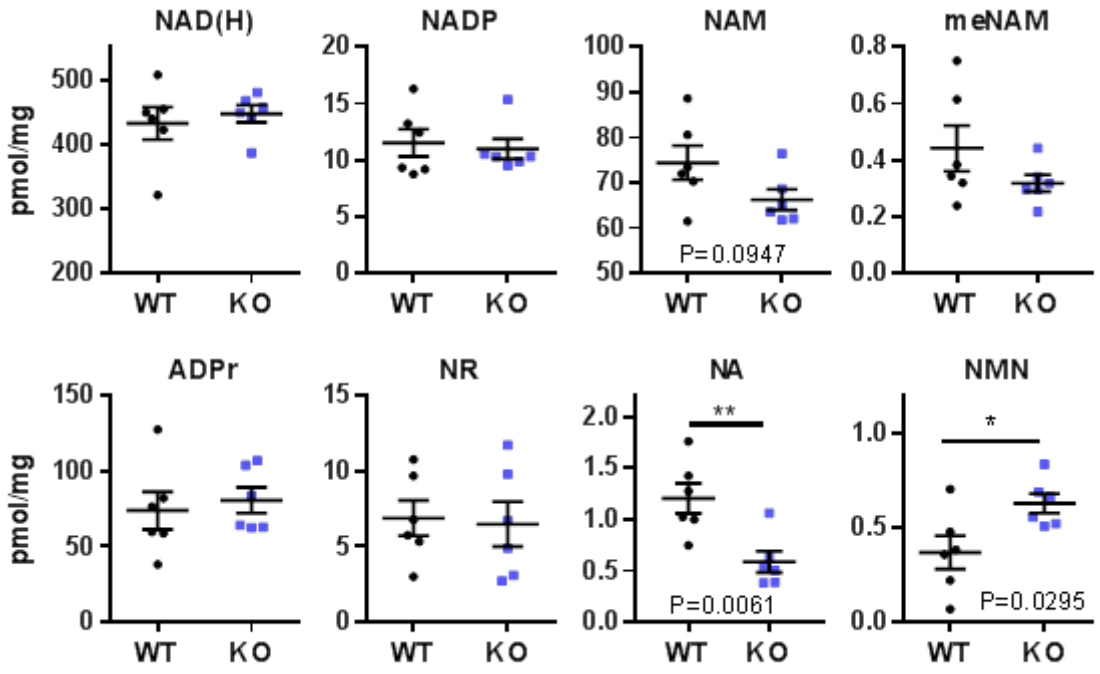

Figure 4.7 NAD$^+$ metabolome of WT and NMRK2KO skeletal muscle

Quantitative LC-MS analysis of NAD$^+$ and related metabolites from quadriceps skeletal muscle of WT and NMRK2KO mice (n=6). All tissues were collected from age matched males and all values in pmol/mg of dry pellet weight. Significance was determined by unpaired t-test (* $p<0.05$, ** $p<0.01$).

4.3.4 Skeletal muscle energy metabolism in WT and NMRK2KO mice

As NAD$^+$ is a central signalling metabolite in energy metabolism, the impact of NMRK2 loss of function on metabolic pathways was assessed [66, 145]. Firstly, expression of genes central to regulating cellular energy metabolism were examined in WT and NMRK2KO TA and soleus tissue by qPCR including; NAD-dependent Sirt1 and Sirt3, and metabolic transcription factors Pgc1α, Pparα and Pparδ [84, 119, 127]. The expression of these major regulators of energy metabolism was unperturbed in both TA and soleus NMRK2KO tissue (figure 4.8A and B). In addition, expression of mitochondrial genes were also examined.

These included mitochondrial uncoupling protein 2 (Ucp2), pyruvate dehydrogenase kinase 4 (Pdk4) and isocitrate dehydrogenase 2 (Idh2) – regulators of glucose metabolism, as well as nuclear respiratory factor 1 (Nrf1), and mitochondrial transcription factor A (Tfam) – key modulatory genes of mitochondrial biogenesis [63, 177]. Ucp2 expression in the TA was the only significantly altered mitochondrial gene examined ($\sim$2 fold increase) (figure 4.8C and D). Together this data shows that loss of NMRK2 function does not lead to vast reprogramming of the metabolic genes tested.

Induction of metabolic signalling through NAD^+ dependent SIRT activation leads to mitochondrial biogenesis [90, 227, 251]. Gene expression is not necessarily reflective of enzyme activity therefore, using a mitochondrial profiling antibody, we examined protein expression of key components in each of the mitochondrial ETC complexes (complex I, II, III, IV and V (or ATP synthase)) as an indicator of changes to mitochondrial biogenesis. Figure 4.8E shows that, of the mitochondrial proteins examined, there was no change to protein expression detected in NMRK2KO mouse quadriceps and TA tissues compared to WT. This data together with the qPCR data indicates that deletion of Nmrk2 does not impede key mitochondrial signalling pathways under basal conditions.

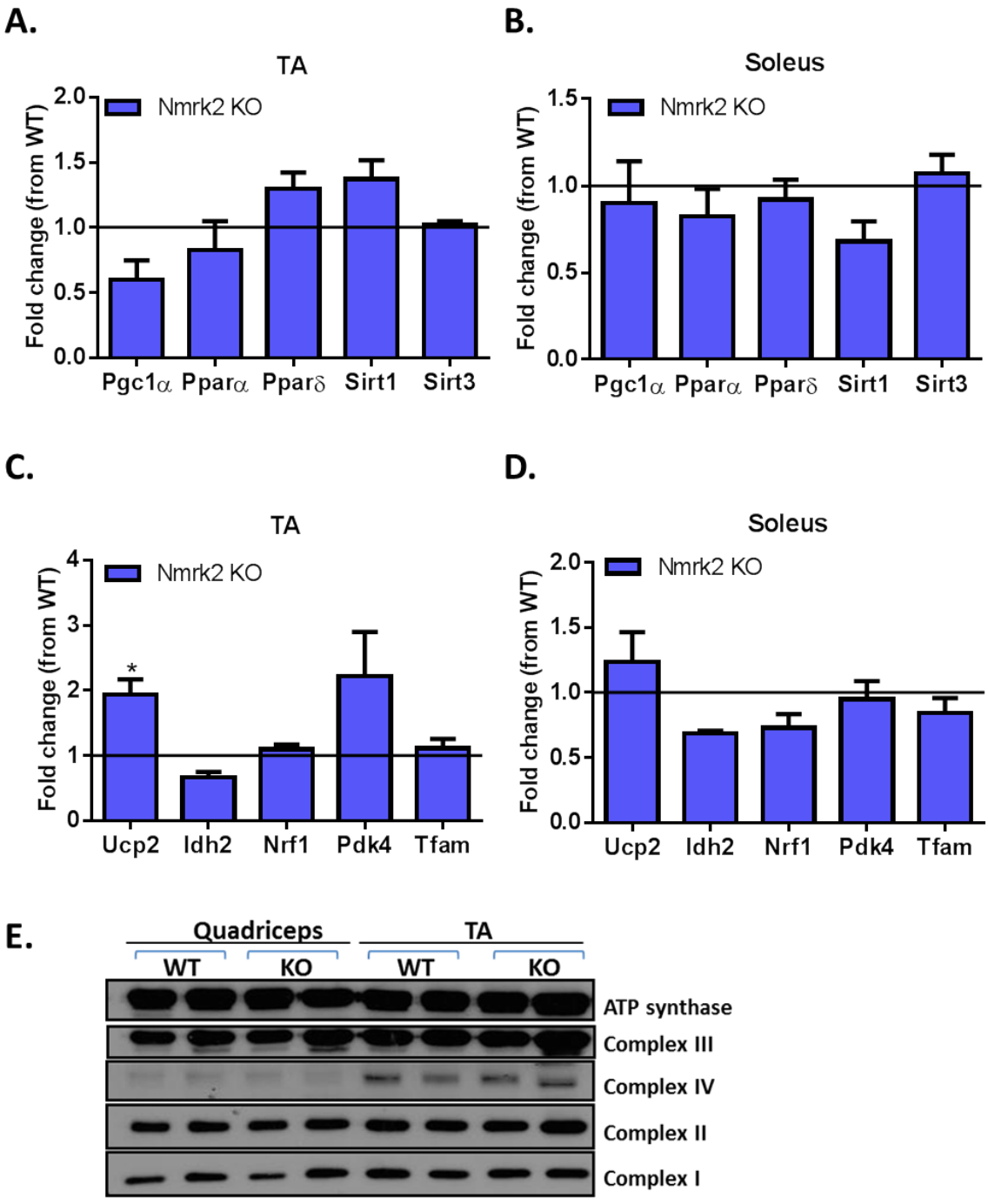

Figure 4.8 Metabolic gene expression profiling of NMRK2KO skeletal muscle

Real-time PCR analysis of key metabolic genes in NMRK2KO (A) TA and (B) soleus skeletal muscle compared to WT. Real-time PCR analysis of key mitochondrial genes in NMRK2KO (C) TA and (D) soleus skeletal muscle compared to WT. (E) Immunoblot analysis of mitochondrial complex protein expression in quadriceps and TA tissue from WT and NMRK2KO mice. All tissues were from age-matched NMRK2KO males and analysis of ΔCT fold change (mean ± SEM) compared to WT controls (presented as solid line at y=1), n=4. Statistical significance was determined by unpaired t-test (* $p<0.05$).

To more directly assess the effect of NMRK2 loss of function on energy metabolism, quantitative LC-MS analysis was used to identify potential changes to metabolite levels (ATP, ADP, inosine, cytidine, uridine, inosine monophosphate (IMP), uridine monophosphate (UMP) and cytidine monophosphate (CMP)) in muscle tissue. From the metabolites examined, figure 4.9 shows that IMP was the only metabolite found to be significantly different in WT and NMRK2KO muscle tissue.

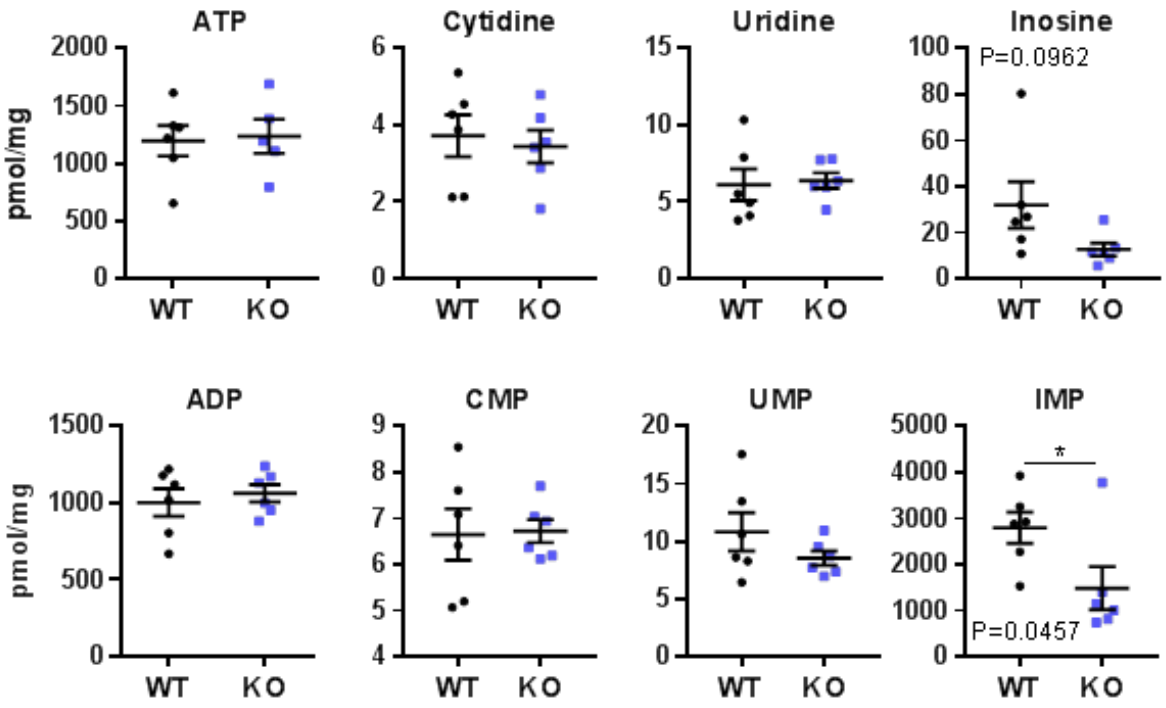

Figure 4.9 LC-MS analysis of energy metabolites in WT and NMRK2KO skeletal muscle

Quantitative LC-MS analysis of ATP, ADP and nucleotide metabolites from quadriceps skeletal muscle of WT and NMRK2KO mice (n=6). All tissues were collected from age matched males and all values in pmol/mg of dry pellet weight. Statistical significance was determined by unpaired t-test (* $p<0.05$).

4.3.5 Functional analysis of NMRK2KO myotubes *in vitro*

Primary myotubes from WT and KO mice were used as *in vitro* models of skeletal muscle. These allowed for higher throughput analysis and enabled the comparison of genetic, pharmacological and nutraceutical interventions in both isolation and combination.

Using the NAD^+ colorimetric assay, previously optimised in C2C12 myotubes, cellular NAD^+, NADH and the NAD/NADH ratio were quantified in primary WT and NMRK2KO myotubes. Interestingly, NAD^+ levels were significantly lower (35.4% ± 8.8) in the NMRK2KO myotubes compared to WT. NADH levels were also reduced in the NMRK2KO myotubes; thereby resulting in an unchanged NAD/NADH ratio (figure 4.10 A).

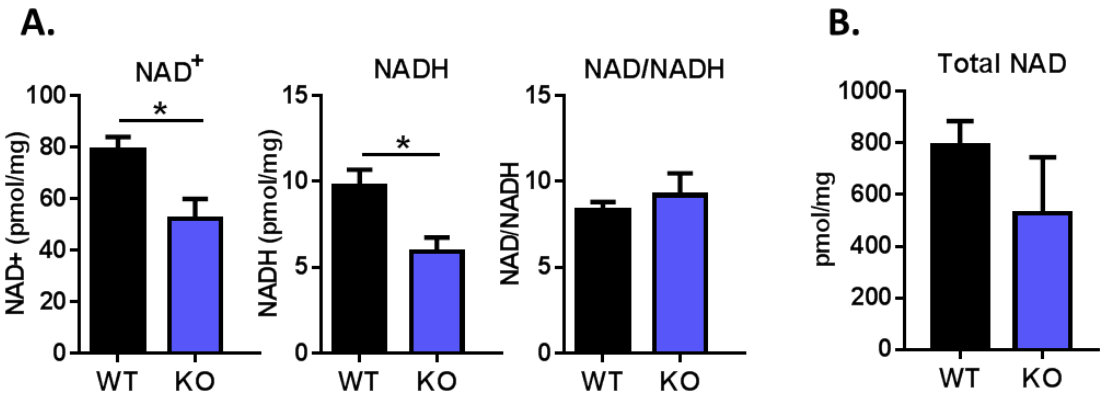

Figure 4.10 NAD^+ content of primary myotubes isolated from WT and NMRK2KO mice

(A) Colorimetric assay analysis of NAD^+, NADH and NAD/NADH in primary myotubes isolated from gastrocnemius muscle of WT and NMRK2KO mice (n=5). (B) Preliminary LC-MS analysis of total NAD(H) in primary myotubes isolated from gastrocnemius muscle of WT and NMRK2KO mice (WT n=3, KO n=2). All data presented as mean ± SEM and statistical significance was determined by unpaired t-test (* $p<0.05$).

This data opposed the unchanged levels seen in tissue and highlights the notion that there are likely to be differences between closed cellular systems and tissue which are exposed to systemic regulation, particularly when examining highly regulated signalling events. Supporting this, preliminary LC-MS analysis of NMRK2KO primary myotubes showed a downward trend, albeit non-significant, in NAD^+ content compared to WT (figure 4.10B).

To confirm NMRK2 as a novel target enzyme for boosting NAD^+ in skeletal muscle, through its ability to salvage NR, primary myotubes were supplemented with NR for 24 hours. Surprisingly, in response to 24 hour NR treatment, NAD^+ content significantly increased in both WT and NMRK2KO myotubes, although NAD^+ levels were still significantly higher in the WT myotubes the percentage of increase from their respective untreated myotubes was similar (~55 %) (figure 4.11A). NAM supplementation (0.5 mM for 24 hours) did not significantly change NAD^+ levels from the untreated control myotubes however there appears to be an upward trend in NAD^+ in the NMRK2KO myotubes (figure 4.11A). Figure 4.11B demonstrates that the corresponding NADH levels show a similar trend to NAD^+ with a significant increase in NADH following NR supplementation in the WT myotubes only. The NAD/NADH ratio was more variable and did not significantly change between genotypes with or without precursor treatment (figure 4.11E).

NAD^+ and its metabolites are continuously interchanged by a range of enzymes; thus, it is possible NR is converted to NAM in NR supplemented NMRK2KO myotubes. Although exogenous NAM supplementation does not lead to enhanced NAD^+, this may be a result of poor cellular uptake, and it is therefore feasible that intracellular conversion of NR to NAM by enzymes such as PNP could still result in increased NAD^+ availability.

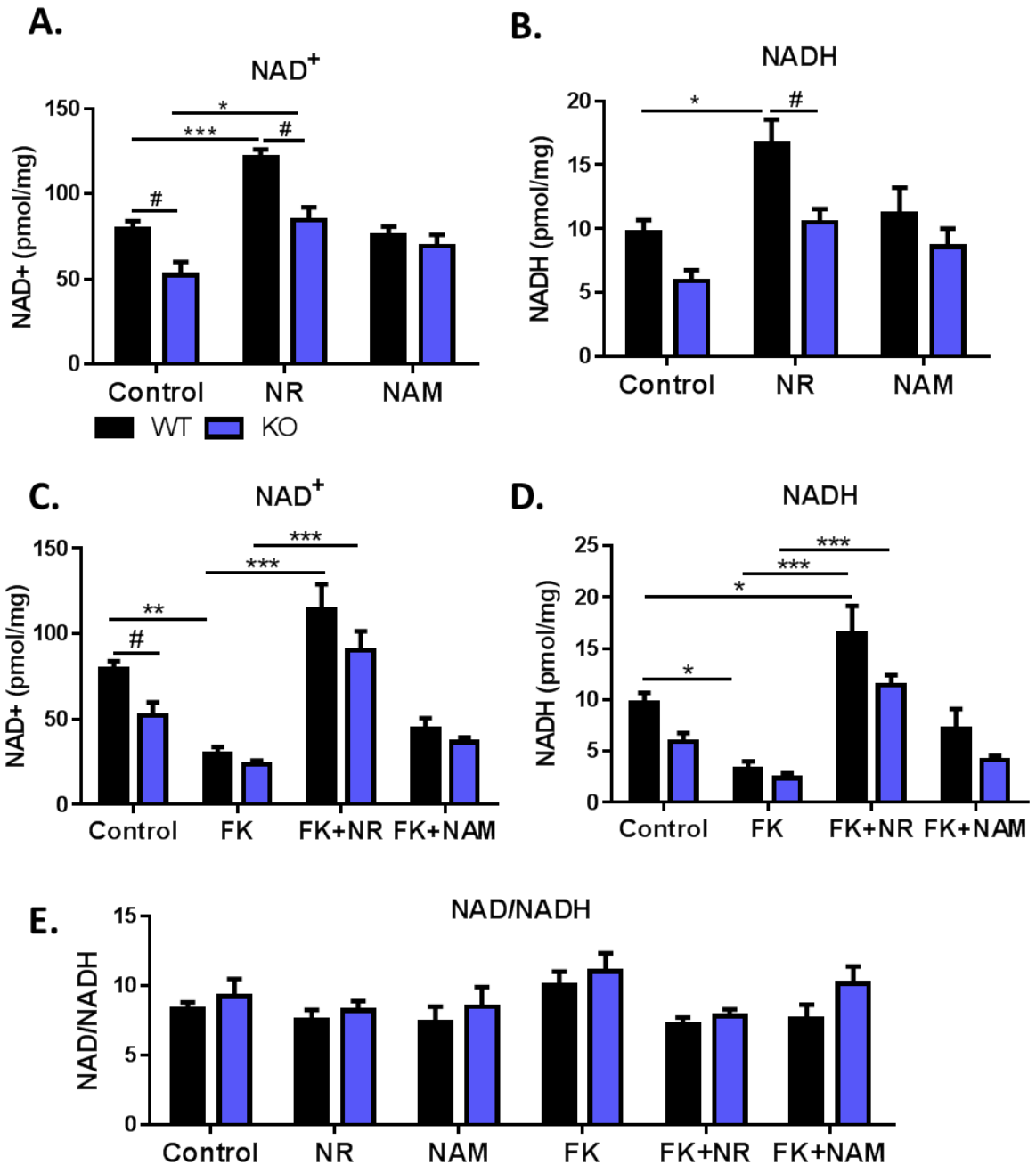

Figure 4.11 NAD^+ content of WT and NMRK2KO myotubes following NAD^+ precursor supplementation

(A) NAD^+ and (B) NADH content of WT and NMRK2KO myotubes following 24 hour treatment with 0.5 mM NR, NAM or vehicle control for 24 hours. (C) NAD^+ and (D) NADH content of WT and NMRK2KO myotubes following 24 hour treatment with NAMPT inhibitor FK866 (100 nM) and supplementation with 0.5 mM NR, NAM or vehicle control for 24 hours. (E) NAD/NADH ratio of WT and myotubes with and without 24 hour 100 nM FK866 and 0.5 mM NR or NAM treatment. All controls and cell treatments n=5 and data presented as mean ± SEM, significance was determined by two-way ANOVA with Tukey's multiple comparisons (* $p<0.05$, ** $p<0.01$, *** $p<0.001$ treatment vs vehicle and # $p<0.05$ WT vs NMRK2KO).

To test this theory and to gain further insight to the relative importance of NMRK2 and NAMPT mediated NAD^+ salvage in skeletal muscle, NAMPT was inhibited with FK866 thereby blocking salvage of NAM to NAD^+. As previously seen in WT myotubes, following 24 hour FK866 treatment NAD^+ levels were significantly depleted in both WT and NMRK2KO myotubes. However, NR supplementation was able the completely recover NAD^+ levels following FK866 treatment in both WT and KO myotubes; significantly enhancing NAD^+ to similar levels to those seen with NR treatment alone (figure 4.11C). In addition, figure 4.11C shows that NAM supplementation with FK866 was unable to rescue NAD^+ content indicating that FK866 is appropriately inhibiting NAMPT. NADH levels again show a similar trend to NAD^+ following FK866 inhibition of NAMPT (figure 4.11D).

Together this data suggests that NR can be metabolised independently of NMRK2 and NAMPT in skeletal muscle. Finally, although the NAD/NADH ratio did not significantly change following FK866 treatment it does show an upward trend in both the WT and KO myotubes which is reversed following NR supplementation (figure 4.11E); suggesting depletion in NAD^+ may lead to a surge in oxidative metabolism.

As this data indicates that NMRK2 and substrate NR can both independently regulate cellular NAD^+ levels in primary myotubes, mitochondrial function was assessed using the Seahorse XF analyser to see whether NMRK2 or NR can regulate mitochondrial oxidative output. Cellular oxygen consumption rate (OCR) provides an indication of oxidative metabolism, and preliminary data in figure 4.12A demonstrates that the maximal mitochondrial respiration of NMRK2KO myotubes may be slightly impaired compared to WT. Moreover, 24 hour NR

treatment appears to enhance both NMRK2KO and WT (to a larger degree) maximal mitochondrial respiration. The corresponding extracellular acidification rate (ECAR), an indicator of glycolysis, shows a downward trend in ECAR in NMRK2KO myotubes compared to WT (figure 4.12A - right). The figure is representative of n=2 and therefore this experiment will require repeating to draw more definitive conclusions.

To investigate whether the potential changes in mitochondrial function in WT and NMRK2KO myotubes following NR treatment is a result of enhanced mitochondrial biogenesis, expression of key proteins from each mitochondrial complex were examined by immunoblot analysis using a mitochondrial profiling antibody. Protein expression in WT and NMRK2KO myotubes was assessed with and without 0.5 mM NR supplementation and in either normal growth DMEM with glucose at 25 mM or in low 6 mM glucose DMEM. This lower glucose concentration acts to deprive cells of glucose and inflict metabolic stress, similar to calorie restriction, and stimulate metabolic adaptation [84, 102]. The immunoblot data in figure 4.12B illustrates that protein expression of all the detected mitochondrial complex proteins in WT and NMRK2KO myotubes was unchanged - with or without NR in both high and low glucose conditions suggesting mitochondrial biogenesis was not induced.

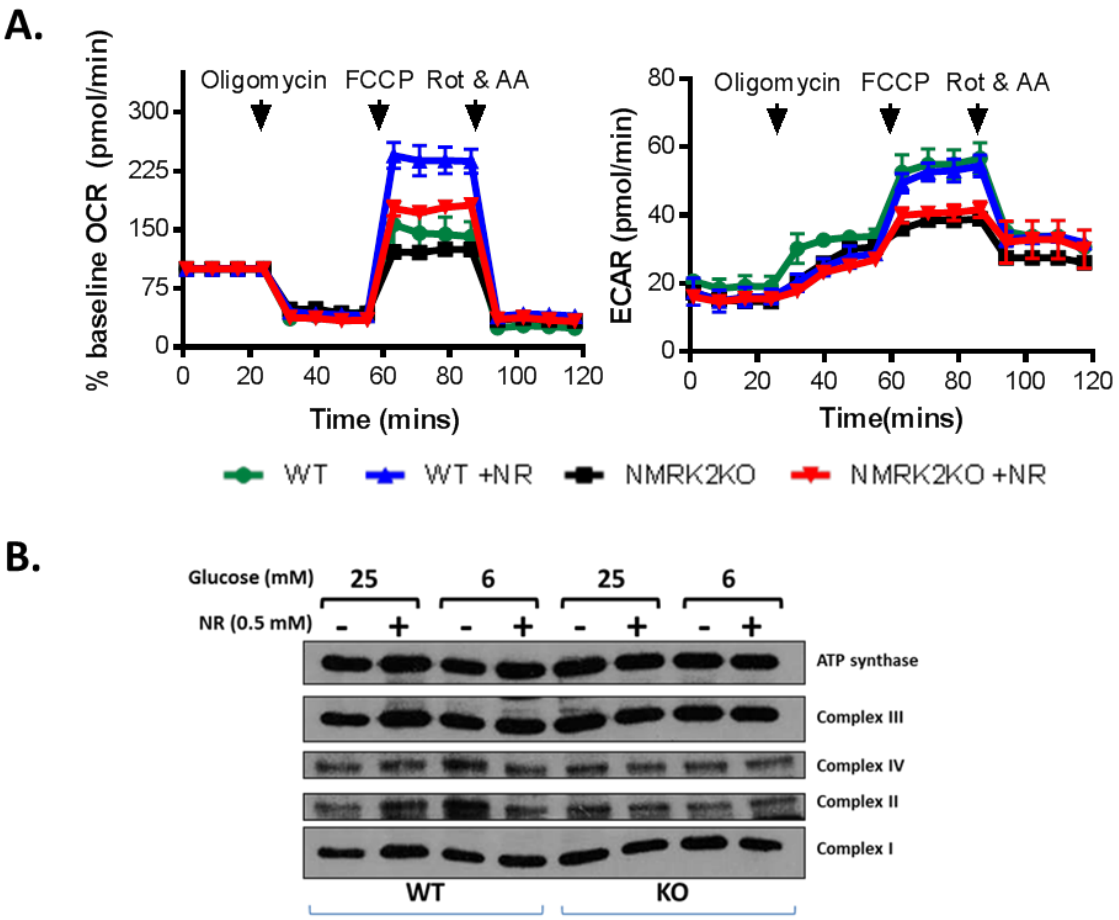

Figure 4.12 Mitochondrial function of WT and NMRK2KO myotubes following NR supplementation

(A) Mitochondrial oxygen consumption rate and extracellular acidification rate as a % of basal levels with in WT and NMRK2KO myotubes following 0.5 mM NR supplementation. (B) Immunoblot analysis of key mitochondrial electron transport chain subunits in WT and NMRK2KO myotubes with and without 24 hour NR treatment and in high and low glucose cell media.

4.3.6 NMRK1 as a mediator of skeletal muscle NAD^+ biosynthesis

The data in this chapter shows that exogenous NR can be metabolised to NAD^+ independently of both NMRK2 and NAMPT. Despite relatively low expression of NMRK1 in skeletal muscle, its salvage of NR is the most likely alternative route to NAD^+. Thus, to investigate a potential role for NMRK1 in NAD^+ salvage, siRNA based gene knockdown (KD) was employed in primary cultures. Nmrk1 KD was investigated in WT and NMRK2KO myotubes to determine the role of NMRK1 and

assess potential redundancy effects in NMRK2KO myotubes. Around 50% KD of Nmrk1 mRNA was achieved (figure 4.13A). NMRK1 Protein KD was not confirmed due to difficulties detecting NMRK1 which is expressed at low levels in myotubes. Nmrk1 KD in WT and NMRK2KO myotubes did not appear to significantly alter the gene expression profiles of NAD^+ salvage genes or other genes involved in mitochondrial and energy metabolism (figure 4.13A and B).

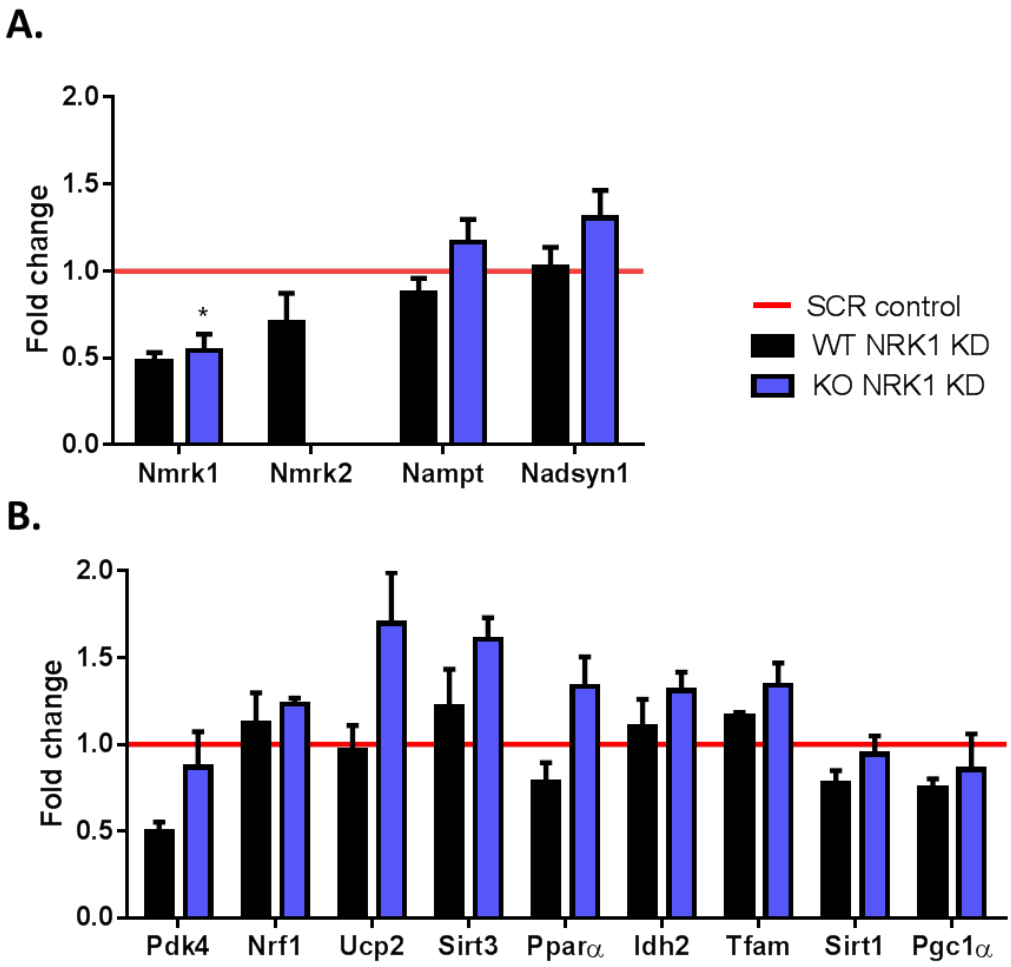

Figure 4.13 Metabolic gene profiles of WT and NMRK2KO myotubes following Nmrk1 knockdown

Real-time PCR analysis of (A) NAD^+ biosynthesis and (B) mitochondrial and energy metabolism genes in WT and NMRK2KO myotubes following transient Nmrk1 knockdown (KD). Data given as fold change of Nmrk1 KD WT myotubes compared to scrambled control treated WT myotubes or Nmrk1 KD of NMRK2KO myotubes compared to scrambled control treated NMRK2KO myotubes. All data presented as mean ± SEM. Nmrk1 KD WT, scrambled NMRK2KO and Nmrk1 KD NMRK2KO myotubes n= 3 and scrambled WT myotubes n=2 thus unpaired t-test statistical analysis on ΔCt values of NMRK2KO myotubes only (* $p<0.05$).

Due to problems with myotube isolation, WT scrambled myotubes were only n=2 and therefore statistical analysis was only determined on ΔCT values from scrambled versus Nmrk1 siRNA transfected NMRK2KO myotubes. It is notable that, although significance could not be established, there may be some downregulation to Nmrk2 expression in WT Nmrk1 KD myotubes (figure 4.13A); potentially a result of off target knockdown.

NAD^+ was measured in primary myotubes following siRNA Nmrk1 KD. Basal levels of NAD^+ were unchanged in Nmrk1 KD myotubes compared to those treated with a scrambled siRNA control (figure 4.14A). Primary myotube cultures were also used to investigate whether NMRK1 can use exogenous NR to boost NAD^+ in skeletal muscle. NAMPT inhibitor FK866 was used to block NAMPT salvage and maximise the NAD^+ boosting effect of NR. NMRK1 precursor salvage was assessed both alone in WT and in combination in NMRK2KO myotubes. Following 24 hour NR treatment, a downward trend was seen in NAD^+ in WT Nmrk1 KD myotubes compared to scrambled treated WT myotubes (figure 4.14B). However, no difference was identified in NMRK2KO myotubes following Nmrk1 KD compared to scrambled treated cells; this may be attributed to the slight upregulation of Nmrk1 seen in NMRK2KO tissue (figure 4.5) and thereby 50% KD leading to potentially WT levels of Nmrk1.

As a downstream vitamin B3 NAD^+ precursor to NAMPT and the NMRK enzymes, NMN was also supplemented into this model as a control to overcome all the pathway blocks and boost NAD^+. Interestingly, despite acting downstream, NMN could not boost NAD^+ to the same extent following Nmrk1 KD in both WT and NMRK2KO myotubes; indicating a possible alternative role for NMRK1 (figure

4.14B). Unfortunately, difficulties replicating the KD data beyond n=3 – either due to issues with siRNA transfection efficiency, particularly in differentiated myotubes, and large scale growth of primary muscle to get the required cells for multi-intervention analysis – resulted in high variability. This data was therefore only used for preliminary analysis of NMRK1 in muscle with no conclusive results found.

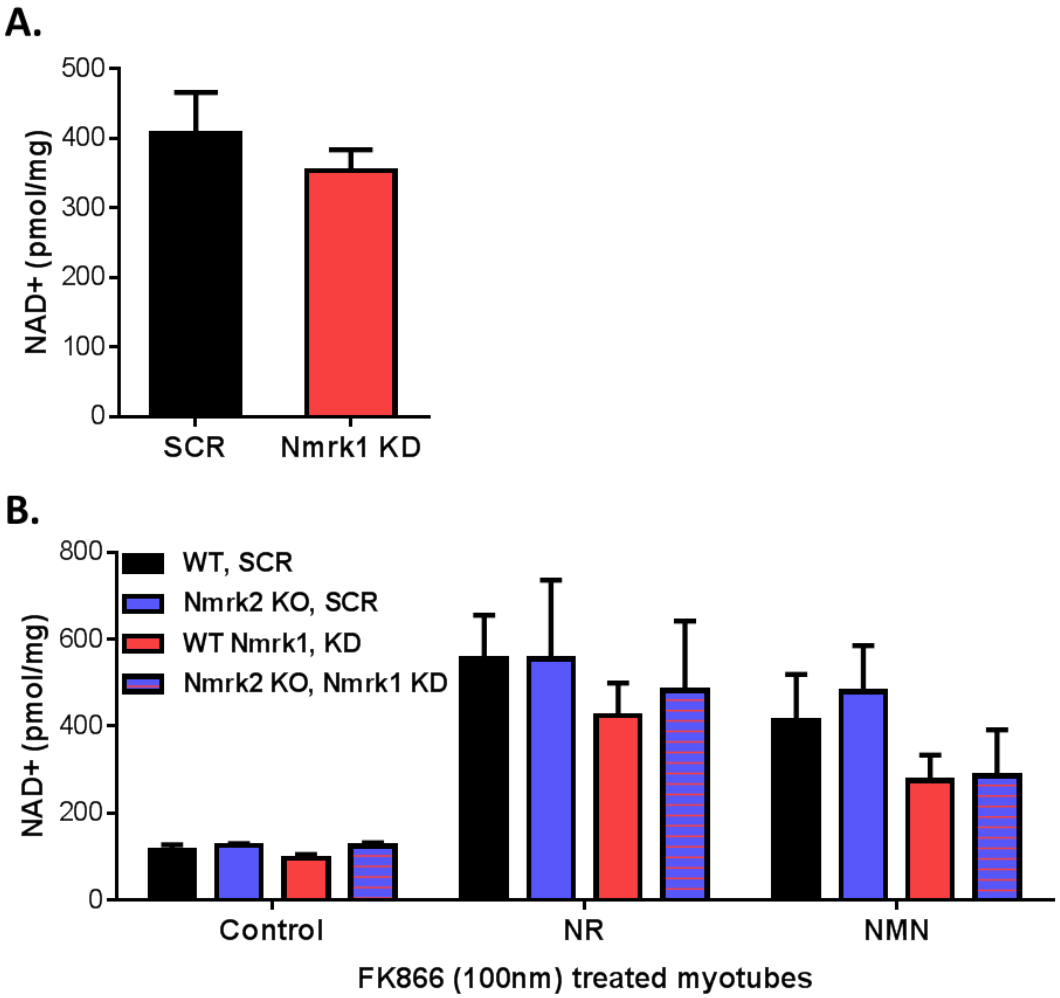

Figure 4.14 Cellular NAD^+ content following Nmrk1 Knockdown

(A) Primary myotube NAD^+ content following Nmrk1 siRNA transfection compared to scrambled (SCR) control. (B) WT and KO myotube NAD^+ content following Nmrk1 siRNA transfection compared to scrambled control. All myotubes were treated with 100 nM FK866 to inhibit NAMPT activity and supplemented with 0.5 mM NR or NMN for 24 hours. All treatment groups were n=3 and data presented as mean ± SEM.

4.3.7 The effects of loss of NMRK function on skeletal muscle cell differentiation and metabolic phenotype *in vitro*

As Nmrk1 KD studies proved limited for analysis of NMRK1 function, NMRK1KO mouse models were acquired (from the lab of Carles Canto, Nestle institute of health sciences, Lausanne). Following this, to assess NMRK enzyme redundancy, NMRK1 and 2 KO mouse breeding programs were also established to generate double NMRK KO (DKO) offspring. With NMRK enzymes highly conserved [142] and NAD^+ availability critical for energy homeostasis it was necessary to firstly identify any global effects loss of NMRK1 and 2 function may have on muscle development and metabolism. Similar to NMRK2KO mice, no gross abnormalities were identified, with mouse behaviour and physical characteristics seemingly normal.

Furthermore, expression of myogenic genes over muscle differentiation in WT, NMRK1KO, NMRK2KO and DKO mouse myotubes was assessed to indicate normal muscle differentiation. Figure 4.15 shows that the loss of NMRK1 and NMRK2 function individually and combined (to eliminate potential NMRK redundancy) did not alter expression of key muscle differentiation markers namely; Acta, MyoD and MyoG (figure 4.15A-C). Myotube morphology also appeared consistent across the different genotypes over differentiation. Thus, this data combined with macroscopic *in vivo* assessment confirms that the NMRKs are not essential for muscle development in mice despite the highly muscle specific nature of NMRK2. This data is contrary to findings in zebrafish, whereby nrk2b was found to be essential for skeletal muscle morphogenesis. This effect however, was shown to be NAD^+ specific and therefore suggests zebrafish skeletal muscle is more reliant of Nrk2b mediated NAD^+ biosynthesis as opposed to Nampt [252].

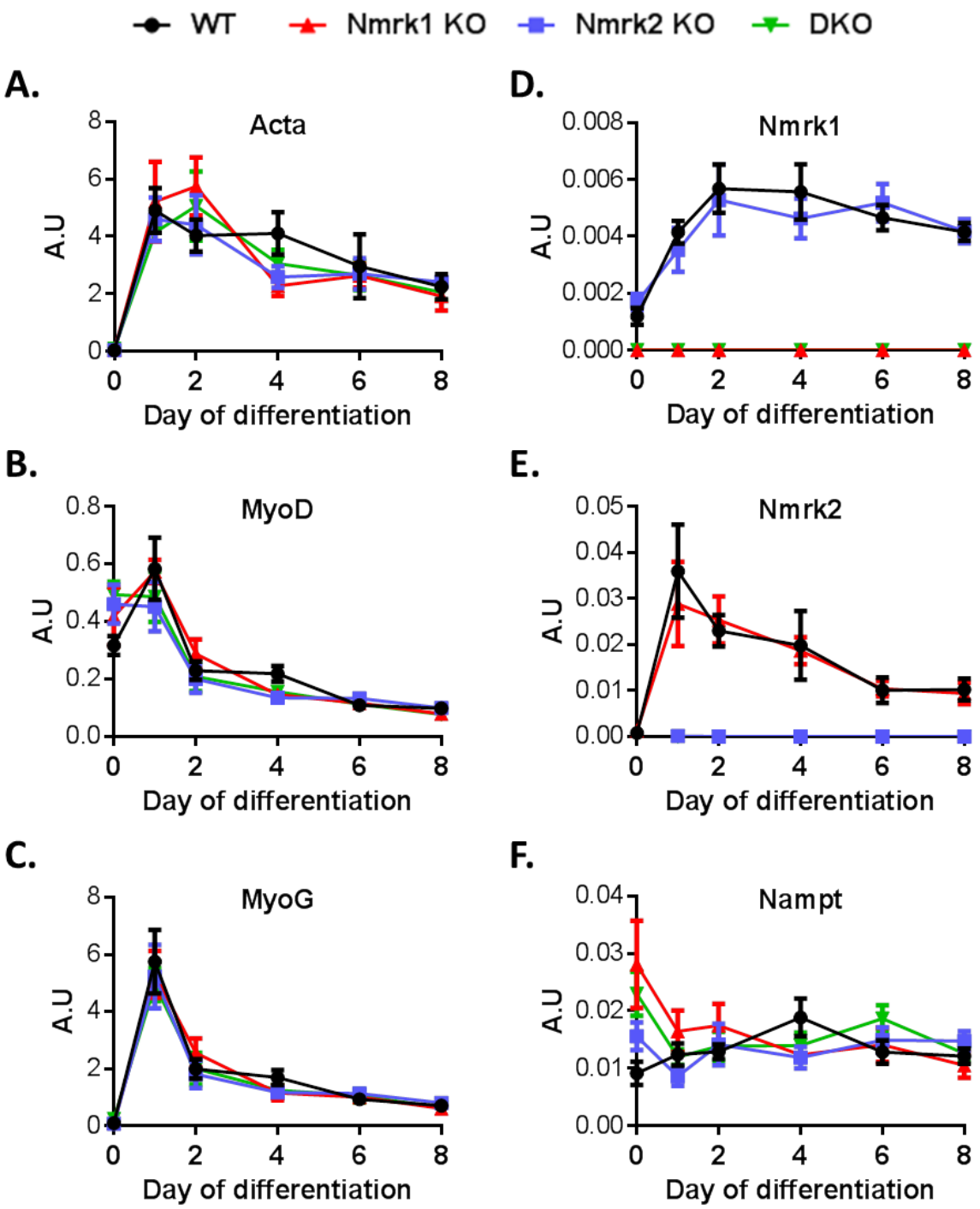

Figure 4.15 NAD^+ Salvage and myogenic gene expression over differentiation in NMRK KO myotubes

Real-time PCR analysis of skeletal muscle myogenic markers (A-C) and NAD^+ salvage genes (D-F) in WT, NMRK1KO, NMRK2KO and DKO isolated muscle cells over 8 days of differentiation to myotubes. A.U values presented as mean ± SEM (n=5).

NAD^+ salvage gene expression was also examined to validate the primary myotube KO models and identify possible redundancy effects following loss of NMRK1 and NMRK2 function. As expected mRNA expression of Nmrk1 and Nmrk2 was absent in their respective single and double NMRK1 and 2 KO myotubes. Expression of NMRK1 and 2 was unchanged from WT levels in NMRK2 and NMRK1 KO myotubes respectively (figure 4.15D and E). Nampt mRNA expression was unchanged from WT levels in both the single NMRK KO and DKO myotubes (figure 4.15F). This data validates the genotype of the myotubes examined whilst indicating minimal NAD^+ biosynthesis enzyme redundancy following loss of NMRK function over differentiation at mRNA level.

4.3.8 NMRKs do not modulate basal skeletal muscle NAD^+ but are essential for exogenous NR and NMN utilisation

The data in figure 4.11 demonstrated that NMRK2KO myotubes can still metabolise exogenous NR to NAD^+, independent of NAMPT, indicating NMRK1 activity in myotubes. NAD^+ was measured in primary myotubes from single and double NMRK KO mice to investigate the individual (and combined) role of NMRKs in basal NAD^+ maintenance and precursor use; with DKO myotubes used to establish possible enzyme redundancy. This work was performed in the Carles Canto laboratory at the Nestlé Institute of Health Sciences, Lausanne, Switzerland with the assistance of Joanna Ratajczak for primary myotube preparation and analysis.

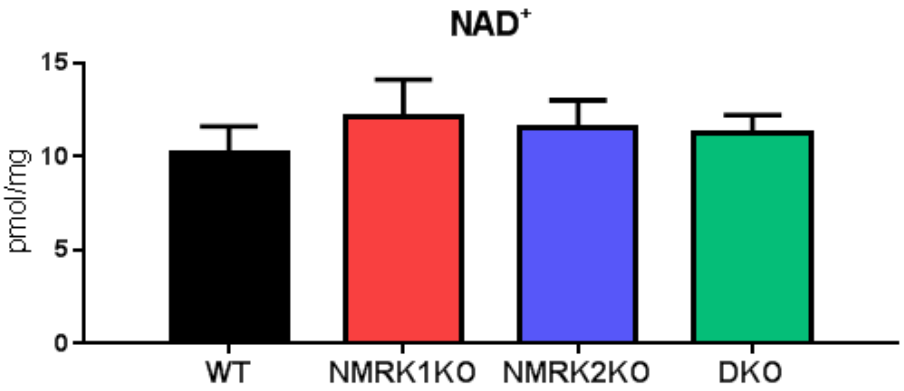

Figure 4.16 NAD$^+$ content of NMRK KO myotubes

Basal NAD$^+$ content of primary myotubes from WT, NMRK1KO, NMRK2KO and NMRK1 and NMRK2 double KO (DKO) mouse skeletal muscle. All data presented as mean ± SEM (n=4-5).

Interestingly, in contrast to previous data (figure 4.10), basal NAD$^+$ levels were unchanged from control in the single and double NMRK deficient models (figure 4.16). Although to a lesser extent than in the WT myotubes, NMRK1KO and NMRK2KO myotubes still exhibited enhanced NAD$^+$ following NR supplementation (figure 4.17A,B left). However, NR was completely unable to increase NAD$^+$ in the DKO myotubes (Figure 4.17C left), suggesting an unbiased NMRK dependence for NR in muscle.

To further understand the role of NMRKs relative to NAMPT and eliminate possible NAMPT redundancy, FK866 was used to inhibit NAMPT and effectively provide a triple loss of function system. As expected, 24 hour NAMPT inhibition by FK866 substantially depleted cellular NAD$^+$ content in all the NMRK loss of function models (Figure 4.17A-C right). NR supplementation could recover, but not boost, NAD$^+$ levels following FK866 inhibition in NMRK2KO and, to a lesser extent, NMRK1KO myotubes (Figure 4.17A,B right). Yet, NR supplementation could not rescue NAD$^+$ depletion in NMRK DKO myotubes (Figure 4.17C right).

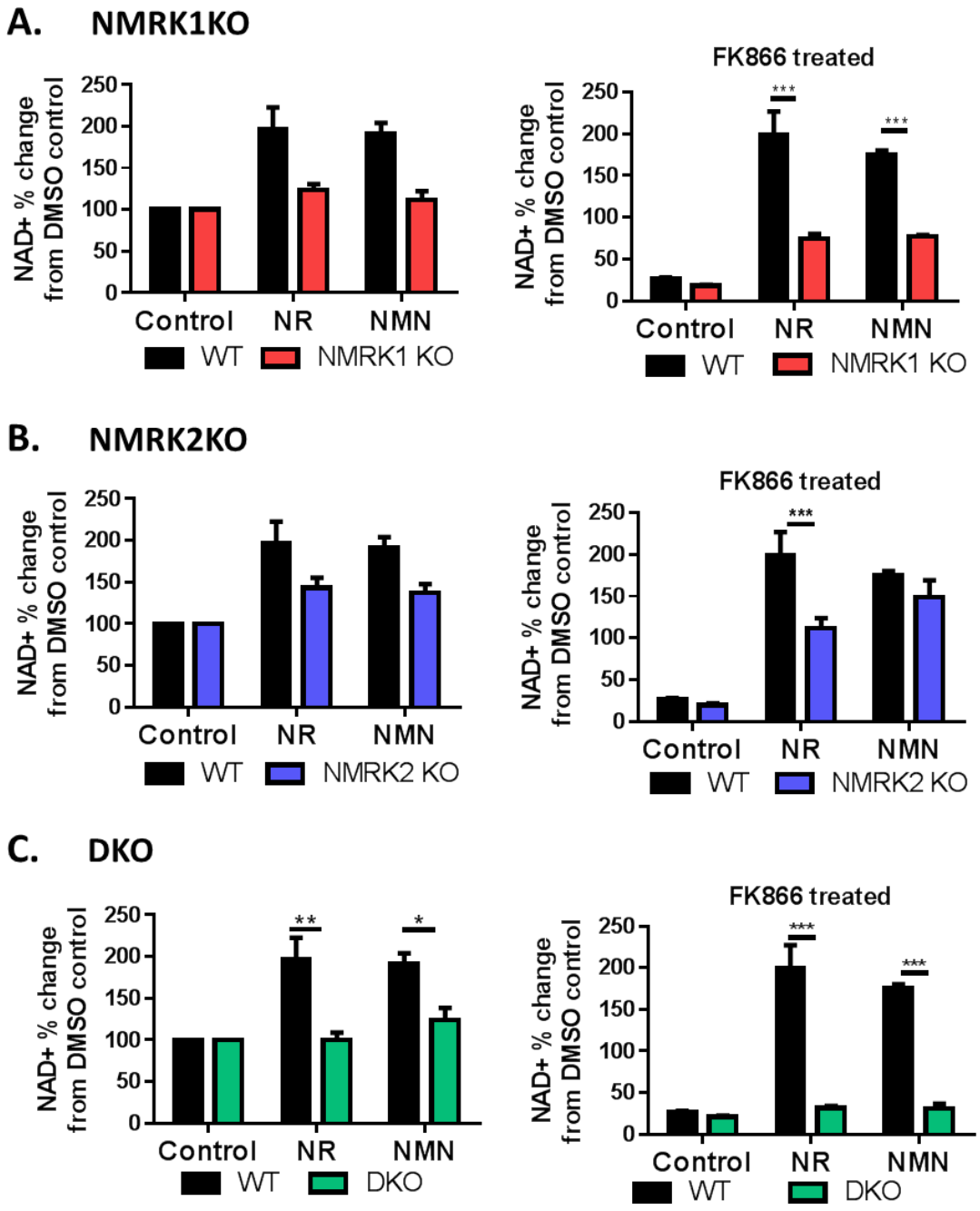

Figure 4.17 NR and NMN salvage to NAD$^+$ in NMRK KO myotubes

Percent change in NAD$^+$ content from control of (A) NMRK1KO (B) NMRK2KO and (C) double KO (DKO) primary myotubes following 24 hour 0.5 mM NR or NMN supplementation compared to WT myotubes (left) and corresponding % change in NAD$^+$ content following 24 hour 100 nM FK866 treatment (right). Data presented as mean ± SEM and significance of actual NAD$^+$ values between WT and KOs was determined by two-way ANOVA with Bonferroni post-tests (n=4-5). (* p<0.05, **p<0.01, ***p<0.001).

In addition, NMN is salvaged to NAD^+ downstream of NAMPT and the NMRKs (figure 4.1) and can significantly boost NAD^+ content and rescue FK866 depletion in WT myotubes (figure 3.9), thus it was used as a control to enhance NAD^+ in all the NMRK loss of function models. As previously seen, NMN supplementation could recover and boost NAD^+ with and without NAMPT inhibition in WT and NMRK2KO myotubes (figure 4.17B). However, and surprisingly, NMN supplementation could not recover NAD^+ depletion in NMRK1 deficient myotubes (figure 4.17A,C).

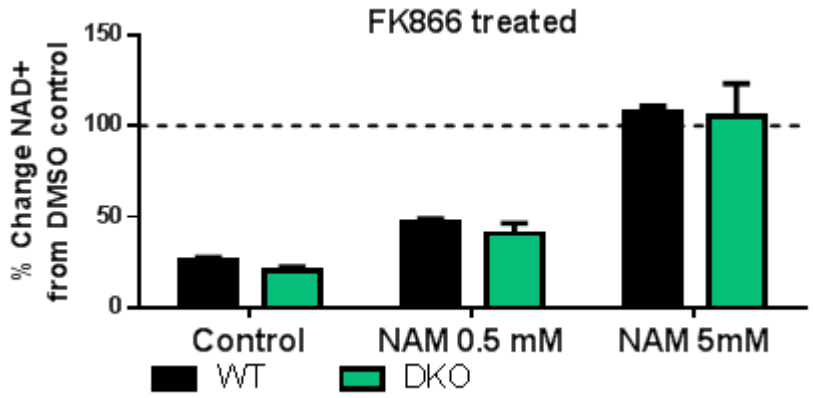

Figure 4.18 NAM salvage to NAD^+ in NMRK DKO myotubes following NAMPT inhibition

Percent change in NAD^+ content of NMRK DKO primary myotubes compared to untreated WT control (dashed line) following 24 hour 100 nM FK866 treatment and 0.5 mM and 5 mM (NAM*10) NAM supplementation. Data presented as mean ± SEM (n=4).

NAM supplementation was used as a further control and was unable to boost NAD^+ at equimolar levels but could enhance NAD^+ and partly overcome NAMPT inhibition at 5 mM (at 50,000 x FK866 concentration) in WT and DKO myotubes (figure 4.18). These data further confirm that NAMPT recycling of NAM is the principal pathway for maintaining NAD^+ homeostasis in skeletal muscle. It also shows that the NMRKs are essential for utilising NR to enhance cellular NAD^+, and identifies a novel role for NMRK1 in the salvage of exogenous NMN.

4.4 Discussion

Skeletal muscle is a central tissue for energy homeostasis; thus loss of muscle mass and function with ageing and chronic disease states manifests hand in hand with metabolic decline [26]. As a critical signalling metabolite in energy metabolism, reduced NAD^+ availability in ageing may compromise the plasticity of muscle in response to metabolic stress [89, 169, 174]. Therefore, a better understanding of NAD^+ turnover in skeletal muscle may elucidate novel strategies to enhance NAD^+ levels and restore metabolic function. Studies have already begun to outline potential muscle specific benefits of enhanced cellular NAD^+ with strategies including, PARP inhibition to limit NAD^+ consumption [92, 127] and supplementation with NAD^+ precursors to drive biosynthesis [178, 201].

Following the identification of Nampt and Nmrk2 as the most predominantly expressed NAD^+ biosynthesis genes in skeletal muscle, this chapter further investigated the importance of these pathways for NAD^+ biosynthesis. NAMPT has already been well characterised as a critical regulator of basal NAD^+ [76, 150, 227] yet little is known about the function of NMRK2. Current studies of NMRKs are mostly limited to yeast and zebrafish models [142, 173, 252, 253]. In yeast models Nmrk1-dependent metabolism of NR was shown to contribute to basal NAD^+ and necessary for Sir2 function and life span extension seen following calorie restriction [253]. Whilst in zebrafish, nrk2b has been shown to regulate cell matrix adhesion complexes during muscle morphogenesis in an NAD^+ dependent manner with nrk2b deficiency leading to muscle abnormalities [173]. Despite these studies indicating an evolutionary conserved importance for NMRK salvage of NR there has been little study beyond this in higher organisms.

Thus, to investigate the function of mammalian NMRK2, a loss of function mouse model was employed. As a novel mouse model with no existing published data, the NMRK2KO mouse was fully validated and loss of mRNA and protein was confirmed. Macroscopic analysis of mice identified behaviour and activity consistent with WT and HET litter mates. Skeletal muscle quantification of NAD^+ and related metabolites showed mostly unchanged metabolite levels in NMRK2KO tissue compared to WT. Although NA was reduced in NMRK2KO muscle, the levels detected even in WT tissue were minimal and therefore this difference is unlikely to have biological relevance. Skeletal muscle NADS (protein encoded by NADsyn1) expression and activity is normally below detectable levels [147] but it is possible the decrease is a result of increased NADS activity as a redundancy response to loss of NMRK2 activity.

Basic profiling of muscle tissue gene and protein expression did not identify any major transcriptional or translational differences in NMRK2KO muscle compared to WT in respect to NAD^+ signalling and energy metabolism. Of the genes investigated, only CD157, Pnp and Ucp2 were found to be significantly changed in TA muscle. Soleus tissue gene expression was less affected by NMRK2 deficiency with only CD157 significantly upregulated. Unfortunately, follow up immunoblot analysis of CD157 protein expression was unsuccessful largely owing to issues with antibody specificity (sc-7115, Santa Cruz, U.S) and its low expression in skeletal muscle. CD157 uses NAD^+ to generate cyclic ADPribose, NAADP and ADPr [98]; its role in numerous cellular signalling pathways from cell proliferation to immune function makes it impossible to predict the relevance of this upregulation [254, 255], notably it is involved in muscle contraction and calcium signalling [255], which may possibly be perturbed in NMRK2KOs given its

muscle specificity. Interestingly, NR has been identified as a substrate for PNP which can dephosphorylate NR to NAM [248]. This change may be an adaptive response to increased NR availability in muscle in NMRK2KO. If PNP metabolism is enhanced this may also explain why a block to NR metabolism via NMRK2 did not lead to a build-up of NR in NMRK2KO muscle. Again, the importance and/or biological significance of changes to Ucp2 expression is difficult to deduce. UCP2 is a mitochondrial uncoupling protein that can regulate cellular ADP:ATP ratio, unlike UCP1 which plays a clear role in brown adipose thermogenesis the specific physiological functions of UCP2 are still poorly understood; with upregulation associated with increased energy expenditure and protective against obesity [256-258].

With the NAD^+ metabolome mostly unperturbed in NMRK2KO tissue, it is unsurprising that the loss of function mice did not present with majorly aberrant NAD^+ signalling and metabolism. Although gene and protein expression levels are good indicators of changes to NAD^+ signalling, they do not identify changes to enzyme activities and post translational signalling events. For example, despite unchanged gene expression to SIRT1 in NMRK2KO muscle, SIRT1 enzyme activity may still be different from WT. Current difficulties measuring SIRT activity in muscle meant that potential changes could not be directly measured in NMRK2 deficient muscle; however, expression of metabolic genes (e.g. Pdk4, Nrf1 and Tfam) that are typically transcriptionally regulated by SIRT activity via PGC1α [63, 259] were unchanged suggesting that SIRT activity is not affected by loss of NMRK2 function.

Initial investigation of NMRK2 deficient myotubes using the colorimetric NAD/NADH assay identified significantly lower NAD^+ levels compared to WT myotubes. Preliminary LC-MS analysis of NMRK2KO myotubes corroborated these findings. Further repetition of LC-MS is necessary to determine significance of this analysis and investigate NAD-related metabolites. The primary cultures required for LC-MS analysis required large up-scaling limiting culture success rates. Thus, this analysis was treated as exploratory with further assessment required to draw any conclusions. The results determined in myotubes opposed those from NMRK2KO tissue analysis and may be attributed to myotubes existing in a closed system with limited substrate availability. It is possible that without multi-tissue and systemic interplay myotube NAD^+ levels are more sensitive to changing.

Furthermore, preliminary data suggests maximal mitochondrial function may be impaired in NMRK2KO mice. NR may enhance maximal mitochondrial function, following uncoupling, in WT, and to a lesser degree in NMRK2KO myotubes. This shows potential functional differences between WT and NMRK2KO myotubes; possibly indicating a diminished oxidative adaptive ability of KO myotubes during metabolic stress, that may be related to NAD^+ availability. Normalisation difficulties due to the small amount of protein per well and the inability to count satellite cells meant data was presented as percent change from basal OCR. Profiling of key mitochondrial complex proteins showed no difference between WT and KO myotubes with or without NR treatment, suggesting mitochondrial content is unchanged and not responsible for any functional differences. However, consistent with the other experiments performed here myotubes were treated with NR for just 24 hours and a longer treatment time may be required to see changes

at a protein level. With that said, taking into account previous literature, these findings in respect to NR supplementation were anticipated. The muscle specific NAMPT overexpressing mouse model exhibited a 50% increase in NAD^+ content yet mitochondrial biogenesis was not induced and oxidative function was unchanged in young mice [240]. With the NAMPT overexpressing mice only demonstrating improvements to metabolic health compared to WTs upon ageing (2 years) [76].

Despite depletion of NAD^+ by FK866, there is a general upward trend in the NAD/NADH ratio, typically thought to push oxidative metabolism. This is unexpected as upon NAD^+ depletion it would be expected that oxidative function would be negatively impacted. Studies have shown that mitochondrial NAD^+ is protected from FK866 depletion for over 24 hours [96] thereby maintaining mitochondrial function and it is possible the NAD/NADH ratio pushes towards NAD^+ as an acute stress response to reduced cytosolic NAD^+ availability to further support oxidative function.

NR supplementation enhanced NAD^+ levels in both WT and NMRK2KO myotubes. The NAD^+ boosting effect of NR was also seen following NAMPT inhibition, thus ruling out potential conversion of NR to NAM and salvage to NAD^+ by NAMPT. This indicated that NMRK1 may be able to metabolise NR in skeletal muscle despite low expression. NMRK1 protein was unsuccessfully detected in WT and NMRK2KO muscle tissue, but mRNA levels were slightly upregulated indicating a possible redundancy effect following loss of NMRK2 function. Initial Nmrk1 KD studies to investigate the potential role of NMRK1 in skeletal muscle biosynthesis were inconclusive due to difficulties reproducing KD efficiency in repeated

experiments. Muscle cells are difficult to transfect and transfections are normally most successful whilst cells are myoblasts. For this study, NAD^+ was measured in fully differentiated myotubes to compare and combine with data from NMRK2KO myotubes and therefore this is likely the reason for inconsistent transfection efficiency.

Therefore, to investigate NMRK1 function in skeletal muscle further, a collaboration with Dr Carles Canto at the Nestle Institute of Health Sciences was established, where NMRK1KO, NMRK2KO and NMRK double KO (DKO) mice were available for analysis. Expression of key differentiation markers showed levels consistent with WT myotubes in the NMRK single and double KO systems, indicating normal myotube differentiation. Furthermore, expression of Nampt and Nmrk1 and Nmrk2 mRNA was unchanged from WT in myotubes (except in corresponding NMRK KO myotubes), indicating a lack of redundancy at a gene level.

NR supplementation of the NMRK KO models showed that NMRK1 and 2 KO myotubes could salvage NR and replete NAD^+ following FK866 depletion, but to a lesser extent than WT. In DKO myotubes NR supplementation was unable to enhance or recover myotube NAD^+, identifying NR metabolism to NAD^+ as NMRK dependent. Despite a much lower level of expression, NMRK1 deficiency appeared to have a greater effect on NR metabolism compared to NMRK2 which may be attributed to its greater affinity for NR [164, 165]. This reinforces the notion that expression levels are a useful indicator but not reliable for assuming enzyme influence. Importantly, the relative expression of Nmrk1 in primary myotubes was

higher than in skeletal muscle tissue (although still considerably lower than Nmrk2); therefore this may have heightened the effects of Nmrk1 salvage *in vitro*.

Although, NMN is metabolised to NAD^+ downstream of NMRKs and NAMPT, exogenous NMN supplementation was unable to be used for NAD^+ salvage in NMRK1KO primary myotubes, implicating NMRK1 in regulating exogenous NMN metabolism. Recent findings by Ratajczak et al. (2016), have also implicated NMRK1 in the regulation of exogenous NMN salvage in hepatocytes; with hepatocytes (which do not express Nmrk2) from NMRK1KO mice unable to use exogenous NMN. This work proposed a need for NMN to be extracellularly metabolised to NR for entry into the cell and then phosphorylated intracellularly by NMRK1 [166].

This follow up analysis using NMRK1, NMRK2 and DKO myotubes failed to replicate the decrease in basal NAD^+ levels previously seen in NMRK2KO myotubes. These myotubes were set up whilst in a different laboratory environment (Lausanne, Switzerland) and therefore there were some unavoidable changes to the experimental set up that may be attributed to the inconsistencies seen here. For example, batch numbers of horse serum, foetal bovine serum and chick embryo extract were different and as previously demonstrated NAD^+ levels are highly sensitive to nutrient availability [116, 135]. Moreover, the myotube cultures for the single and double KO experiments had some fibroblast contamination that is not normally seen in primary muscle set up (although myotubes were still predominant). Muscle tissue consists of a mix of muscle cells and connective tissue and therefore, although most of the fibroblasts are separated from myofibres during set up, small amounts of fibroblast contamination

is expected in cultures [260, 261]. The increase seen was consistent across all the cultures (from 20 mice) done in the secondary laboratory environment and may be a result of differences to serums or possibly due to culture plate differences. Unfortunately, these culture differences were unanticipated and as both mouse availability and time was limiting to this part of the investigation it could not be repeated to determine fibroblast influence on NAD^+ levels. Importantly, all the NMRK KO models exhibited global loss of function and therefore fibroblast contamination should not influence functional investigations. The inconsistencies in this data again highlights the highly dynamic and sensitive nature of NAD^+ signalling and shows the difficulties faced whilst trying to accurately measure changes following intervention.

This chapter presents novel findings in regards to skeletal muscle NAD^+ biosynthesis pathways. Despite, identifying an essential role for NMRKs in NR salvage, initial investigations show no impairments to NAD^+ signalling, muscle development and energy metabolism in the loss of function mouse models. However, the muscle specificity of NMRK2 suggests it may still be an important enzyme in skeletal muscle. These studies outlined the importance of different NAD^+ biosynthesis pathways under basal conditions. Despite a minimal role for NMRKs under basal conditions, skeletal muscle is highly adaptive to metabolic stress and therefore they may have a redundancy function to support NAMPT salvage activity in response to stress.

Chapter 5 Preliminary *in vivo* assessment of NMRK2 deficient mice

(All *in vivo* experiments and tissue collection were conducted at University of Birmingham; fibre-typing analysis was performed by Dr Gabriela da Silva Xavier post-collection at Imperial College London)

5.1 Introduction

Skeletal muscle has a remarkable ability to adapt in response to metabolic stress and meet the high energy requirements for muscle contraction [31, 32, 46]. It acts as a critical modulator of systemic energy metabolism and adapts acutely and chronically to everyday stresses that threaten energy homeostasis including, exercise and calorie restriction [30, 46, 177]. This critical function is regulated through the energy sensing enzymes AMPK and SIRTs. When cellular ATP levels decrease, AMPK is activated and can directly phosphorylate PGC1α and upregulate its transcription [62]. Furthermore, AMPK can phosphorylate NAMPT and enhance recycling of NAM to NAD^+; a surge in cellular NAD^+ availability stimulates SIRT activity and results in deacetylation of PGC1α [244]. This post-translational modification activates PGC1α, inducing global transcriptional reprogramming of metabolic genes in favour of ATP generation [63, 251].

The importance of NAD^+ biosynthesis in skeletal muscle metabolism

NAD^+ dependent SIRT-mediated metabolic signalling was classically identified in yeast whereby induction of Sir2 by calorie restriction enhanced lifespan [262]. Since then, the vast benefits of calorie restriction and induction of SIRTs have been elucidated [84, 263].

In mammals, fasting and calorie restriction is associated with enhanced NAMPT activity and NAD^+ availability to support SIRT action [84]. The dependence of SIRT activity on NAD^+ demonstrates the importance of replenishing NAD^+ following consumption [90, 99]. Data presented in this thesis supports previous research that shows NAMPT to be an essential enzyme for NAD^+ biosynthesis in skeletal muscle [76]. Pharmacological inhibition of NAMPT leads to a severe

depletion of cellular NAD^+ and ultimately cell death. Complete loss of NAMPT function in mice is incompatible with life but inducible tissue specific models have been generated [76, 168, 264, 265]. Surprisingly, studies of muscle specific NAMPT KO mice showed that young mice did not manifest with major abnormalities despite exhibiting a staggering 85% decrease in intramuscular NAD^+ content [76]. However, a degenerative muscle phenotype was seen over ageing, with these mice manifesting with fibre degeneration, loss of muscle strength and endurance exercise capacity. Treatment with NR restored muscle function highlighting the importance of NAD^+ availability to muscle health, irrespective of NAMPT activity [76]. The physiological relevance of loss of NAMPT function in terms of non-genetically altered mice has also been investigated; with a concomitant decline in NAMPT and NAD^+ identified in aged rat muscle [89, 174]. Exercise can increase both NAD^+ and NAMPT expression in aged muscle and has been proposed to slow the progression of age-related metabolic decline through SIRT1 mediated effects [174]. Together these studies demonstrate the importance of maintaining NAD^+ turnover in skeletal muscle and the potential metabolic benefits of preserving NAD^+ signalling during ageing.

NMRKs as a nutraceutical targets against metabolic decline

Data presented here indicates that, unlike NAMPT, the NMRK enzymes have little influence on resting metabolism in muscle, with NMRK deficient mice presenting with normal NAD^+ signalling and energy metabolism. However, their ability to exclusively metabolise exogenous NR, and dictate the use of exogenous NMN, to enhance NAD^+ makes them valuable therapeutic targets. With NAMPT self-limiting, and NAM excess inhibitory to SIRT activity [152], this alternative biosynthesis pathways has provided much research interest. NR supplementation

has already been demonstrated to protect against many of the global metabolic consequences of HFD induced metabolic decline in mice [199]. Moreover, in models of muscle dystrophy NR supplementation could improve muscle function; with enhanced mitochondrial function and structural proteins and reduced inflammation, fibrosis and senescent stem cells [242, 266].

Most of the research to date has focussed on the use of NR as a means to ameliorate or reverse models of metabolic impairment. However, despite its highly conserved and muscle specific nature, the function of NMRK2 beyond salvage of NR is still unknown. It is possible that it plays a supporting role for NAMPT during metabolic stress that is not apparent during basal metabolism. Using NMRK2KO mice, this chapter aims to investigate the role of NMRK2 during metabolic stress following in vivo interventions including fasting, HFD challenge and exercise. These studies will be the first to investigate the importance of NMRK2 during metabolic stress and the potential impact NMRK2 deficiency may have on metabolic adaptation.

5.2 Materials and Methods

5.2.1 Animal care

Heterozygous breeding of the NMRK2KO mouse line provided litter matched WT and KO cohorts. Animals were all kept in an enriched, pathogen–free environment at around 21-23°C with 12 hour light/dark cycles. Unless otherwise stated standard chow and water was available *ad libitum*.

5.2.2 High fat diet (HFD)

From 10 weeks of age, mice were fed a commercially available high fat chow (Brogaarden, Denmark) for 16 weeks. The mice were weighed before starting the HFD and once a week until the end of the diet.

5.2.3 Glucose tolerance test (GTT)

GTTs were performed following 6 hours of food restriction. Small incisions were made to superficial vessels on the tails of each mouse and a drop of blood collected on Accu-Chek blood glucose strips (Boots, UK) and read using a glucometer to provide a baseline blood glucose reading. Following this, glucose (2g/kg) was administered by I.P injection and blood glucose was measured at 15 min, 30 min, 60 min and 120 min – post glucose administration. Animals were monitored during and following the procedure for any signs of unexpected stress.

5.2.4 *In vivo* metabolic phenotyping

Mice were weighed and placed into the PhenoMaster (TSE) with their original litter mates and in their original cages for 24 hours to acclimate to the new environment. Following this, the mice were separated and housed individually for 72 hours within the PhenoMaster. The first 24 hours allowed acclimatisation to

isolation, and indirect calorimetry data was collected during the subsequent 48 hours (section 2.13.7). Body weight, food and drink intake was monitored throughout.

5.2.5 Fasting

Mice were single housed in clean cages and had no access to food for 16 hours before tissue collection. Mice had normal access to water and were kept in normal housing conditions.

5.2.6 Treadmill exercise

Following a short acclimatisation period, mice were exercised on specialised treadmills for 1 hour 3 times a week at a speed of 0.2 m/s and a 15% incline. Upon stopping mice were encouraged to run and were briefly blown with air if they failed to re-join the treadmill (up to a maximum of 3 times).

5.2.7 Tissue collection

Tissues were collected at 10-11 AM to minimise circadian changes. Mice were culled by schedule 1 cervical dislocation and tissues were immediately collected and either snap frozen in liquid nitrogen or placed in the required buffer or fixing agent.

5.2.8 Fibre-typing

Muscle sections were fibre typed by Dr Gabriella Da Silva Xavier (Imperial College London), using immunofluorescence following an established protocol. Briefly, 10 µm sections of were cut using a cryostat and mounted onto slides. Primary antibodies detecting different myosin heavy chain subunits were added, followed by fluorescent secondary antibodies. Sections were formalin fixed, mounted and

then analysed using a Zeiss Axio Observer inverted microscope (Carl Zeiss, Germany). Fibres were manually counted across the entire section using Image J (Fiji) software and recorded as positive for each fibre expressing the relevant visible colour (section 2.14).

5.2.9 High resolution respirometry - Oroboros

Excised muscles were placed in ice cold BIOPS buffer and carefully separated into clusters. Fibre clusters were transferred into ice cold BIOPS buffer with saponin (at 5 mg / ml of BIOPS) and incubated at 4° C for 30 minutes on a shaker to permeabilise. Fibres were then dried and 5 mg of fibres were transferred into ice cold mitochondrial respiration medium (MiRO5) and placed into Oroboros respirometer chambers. Once airflow stabilised substrates were sequentially added as follows; 0.5 mM malate, 55 µM palmitoyl, 10 mM glutamate, 5 mM ADP, 10 µM cytochrome, 10 mM succinate, 0.5 µM FCCP, 0.5 µM rotenone and finally 2.5 µM antimycin A.

5.2.10 RNA extraction

RNA was extracted from 20 mg of tissue using TRI-reagent (Invitrogen). RNA quality was determined by visualisation on a 1.5% agarose gel and quantified using a nanodrop. 1 µg of RNA was used for reverse transcription (see section 2.6).

5.2.11 qPCR

qPCR was performed in a 384-well plate in single-plex format using Assay on Demand primers and probes (Applied Biosystems) (section 2.6.4). The PCR plates were placed in the real-time ABI7500 system and amplified using the following protocol: 95^{o}C for 10 minutes then 40 cycles of 95^{o}C for 15 seconds and

60^{o}C for 1 minute using an. The resulting Ct values were used to obtain deltaCt (dCt) values.

5.3 Results

5.3.1 Regulation of NAD^+ biosynthesis in fasted skeletal muscle

Fasting is known to induce metabolic adaptation through SIRT signalling to reprogram energy metabolism when glucose levels are low and maintain ATP production [84]. To examine the effect of fasting on NAD^+ biosynthesis genes in skeletal muscle, mice were fasted overnight and tissue was collected. qPCR analysis of fasted muscle tissue identified a significant increase in Nampt expression supporting previous evidence. Interestingly, Nmrk2 expression is significantly supressed in fasted muscle, although the reason for this downregulation is not immediately apparent. Alternative NAD^+ salvage genes, Nmrk1 and NADsyn1 were not significantly regulated in fasting muscle (figure 5.1). These transcriptional changes seen in skeletal muscle following acute fasting highlights the dynamic nature of muscle in response to metabolic stress.

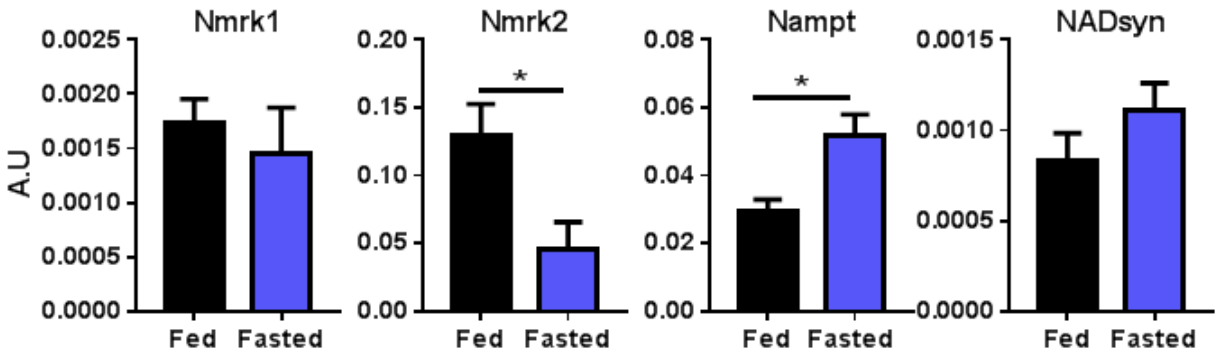

Figure 5.1 NAD^+ biosynthesis gene expression in fed and fasted skeletal muscle

Real-time PCR analysis of NAD^+ biosynthesis genes (Nmrk1, Nmrk2, Nampt and NADsyn1) from skeletal muscle of mice either fed *ab libitum* or following a 16 hour overnight fast (n=4). Data presented as mean A.U values ± SEM and significance determined by unpaired t-test (* $p<0.05$).

5.3.2 Metabolic phenotyping of NMRK2KO mice following High fat diet challenge

HFD challenge in mice is well characterised to induce obesity and associated co-morbidities such as insulin resistance [199, 267]. To determine whether NMRK2 plays an important support role during perturbed metabolism, WT and NMRK2KO mice were subjected to HFD feeding and metabolic parameters were examined. On average the weight of both WT and KO mice increased by nearly 100% following 12 weeks of HFD with no genotype difference apparent (figure 5.2A).

Fasting blood glucose levels were similar in WT and NMRK2KO mice at 10.7 ± 0.5 and 11.1 ± 0.7 mmol/L respectively**.** Normal chow fed WT controls exhibited significantly lower fasting blood glucose levels of 8.3 ± 0.3 mmol/L, suggesting HFD induced hyperglycaemia. Glucose tolerance tests (GTT) showed both WT and KO mice to have impaired glucose clearance from the blood following glucose I.P compared to normal chow fed mice (grey), with levels still not returned to basal fasting glucose after 2 hours – demonstrating high fat diet induced insulin resistance (figure 5.2B). Interestingly, NMRK2KO mice seemed to initially exhibit higher blood glucose levels following I.P injection, with an upward trend seen in area under the curve (AUC), indicating that NMRK2KO mice are less able to modulate glucose metabolism (figure 5.2C).

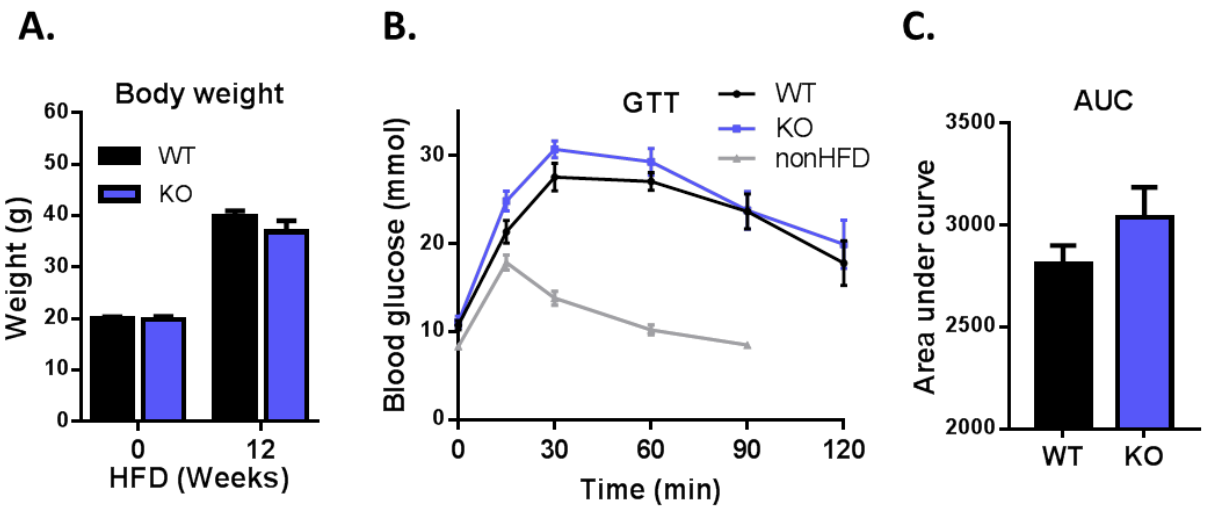

Figure 5.2 NMRK2KO mouse glucose metabolism following HFD

(A) Total body weight of WT and NMRK2KO mice before (3 months old) and after (6months old) 12 weeks of high fat diet (HFD) feeding. (B) Corresponding glucose tolerance test curve, (with a WT chow fed GTT provided for diet comparison - grey) and (C) area under the curve, of HFD fed WT and NMRK2KO mice. All data was collected from age-matched female mice (n=9) and presented as mean ± SEM.

Using PhenoMaster technology (TSE, Germany), mice were single housed in metabolic cages and gas exchange was continuously monitored over a 72 hour period for indirect calorimetry analysis. The respiratory exchange ratio (RER) is defined by the amount of CO_2 produced divided by O_2 used and provides an indication of the fuel used to support metabolism based on the degree of oxygen used. A respiratory quotient (RQ) of 1 is representative of pure carbohydrate metabolism (normally during active periods) where as an RQ of 0.7 implies pure fatty acid oxidation (inactive periods) [268-270]. Figure 5.3A demonstrates that HFD fed mice have impaired metabolic flexibility with the RER curves remaining relatively flat compared to normal chow fed mice. Normal chow fed mice can adapt metabolism throughout periods of activity and rest; with a higher use of carbohydrates during periods of activity (at night) and a switch to fatty acids metabolism during periods of rest (daytime). Here, following chronic high fat diet feeding NMRK2KO mice demonstrate a downward shift in RER which is more

prominent during night time periods of activity implying they are further metabolically impaired (figure 5.3B).

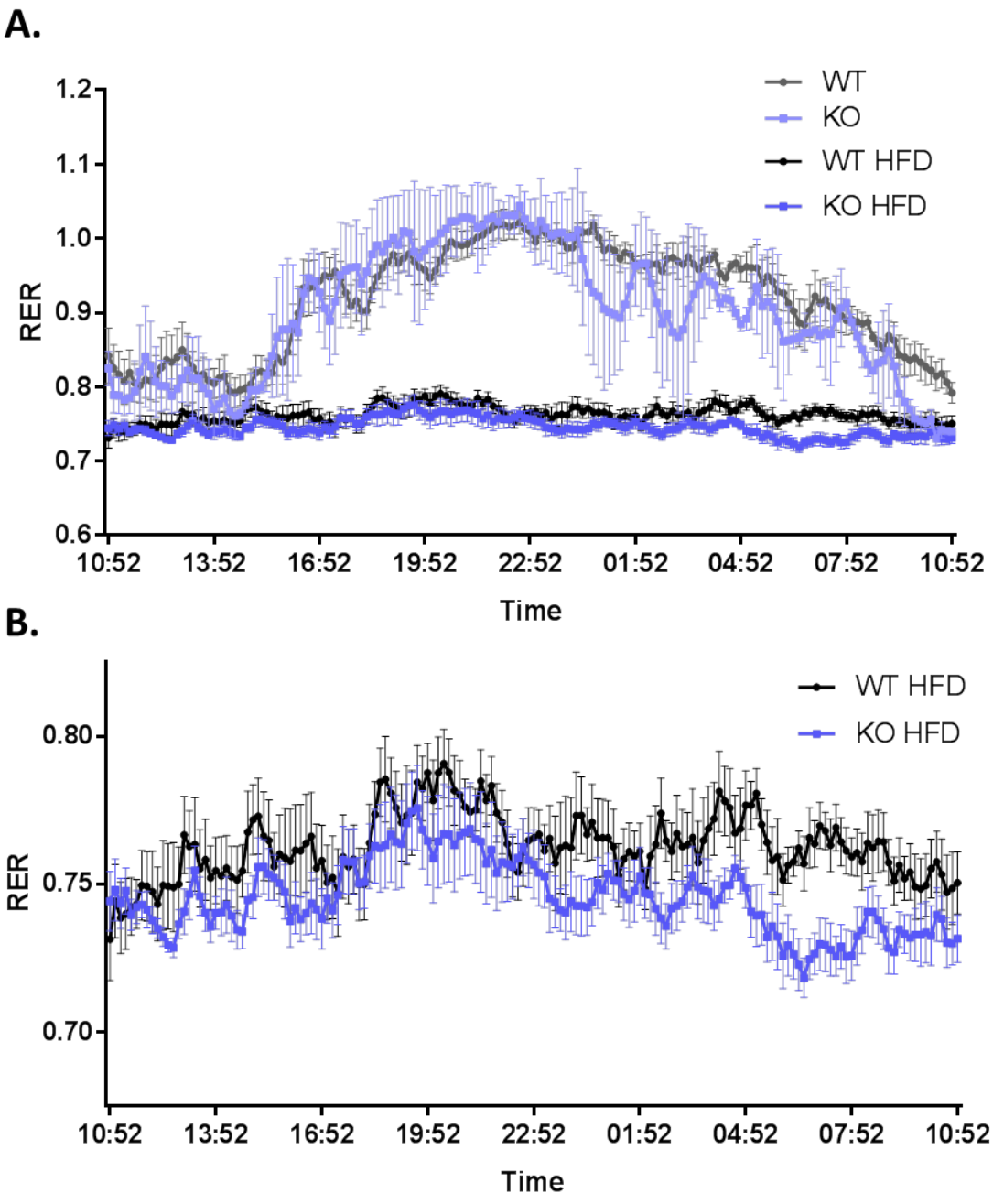

Figure 5.3 *In vivo* metabolic phenotyping of HFD fed WT and NMRK2KO mice

(A) Respiratory exchange ratio (RER) of WT and NMRK2KO mice fed normal chow (faded, upper lines) and high fat diet over 24 hours. (B) A closer look at the RER of HFD fed WT and NMRK2 KO mice. (RER readings were taken every 9 minutes and all mice were female at 6-7 months old HFD WT n=6, HFD KO n=9, chow fed WT and KO n=2). All data presented as mean ± SEM.

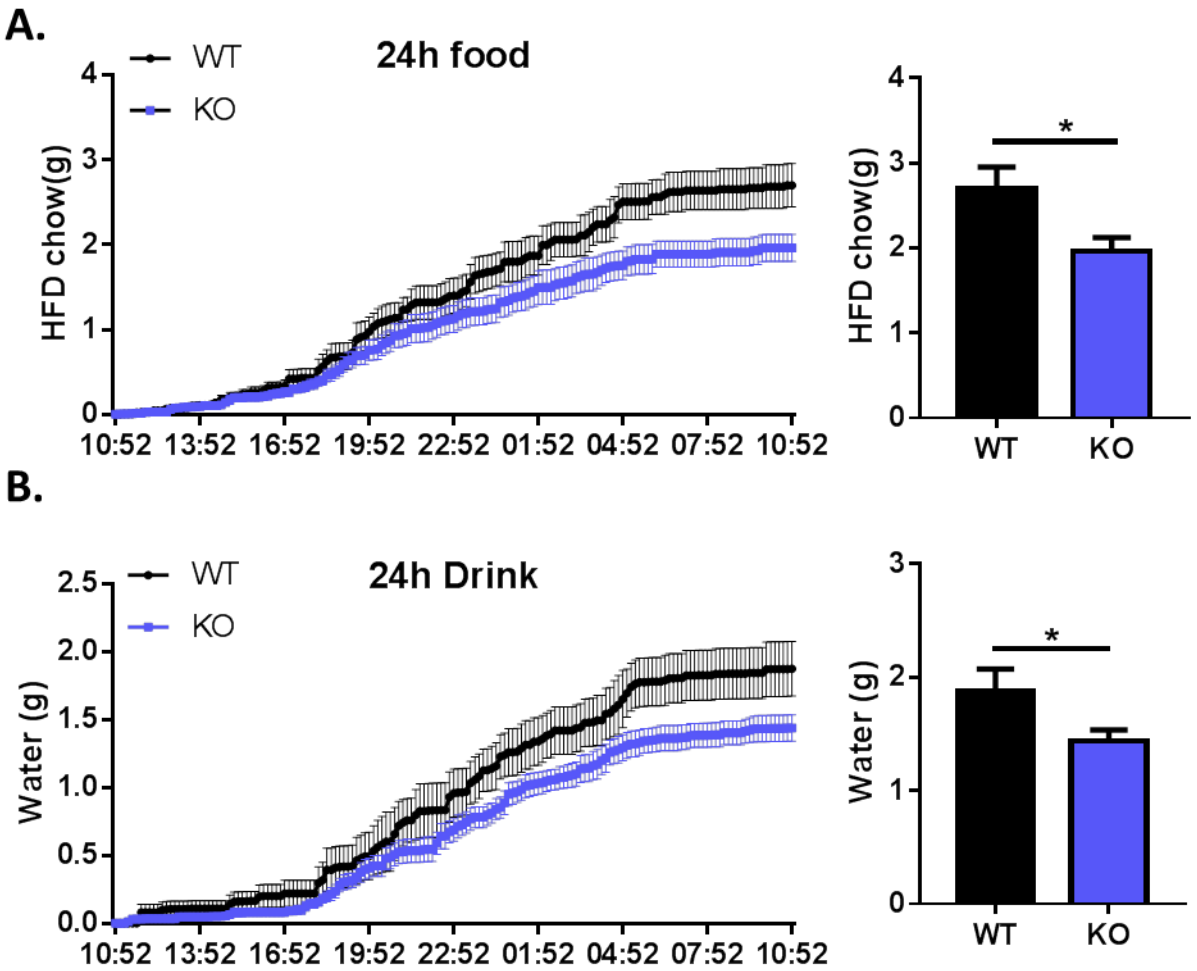

Figure 5.4 Food and drink consumption of WT and NMRK2KO mice in PhenoMaster housing

Cumulative (left) and total (right) 24 hour food (A) and drink (B) intake of high fat diet fed mice placed in the PhenoMaster. (Consumption was measured every 9 minutes and all mice were female at 6-7 months old WT n=6, KO n=9). All data presented as mean ± SEM, significance was determined by unpaired t-test analysis (* $p<0.05$).

Food and drink intake was also monitored and surprisingly NMRK2KO mice appeared to eat less HFD food than WT mice (figure 5.4A). The reduced food intake was seen consistently over the entire experiment rather than a factor of delayed feeding, and feeding frequency was not affected. This difference in food intake likely explains the shift in RER yet the biological significance of this is still unknown. Water intake was also significantly reduced between genotypes (figure

5.4B). Mice that did not take to the metabolic housing did not eat or drink at all leading to weight loss and removal from the PhenoMaster system before experimental readings were taken. All the mice included in the experimental analysis ate and drank gradually over the entire data collection period with no major weight loss. This suggests the NMRK2KO did not consume less food and water due to distress as water intake is was not neglected. Unfortunately, mouse activity could not be measured using this particular set up and therefore differences owed to changes in physical activity could not be determined.

Finally, the oxidative capacity of skeletal muscle from HFD fed WT and NMRK2KO mice was examined. Muscles were collected from mice and intact muscle fibres were dissociated and examined using Oroboros based high resolution respirometry to provide real-time analysis of mitochondrial function. A sequence of reagents were added to test mitochondrial output in response to substrates (malate, palmitoyl carnitine, glutamate, ADP, cytochrome c and succinate), followed by uncoupling agent FCCP, and inhibitors of mitochondrial respiration, rotenone and antimycin A. Mitochondrial response to Malate, palmitoyl carnitine and glutamate appeared blunted in NMRK2KO however maximal mitochondrial output of NMRK2KO muscle fibres was not significantly different from WT (figure 5.5). This data suggests mitochondrial function is not further impaired in NMRK2 deficient muscle following metabolic challenge.

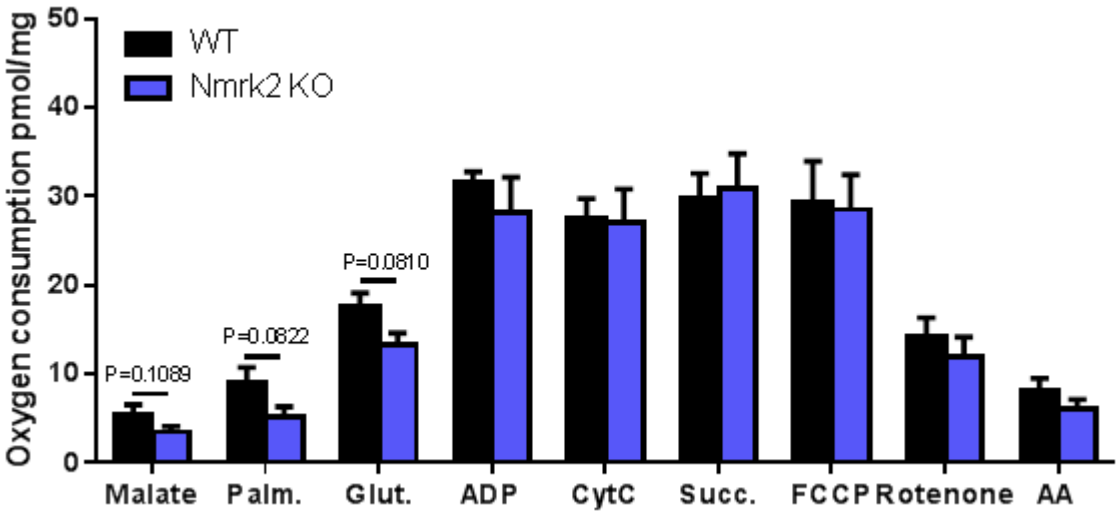

Figure 5.5 High resolution respirometry of skeletal muscle from HFD fed WT and NMRK2KO mice

Mitochondrial function of quadriceps muscle fibres collected from HFD fed WT and NMRK2KO mice was assessed by Oroboros based high resolution respirometry. A succession of substrates were added to the fibres including 0.5 mM malate, 55 µM palmitoyl carnitine (Palm.), 10 mM glutamate (Glut.), 5 mM ADP, 10 mM succinate (Succ.), 10 µM cytochrome *c* (CytC), 0.5 µM FCCP, 0.5 µM rotenone and 2.5 µM antimycin A (AA). Muscle was collected from females at 6-7 months old (WT n=4, KO n=6 and data presented as mean ± SEM).

5.3.3 Fibre-typing of NMRK2KO mice following endurance exercise

The muscle specific nature of NMRK2 and its regulation in muscle differentiation suggests it may have a role in muscle fibre organisation. Muscle development is seemingly unaffected by NMRK2 loss of function with mouse behaviour normal, muscle bed weights unchanged and expression of myotube differentiation markers consistent with WT. Thus, to test whether NMRK2 is important following metabolic stress, an endurance exercise pilot study was set up using WT (n=3) and NMRK2KO (n=3) mice. Endurance exercise induces metabolic adaptation and promotes an oxidative fibre type shift in skeletal muscle [23]. All the mice completed the 6 week endurance exercise protocol successfully, notes were taken and no obvious differences in performance was noticed. Average mouse bodyweight was also consistent between WT and NMRK2KO mice (figure 5.6A).

Following the exercise protocol, mouse tissue beds were weighed and average muscle weights were similar between WT and NMRK2KOs (figure 5.6B).

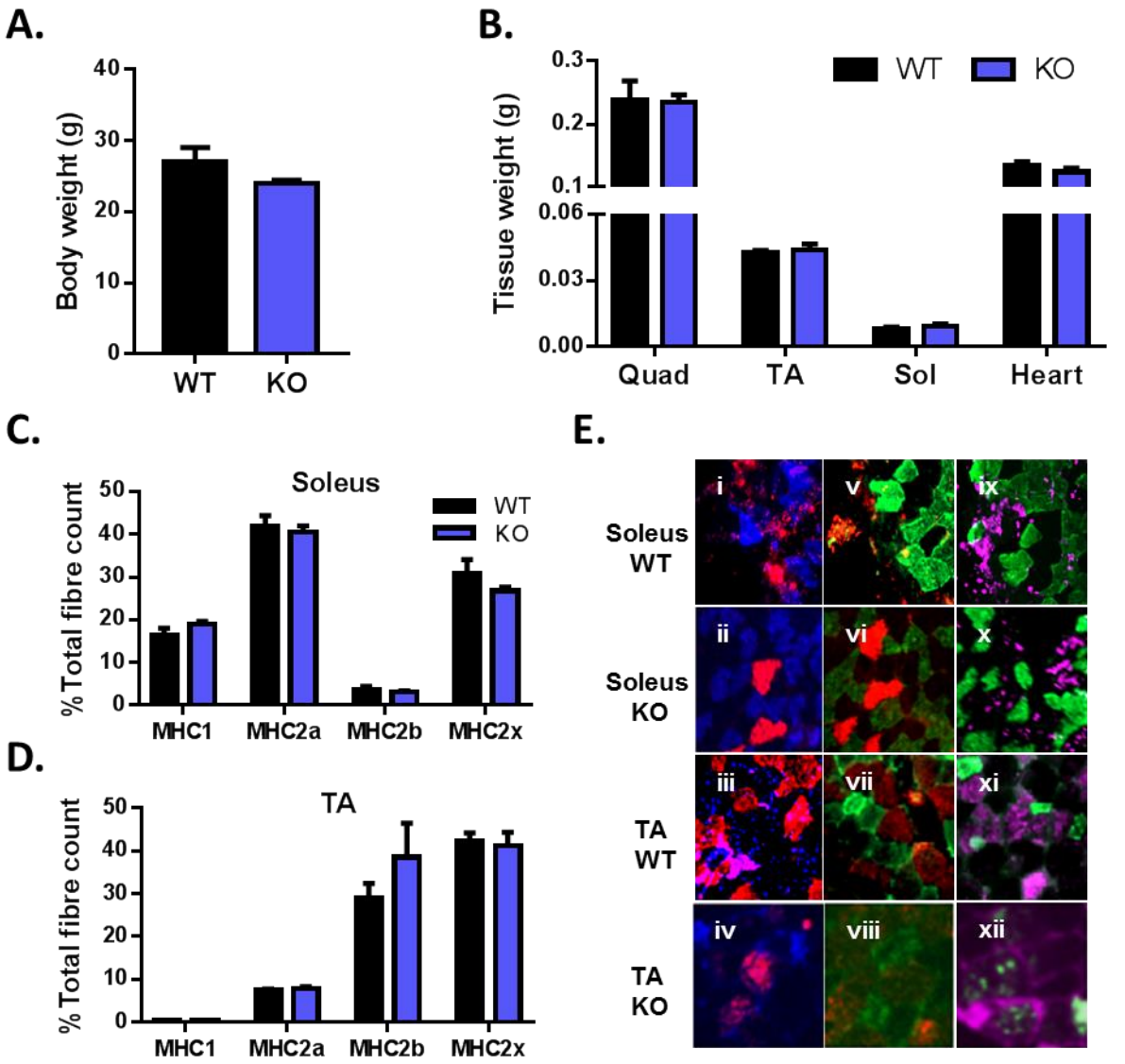

Figure 5.6 NMRK2KO mouse muscle phenotyping following endurance exercise training

(A) Whole body weight and (B) skeletal and cardiac muscle bed weight of WT and NMRK2KO mice following 6 weeks of endurance exercise training. Fibre-type composition of (C) soleus and (D) TA skeletal muscle from WT and NMRK2KO mice following 6 weeks of endurance exercise training. (E) Corresponding representative images of MHC expression. Cross section (i-iv) incubated with BA-F8 and BF-F3 (CK1a) showing MHC I (blue) and IIB (red) expressing fibres. Cross section (v-viii) incubated with SC-71 and BF-F3 (CK1b) showing MHC IIA (green) and IIB (red) expressing fibres. Cross section (ix-xii) incubated with SC-71 and 6H1 (CK2) showing MHC IIA (green) and IIX (purple) expressing fibres. All data n=3, females and presented as mean ± SEM.

Muscle fibre typing by immunofluorescence was employed to examine potential differences to muscle fibre composition. As expected, TA muscle had a larger proportion of type 2b and 2x fibres with minimal type 1 and 2a fibres, whereas oxidative soleus tissue exhibited much larger proportions of type 1 and 2a fibres (figure 5.6C and D). NMRK2KO fibre type composition was consistent with WT following endurance exercise (figure 5.6 C and D); indicating that NMRK2 is not an essential gene in regulating fibre type composition. Representative images of WT and KO soleus and TA muscle fibre typing are provided (figure 5.6E).

5.5 Discussion

The muscle specificity and conserved nature of NMRK2 across species implicates a role for it in skeletal muscle function [142]. Data presented in this thesis has determined its role in NAD^+ biosynthesis to be minimal under basal metabolism with NAMPT activity crucial for maintaining NAD^+ levels. Therefore, it was postulated that NMRK2 may function in skeletal muscle to support NAMPT activity during metabolic stress when NAD^+ turnover is enhanced through elevated SIRT activity [119, 227]. Skeletal muscle is a highly metabolic tissue and, unlike liver tissue which has numerous routes to NAD^+ [139, 166], it appears to be predominantly reliant on NAMPT activity. This chapter investigates the metabolic phenotype of NMRK2 deficient mice *in vivo* in response to metabolic interventions to evaluate a possible role for NMRK2 in NAD^+ salvage when NAMPT activity is maximal.

Cohorts of mice were investigated following either overnight fasting, HFD feeding or endurance exercise. NMRK2KO mice assumed normal activity as compared to WT following the interventions and showed no major signs of metabolic impairment. Absence of major phenotypical abnormalities in NMRK2KO mice following metabolic stress was unsurprising considering the lack of changes to mouse behaviour, NAD^+ signalling and energy metabolism detected under basal conditions. This indicates that NAD^+ signalling is sufficient during metabolic stress to support energy homeostasis. The robust nature of NAD^+ signalling *in vivo* has been demonstrated in muscle specific NAMPT KO mouse models where young mice exhibit a relatively mild phenotype considering the large loss of NAD^+ [76].

Interestingly, there were some indications NMRK2 deficient mice were more metabolically impaired than WT by high fat diet induced obesity. Although WT and NMRK2 mice were equally hyperglycaemic, NMRK2 mice appeared slower at clearing glucose following GTTs suggesting increased insulin resistance. An insulin tolerance test would be a useful follow up test to determine insulin sensitivity of WT and NMRK2KOs. A downward shift in RER was also seen in NMRK2KO mice during night time activity periods. RER is defined by the volume of CO_2 generated divided by the volume of O_2 used and can be used as an estimate of the respiratory quotient (RQ). A RQ of 1 indicates pure carbohydrate metabolism whereas a RQ of 0.7 indicates pure fatty acid oxidation. This theory is based on a larger amount of oxygen needed to fully metabolised fatty acids in comparison to glucose [269]. During wake periods glucose metabolism is normally favoured and fat oxidation favoured during fasted sleep periods [270]. However, diets with a high fat content lead to enhanced fat oxidation [271, 272]. Therefore, these data suggest that NMRK2KO mice are more metabolically inflexible than WT, and are more reliant on fat oxidation. The shift is likely to be related to the reduced food intake seen by NMRK2KO mice whereby fat stores are being mobilised for energy production. Extensive nutritional studies have shown food intake to have considerable impact on RQ [263, 273-275].

The relevance of these metabolic differences in terms of NMRK2 function remains unclear. However, regulation of food intake by the hormone ghrelin has been previously shown to be UCP2 dependent with induction of mitochondrial respiration by UCP2 vital [258]. NMRK2KO mice exhibited upregulated Ucp2 expression in TA muscle and thereby expression may also be altered in neurons; possibly providing a link between NMRK2 and food intake. Furthermore, a recent

study showed, by indirect–calorimetry, that metabolic flexibility was significantly improved in mice fed an obesogenic diet when NR (30 mg/kg) was supplemented; a finding that was not found in mice fed a balanced diet [276]. This again indicates that NMRK salvage of NR to NAD^+ may be important for maintaining metabolic health and may also be a useful therapeutic strategy against to metabolic disruption.

Previous studies have shown that exogenous NR, metabolised to NAD^+ by NMRK activity, can protect against the effects of high fat diet induced obesity and diabetes [178, 199]. Although, skeletal muscle NMRK activity may be limited by NR availability, it is possible that endogenous NR can be generated and delivered from other tissues *in vivo* and used in muscle during metabolic decline. Thus, NMRK2KO mice are unable to use NR as an alternative NAD^+ source leading to further metabolic disruption. As the HFD feeding was a pilot study the 'n' numbers for each genotype were limited (WT= 6, KO= 9), and some mice were removed from the study before analysis due to skin sores. Consequently, statistical significance for GTTs and indirect calorimetry was not reached. Further biological replicates are now required to determine statistical significance before commencing new mechanistic studies to investigate the metabolic differences indicated here.

Mitochondrial function of muscle fibres from NMRK2KO mice did not appear impaired compared to WT after HFD. However, these findings must be confirmed by repeated analysis. In exchange for high resolution respirometry, Oroboros technology is low throughput with only 2 chambers to run just 2 samples per experiment. Consequently, samples had to be run at different times post-harvest,

introducing greater amounts of variability and the possibility of diminished viability of the myofibres analysed after longer periods of time post collection.

Skeletal muscle metabolic adaptation to exercise has shown to be dependent on NAMPT; with increased recycling of NAM to NAD^+ to support SIRT activity [227]. In muscle specific NAMPT loss of function mice, treadmill exercise performance progressively deteriorated with age compared to age-matched WTs [76]. Despite, its high expression in muscle the impact of NMRK2 activity during exercise-induced metabolic adaptation has not previously been investigated. Initial data from the pilot endurance exercise study did not determine any effects of loss of NMRK2 function on exercise performance, muscle size (by weight) and fibre type composition. This indicates that NMRK2 is not vital for exercise-induced metabolic adaptation and fibre type 'shifting', however further molecular analysis of tissues is required. Due to the terms of the Home Office licence, the mice here were trained to a set amount of exercise and not run to exhaustion. It is possible that performance differences may have been seen between WT and KO mice if they were exercised to their limits.

Interestingly overnight fasting resulted in significant downregulation of Nmrk2; yet in numerous models of muscle damage and myopathy Nmrk2 expression is greatly upregulated [277-280]. Loss of NMRK2 function appears to have little effect on muscle metabolism and development; which poses new questions of why NMRK2 is so heavily regulated by these different scenarios and what factors are involved in its regulation. It may be that the sole function of NMRK2 is to salvage NR to NAD^+, with regulation of NMRK2 expression a previously important response mechanism to metabolic stress to drive NAD^+ biosynthesis in skeletal

muscle. Alternatively, changes to modern day diets and food processing may have led to wide spread NR deficiency, effectively making NMRK2 activity redundant [281]. If this was to be the case, then a major positive outcome of this understanding is that NR supplementation, to drive NMRK mediated NAD^+ biosynthesis, could be an extremely useful tool for protecting against metabolic disease, particularly with NAMPT depletion during age-related metabolic decline [174]. Oral bioavailability of NR has been recently demonstrated and although clinical studies with NR are in their infancy currently no major adverse effects have been determined [201].

Alternatively, regulation of Nmrk2 in response to muscle injury and during differentiation may implicate a function in muscle regeneration [277, 280]. The importance of this function would unlikely be noticed in young healthy mice but may be more apparent in aged, sarcopenic muscle. Skeletal muscle is enriched with satellite cells and, with the right cues, it has a great capacity to regenerate [11]. Zebrafish models of Nrk2b deficiency (orthologue of Nmrk2) support a role for Nmrk2 in muscle development. They show Nrk2b is essential for correct formation of cell matrix adhesion complexes and Nrk2b deficient zebrafish exhibit abnormal muscle development due to incorrect laminin polymerisation [252]. This phenotype can be rescued with exogenous NAD^+ highlighting that the NAD^+ salvage function of Nrk2b is critical [252]. Further evidence supporting an important function for Nrk2b in zebrafish muscle health was seen in models of dystrophy. Nrk2b mediated NAD^+ biosynthesis following vitamin b3 supplementation led to repressed muscle fibre degeneration in dystrophic zebrafish embryos [173]. The most likely reason this more extreme phenotype is not seen in mice is because NAMPT salvage predominates. Again, this further implicates NMRK2 as an

important target to promote muscle health particularly if NAMPT function is compromised.

These initial *in vivo* studies of NMRK2KO mice are the first to investigate the role of NMRK2 following metabolic challenge. Despite NMRK2 deficient mice displaying no gross abnormalities these studies do indicate some metabolic impairment. The criticality of NAD^+ for energy production and metabolism necessitates robust signalling with immense redundancy capable of withstanding metabolic stress [32, 66, 86, 145]. Thus, even with metabolic challenge NAMPT activity, and possibly NMRK1 redundancy, are still able to maintain adequate NAD^+ turnover. It may be the true importance of NMRK2 in skeletal muscle is uncovered in models of NAMPT deficiency such as during ageing [169, 174].

Chapter 6 Final discussion

NAD^+ is now widely recognised as a central mediator of energy metabolism. Skeletal muscle is a highly plastic metabolic tissue that can adapt in response to metabolic stress to maintain energy homeostasis [1, 26, 239]. The growing global ageing population means sarcopenia has become a major public health issue, with a degenerative loss of muscle mass and function not only leading to muscle weakness but also negatively impacting on systemic metabolic health [182, 184].

Aberrant NAD^+ signalling has been associated with several pathophysiological states [76, 89, 99, 169, 170], and initial examination of young versus aged mouse muscle tissue identified a decline in NAD^+ and ATP, supporting previous research associating perturbed NAD^+ and energy metabolism in ageing [130, 174].

Numerous therapeutic strategies targeting NAD^+ signalling have been employed to prevent or improve metabolic decline [170, 178, 199, 229, 242]. The positive health effects of NAD^+ enrichment following precursor supplementation have now been widely studied in disease settings [158, 169, 199, 200, 204, 205, 207, 226, 282-284]. Treatment with NA derivative acipimox increased mitochondrial metabolism yet its therapeutic potential is limited due to adverse effects leading to poor patient compliance [196]. Recent research by Zhang et al. has already shown encouraging therapeutic potential of repleting NAD^+ directly in skeletal muscle. They showed that NR treatment revitalized muscle stem cells in aged mice and improved mitochondrial function, and in mouse models of muscular dystrophy, NR increased muscle fibre regeneration through reactivation of senescent muscle stem cells [266].

With the mounting evidence supporting the notion that enhancing NAD^+ availability has health benefits in the context of the chronic diseases of ageing, and the

possibility of doing so by supplementation with readily available NAD^+ precursor vitamin B3s [86, 169, 170, 229, 284]; it is necessary to determine the importance of the different NAD^+ salvage enzymes in tissues to target NAD^+ biosynthesis. Thus, this thesis explored NAD^+ salvage and biosynthesis in skeletal muscle, as a major metabolic target tissue in the context of healthy ageing, and focussed in on identifying the role of the NMRKs as regulators of NR conversion to NAD^+ [142].

NAD^+ biosynthesis in skeletal muscle appears restricted to two main salvage pathways involving the rate-limiting enzymes NAMPT, NMRKs and NMNAT. While NAMPT and, to a degree NMRK1, display ubiquitous expression; NMRK2 displays a muscle restricted pattern. *De novo* NAD^+ biosynthesis and the Preiss-Handler NA salvage pathway play a minimal role in skeletal muscle with limited or undetectable levels of expression of rate limiting enzymes and metabolites. This supports previous metabolic enzyme activity profiling that demonstrated undetectable NAD synthase activity in skeletal muscle – the final rate limiting enzyme for both *de novo* biosynthesis and NA salvage [147].

Inhibition of NAMPT enzymatic activity leads to severe NAD^+ depletion that ultimately leads to cell death, identifying its vital role in muscle metabolism. These findings support recent studies by Frederick et al. (2016) that showed NAMPT to be vital for skeletal muscle NAD^+ biosynthesis using a muscle specific loss of function mouse model. They found an 85% reduction in muscle NAD^+, impaired mitochondrial function, loss of fibre integrity and muscle strength and performance over age; delineating the importance of NAMPT for local NAD^+ turnover and muscle health and metabolism [76].

Although NAMPT is a critical regulator of basal NAD^+ biosynthesis [227], exogenous NAM appears to be a poor precursor for NAD^+ boosting in muscle cells compared to NR and NMN which can significantly increase NAD^+ when supplemented even with FK866 induced NAD^+ depletion.

Considering the ability of NR to increase NAD^+, the role of the NMRKs was examined in skeletal muscle. Despite highly specific expression of NMRK2 in skeletal muscle, NMRK2 loss of function has no effect on basal NAD^+ turnover in muscle tissue. Analysis of NMRK1KO and DKO models showed there was no enzyme redundancy effect with basal NAD^+ content unchanged in all the loss of function models. Characterisation of the loss of function mice did not identify adverse NAD^+ signalling or indicate any major impairment to muscle health and metabolism. HFD diet induced metabolic decline did identify some possible metabolic impairment in NMRK2KO mice but the significance and biological relevance of these are yet to be determined. Together these data indicate that the NMRKs are not critical regulators of basal NAD^+ turnover in muscle and are not essential for muscle development and metabolism.

Findings from loss of function myotube models confirmed that NR is exclusively metabolised by the NMRK enzymes in skeletal muscle; with no change to cellular NAD^+ levels in DKO primary myotubes following NR supplementation. The cellular consequences of NAD^+ depletion by NAMPT fully demonstrate the criticality of maintaining sufficient NAD^+ levels and implicate a potential supporting role by NMRKs to maintain NAD^+ during metabolic or cellular stress. This role is however restricted to NR availability in skeletal muscle. Upon exogenous NR supplementation and thereby increasing precursor availability, NMRK-mediated

NAD^+ biosynthesis can restore the consequences of NAD^+ depletion and greatly enhance NAD^+ content.

The natural availability of NR in the diet [192], and its ability to restore and boost cellular NAD^+ pools, makes NMRK salvage a promising therapeutic target particularly during physiological decline, such as ageing, where NAD^+ content and NAMPT expression have been shown to be mutually reduced [89, 174]. Exercise studies to enhance both NAMPT and NAD^+ following age-related metabolic decline have indicated that preserving NAD^+ signalling can help prevent impaired energy metabolism [174]. Unlike NAMPT, basal NAD^+ turnover is not reliant on NMRK activity and its restriction by cellular NR availability provides a great amount of scope for exogenous NR supplementation to drive NMRK activity and augment NAD^+.

Despite, the ability of NR to rescue the consequences of FK866-mediated NAD^+ depletion and some of the effects of metabolic challenge *in vivo* [178, 199], data presented here suggests that enhancing NAD^+ availability in skeletal muscle by NR supplementation does not stimulate NAD^+ signalling or enhance oxidative metabolism of 'healthy' muscle cells. This data supports work whereby muscle NAD^+ content was enhanced using a muscle specific NAMPT overexpressing mouse model; despite a 50% increase in NAD^+, mitochondrial biogenesis and function was not found to be enhanced in young mice [240]. Nonetheless, these data support the notion that muscle has certain redundancy in its ability to metabolise NR and therefore NMN. Oral NR administration to humans has recently been demonstrated to be effective in boosting circulating and hepatic NAD^+ levels, and evidence of NR exerting a greater effect than equimolar amounts

of NAM and NAD^+ [201]. Interestingly in mice, chronic supplementation of NR in drinking water had minimal impact on skeletal muscle NAD^+ levels despite NR resulting in part recovery of a loss of NAD^+ phenotype [76]. Following this, acute oral supplementation with labelled NR (200 mg/kg) was shown to reach the liver and contribute to NAD^+ turnover, yet in muscle tissue, only a small fraction of labelled NR was detectable. The label pattern indicated that the majority of supplemented NR was broken down and resynthesized to NAD^+ rather than being incorporated intact. This was further supported by large increases to circulating NAM levels, trace levels of NR and unchanged NMN. Together this suggests poor delivery of NR to muscle in vivo [76]. Further work is required to determine the importance of effective muscle NAD^+ repletion via NR and NMN in the context of the NMRKs.

It was initially postulated that NMRK2 would contribute to a greater degree than NMRK1 in skeletal muscle NR salvage, due to its predominant muscle specific expression, yet the findings here showed that although NMRK2 can mediate NR salvage, NMRK1 may play a more prominent role. Data presented here point to NMRK1 being a more critical gate keeper for NR and NMN salvage and point to NMRK2 having an additional role in cellular metabolism involving NR phosphorylation. Indeed, the notion that Nmrk2 is regulated by low NAD^+ may show it to be more important for switching to NR/NMN metabolism during stress responses.

The absence of a gross NAD^+ relatable phenotype in young mice may not be unexpected given the NAMPT MKO mice are viable and without major abnormalities when young despite great loses to NAD^+ and ATP [76]. This does

pose the question as to the role of NMRK2. The highly conserved nature of the NMRKs across species and the greatly responsive regulation of NMRK2 during cellular and metabolic stress highlight an importance for NR metabolism [167, 277, 280]. Like NAM, NR can be metabolized in the gut from NAD^+ found in the food we eat [171]. Existence of NR in the circulation is key in terms of its use exogenously; with NR availability indicated by the residence of pathogens that rely on exogenous NR for NAD^+ biosynthesis to survive in humans such as Haemophilus influenza [285].

NMRK2 may have a role in NAD^+ biosynthesis during metabolic decline or possibly an alternative role distinct from NAD^+ signalling. The enriched expression of NMRK2 in glycolytic TA muscle again provides an interesting fibre-type expression pattern that may have metabolic relevance; yet fibre-typing of NMRK2KO muscle showed no abnormality to fibre-type distribution or morphology. Further mechanistic work is now required to understand the regulation of NMRK2 and whether its highly dynamic modulation is of biological importance or a result of off target regulation during muscle stress responses. Alternatively, this fibre-type specific expression, may implicate a wider metabolic role for NMRK2. Expression is highly regulated during fasting and NMRK2 null mice exhibit a potentially impaired metabolic phenotype following high fat diet induced obesity. Nmrk2 may be part of a transcriptionally regulated metabolic switch dictating carbohydrate (or specifically glycolytic) metabolism over lipid metabolism. For example, Nmrk2 is downregulated during fasting, when energy metabolism is predominantly sourced from lipid oxidation and [273], in keeping with this, HFD fed NMRK2KO mice show lower flexibility to switch from lipid to carbohydrate metabolism. Whereas, expression is enriched in glycolytic TA

muscle, during myotube fusion and injury (or possibly regeneration) [280]; with the latter scenarios when the cell may be more reliant on glycolytic metabolism.

In summary, the data in this thesis demonstrates a limited set of NAD^+ biosynthesis genes in skeletal muscle (figure 6.1). NAMPT-mediated NAD^+ salvage in skeletal muscle is vital. Although NMRK1 and 2 can both salvage NR to NAD^+, this process appears restricted to substrate availability with exogenous delivery leading to enhanced NAD^+. Despite the criticality of NAMPT for maintaining basal NAD^+ turnover, exogenous NAM delivery doesn't not exhibit the same NAD^+ boosting effects of NR and NMN. NAD^+ levels must be tightly controlled for metabolic homeostasis to persist; therefore, NAMPT enzyme activity must be tightly regulated. High NAD^+ results in inhibition of NAMPT enzyme activity (as an immediate regulatory response) and therefore this feedback leaves little scope to boost NAD^+ via NAMPT overexpression or NAM supplementation.

Although not essential to basal NAD^+ metabolism, the NMRKs allow an alternative adaptive route to NAD^+ through the salvage of NR, independent of NAMPT which may be important during age-related metabolic decline where a concomitant reduction to both NAMPT and NAD^+ has been demonstrated [174]. NR can completely restore the effects of NAD^+ depletion via NAMPT inhibition, highlighting that it is solely NAD^+ availability that regulates signalling. Therefore, NR as a naturally available vitamin B3 to enhance NAD^+ could be an extremely useful way to target metabolic decline in skeletal muscle.

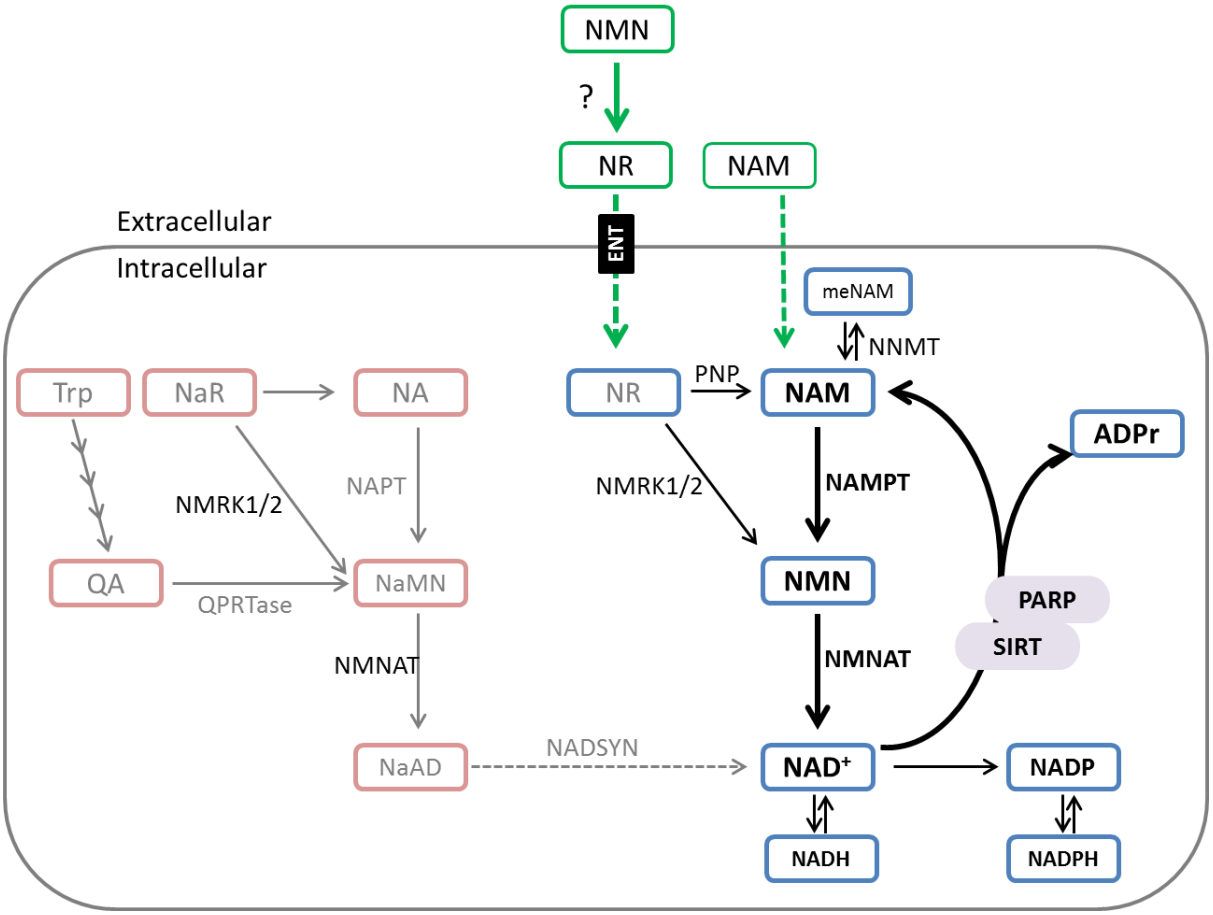

Figure 6.1 Overview of skeletal muscle NAD$^+$ biosynthesis pathways

A schematic of NAD$^+$ biosynthesis pathways in skeletal muscle. The metabolites detectable, and enzymes expressed, in healthy skeletal muscle are outlined in black and/or blue boxes. Recycling of NAM to NAD$^+$ is vital for maintaining basal NAD$^+$ availability. Although NMRK1 and 2 are expressed in muscle, their activity has little influence on basal NAD+ turnover due to limited NR availability. However, delivery of exogenous NR or NMN (in an NMRK dependent manner) can increase basal NAD$^+$ levels to a greater extent than NAM (supplementation strategies outlined in green). The NAD$^+$ biosynthesis enzymes and metabolites thought to play a minimal role in skeletal muscle have been presented in grey and/or red boxes (left).

Appendix A - PCR primer sequences

Primer	Forward	Reverse
Nmrk2 (mouse)	5'-AAACTCATCATAGGCATTGGAGG-3'	5'-TTAGATGGCATGAAGTCCCCG-3'
Nmrk2 WT (mouse)	5'-CCAAATAGCAGTCGGAGAGG-3'	5'-GCAAACTTGTGTGGATCCTTC-3'
Nmrk2 Mutant (mouse)	5'-CGGTCGCTACCATTACCAGT-3'	5'-GGGACATGCCCTCCTATGTA-3'
nmrk1 (zebrafish)	5'-GAAACCCACAGCATCAGAGC-3'	5'-AGGTACATGGGCCAAACGTA-3'
nmrk2 (zebrafish)	5'-CCACCACATCTGACCCTGAT-3'	5'-TCCAAGCTGCTGTTCTCCAT-3'
mibp (zebrafish)	5'-TAAATTTGCTCGCTCCCACG-3'	5'-GGCCACACATGACCATCAAA-3'
mibp2 (zebrafish)	5'-CATTGGTATCGGAGGGGTCA-3'	5'-CCGTGGGATCTCTCGAACTT-3'

The forward and reverse sequences of PCR primers used in this thesis. All primers were made to order from Sigma Aldrich, UK.

Appendix B – Assay on demand TaqMan probes

Gene	Product number
Nmrk1	**Mm00521051_m1**
Nmrk2	**Mm01172895_m1**
Nampt	**Mm00451938_m1**
Nmnat1	**Mm01257929_m1**
Nadsyn1	**Mm00513448_m1**
Ucp2	**Mm00627599_m1**
Tfam	**Mm00447485_m1**
Nrf1	**Mm01135606_m1**
Pparα	**Mm00440939_m1**
Parp1	**Mm01321084_m1**
Pdk4	**Mm01166879_m1**
Sirt1	**Mm01168521_m1**
Sirt3	**Mm00452131_m1**
Pnp	**Mm00840006_m1**
Nt5e (ENT5)	**Mm00501910_m1**
Bst1 (CD157)	**Mm00477672_m1**
Nnmt	**Mm00447994_m1**
Idh2	**Mm00612429_m1**
Pgc1α	**Mm01208835_m1**
Pparδ	**Mm00803184_m1**
MyoG	**Mm00446194_m1**
MyoD1	**Mm00440387_m1**

Appendix C – Immunoblotting antibodies

NAME	Supplier, product #	Dilution	Secondary
Primary Antibody			
NMRK1	BioGenes (Germany)*	1:1000	Anti-Rabbit
NMRK2	BioGenes (Germany)*	1:2000	Anti-Rabbit
NAMPT (PBEF)	Bethyl (USA), A300-372A	1:1000	Anti-Rabbit
α-Tubulin (B-7)	Santa Cruz Biotech. (USA), SC-5286	1:1000	Anti-Mouse
β-Actin	Cell signalling (USA), #12262	1:1000	Anti-Mouse
Total OXPHOS (Mito-profile)	Abcam (UK), ab110413	1:1000	Anti-Mouse
GAPDH	Cell signalling (USA), #2118	1:2000	Anti-Rabbit
Secondary Antibody			
Anti-mouse-HRP	Dako (Denmark), P0161	1:10000	N/A
Anti-Rabbit-HRP	Dako (Denmark), P0448	1:10000	N/A

*Specifically generated by request

Appendix D – LC-MS/MS metabolite parameters

Metabolite	Transition (m/z)	CE[a]	Cone volt.	RT (min)	*k'*	LOQ this study (pmol)[b]
Nam	123 > 96	16	32	9.82	6	0.6
NA	124 > 53	26	32	8.35	5	2.5
Cytidine	244 > 112	18	18	11.14	7	0.01
Uridine	245 > 113	16	18	11.5	7	3.1
NR	255 > 123	12	14	8.98	5.4	0.01
NAR	256 > 124	13	14	10.33	6.4	0.1
Inosine	269 > 137	12	12	12.88	8.2	0.03
CMP	324 > 112	22	16	2.97	1.1	0.09
UMP	325 > 97	12	20	4.11	1.9	0.06
NMN	335 > 123	12	16	8.92	5.4	1
NAMN	336 > 124	12	18	4.2	2	0.06
IMP	349 > 137	22	14	9.65	5.9	0.1
ADP	428 > 136	26	30	10.43	6.5	0.03
ATP	508 > 410	16	30	10.51	6.5	1
ADPr	560 > 348	16	26	11.08	6.9	0.02
NAD^+	664 > 428	26	26	13.64	8.7	0.19
NAAD	665 > 428	24	24	11.89	7.5	0.02
NADH	666 > 649	20	26	12.98	12	0.19
NADP	744 > 604	18	26	12.01	7.6	0.06
NADPH	745 > 729	48	28			

[a]collision energy
[b]LOQ of method described in this paper

Details of metabolite detection parameters and sensitivity for selective reaction monitoring (SRM) as previously established by Trammell et al. With details of ion transitions given as mass to charge ratio (m/z), collision energy (CE) retention time (RT), retention capacity (K') and limits of quantification (LOQ) [224].

Appendix E – Associated Manuscript

Nicotinamide riboside kinases display redundancy in mediating nicotinamide mononucleotide and nicotinamide riboside metabolism in skeletal muscle cells

Original Article

MOLECULAR METABOLISM

Nicotinamide riboside kinases display redundancy in mediating nicotinamide mononucleotide and nicotinamide riboside metabolism in skeletal muscle cells

Rachel S. Fletcher [1,2], Joanna Ratajczak [3,4], Craig L. Doig [1,2], Lucy A. Oakey [2], Rebecca Callingham [5], Gabriella Da Silva Xavier [5], Antje Garten [1,6], Yasir S. Elhassan [1,2], Philip Redpath [7], Marie E. Migaud [7], Andrew Philp [8], Charles Brenner [9], Carles Canto [3,4], Gareth G. Lavery [1,2,*]

ABSTRACT

Objective: Augmenting nicotinamide adenine dinucleotide (NAD^+) availability may protect skeletal muscle from age-related metabolic decline. Dietary supplementation of NAD^+ precursors nicotinamide mononucleotide (NMN) and nicotinamide riboside (NR) appear efficacious in elevating muscle NAD^+. Here we sought to identify the pathways skeletal muscle cells utilize to synthesize NAD^+ from NMN and NR and provide insight into mechanisms of muscle metabolic homeostasis.

Methods: We exploited expression profiling of muscle NAD^+ biosynthetic pathways, single and double nicotinamide riboside kinase 1/2 (NRK1/2) loss-of-function mice, and pharmacological inhibition of muscle NAD^+ recycling to evaluate NMN and NR utilization.

Results: Skeletal muscle cells primarily rely on nicotinamide phosphoribosyltransferase (NAMPT), NRK1, and NRK2 for salvage biosynthesis of NAD^+. NAMPT inhibition depletes muscle NAD^+ availability and can be rescued by NR and NMN as the preferred precursors for elevating muscle cell NAD^+ in a pathway that depends on NRK1 and NRK2. Nrk2 knockout mice develop normally and show subtle alterations to their NAD+ metabolome and expression of related genes. NRK1, NRK2, and double KO myotubes revealed redundancy in the NRK dependent metabolism of NR to NAD^+. Significantly, these models revealed that NMN supplementation is also dependent upon NRK activity to enhance NAD^+ availability.

Conclusions: These results identify skeletal muscle cells as requiring NAMPT to maintain NAD^+ availability and reveal that NRK1 and 2 display overlapping function in salvage of exogenous NR and NMN to augment intracellular NAD^+ availability.

Keywords Skeletal muscle; NAD^+; Energy metabolism; Nicotinamide riboside

1. INTRODUCTION

Nicotinamide adenine dinucleotide (NAD^+) was first described as a vital cofactor in cellular redox reactions important to cellular energy metabolism [1,2]. NAD^+ also serves as a consumed substrate for enzymes such as sirtuins that post translationally modify proteins by deacetylation, yielding nicotinamide (NAM) and 2′-and 3-O-acetyl-ADP ribose in the process [3]. Sirtuins have been characterized as regulatory sensors that coordinate metabolic and transcriptional adaptations to cellular and tissue energy requirements [4,5].

Skeletal muscle requires a high turnover of ATP to sustain contraction, facilitated by glycolysis and oxidative phosphorylation, which depend on the redox functions of NAD^+ [6]. Because of the activity of NAD^+ consuming enzymes, replenishment of NAD^+ through biosynthesis and salvage pathways is vital [7,8]. NAD^+ can be synthesized de novo from tryptophan and by salvage of nicotinic acid (NA), a form of vitamin B3, via the Preiss-Handler pathway [9,10]. Along with NA, nicotinamide (NAM) is also called vitamin B3 (collectively termed niacin) and as a nutrient or by recycling following NAD^+ consumption, is metabolized by nicotinamide phosphoribosyltransferase (NAMPT) to nicotinamide mononucleotide (NMN), which is converted to NAD^+ via NMN adenylyltransferases (NMNAT) [11]. A final route to NAD^+ is the salvage and phosphorylation of the recently discovered form of vitamin B3 nicotinamide riboside (NR) to NMN, through the nicotinamide riboside

[1]Institute of Metabolism and Systems Research, 2nd Floor IBR Tower, University of Birmingham, Birmingham, B15 2TT, UK [2]Centre for Endocrinology, Diabetes and Metabolism, Birmingham Health Partners, Birmingham, B15 2TH, UK [3]Nestlé Institute of Health Sciences (NIHS), Lausanne, CH-1015, Switzerland [4]Ecole Polytechnique Fédérale de Lausanne, Switzerland [5]Section of Cell Biology and Functional Genomics, Department of Medicine, Imperial College London, London, W12 0NN, UK [6]Leipzig University, Hospital for Children and Adolescents, Center for Pediatric Research, Liebigstrasse 19-21, 04103, Leipzig, Germany [7]Mitchell Cancer Institute, 1660 Springhill Avenue, Mobile, AL, 36604, USA [8]School of Sport Exercise and Rehabilitation Sciences, University of Birmingham, Edgbaston, Birmingham, B15 2TT, UK [9]Department of Biochemistry, Carver College of Medicine, University of Iowa, Iowa City, IA, 52242, USA

*Corresponding author. Wellcome Trust Senior Research Fellow, Institute of Metabolism and Systems Research, University of Birmingham, Edgbaston, Birmingham, B15 2TT, UK. Fax: +44 121 415 8712. E-mail: g.g.lavery@bham.ac.uk (G.G. Lavery).

Received May 5, 2017 • Revision received May 22, 2017 • Accepted May 24, 2017 • Available online xxx

http://dx.doi.org/10.1016/j.molmet.2017.05.011

kinase 1 and 2 (NRK1 and 2) pathway [2,12,13]. Despite mammalian cells demonstrating pathway diversity for maintaining NAD^+ levels in various tissues, the relative contribution of these pathways to NAD^+ biosynthesis in skeletal muscle remained unclear. The metabolic benefits of augmenting muscle NAD^+ availability is being realized through the application of NAD^+ precursor supplementation strategies. Historically, NA and NAM supplementation has been used to treat hypercholesterolemia and pellagra [14]. However, undesirable side effects in humans have limited their utility. NA causes flushing through activation of the GPR109A receptor in a large proportion of patients, leading to poor compliance [15]. Large doses of NAM are required to increase NAD^+ leading to adverse effects and NAM mediated inhibition of sirtuin activity [16,17]. The NA derivative Acipimox has shown the potential of using NAD^+ precursors to improve and enhance mitochondrial function and ATP content of skeletal muscle in the context of diabetes [15].

NMN and NR have emerged as NAD^+ precursors with the potential to circumvent the adverse side effects associated with high dose niacin and augment NAD^+ synthesis and sirtuin activity [18]. NMN, being an intermediate of NAD^+ biosynthesis, has been used to successfully ameliorate a number of pathological scenarios, including normalization of glucose tolerance in diet induced diabetes [19], and is able to restore mitochondrial function in aged muscle [20,21]. Dietary supplementation of NR in mice can negate the metabolic consequences of high fat diet and increase oxidative performance [22], delay disease progression in mice with mitochondrial myopathy, inducing sirtuin dependent mitochondrial biogenesis and the mitochondrial unfolded protein response [23]. In addition, NR improves glycemic control and opposes development of diabetic neuropathy in mice and allows rats to resist development of chemotherapeutic neuropathy [24,25]. Importantly, NR has been shown to safely elevate human NAD^+ metabolism [26].

NAD^+ precursor utilization pathways in muscle require further definition. Naturally available NR is phosphorylated to NMN by the NR kinases (NRKs encoded by *Nmrk1* and *2*) [12,27], highly conserved enzymes, but little is known of their roles in skeletal muscle [12]. It is unclear whether NMN is truly available to muscle as an intermediate of NAD^+ biosynthesis or is dependent on NRKs as a consequence of extracellular metabolism to NR prior to cellular uptake and incorporation into the cellular NAD^+ pool [28]. Here we investigate NRK expression in skeletal muscle and define the influence of NRKs on NR and NMN metabolism to NAD^+ in loss-of-function muscle cells derived from *Nmrk*1 and 2 knockout mice (NRK1KO, NRK2KO). We show that the NRKs have overlapping and redundant activity in muscle cells critical to the conversion of exogenous NR and NMN to NAD^+.

2. MATERIALS AND METHODS

Unless otherwise specified all materials and reagents were acquired from Sigma–Aldrich, UK.

2.1. Animal care

Mice were group housed in a standard temperature (22 °C) and humidity-controlled environment with 12:12- hour light:dark cycle. Nesting material was provided and mice had ad libitum access to water and standard chow. Mice were sacrificed using schedule one cervical dislocation and tissues were immediately. All experiments were in groups of up to 6 and conducted within the UK Home office regulations.

2.2. Generation of NRK loss of function mice

NRK2KO mice were acquired from the Jackson Laboratory. The *Nmrk2* KO mutant allele was generated on a C57BL/6NTac background through the Knockout Mouse Phenotyping Program (KOMP2). A ZEN-UB1 Velocigene cassette (beta-galactosidase coding sequence from E. coli lacZ gene; polyadenylation signal; loxP site; promoter from the human ubiquitin C gene; neomycin phosphotransferase; polyadenylation signal; loxP site) was inserted through homologous recombination into the gene in place of all coding exons inhibiting transcription. Deletion of *Nmrk2* was validated by qPCR and immunoblotting.

NRK1KO mice generated on a C57BL/6NTac background have been previously described [28].

2.3. Exercise and fibre-typing

As a preliminary experiment, mice ($n = 3$) were acclimatized to the treadmill environment and exercised 3 times a week for 1 h at 0.25 M/Sec, at a 10° incline for 6 weeks.

Muscle sections were fiber typed using immunofluorescence following an established protocol [29–31]. Briefly, 10 μm sections were cut using a cryostat and mounted onto slides. Primary antibodies detecting different myosin heavy chain subunits (BA-F8 – MHC1 (1:50), BF-F3 – MHC IIb (1:100), SC-71 (1:600) – MHC IIa, 6H1 – MHC IIx (1:50)) (Developmental Studies Hybridoma Bank, University of Iowa) were added, followed by fluorescent secondary antibodies (IgG AF 647– Blue (1:500), IgM AF 555 – Red (1:500), IgG AF 488 – Green (1:500)). Sections were formalin fixed and mounted and then analyzed using a Zeiss Axio Observer inverted microscope (Carl Zeiss, Germany). Fibers were manually counted across the entire section using Image J (Fiji) software and recorded as positive for each fiber expressing the relevant visible color.

2.4. RNA extraction and qPCR

RNA was extracted from tissue and cells using TRI-reagent (Invitrogen). RNA quality was determined by visualization on a 1.5% agarose gel and quantified using a nanodrop. Reverse transcription was conducted using 500 ng RNA that was incubated with 250 μM random hexamers, 5.5 mM $MgCl_2$, 500 μM dNTPs, 20 units RNase inhibitor 63 units multiscribe reverse transcriptase, and 1× reaction buffer. Reverse transcription was performed using a thermocycler set at the following conditions: 25 °C for 10 min and 37 °C for 120 min before the reaction was terminated by heating to 85 °C for 5 min qPCR was performed in a 384-well plate in single-plex format. Primers and probes were purchased as Assay on Demand (FAM) products (Applied Biosystems). Total reaction volumes used were 10 μl containing Taqman Universal PCR mix (Applied Biosystems). All Ct values were normalized to 18s rRNA (VIC) (Applied Biosystems). The real-time PCR reaction was performed under the following protocol: 95 °C for 10 min, then 40 cycles of 95 °C for 15 s, and 60 °C for 1 min using an ABI7500 system. Data were collected as Ct values and used to obtain deltaCt (dCt) values.

2.5. Western blotting

Protein lysates were extracted from tissues in RIPA buffer (50 mmol/l Tris pH 7.4, 1% NP40, 0.25% sodium deoxycholate, 150 mmol/l NaCl, 1 mmol/l EDTA) and protease/phosphatase inhibitor cocktail (Roche, Lewes, U.K.). Total protein concentration was quantified by Bio-Rad assay. Total proteins (25 μg) were resolved on a 12% SDS-PAGE gel and transferred onto a nitrocellulose membrane. Primary antibodies specific for NRK1/2 were generated and affinity purified by BioGenes (GmbH) Berlin, Germany and used at a 1:2000 dilution. Primary antibodies including NAMPT (Abcam, USA), β-Actin (Cell Signaling, USA, #12262) and α-Tubulin (Santa Cruz, USA, SC-5286) were all commercially available and used at a 1:1000 dilution.

MOLECULAR METABOLISM

Secondary anti-mouse and anti-rabbit antibodies conjugated with HRP (Dako, Denmark) were added at a dilution of 1/10,000. Equal loading of protein content was verified using beta-actin and alpha-tubulin and bands visualized using ECL detection system (GE Healthcare, UK).

2.6. Preparation of tissue fractions

Muscle tissue was homogenized in sucrose buffer (0.25 M sucrose, 20 mM HEPES) and centrifuged at 1000 *g* for 10 min at 4 °C. The supernatant was transferred to a new tube and centrifuged at 12,000 *g* for 10 min at 4 °C. The mitochondrial fraction was pelleted and re-suspended in sucrose buffer and the supernatant was transferred to ultracentrifuge tubes and, following careful balancing, centrifuged at 100,000 *g* for 1 h at 4 °C. The supernatant containing the cytosolic fraction was transferred to a new tube and the pellet was re-suspended in MOPs buffer (100 mM KCl, 20 mM NaCl, 1 mM MgCl2, 20 mM MOPs) and washed 3 times by pelleting at 100,000 *g*. The microsomal pellet was re-suspended in MOPs buffer and snap frozen.

2.7. Primary muscle culture

Gastrocnemius tissue was excised from hind limbs of mice and digested in DMEM with 0.2% collagenase at 37 °C for 2 h. Digested tissue was washed in DMEM, and media was expelled vigorously onto the muscle to allow single myofibers to detach. Myofibers were then placed in pre-set matrigel (BD biosciences) coated wells in DMEM supplemented with 30% (v/v) FCS, 10% (v/v) HS, 1% (v/v) P/S, 2 mM L-glutamine, 1% (v/v) chick embryo extract (CEE) (Seralab, UK), and 0.1% of fibroblast growth factor (FGF) (Peprotech). Following satellite cell migration, media was replaced with proliferation media (DMEM with 10% (v/v) HS, 1% (v/v) P/S and 0.5% (v/v) CEE). Upon 70–80% confluence, media was replaced with Differentiation media (DMEM supplemented with 2% (v/v) HS, 0.5% (v/v) CE,E and 1% (v/v) P/S) and cells were differentiated for 6 days.

2.8. Cell treatments

Cells were treated in serum free media with 1 μM FK866 or DMSO as a vehicle control for 24, 48 or 72 h. Cells were supplemented with 0.5 mM NR (ChromaDex, USA), 0.5 mM NAR, 0.5 or 5 mM NAM and 0.5 mM NMN for 24 h. A concentration of 0.5 mM for cell treatments was used to provide a maximal effect on cellular NAD^+ content following preliminary dose response experiments and previously published work in myotubes [22].

2.9. NAD^+ measurements

2.9.1. NAD^+ by cycling assay

NAD^+ was extracted from primary myotubes and quantified using EnzyChrom NAD/NADH Assay kit (BioAssay Systems) according to the manufacturer's instructions.

2.9.2. NAD^+ by HPLC

Total NAD was measured by reversed-phase HPLC using the Chromaster Purospher STAR RP-18 endcapped 3 μm Hibar RT 150-3 HPLC column (Merck). Frozen mouse muscle tissue (10 mg) was lysed in 100 μl 1 M perchloric acid. Samples were incubated on ice samples for 10 min, centrifuged and the supernatant was neutralized with 3 M potassium carbonate. After repeated centrifugation, samples were analyzed as previously described [32].

2.10. Targeted NAD^+ metabolomics

20 mg of pulverised tissue samples were placed in Eppendorf tubes on dry ice. Metabolites were extracted in 0.2 ml of ice cold LCMS grade methanol and kept on ice before adding 300 μl of internal standard (diluted 1:300 in LC-MS grade water). Samples were briefly sonicated in an acetone water bath (at −4 °C), returned to ice, and then incubated at 85 °C for 5 min, shaking at 1050 rpm. Samples were cooled on ice for 5 min and centrifuged. Supernatant was dried using a speed vacuum. The dried extract was resuspended in 40 μl of either LC-MS grade water for acid extract or 10 mM ammonium acetate for alkaline extract and transferred to a Waters Polypropylene 0.3 ml plastic screw-top vial and analyzed by LC-MS/MS [33] using the ACQUITY UPLC H-class system.

2.11. Respirometry

C2C12 cells were differentiated into fully fused myotubes for 5 days. Respiratory output and mitochondrial stress tests were performed with C2C12 myotubes in XF-Assay media (Agilent Technologies) supplemented with 25 mM glucose, 0.5 mM sodium pyruvate, pH 7.4, maintained for 1 h at 37 °C in 0% CO_2 prior to Seahorse extracellular flux analysis. Extracellular flux analysis was performed using the Seahorse XF analyser following manufacturer's instructions (Agilent Technologies).

2.12. Cell viability and apoptosis

C2C12 cells were seeded in a 96 well plate and differentiated for 5 days. Cell viability and apoptosis were assessed using the ApoLive-Glo™ multiplex assay (Promega) according to the manufacturer's instructions.

2.13. Statistical analysis

Unpaired Students *t*-test or ANOVA statistical comparisons were made using GraphPad Software Inc. Prism version 6. Data are presented as mean ± SEM with statistical significance determined as * = $P < 0.05$, ** = $P < 0.01$, *** = $P < 0.001$. Statistical analysis of real-time PCR data was determined using dCt values.

3. RESULTS

3.1. NRK2 expression exhibits highly conserved skeletal muscle specificity

NAMPT and NADsyn1 act as rate limiting enzymes in the best characterized mammalian NAD^+ biosynthesis pathways, with NADsyn1 the common final step in de novo synthesis and Preiss-Handler salvage pathways (Figure 1A) [34]. NRK 1 and 2 were more recently identified as NAD^+ salvage enzymes involved in a novel NR dependent route to NAD^+ [12] (Figure 1A). To better understand the roles the NRKs play in the context of the rate limiting enzymes NAMPT and NADsyn1, we examined their expression in a range of tissues to determine tissue specificity.

Using real-time PCR we show that *Nmrk1* is ubiquitously expressed, with particularly high expression in kidney, while *Nmrk2* exhibits high specificity to skeletal muscle (Figure 1B,C). *Nampt* is ubiquitously expressed across different tissue types as previously described (Figure 1D) [35], and *NADsyn1* shows greatest expression in liver and kidney tissue, consistent with previous data (Figure 1E) [36]. Nmnat1, common to all NAD^+ biosynthetic pathways for conversion of NMN to NAD^+, is ubiquitously expressed (Figure 1F). We went on to endorse these findings using Western blot analysis. While low levels of NRK1 are detectable in muscle, it was prominently detected in whole kidney and liver lysates (Figure 1G). For NRK2 we confirmed its muscle specificity. We also confirmed the ubiquitous expression of NAMPT (Figure 1G).

Using previously generated microarray data for soleus and tibialis anterior (TA) skeletal muscle [37], we further evaluated the relative

Original Article

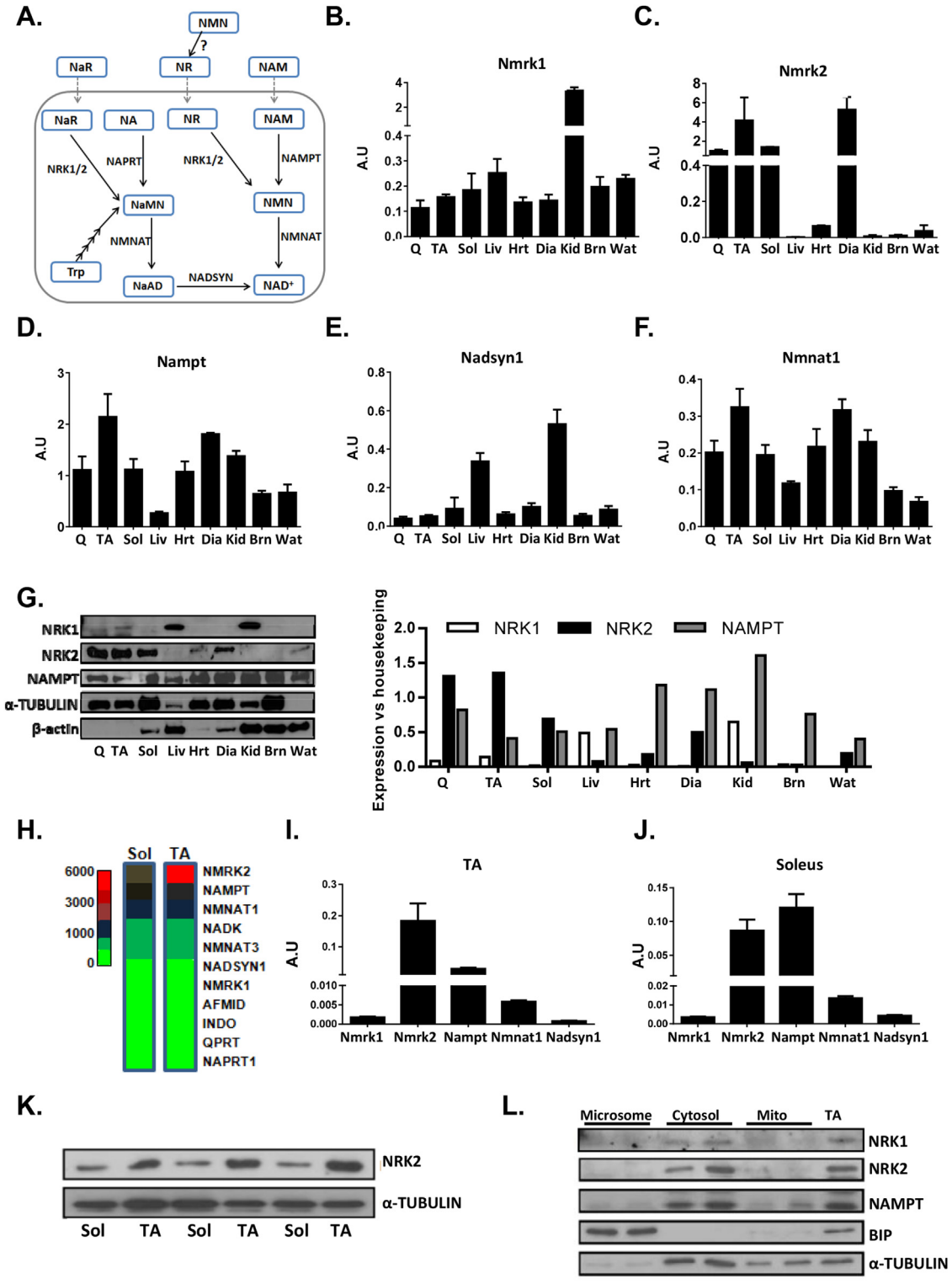

Figure 1: NAD$^+$ biosynthesis pathways in skeletal muscle. (A) An illustration of the known NAD+ biosynthesis pathways identified in mammalian cells with exogenous precursor supplementation strategies illustrated with dashed lines. NAD$^+$ can be synthesized de novo from tryptophan (Trp) and following multiple enzymatic reactions is converted to nicotinic acid mononucleotide (NaMN) and then nicotinic acid dinucleotide (NaAD) by nicotinamide mononucleotide adenylyltransferase (NMNAT) activity, before the final conversion to NAD$^+$ by NAD synthase (NADSYN). NAD+ can be salvaged from precursors nicotinic acid riboside (NaR) and nicotinic acid (NA) by nicotinamide riboside kinases (NRK1/2) and nicotinic acid phosphoribosyltransferase (NAPRT) respectively to NaMN and follow the same final steps. Finally, nicotinamide riboside (NR) and nicotinamide (NAM) are salvaged by NRKs and nicotinamide phosphoribosyltransferase (NAMPT) respectively to nicotinamide mononucleotide (NMN) and finally to NAD$^+$ by NMNAT activity. Real-time PCR mRNA expression of *Nmrk1* **(B)**, *Nmrk2* **(C)**, *Nampt* **(D)**, Nadsyn1 **(E),** and Nmnat1 **(F)** across metabolic tissues. **(G)** Protein expression of NRK1, NRK2, and NAMPT across metabolic tissues with corresponding densitometry compared to housekeeping protein (α-Tubulin for all tissues except liver and Wat which are compared to β-actin expression). **(H)** Microarray of NAD$^+$ biosynthesis genes in tibialis anterior (TA) and soleus (Sol) skeletal muscle tissue (n = 3). Real-time PCR mRNA expression of rate limiting NAD biosynthesis genes in TA **(I)** and soleus **(J)** muscle (n = 4). **(K)** NRK2 protein expression in TA and soleus muscle tissue. **(L)** NRK1, NRK2, and NAMPT protein expression in cytosolic, mitochondrial and microsomal fractions of skeletal muscle. (Q = quadriceps, TA = tibialis anterior, Sol = soleus, Liv = liver, Hrt = heart, Dia = diaphragm, Kid = kidney, Brn = brain and Wat = white adipose tissue).

MOLECULAR METABOLISM

expression of NAD^+ biosynthesis and salvage genes. We identified *Nmrk2*, *Nampt*, and *Nmnat1* as the most abundantly expressed genes in soleus and TA muscle (Figure 1H). We used real-time PCR to confirm these findings and show that *Nmrk2* is the most predominantly expressed NAD^+ biosynthesis gene in fast twitch tibialis anterior muscle compared to slow twitch fibre rich soleus muscle (Figure 1I,J). Western blots of soleus and tibialis anterior muscle lysates corroborated with the mRNA expression analysis, suggesting some muscle beds are enriched with NRK2 (Figure 1K). Finally, we addressed subcellular localization of the NRKs and NAMPT. Following fractionation of skeletal muscle tissue enriched into microsomes, cytosol, and mitochondria we show that NRK2, NRK1, and NAMPT are predominantly localized to cytosol (Figure 1L).

Although the role of NAMPT-mediated NAD^+ biosynthesis has been characterized in skeletal muscle [38,39], the function of NRK1 and NRK2 in particular, given its muscle restricted expression, and their relative contribution to NAD^+ biosynthesis and homeostasis remained ill defined.

To further examine the specific roles of the NRKs, we investigated mRNA and protein expression during C2C12 and primary muscle myotube differentiation. In C2C12 cultures, NRK1 demonstrated low level expression with respect to NRK2, rising to maximal expression at day 8 (Figure 2A,D). In contrast, NRK2 expression was upregulated during differentiation, peaking at day 4 around the time of myotube fusion (Figure 2B,D). NAMPT expression remained constant throughout differentiation (Figure 2C,D). We expanded this analysis to examine primary cultures of muscle cells derived from hind limbs of WT mice as a more physiologically relevant scenario. We used Myogenin (MyoG), Myogenic differentiation 1 (MyoD), and α-actin 1 (ACTA1) as markers of differentiation in our primary system, with all genes displaying anticipated profiles of expression for normal muscle cell differentiation (Sup. 1A). *Nmrk1*, *Nmrk2*, and *Nampt* showed similar patterns of differentiation as seen in C2C12s (Figure 2A—C). In addition, we showed that Nmnat1 is constitutively expressed during primary myotube differentiation (Sup. 1A). These data support the notion of a highly conserved and specific function for NRK2 in skeletal muscle.

3.2. NAD^+ turnover in skeletal muscle is predominantly regulated by NAMPT salvage of NAM, yet NR proves a more valuable precursor for augmenting NAD^+

As the NA Preiss-Handler pathway is mostly restricted to liver NAD^+ biosynthesis and NA treatment is limited due to adverse effects, we aimed to establish the NAD^+ precursors and the pathways that could be used to enhance NAD^+ content in skeletal muscle [15,34]. Metabolic enzyme activity profiling data suggest that the amidated routes to NAD^+, mediated by the NAMPT and NRK salvage pathways, prevail as the main biosynthetic routes to NAD^+ in muscle, which is corroborated by our tissue expression data and molecular analysis [34].

To further assess this, we supplemented primary-derived myotubes with NAD^+ precursors that could be utilized by NRK or NAMPT pathways; NAR (non-amidated version of NR), NR, NMN, and NAM (Figure 1A) and quantified NAD^+ using a cycling assay. NAR, like NR, is metabolized by NRKs to NAMN and then to NAAD by NMNATs [40]. However, NAAD requires final amidation to NAD^+ via NAD synthetase [41]. We found that NAR was unable to augment the NAD^+ pool in muscle cells, whereas both NR and NMN supplementation significantly increased NAD^+ in myotubes by almost 2-fold. However equivalent concentrations of NAM did not significantly enhance NAD^+, with 10-fold excess NAM required to increase NAD^+ (Figure 3A). NAMPT is considered the rate limiting step for NAD^+ salvage and synthesis in skeletal muscle [38] but has not been explored in detail in the context of NRKs. We examined precursor salvage and NAD^+ levels in myotubes treated with the potent NAMPT inhibitor FK866 [42]. NAMPT is indeed essential for basal NAD^+ homeostasis with NAD^+ levels severely depleted (by more than 70%) following 24 h of inhibition. This depletion was completely reversed by NR and NMN supplementation, and both precursors were still able to boost NAD^+ to the same extent as without FK866 treatment confirming that NR and NMN salvage is independent of NAMPT (Figure 3B).

To gain further insight into the activity of NR, we used LC-MS-based targeted quantitative metabolomics. Table 1 shows levels of key NAD^+ metabolites in primary myotubes treated with FK866 and NR. As expected, NAD(H) levels significantly increase following NR supplementation, and, importantly, here we identify a large increase in cellular NR and NMN from control cells 24 h following cell treatments. Interestingly, metabolites of NAD^+ consumption, NAM and ADP ribose (ADPr), were not altered by NR treatment but levels were reduced following FK866-induced NAD^+ depletion, suggesting NAD^+ availability is only rate limiting to NAD^+ signaling below normal levels (Table 1). NA and other metabolites from the Preiss-Handler and de novo NAD^+ biosynthesis pathways were undetected in primary myotubes.

NAD^+ is vital to mitochondrial respiration so we demonstrated the importance of NAMPT for maintaining NAD^+ turnover by treating C2C12 myotubes with FK866 for 72 h. Inhibition of NAMPT significantly reduced basal and maximal respiration, which was fully rescued by treatment with NR for the final 24 h (Figure 3C). NR alone did not enhance mitochondrial respiration above untreated levels (Figure 3C). Concordantly, apoptosis was stimulated in C2C12 myotubes after 48—72 h of NAMPT inhibition. NR supplementation completely prevented this effect (Sup. 1B).

Changes in NAD^+ availability and muscle cell energetics as a result of NAMPT inhibition are known to stimulate elevated rates of NAMPT gene transcription through AMPK activity; however, the effects on NRKs in this context are unknown [43,44]. Using real-time PCR, we show that cellular mRNA expression of NAD^+ salvage genes is tightly regulated by NAD^+ availability. NAD^+ depletion by FK866 resulted in upregulation of *Nmrk2* and *Nampt* and downregulation of *Nmrk1* (Figure 3D). Repletion of NAD^+ by NR supplementation returned mRNA levels of all genes back to that of untreated control and NR treated cells (Figure 3D).

These data demonstrate that NAMPT is crucial for basal NAD^+ biosynthesis. NR supplementation can completely rescue NAMPT inhibition through NRK-mediated NAD^+ salvage. These data suggest that NRK activity is independently capable of maintaining cellular NAD^+ and that NR availability may restrict NRK activity under basal conditions.

3.3. Loss of NRK2 function does not impair skeletal muscle mass or fiber type distribution in young mice

To further elucidate the roles of the NRKs in skeletal muscle NAD^+ salvage, we focused on the muscle-specific importance of NRK2 and have generated a model with constitutive ablation of the *Nmrk2* gene (NRK2KO). NRK2KO mice were born at anticipated Mendelian ratios and displayed no gross abnormalities. No *Nmrk2* mRNA or protein could be detected in any NRK2KO tissue examined, which included a range of skeletal and cardiac tissues (Figure 4A—B). 12—14 week old male and female mice were equivalent to WT control mice in terms of total body weight and lean mass for a range of muscle beds (Figure 4C—D). To induce metabolic stress and examine a role for NRK2 in skeletal muscle metabolic adaption, mice were subjected to an endurance exercise protocol. Again, total body weight and lean mass for a range of muscle beds were unchanged in NRK2KO mice (Figure 4E—F). Assessment of

Original Article

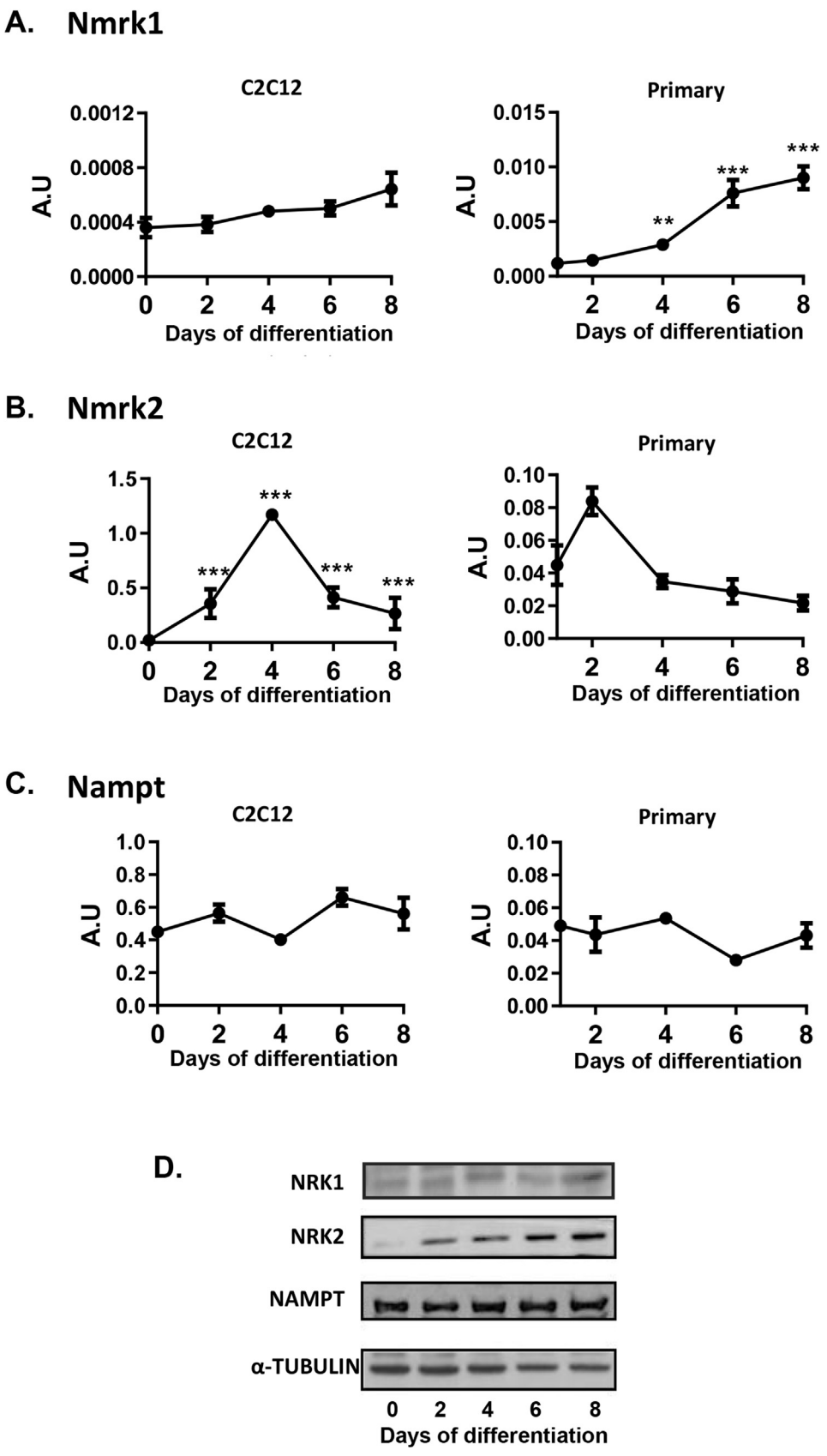

Figure 2: Patterns of NAD$^+$ biosynthesis gene expression during skeletal muscle differentiation and muscle development. 8 day differentiation time course of *Nmrk1* **(A)**, *Nmrk2* **(B)**, and *Nampt* **(C)** mRNA expression in C2C12 and primary myotubes (n = 3–4). 8-day C2C12 myotube differentiation time course of NAD$^+$ biosynthesis enzyme protein expression **(D)**.

MOLECULAR METABOLISM

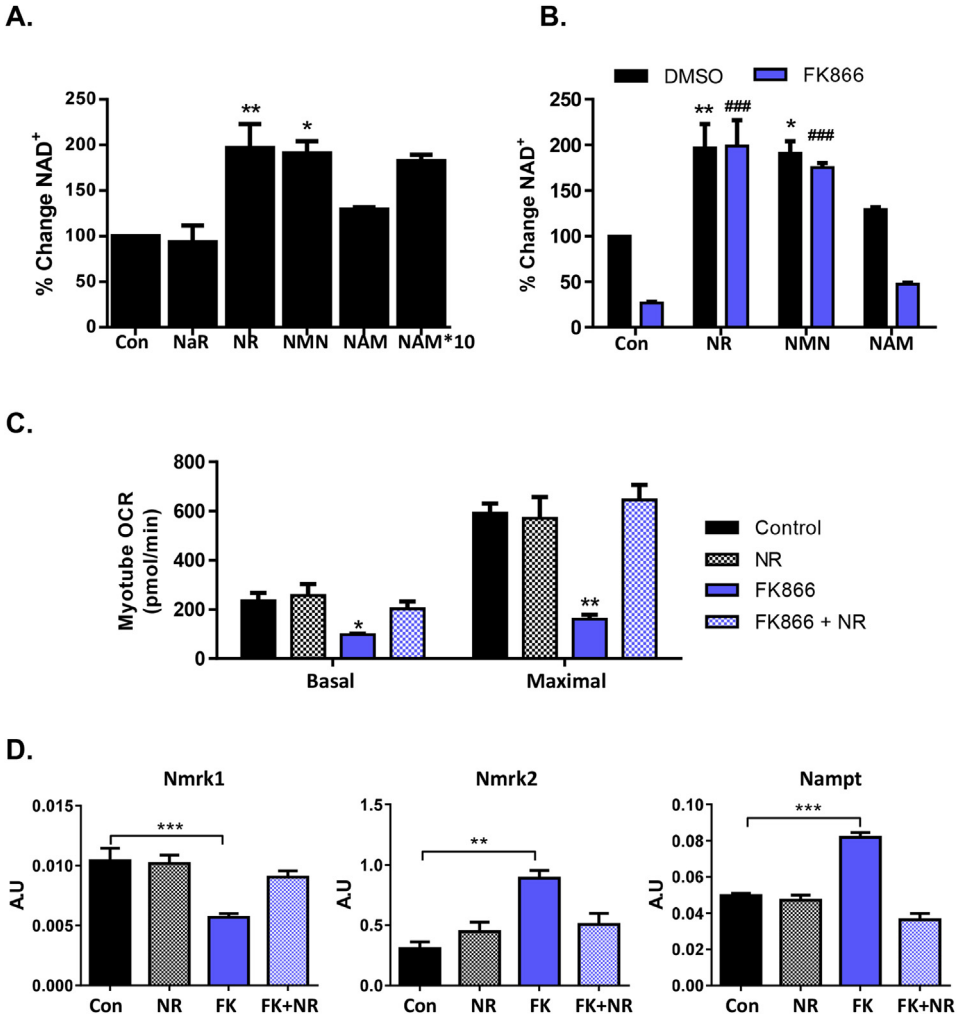

Figure 3: Precursor availability and skeletal muscle NAD$^+$ biosynthesis. (A) Primary myotube NAD$^+$ levels following 24 h 0.5 mM NAD$^+$ precursor supplementation (n = 4) determined using an NAD$^+$ cycling assay. **(B)** Primary myotube NAD$^+$ content following 24 h 0.5 mM NAD precursor supplementation with or without FK866 inhibition of NAMPT (* = significant from DMSO control and # = significant from FK866 treated control) (n = 4) determined using the NAD$^+$ cycling assay. **(C)** Basal and maximal mitochondrial respiration following 24 h NR supplementation with or without FK866 inhibition (n = 3). **(D)** Transcriptional regulation of NAD$^+$ biosynthesis genes, *Nmrk1*, *Nmrk2*, and *Nampt* following 24 h NR supplementation with or without FK866 inhibition of NAMPT (n = 3).

muscle fiber cross-sectional area showed no significant differences in proportions of fibre size in NRK2KO quadriceps compared to WT (Figure 4G). Similarly, muscle fiber type distribution assessed for myosin heavy chains (MHC) MHC1, MHC2a, MH2b, and MHCX in slow twitch rich soleus, and fast twitch rich TA muscle were normal and at expected proportions (Figure 4H–I).

3.4. NRK2 deficiency minimally impacts the skeletal muscle NAD$^+$ metabolome

Recent evidence has shown that NR can elevate muscle NAD$^+$ when administered to mice or cultured cells [22]. To ascertain the effect of NRK2 deficiency on muscle levels of NAD$^+$ and related metabolites we used LC-MS-based targeted quantitative NAD$^+$ metabolomics [33]. This method allows quantification of NAD$^+$ as well as associated metabolites to determine the wider effect loss of NRK2 has on NAD$^+$ metabolism. Surprisingly, NAD$^+$ levels in quadriceps tissue from NRK2KO mice were shown not to be deficient compared to WT control tissue (Figure 5A). The NAD$^+$ precursors NR and NAM were unchanged, but a significant increase in NMN was detected (Figure 5C). Furthermore, no differences in NADP, ATP, ADP, or the NAD$^+$ consumption product ADPr were detected (Figure 5A). To confirm the NAD$^+$ data generated by LC-MS, NAD$^+$ levels were independently measured using a colorimetric cycling assay and by HPLC [32], which

Table 1 — Targeted LC-MS NAD$^+$ metabolome of primary myotubes treated with NR (0.5 mM) and/or FK866 (100 nM).

Metabolites (pmol/mg)	Control	NR	FK866	FK866 + NR
NAD(H)	790.2 ± 54.3	1968.1 ± 518.1*†	253.8 ± 25.7	1564.4 ± 207.6†
NADP(H)	90.5 ± 3.1	186.4 ± 62.1	55.1 ± 23.5	98.4 ± 20.1
NR	4.9 ± 0.6	73.6 ± 9.5*†	9.9 ± 2.0	112.1 ± 11.2*†
NAM	834.2 ± 29.8	1064.2 ± 172.4†	354.1 ± 43.3*	973.1 ± 75.8†
ADPr	535.3 ± 198.4	400.2 ± 54.1	326.6 ± 86	537.5 ± 104.3
NMN	ND	107.9 ± 26.5*†	3.8 ± 0.7	79.6 ± 12.1*†
Na	ND	ND	ND	ND
NaR	ND	1.7 ± 0.2*†	0.1 ± 0.1	1.9 ± 0.2*†
NaAD	ND	14.9 ± 5.6*†	ND	8.4 ± 2
NaMN	ND	ND	ND	ND

*Significant to control, †significant to FK866 treated, n = 3.

Original Article

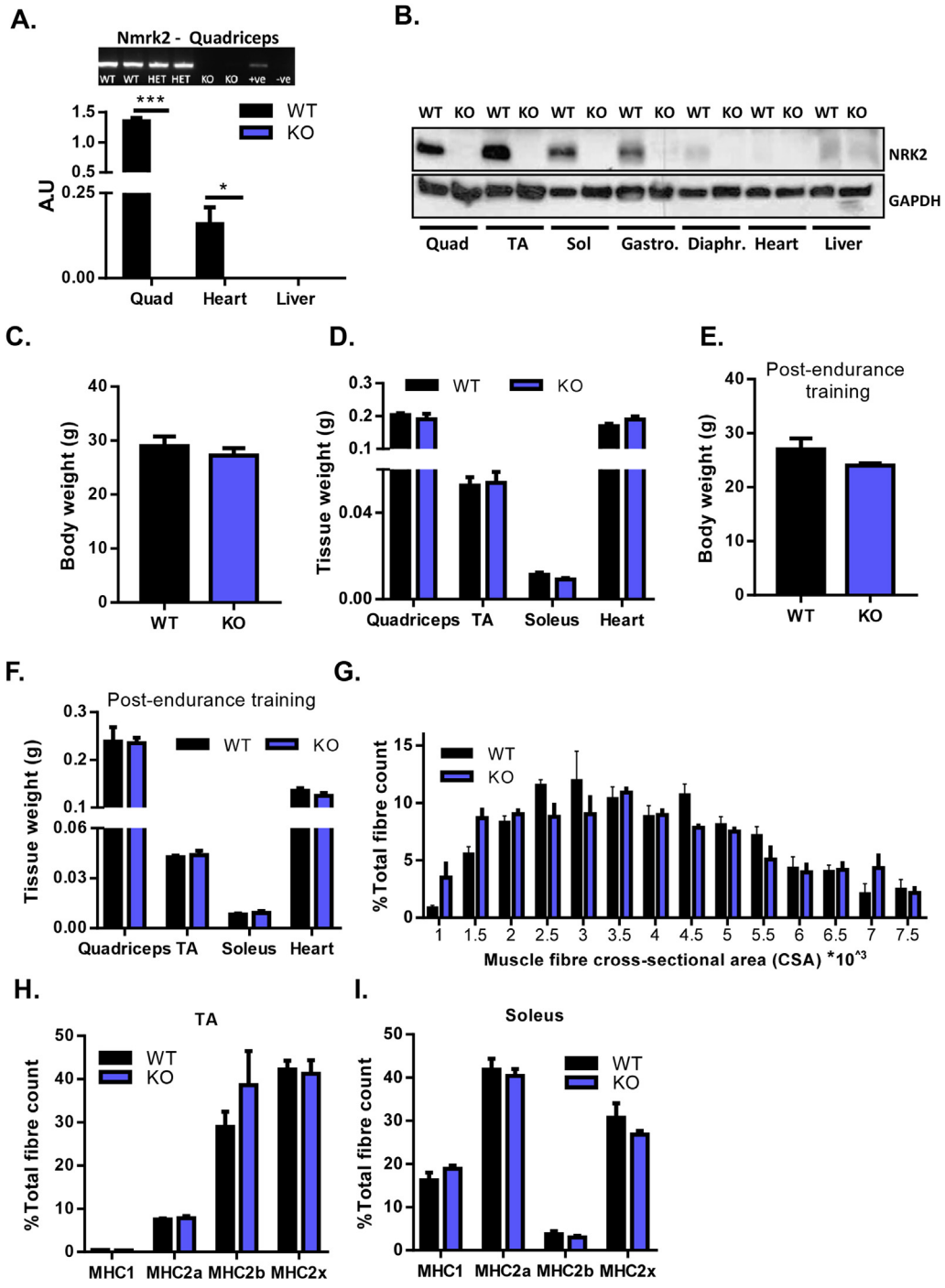

Figure 4: Validation and characterization of NRK2KO mice. (A) mRNA expression of *Nmrk2* in WT and NRK2KO quadriceps muscle, heart, and liver tissue. **(B)** Protein expression of NRK2 across metabolic tissues from WT and NRK2KO mice. **(C)** Whole body weight of 12 week old WT and NRK2KO mice. **(D)** Tissue weight of skeletal and cardiac muscle from 12 week old WT and NRK2KO mice. **(E)** Whole body weight of WT and NRK2KO mice following 6 weeks of endurance exercise training. **(F)** Tissue weight of skeletal and cardiac muscle from WT and NRK2KO mice following 6 weeks of endurance exercise training. **(G)** Muscle fiber cross-sectional area as a proportion of all fibers in WT and NRK2KO quadriceps. Fiber-type composition of TA **(H)** and soleus **(I)** skeletal muscle from WT and NRK2KO mice following 6 weeks of endurance exercise training. (All data n = 3–6).

confirmed that there were no significant alterations to tissue NAD^+ and NADH levels (Sup. 1C–D).

Finally, we examined the expression of key NAD^+ salvage and biosynthetic genes in response to loss of *Nmrk2*. We did not detect any adaptive changes in *Nmrk1* or *Nampt* but did detect increased expression of Pnp (2-fold) and CD157 (4-fold) (Figure 5B). Purine Nucleoside Phosphorylase (PNP) is involved in purine metabolism and has activity to convert NR to NAM [45]. CD157 has NAD^+ nucleotidase activity liberating cADP-ribose and NAM [46]. These adaptive responses in gene expression, to compensate for loss of NRK2 in living mice, may have more long-term consequences for NAD^+ salvage and require further assessment.

MOLECULAR METABOLISM

3.5. NRKs are essential for exogenous NR and NMN utilization to NAD^+ in cultured muscle cells

To better understand the interactions and contributions of muscle NRK 1, NRK2, and NAMPT to NR and NMN precursor salvage we employed a primary muscle culture system to derive myotubes with combinatorial single, double, and triple NRK1/2 and NAMPT loss of function. These experiments were conducted using NRK1 and 2KO mice as reported by Ratajczak et al. [28]. Firstly, due to the highly muscle-specific nature of NRK2, we assessed expression of key muscle differentiation markers and NAD^+ signaling genes over myotube differentiation in all the NRKKO models and found that expression was not altered, confirming that the NRKs are not essential for myotube differentiation (Sup. 2A,B).

Basal NAD^+ levels in NRK single or double KO (DKO) cells were comparable to those of WT cells (Sup. 2C). Similarly, but to a lesser extent than in the WT myotubes, single NRK1KO and NRK2KO myotubes were still able to enhance NAD^+ levels following NR supplementation, more so in NRK2KO cells compared to NRK1KO cells (43.25% increase in NAD+ versus 23.5%), suggesting functional redundancy of the NRKs to generate NAD^+ from available NR. However, NR was unable to increase NAD^+ in double KO cells with less than a 1% change from untreated (Figure 6A–C, left).

In hepatocytes, extracellular NMN is converted to NR extracellularly such that both NR and NMN require NRK1 activity to convert these compounds to intracellular NMN and NAD^+ [28]. In unstressed NAD^+ replete cells NMN supplementation could not augment NAD^+ levels in NRK1KO, and to a lesser degree NRK2KO, such that double KO cells are effectively unresponsive to NMN (Figure 6A–C, left).

We then examined the ability of NR and NMN to rescue cells depleted of NAD^+ following 24 h NAMPT inhibition (Figure 6A–C, right). NAMPT inhibition substantially depleted cellular NAD^+ content in WT and all the NRK loss of function cell cultures (Figure 6A–C, right). NR and NMN were able to recover, but not boost, NAD^+ levels following FK866 inhibition in NRK2KO and, to a lesser extent, NRK1KO myotubes. However, neither NR nor NMN supplementation was able to recover NAD^+ depletion in DKO myotubes, again clearly indicating the NRK dependency of NMN conversion to NAD^+ (Figure 6A–C, right). In all instances, 10-fold excess NAM (5 mM) is required to overcome NAMPT inhibition (Sup. 2D).

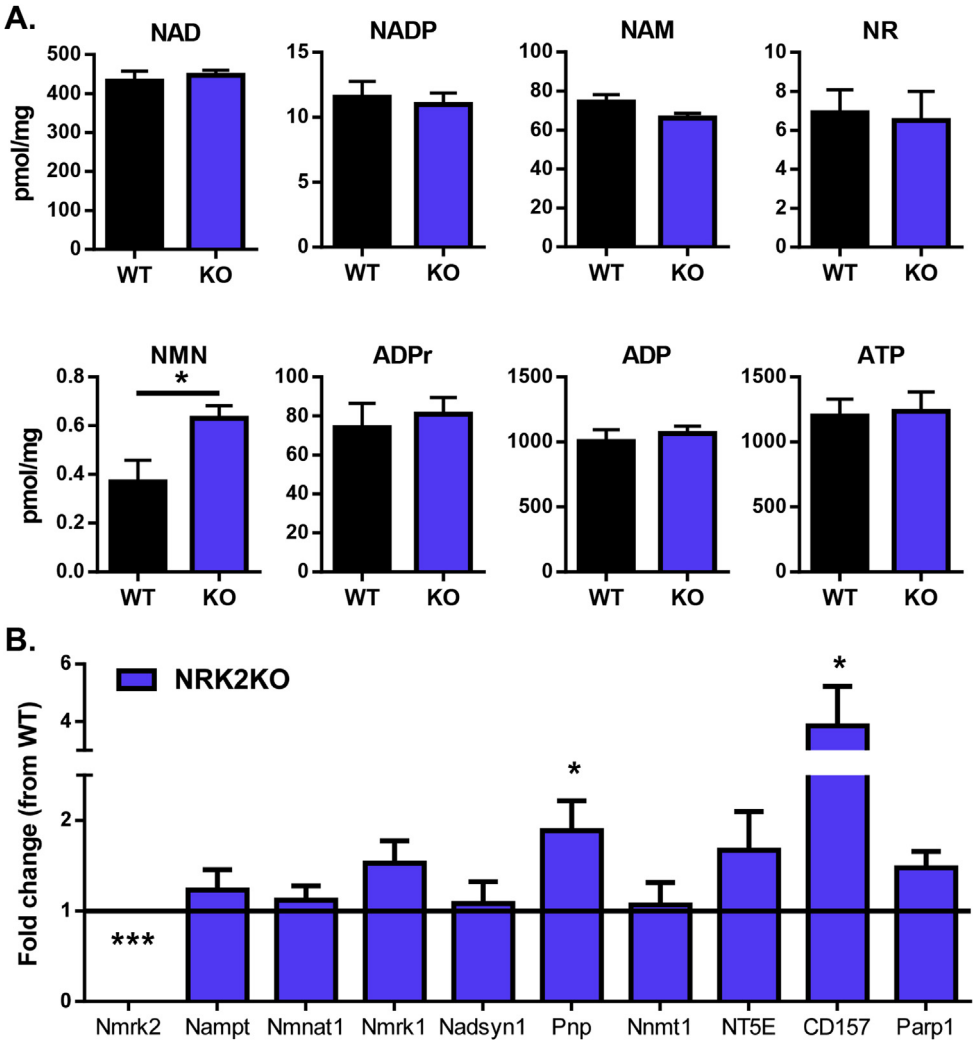

Figure 5: NAD^+ availability and signaling in NRK2KO mice. (A) LCMS-based targeted NAD^+ metabolomics to quantify NAD^+ and related metabolite levels in WT and NRK2KO skeletal muscle tissue (n = 6). **(B)** Fold change in mRNA expression of NAD^+ related signaling genes in NRK2KO skeletal muscle compared to WT (at Y axis = 1) (n = 4).

Original Article

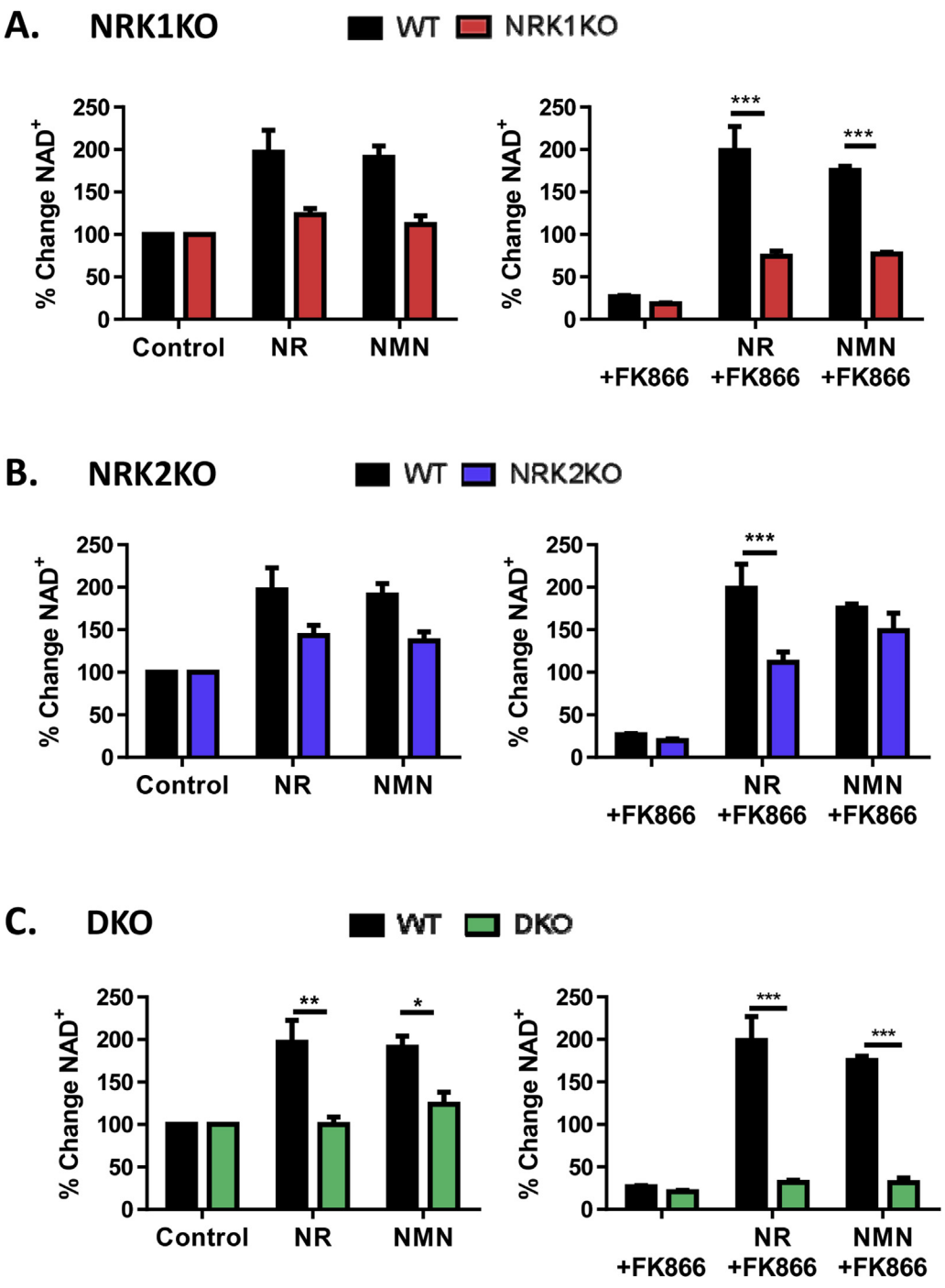

Figure 6: Manipulations to skeletal muscle NAD$^+$ biosynthesis pathways. (A) NRK1KO, **(B)** NRK2KO, and **(C)** NRK double KO (DKO) primary myotubes supplemented with 0.5 mM NAD$^+$ precursors for 24 h (left) and corresponding primary myotubes supplemented with 0.5 mM NAD$^+$ precursors for 24 h following 1 μM FK866 mediated NAMPT inhibition (right). For clarity, all data is presented as percent change in NAD$^+$ compared to DMSO only control (100%) (all groups n = 4 and significance determined between WT and corresponding KO from actual NAD$^+$ content by two-way ANOVA using Bonferroni's post-test).

These data show that while NAMPT is the primary pathway for maintaining NAD$^+$ turnover in skeletal muscle, the NRKs are essential for utilizing exogenous NR and NMN to enhance cellular NAD$^+$.

4. DISCUSSION

Mounting evidence supports the notion that enhancing tissue NAD$^+$ availability has beneficial effects on metabolic health in the context of metabolic disease and physiological decline [22,23,47–49]. The leading method to accomplish NAD$^+$ augmentation is through dietary supplementation with NR and NMN. Although they have a similar capacity to raise NAD$^+$ and promote metabolic benefit, the tissue-specific routes of their metabolism remain obscure. Skeletal muscle exhibits a decline in NAD$^+$ in a number of physiological, metabolic, and genetic scenarios, all associated with defects in muscle physiology and mitochondrial function [7,50,51]. Here we have explored NAD$^+$

MOLECULAR METABOLISM

salvage and biosynthesis in skeletal muscle and identified NRKs as critical to the availability of both NR and NMN to NAD^+ in skeletal muscle cells.

NAD^+ biosynthesis in skeletal muscle appears restricted to two main salvage pathways involving the rate-limiting enzymes NAMPT, NRKs, and NMNAT. While basal NAMPT and, to a degree, NRK1 display ubiquitous expression, NRK2 displays a muscle restricted pattern at mRNA and protein level. De novo NAD^+ biosynthesis and the Preiss-Handler NA salvage pathway play a minimal role in skeletal muscle with limited or undetectable levels of expression of rate limiting enzymes and metabolites. This supports previous metabolic enzyme activity profiling data that found enzyme activity of NAD synthase — the final rate limiting enzyme for both de novo biosynthesis and NA salvage — to be undetectable in skeletal muscle [34]. We endorse this by showing that unlike NR, the acid version NaR, which is metabolized by the NRKs and NMNATs — but also requires NAD synthase activity for final conversion to NAD^+ [40,41] — does not appear able to act as an exogenous NAD^+ precursor in skeletal muscle.

Depletion of NAMPT activity in muscle leads to a severe reduction (85%) in muscle NAD^+ availability; yet, at least for young mice, no gross NAD^+ relatable phenotype was observed [38]. However, with advancing age (7 months), this chronic reduction in NAD^+ manifests with impaired mitochondrial function, loss of muscle fiber integrity, strength, and performance [38]. Although NAMPT is critical to basal NAD^+ biosynthesis, exogenous NAM appears to be a poor precursor for NAD^+ boosting in muscle compared to NR and NMN due to poor conversion to NAD^+ and its inhibitory activity towards sirtuins [52]. We found that NR supplementation could significantly boost NAD^+ in the context of reduced NAD^+ levels following NAMPT inhibition and rescue concurrent defects in mitochondrial energy metabolism. Despite NR rescuing NAD^+ depletion and some of the effects of metabolic challenge *in vivo* [22], our data suggest that increasing NAD^+ availability in skeletal muscle by NR supplementation does not enhance oxidative metabolism of 'healthy' NAD^+ replete muscle cells. Muscle-specific NAMPT overexpressing mice showed that a 50% increase in NAD^+ could not stimulate mitochondrial biogenesis or enhance mitochondrial metabolism in young skeletal muscle [53]. Our results show that when NAD^+ is enhanced through NR supplementation, NAM and ADPr levels are unchanged, whereas there is a decrease following NAD^+ depletion (Table 1). As NAM and ADPr are metabolites of NAD^+ signaling (products of SIRT based NAD^+ consumption) [54], this indicates that although a reduction of NAD^+ can limit NAD^+ signaling and ultimately hinder mitochondrial metabolism, basal NAD^+ content alone is not limiting to NAD^+ signaling, at least in healthy skeletal muscle.

Though NRK2 appears to be restricted to muscle, loss-of-function had no effect on basic parameters of muscle physiology, perhaps reflecting the unstressed nature of young muscle in this study, and in line with the work of Frederick et al. [38]. Again, this also suggests that NAMPT is more than sufficient to match NAD^+ recycling to its metabolic clearance. Measuring the quadriceps tissue NAD^+ related metabolome was unremarkable other than for a 50% increase in NMN. Similarly, NAMPT and NRK1 were unaffected at the level of gene expression and may suggest that no overt stress response was initiated. However, we did note elevation in the expression of *Pnp* and *CD157*. PNP can convert NR to NAM and CD157 converts extracellular NAD+ to ADPr and NAM [45,46]. While this does not manifest as raised NAM level in muscle, it may reflect raised NMN that serves to balance NAD^+ availability suggesting a minor adaptation to the loss of NRK2.

We originally postulated that NRK2 would be more important than NRK1 in skeletal muscle for NR salvage due to its predominant expression. However, our *in vivo* data and work by Ratajczak et al. showing that NRK1 controls NR and NMN metabolism in mammalian cells [28] led us to examine more closely the dependency of NR and NMN on each NRK. Using combinatorial muscle cultures of single and double NRK1/2 KO cells we confirmed that NR is exclusively metabolized by the NRK enzymes in skeletal muscle with no change to cellular NAD^+ levels in DKO primary myotubes following NR supplementation, which was strikingly evident in NAD^+ depleted cells. Both NRK1 and NRK2 single KO cells demonstrate a level of redundancy in their ability to respond to NR, though clearly being submaximal compared to control cells.

NMN is metabolized to NAD^+ downstream of NRKs and NAMPT, yet exogenous NMN supplementation was unable to be metabolized to NAD^+ in DKO cells, again most strikingly in the context of severe NAD^+ depletion. While there is a level of redundancy in the single KO cells, the data implicate NRK1 as being more critical for regulating NMN entry into the cell. Recent findings by Ratajczak et al. have shown that NRK1 regulates exogenous NMN salvage in liver tissue and cells. They identified a requirement for NMN to be metabolized extracellularly to NR before hepatic uptake, then re-phosphorylated by NRK1 back to NMN [28]. Similar data also have highlighted that human cells can metabolize NMN to NR intracellularly utilizing cytosolic 5′-nucleotidases [40]. The data presented here in primary WT and loss-of-function myotubes corroborate these findings and reveal the NRKs critical role for both NR and NMN conversion to NAD^+.

Positive health effects of enhancing NAD^+ availability have been demonstrated in muscle [55]. Acipimox (NA analogue) treatment improved aspects of mitochondrial physiology in type 2 diabetic muscle. However, the effects on NAD^+ availability were small and the mechanisms unclear, and the therapeutic potential of acipimox limited due to a range of adverse effects including insulin resistance and GPR109A receptor activation leading to flushing and therefore poor compliance [15]. The inhibition of PARPs, sparing and elevating NAD^+, leading to enhanced mitochondrial function and biogenesis through activation of SIRT1-PGC-1α axis has been demonstrated as being effective in muscle [56—58].

However, supplementation with NR and NMN to boost cellular NAD^+ pools in a range of scenarios appears to be the most promising strategy [19,20,22,48,51,59—63]. NR and NMN based NAD^+ repletion in skeletal muscle can revitalize stem cells and augment physiological and mitochondrial function in aged mice [49]. Furthermore, NAD^+ can also act to regulate protein—protein interactions that influence DNA repair through control of PARP activity, and NMN or NR repletion of NAD^+ in ageing could support efficient DNA repair capacity while maintaining the positive effects of sirtuin activation [64].

While NR is naturally available in the human diet, with appreciable levels measured in milk, the main source of NR, NMN, NAM, and NA is the NAD(P) (H) pool available through the digestion of whole, unprocessed food [27]. Oral NR administration to humans has recently demonstrated effectiveness in boosting circulating and white blood cell NAD^+ levels, with further work required to determine the importance for muscle NAD^+ repletion [26].

These data establish that muscle has a level of redundancy in its ability to metabolize NR and therefore NMN. Despite NRK2 being restricted to muscle and being highly expressed, basal NAD^+ turnover does not seemingly require NRK activity. However, NRK1 and to a smaller degree NRK2 are gate-keepers of NR and NMN salvage. Importantly, NAD^+ depletion and energetic stress can lead to augmented NRK2 expression in a range of tissues such as neurons, cardiac, and skeletal muscle [65—67]. Thus, beyond basal NAD^+ turnover, regulated NRK2 activity may serve an additional role in cellular metabolism involving

NR phosphorylation, potentially more critical to stress adaptation when there is need to enhance NR/NMN metabolism to defend metabolic integrity.

AUTHOR CONTRIBUTIONS

GGL and CC conceived and designed the study. RSF, JR, CLD, and LAO performed the experiments. RC, GSX, AG, and YE contributed to experiments. PR, MM, and CB contributed reagents, technology and critical evaluation of the manuscript. RSF, AP, and GGL wrote and CB edited the manuscript.

ACKNOWLEDGMENTS

This work was supported by an MRC PhD studentship, a Wellcome Trust Senior Fellowship (GGL-104612/Z/14/Z), a Marie Sklodowska-Curie grant (AG-No 705869), the Nestlé Institute of Health Sciences, the Roy J. Carver Trust and National Institutes of Health (CB-R21-AA022371). Seahorse metabolic flux analysis was performed through the University of Birmingham Mitochondrial Profiling Centre, an open access facility supported by the Medical Research Council and the University of Birmingham Dynamic Investment Fund. We thank ChromaDex (Irvine, California) for nicotinamide riboside and helpful discussions. We thank Agnieszka Zielinska for technical support.

CONFLICT OF INTEREST

JR and CC are employees of the Nestlé Institute of Health Sciences.

APPENDIX A. SUPPLEMENTARY DATA

Supplementary data related to this article can be found at http://dx.doi.org/10.1016/j.molmet.2017.05.011.

REFERENCES

[1] Belenky, P., Bogan, K.L., Brenner, C., 2007. NAD+ metabolism in health and disease. Trends in Biochemical Sciences 32(1):12–19.

[2] Bogan, K.L., Brenner, C., 2008. Nicotinic acid, nicotinamide, and nicotinamide riboside: a molecular evaluation of NAD+ precursor vitamins in human nutrition. Annual Review of Nutrition 28(1):115–130.

[3] Mouchiroud, Laurent, Houtkooper, Riekelt H., Moullan, Norman, Katsyuba, Elena, Ryu, Dongryeol, Cantó, Carles, et al., 2013. The NAD+/sirtuin pathway modulates longevity through activation of mitochondrial UPR and FOXO signaling. Cell 154(2):430–441.

[4] Amat, R., Planavila, A., Chen, S.L., Iglesias, R., Giralt, M., Villarroya, F., 2009. SIRT1 controls the transcription of the peroxisome proliferator-activated receptor-gamma Co-activator-1alpha (PGC-1alpha) gene in skeletal muscle through the PGC-1alpha autoregulatory loop and interaction with MyoD. Journal of Biological Chemistry 284(33):21872–21880.

[5] Canto, C., Jiang, L.Q., Deshmukh, A.S., Mataki, C., Coste, A., Lagouge, M., et al., 2010. Interdependence of AMPK and SIRT1 for metabolic adaptation to fasting and exercise in skeletal muscle. Cell Metabolism 11(3):213–219.

[6] Hood, D.A., Irrcher, I., Ljubicic, V., Joseph, A.-M., 2006. Coordination of metabolic plasticity in skeletal muscle. Journal of Experimental Biology 209(12):2265–2275.

[7] Koltai, E., Szabo, Z., Atalay, M., Boldogh, I., Naito, H., Goto, S., et al., 2010. Exercise alters SIRT1, SIRT6, NAD and NAMPT levels in skeletal muscle of aged rats. Mechanisms of Ageing and Development 131(1):21–28.

[8] Egan, B., Zierath, Juleen R., 2013. Exercise metabolism and the molecular regulation of skeletal muscle adaptation. Cell Metabolism 17(2):162–184.

[9] Preiss, J., Handler, P., 1958. Biosynthesis of diphosphopyridine nucleotide: I. Identification of intermediates. Journal of Biological Chemistry 233(2):488–492.

[10] Preiss, J., Handler, P., 1958. Biosynthesis of diphosphopyridine nucleotide: II. Enzymatic aspects. Journal of Biological Chemistry 233(2):493–500.

[11] Garten, A., Petzold, S., Körner, A., Imai, S-i, Kiess, W., 2009. Nampt: linking NAD biology, metabolism and cancer. Trends in Endocrinology & Metabolism 20(3):130–138.

[12] Bieganowski, P., Brenner, C., 2004. Discoveries of nicotinamide riboside as a nutrient and conserved NRK genes establish a Preiss-Handler independent route to NAD+ in fungi and humans. Cell 117(4):495–502.

[13] Tempel, W., Rabeh, W.M., Bogan, K.L., Belenky, P., Wojcik, M., Seidle, H.F., et al., 2007. Nicotinamide riboside kinase structures reveal new pathways to NAD+. PLoS Biology 5(10):e263.

[14] Gille, A., Bodor, E.T., Ahmed, K., Offermanns, S., 2008. Nicotinic acid: pharmacological effects and mechanisms of action. Annual Review of Pharmacology and Toxicology 48(1):79–106.

[15] van de Weijer, T., Phielix, E., Bilet, L., Williams, E.G., Ropelle, E.R., Bierwagen, A., et al., 2015. Evidence for a direct effect of the NAD+ precursor acipimox on muscle mitochondrial function in humans. Diabetes 64(4):1193–1201.

[16] Revollo, J.R., Grimm, A.A., Imai, S.-i., 2004. The NAD biosynthesis pathway mediated by nicotinamide phosphoribosyltransferase regulates Sir2 activity in mammalian cells. Journal of Biological Chemistry 279(49):50754–50763.

[17] Zarzuelo, M.J., López-Sepúlveda, R., Sánchez, M., Romero, M., Gómez-Guzmán, M., Ungvary, Z., et al., 2013. SIRT1 inhibits NADPH oxidase activation and protects endothelial function in the rat aorta: implications for vascular aging. Biochemical Pharmacology 85(9):1288–1296.

[18] MacKay, D., Hathcock, J., Guarneri, E., 2012. Niacin: chemical forms, bioavailability, and health effects. Nutrition Reviews 70(6):357–366.

[19] Yoshino, J., Mills, K.F., Yoon, M.J., Imai, S., 2011. Nicotinamide mononucleotide, a key NAD(+) intermediate, treats the pathophysiology of diet- and age-induced diabetes in mice. Cell Metabolism 14(4):528–536.

[20] Mendelsohn, A.R., Larrick, J.W., 2014. Partial reversal of skeletal muscle aging by restoration of normal NAD(+) levels. Rejuvenation Research 17(1):62–69.

[21] Gomes, A.P., Price, N.L., Ling, A.J., Moslehi, J.J., Montgomery, M.K., Rajman, L., et al., 2013. Declining NAD(+) induces a pseudohypoxic state disrupting nuclear-mitochondrial communication during aging. Cell 155(7):1624–1638.

[22] Cantó, C., Houtkooper Riekelt, H., Pirinen, E., Youn Dou, Y., Oosterveer Maaike, H., Cen, Y., et al., 2012. The NAD+ precursor nicotinamide riboside enhances oxidative metabolism and protects against high-fat diet-induced obesity. Cell Metabolism 15(6):838–847.

[23] Khan, N.A., Auranen, M., Paetau, I., Pirinen, E., Euro, L., Forsstrom, S., et al., 2014. Effective treatment of mitochondrial myopathy by nicotinamide riboside, a vitamin B3. EMBO Molecular Medicine 6(6):721–731.

[24] Hamity, M.V., White, S.R., Walder, R.Y., Schmidt, M.S., Brenner, C., Hammond, D.L., 2017. Nicotinamide riboside, a form of vitamin B3 and NAD+ precursor, relieves the nociceptive and aversive dimensions of paclitaxel-induced peripheral neuropathy in female rats. Pain 158(5):962–972.

[25] Trammell, S.A., Weidemann, B.J., Chadda, A., Yorek, M.S., Holmes, A., Coppey, L.J., et al., 2016. Nicotinamide riboside opposes type 2 diabetes and neuropathy in mice. Science Reports 6:26933.

[26] Trammell, S.A., Schmidt, M.S., Weidemann, B.J., Redpath, P., Jaksch, F., Dellinger, R.W., et al., 2016. Nicotinamide riboside is uniquely and orally bioavailable in mice and humans. Nature Communications 7:12948.

[27] Trammell, S.A., Yu, L., Redpath, P., Migaud, M.E., Brenner, C., 2016. Nicotinamide riboside is a major NAD+ precursor vitamin in cow milk. Journal of Nutrition 146(5):957–963.

MOLECULAR METABOLISM

[28] Ratajczak, J., Joffraud, M., Trammell, S.A., Ras, R., Canela, N., Boutant, M., et al., 2016. NRK1 controls nicotinamide mononucleotide and nicotinamide riboside metabolism in mammalian cells. Nature Communications 7:13103.

[29] Kammoun, M., Cassar-Malek, I., Meunier, B., Picard, B., 2014. A simplified immunohistochemical classification of skeletal muscle fibres in mouse. European Journal of Histochemistry 58(2):2254.

[30] Sawano, S., Komiya, Y., Ichitsubo, R., Ohkawa, Y., Nakamura, M., Tatsumi, R., et al., 2016. A one-step immunostaining method to visualize rodent muscle fiber type within a single specimen. PLoS One 11(11).

[31] Bloemberg, D., Quadrilatero, J., 2012. Rapid determination of myosin heavy chain expression in rat, mouse, and human skeletal muscle using multicolor immunofluorescence analysis. PLoS One 7(4):e35273.

[32] Penke, M., Larsen, P.S., Schuster, S., Dall, M., Jensen, B.A.H., Gorski, T., et al., 2015. Hepatic NAD salvage pathway is enhanced in mice on a high-fat diet. Molecular and Cellular Endocrinology 412:65–72.

[33] Trammell, S.A., Brenner, C., 2013. Targeted, LCMS-based metabolomics for quantitative measurement of NAD(+) metabolites. Computational and Structural Biotechnology Journal 4:e201301012.

[34] Mori, V., Amici, A., Mazzola, F., Di Stefano, M., Conforti, L., Magni, G., et al., 2014. Metabolic profiling of alternative NAD biosynthetic routes in mouse tissues. PLoS One 9(11):e113939.

[35] Samal, B., Sun, Y., Stearns, G., Xie, C., Suggs, S., McNiece, I., 1994. Cloning and characterization of the cDNA encoding a novel human pre-B-cell colony-enhancing factor. Molecular and Cellular Biology 14(2):1431–1437.

[36] Hara, N., Yamada, K., Terashima, M., Osago, H., Shimoyama, M., Tsuchiya, M., 2003. Molecular identification of human glutamine- and ammonia-dependent NAD synthetases. Carbon-nitrogen hydrolase domain confers glutamine dependency. Journal of Biological Chemistry 278(13):10914–10921.

[37] Lavery, G.G., Walker, E.A., Turan, N., Rogoff, D., Ryder, J.W., Shelton, J.M., et al., 2008. Deletion of Hexose-6-phosphate dehydrogenase activates the unfolded protein response pathway and induces skeletal myopathy. Journal of Biological Chemistry 283(13):8453–8461.

[38] Frederick, D.W., Loro, E., Liu, L., Davila Jr., A., Chellappa, K., Silverman, I.M., et al., 2016. Loss of NAD homeostasis leads to progressive and reversible degeneration of skeletal muscle. Cell Metabolism 24(2):269–282.

[39] Kim, J.S., Yoon, C.S., Park, D.R., 2014. NAMPT regulates mitochondria biogenesis via NAD metabolism and calcium binding proteins during skeletal muscle contraction. Journal of Exercise Nutrition & Biochemistry 18(3):259–266.

[40] Kulikova, V., Shabalin, K., Nerinovski, K., Dolle, C., Niere, M., Yakimov, A., et al., 2015. Generation, release, and uptake of the NAD precursor nicotinic acid riboside by human cells. Journal of Biological Chemistry 290(45):27124–27137.

[41] Bieganowski, P., Pace, H.C., Brenner, C., 2003. Eukaryotic NAD+ synthetase Qns1 contains an essential, obligate intramolecular thiol glutamine amidotransferase domain related to nitrilase. Journal of Biological Chemistry 278(35):33049–33055.

[42] Hasmann, M., Schemainda, I., 2003. FK866, a highly specific noncompetitive inhibitor of nicotinamide phosphoribosyltransferase, represents a novel mechanism for induction of tumor cell apoptosis. Cancer Research 63(21):7436–7442.

[43] Fulco, M., Cen, Y., Zhao, P., Hoffman, E.P., McBurney, M.W., Sauve, A.A., et al., 2008. Glucose restriction inhibits skeletal myoblast differentiation by activating SIRT1 through AMPK-mediated regulation of Nampt. Developmental Cell 14(5):661–673.

[44] Schuster, S., Penke, M., Gorski, T., Gebhardt, R., Weiss, T.S., Kiess, W., et al., 2015. FK866-induced NAMPT inhibition activates AMPK and downregulates mTOR signaling in hepatocarcinoma cells. Biochemical and Biophysical Research Communications 458(2):334–340.

[45] Belenky, P., Christensen, K.C., Gazzaniga, F., Pletnev, A.A., Brenner, C., 2009. Nicotinamide riboside and nicotinic acid riboside salvage in fungi and mammals. Quantitative basis for Urh1 and purine nucleoside phosphorylase function in NAD+ metabolism. Journal of Biological Chemistry 284(1):158–164.

[46] Ishihara, K., Hirano, T., 2000. BST-1/CD157 regulates the humoral immune responses in vivo. Chemical Immunology 75:235–255.

[47] Uddin, G.M., Youngson, N.A., Sinclair, D.A., Morris, M.J., 2016. Head to head comparison of short-term treatment with the NAD(+) precursor nicotinamide mononucleotide (NMN) and 6 weeks of exercise in obese female mice. Frontiers in Pharmacology 7:258.

[48] de Picciotto, N.E., Gano, L.B., Johnson, L.C., Martens, C.R., Sindler, A.L., Mills, K.F., et al., 2016. Nicotinamide mononucleotide supplementation reverses vascular dysfunction and oxidative stress with aging in mice. Aging Cell 15(3):522–530.

[49] Zhang, H., Ryu, D., Wu, Y., Gariani, K., Wang, X., Luan, P., et al., 2016. NAD$^+$ repletion improves mitochondrial and stem cell function and enhances life span in mice. Science 352(6292):1436–1443.

[50] Braidy, N., Guillemin, G.J., Mansour, H., Chan-Ling, T., Poljak, A., Grant, R., 2011. Age related changes in NAD+ metabolism oxidative stress and Sirt1 activity in Wistar rats. PLoS One 6(4):e19194.

[51] Ryu, D., Zhang, H., Ropelle, E.R., Sorrentino, V., Mázala, D.A.G., Mouchiroud, L., et al., 2016. NAD$^+$ repletion improves muscle function in muscular dystrophy and counters global PARylation. Science Translational Medicine 8(361), 361ra139-361ra139.

[52] Lee, S.J., Choi, S.E., Jung, I.R., Lee, K.W., Kang, Y., 2013. Protective effect of nicotinamide on high glucose/palmitate-induced glucolipotoxicity to INS-1 beta cells is attributed to its inhibitory activity to sirtuins. Archives of Biochemistry and Biophysics 535(2):187–196.

[53] Frederick, D.W., Davis, J.G., Davila Jr., A., Agarwal, B., Michan, S., Puchowicz, M.A., et al., 2015. Increasing NAD synthesis in muscle via nicotinamide phosphoribosyltransferase is not sufficient to promote oxidative metabolism. Journal of Biological Chemistry 290(3):1546–1558.

[54] Jing, E., O'Neill, B.T., Rardin, M.J., Kleinridders, A., Ilkeyeva, O.R., Ussar, S., et al., 2013. Sirt3 regulates metabolic flexibility of skeletal muscle through reversible enzymatic deacetylation. Diabetes 62(10):3404–3417.

[55] Dolle, C., Skoge, R.H., Vanlinden, M.R., Ziegler, M., 2013. NAD biosynthesis in humans—enzymes, metabolites and therapeutic aspects. Current Topics in Medicinal Chemistry 13(23):2907–2917.

[56] Bai, P., Cantó, C., Oudart, H., Brunyánszki, A., Cen, Y., Thomas, C., et al., 2011. PARP-1 inhibition increases mitochondrial metabolism through SIRT1 activation. Cell Metabolism 13(4):461–468.

[57] Mohamed, J.S., Hajira, A., Pardo, P.S., Boriek, A.M., 2014. MicroRNA-149 inhibits PARP-2 and promotes mitochondrial biogenesis via SIRT-1/PGC-1alpha network in skeletal muscle. Diabetes 63(5):1546–1559.

[58] Pirinen, E., Canto, C., Jo, Y.S., Morato, L., Zhang, H., Menzies, K.J., et al., 2014. Pharmacological inhibition of poly(ADP-ribose) polymerases improves fitness and mitochondrial function in skeletal muscle. Cell Metabolism 19(6):1034–1041.

[59] Brown, K.D., Maqsood, S., Huang, J.Y., Pan, Y., Harkcom, W., Li, W., et al., 2014. Activation of SIRT3 by the NAD(+) precursor nicotinamide riboside protects from noise-induced hearing loss. Cell Metabolism 20(6):1059–1068.

[60] Long, A.N., Owens, K., Schlappal, A.E., Kristian, T., Fishman, P.S., Schuh, R.A., 2015. Effect of nicotinamide mononucleotide on brain mitochondrial respiratory deficits in an Alzheimer's disease-relevant murine model. BMC Neurology 15:19.

[61] Revollo, J.R., Korner, A., Mills, K.F., Satoh, A., Wang, T., Garten, A., et al., 2007. Nampt/PBEF/visfatin regulates insulin secretion in beta cells as a systemic NAD biosynthetic enzyme. Cell Metabolism 6(5):363–375.

[62] Ramsey, K.M., Mills, K.F., Satoh, A., Imai, S., 2008. Age-associated loss of Sirt1-mediated enhancement of glucose-stimulated insulin secretion in beta cell-specific Sirt1-overexpressing (BESTO) mice. Aging Cell 7(1):78–88.

[63] Caton, P.W., Kieswich, J., Yaqoob, M.M., Holness, M.J., Sugden, M.C., 2011. Nicotinamide mononucleotide protects against pro-inflammatory cytokine-

mediated impairment of mouse islet function. Diabetologia 54(12):3083–3092.

[64] Li, J., Bonkowski, M.S., Moniot, S., Zhang, D., Hubbard, B.P., Ling, A.J.Y., et al., 2017. A conserved NAD^+ binding pocket that regulates protein-protein interactions during aging. Science 355(6331):1312–1317.

[65] Sasaki, Y., Araki, T., Milbrandt, J., 2006. Stimulation of nicotinamide adenine dinucleotide biosynthetic pathways delays axonal degeneration after axotomy. The Journal of Neuroscience 26(33):8484–8491.

[66] Aguilar, C.A., Shcherbina, A., Ricke, D.O., Pop, R., Carrigan, C.T., Gifford, C.A., et al., 2015. In vivo monitoring of transcriptional dynamics after lower-limb muscle injury enables quantitative classification of healing. Scientific Reports 5:13885.

[67] Xu, W., Barrientos, T., Mao, L., Rockman, H.A., Sauve, A.A., Andrews, N.C., 2015. Lethal cardiomyopathy in mice lacking transferrin receptor in the heart. Cell Reports 13(3):533–545.

References

1. Frontera, W.R. and J. Ochala, *Skeletal Muscle: A Brief Review of Structure and Function.* Calcified Tissue International, 2015. **96**(3): p. 183-195.
2. MURAKAMI, U. and K. UCHIDA, *Contents of Myofibrillar Proteins in Cardiac, Skeletal, and Smooth Muscles.* Journal of Biochemistry, 1985. **98**(1): p. 187-197.
3. Qazi, T.H., et al., *Biomaterials based strategies for skeletal muscle tissue engineering: Existing technologies and future trends.* Biomaterials, 2015. **53**: p. 502-521.
4. Wang, L., et al., *Nanofiber Yarn/Hydrogel Core-Shell Scaffolds Mimicking Native Skeletal Muscle Tissue for Guiding 3D Myoblast Alignment, Elongation, and Differentiation.* ACS Nano, 2015. **9**(9): p. 9167-79.
5. Bian, W., et al., *Local Tissue Geometry Determines Contractile Force Generation of Engineered Muscle Networks.* Tissue Engineering. Part A, 2012. **18**(9-10): p. 957-967.
6. Ferrante, M.I., et al., *Troponin T is essential for sarcomere assembly in zebrafish skeletal muscle.* Journal of Cell Science, 2011. **124**(4): p. 565-577.
7. Gilev, V.P., *A study of myofibril sarcomere structure during contraction.* J Cell Biol, 1962. **12**: p. 135-47.
8. Christ, B. and C.P. Ordahl, *Early stages of chick somite development.* Anat Embryol (Berl), 1995. **191**(5): p. 381-96.
9. Rudnicki, M.A., et al., *MyoD or Myf-5 is required for the formation of skeletal muscle.* Cell, 1993. **75**(7): p. 1351-9.
10. Wang, Y. and R. Jaenisch, *Myogenin can substitute for Myf5 in promoting myogenesis but less efficiently.* Development, 1997. **124**(13): p. 2507-13.
11. Fu, X., H. Wang, and P. Hu, *Stem cell activation in skeletal muscle regeneration.* Cellular and Molecular Life Sciences, 2015. **72**(9): p. 1663-1677.
12. Cornelison, D.D. and B.J. Wold, *Single-cell analysis of regulatory gene expression in quiescent and activated mouse skeletal muscle satellite cells.* Dev Biol, 1997. **191**(2): p. 270-83.
13. Simionescu-Bankston, A. and A. Kumar, *Noncoding RNAs in the regulation of skeletal muscle biology in health and disease.* J Mol Med (Berl), 2016. **94**(8): p. 853-66.
14. Robison, P., et al., *Impaired Calcium Signaling in Muscle Fibers from Intercostal and Foot Skeletal Muscle in a Cigarette Smoke-Induced Mouse Model of COPD.* Muscle Nerve, 2016.
15. Huxley, A.F. and R. Niedergerke, *Structural Changes in Muscle During Contraction: Interference Microscopy of Living Muscle Fibres.* Nature, 1954. **173**(4412): p. 971-973.
16. Huxley, H. and J. Hanson, *Changes in the Cross-Striations of Muscle during Contraction and Stretch and their Structural Interpretation.* Nature, 1954. **173**(4412): p. 973-976.
17. Huxley, H.E., *The Mechanism of Muscular Contraction.* Science, 1969. **164**(3886): p. 1356-1366.
18. Agbulut, O., et al., *Myosin heavy chain isoforms in postnatal muscle development of mice.* Biol Cell, 2003. **95**(6): p. 399-406.
19. Schiaffino, S. and C. Reggiani, *Fiber types in mammalian skeletal muscles.* Physiol Rev, 2011. **91**(4): p. 1447-531.

20. Thorstensson, A. and J. Karlsson, *Fatiguability and fibre composition of human skeletal muscle.* Acta Physiol Scand, 1976. **98**(3): p. 318-22.
21. Ciciliot, S., et al., *Muscle type and fiber type specificity in muscle wasting.* Int J Biochem Cell Biol, 2013. **45**(10): p. 2191-9.
22. Zierath, J.R. and J.A. Hawley, *Skeletal muscle fiber type: influence on contractile and metabolic properties.* PLoS Biol, 2004. **2**(10): p. e348.
23. Rockl, K.S., et al., *Skeletal muscle adaptation to exercise training: AMP-activated protein kinase mediates muscle fiber type shift.* Diabetes, 2007. **56**(8): p. 2062-9.
24. van den Borst, B., et al., *Loss of quadriceps muscle oxidative phenotype and decreased endurance in patients with mild-to-moderate COPD.* J Appl Physiol (1985), 2013. **114**(9): p. 1319-28.
25. Gannon, J., et al., *Drastic increase of myosin light chain MLC-2 in senescent skeletal muscle indicates fast-to-slow fibre transition in sarcopenia of old age.* Eur J Cell Biol, 2009. **88**(11): p. 685-700.
26. Argiles, J.M., et al., *Skeletal Muscle Regulates Metabolism via Interorgan Crosstalk: Roles in Health and Disease.* J Am Med Dir Assoc, 2016. **17**(9): p. 789-96.
27. Baron, A.D., et al., *Rates and tissue sites of non-insulin- and insulin-mediated glucose uptake in humans.* Am J Physiol, 1988. **255**(6 Pt 1): p. E769-74.
28. Guridi, M., et al., *Alterations to mTORC1 signaling in the skeletal muscle differentially affect whole-body metabolism.* Skeletal Muscle, 2016. **6**(1): p. 1-14.
29. Guridi, M., et al., *Activation of mTORC1 in skeletal muscle regulates whole-body metabolism through FGF21.* Sci Signal, 2015. **8**(402): p. ra113.
30. Hawley, J.A., et al., *Nutritional modulation of training-induced skeletal muscle adaptations.* Journal of Applied Physiology, 2011. **110**(3): p. 834-845.
31. Canto, C., et al., *Interdependence of AMPK and SIRT1 for metabolic adaptation to fasting and exercise in skeletal muscle.* Cell Metab, 2010. **11**(3): p. 213-9.
32. White, A.T. and S. Schenk, *NAD+/NADH and skeletal muscle mitochondrial adaptations to exercise.* American Journal of Physiology - Endocrinology and Metabolism, 2012. **303**(3): p. E308-E321.
33. Dodson, S., et al., *Muscle wasting in cancer cachexia: clinical implications, diagnosis, and emerging treatment strategies.* Annu Rev Med, 2011. **62**: p. 265-79.
34. Park, S.W., et al., *Excessive Loss of Skeletal Muscle Mass in Older Adults With Type 2 Diabetes.* Diabetes Care, 2009. **32**(11): p. 1993-1997.
35. Kim, H.C., M. Mofarrahi, and S.N. Hussain, *Skeletal muscle dysfunction in patients with chronic obstructive pulmonary disease.* Int J Chron Obstruct Pulmon Dis, 2008. **3**(4): p. 637-58.
36. Haman, F., et al., *Effect of cold exposure on fuel utilization in humans: plasma glucose, muscle glycogen, and lipids.* J Appl Physiol (1985), 2002. **93**(1): p. 77-84.
37. Ponticos, M., et al., *Dual regulation of the AMP-activated protein kinase provides a novel mechanism for the control of creatine kinase in skeletal muscle.* EMBO J, 1998. **17**(6): p. 1688-99.
38. Hultman, E., *Fuel selection, muscle fibre.* Proc Nutr Soc, 1995. **54**(1): p. 107-21.
39. Burton, D.A., K. Stokes, and G.M. Hall, *Physiological effects of exercise.* Continuing Education in Anaesthesia, Critical Care & Pain, 2004. **4**(6): p. 185-188.
40. Conley, K.E., *Mitochondria to motion: optimizing oxidative phosphorylation to improve exercise performance.* J Exp Biol, 2016. **219**(Pt 2): p. 243-9.

41. van Hall, G., *The Physiological Regulation of Skeletal Muscle Fatty Acid Supply and Oxidation During Moderate-Intensity Exercise.* Sports Med, 2015. **45 Suppl 1**: p. S23-32.
42. Adibi, S.A., et al., *Amino acid levels in plasma, liver, and skeletal muscle during protein deprivation.* Am J Physiol, 1973. **225**(2): p. 408-14.
43. Wagenmakers, A.J., *Muscle amino acid metabolism at rest and during exercise: role in human physiology and metabolism.* Exerc Sport Sci Rev, 1998. **26**: p. 287-314.
44. Milan, G., et al., *Regulation of autophagy and the ubiquitin-proteasome system by the FoxO transcriptional network during muscle atrophy.* Nat Commun, 2015. **6**: p. 6670.
45. Karlsson, J. and B. Saltin, *Lactate, ATP, and CP in working muscles during exhaustive exercise in man.* J Appl Physiol, 1970. **29**(5): p. 596-602.
46. Egan, B. and Juleen R. Zierath, *Exercise Metabolism and the Molecular Regulation of Skeletal Muscle Adaptation.* Cell Metabolism, 2013. **17**(2): p. 162-184.
47. Howald, H., et al., *Influences of endurance training on the ultrastructural composition of the different muscle fiber types in humans.* Pflugers Arch, 1985. **403**(4): p. 369-76.
48. West, D.W., et al., *Human exercise-mediated skeletal muscle hypertrophy is an intrinsic process.* Int J Biochem Cell Biol, 2010. **42**(9): p. 1371-5.
49. Mikines, K.J., et al., *Effect of physical exercise on sensitivity and responsiveness to insulin in humans.* Am J Physiol, 1988. **254**(3 Pt 1): p. E248-59.
50. Hinton, P.S., P. Nigh, and J. Thyfault, *Effectiveness of resistance training or jumping-exercise to increase bone mineral density in men with low bone mass: A 12-month randomized, clinical trial.* Bone, 2015. **79**: p. 203-12.
51. Deckx, N., et al., *12 Weeks of Combined Endurance and Resistance Training Reduces Innate Markers of Inflammation in a Randomized Controlled Clinical Trial in Patients with Multiple Sclerosis.* Mediators Inflamm, 2016. **2016**: p. 6789276.
52. Lopes, A.L., et al., *The effects of diet- and diet plus exercise-induced weight loss on basal metabolic rate and acylated ghrelin in grade 1 obese subjects.* Diabetes Metab Syndr Obes, 2013. **6**: p. 469-75.
53. Copeland, W.C. and M.J. Longley, *Mitochondrial genome maintenance in health and disease.* DNA Repair (Amst), 2014. **19**: p. 190-8.
54. Ye, F., et al., *High-throughput sequencing in mitochondrial DNA research.* Mitochondrion, 2014. **17**: p. 157-63.
55. Gray, M.W., G. Burger, and B.F. Lang, *Mitochondrial Evolution.* Science, 1999. **283**(5407): p. 1476-1481.
56. Reznick, R.M., et al., *Aging-associated reductions in AMP-activated protein kinase activity and mitochondrial biogenesis.* Cell Metab, 2007. **5**(2): p. 151-6.
57. Irrcher, I., et al., *PPARgamma coactivator-1alpha expression during thyroid hormone- and contractile activity-induced mitochondrial adaptations.* Am J Physiol Cell Physiol, 2003. **284**(6): p. C1669-77.
58. Wu, Z., et al., *Mechanisms controlling mitochondrial biogenesis and respiration through the thermogenic coactivator PGC-1.* Cell, 1999. **98**(1): p. 115-24.
59. Puigserver, P., et al., *A cold-inducible coactivator of nuclear receptors linked to adaptive thermogenesis.* Cell, 1998. **92**(6): p. 829-39.

60. Winder, W.W., et al., *Activation of AMP-activated protein kinase increases mitochondrial enzymes in skeletal muscle.* J Appl Physiol (1985), 2000. **88**(6): p. 2219-26.
61. Xiao, B., et al., *Structure of mammalian AMPK and its regulation by ADP.* Nature, 2011. **472**(7342): p. 230-3.
62. Jager, S., et al., *AMP-activated protein kinase (AMPK) action in skeletal muscle via direct phosphorylation of PGC-1alpha.* Proc Natl Acad Sci U S A, 2007. **104**(29): p. 12017-22.
63. Gerhart-Hines, Z., et al., *Metabolic control of muscle mitochondrial function and fatty acid oxidation through SIRT1/PGC-1alpha.* EMBO J, 2007. **26**(7): p. 1913-23.
64. Meyerhof, O. and P. Oesper, *Ther mechanism of the oxidative reaction in fermentation.* The Journal of biological chemistry 1947. **170**(1).
65. Barron, J.T., L. Gu, and J.E. Parrillo, *NADH/NAD redox state of cytoplasmic glycolytic compartments in vascular smooth muscle.* Am J Physiol Heart Circ Physiol, 2000. **279**(6): p. H2872-8.
66. Houtkooper, R.H., et al., *The secret life of NAD+: an old metabolite controlling new metabolic signaling pathways.* Endocr Rev, 2010. **31**(2): p. 194-223.
67. Warburg, O., *Hydrogen-transferring co-enzyme, its composition and mode of functioning.* Biochem. Z. , 1935. **280**: p. 157-205.
68. Di Stefano, M. and L. Conforti, *Diversification of NAD biological role : the importance of location.* FEBS Journal, 2013. **280**(19): p. 4711-4728.
69. Baker, B.Y., et al., *High-resolution crystal structures of the photoreceptor glyceraldehyde 3-phosphate dehydrogenase (GAPDH) with three and four-bound NAD molecules.* Protein Sci, 2014. **23**(11): p. 1629-39.
70. Kerbey, A.L., P.M. Radcliffe, and P.J. Randle, *Diabetes and the control of pyruvate dehydrogenase in rat heart mitochondria by concentration ratios of adenosine triphosphate/adenosine diphosphate, of reduced/oxidized nicotinamide-adenine dinucleotide and of acetyl-coenzyme A/coenzyme A.* Biochemical Journal, 1977. **164**(3): p. 509-519.
71. Aubert, G., et al., *The Failing Heart Relies on Ketone Bodies as a Fuel.* Circulation, 2016. **133**(8): p. 698-705.
72. Rindler, P.M., et al., *Redox regulation of insulin sensitivity due to enhanced fatty acid utilization in the mitochondria.* American Journal of Physiology - Heart and Circulatory Physiology, 2013. **305**(5): p. H634-H643.
73. Chen, J.-Q. and J. Russo, *Dysregulation of glucose transport, glycolysis, TCA cycle and glutaminolysis by oncogenes and tumor suppressors in cancer cells.* Biochimica et Biophysica Acta (BBA) - Reviews on Cancer, 2012. **1826**(2): p. 370-384.
74. Tan, B., et al., *Pharmacological inhibition of nicotinamide phosphoribosyltransferase (NAMPT), an enzyme essential for NAD+ biosynthesis, in human cancer cells: metabolic basis and potential clinical implications.* J Biol Chem, 2013. **288**(5): p. 3500-11.
75. Ju, H.Q., et al., *Regulation of the Nampt-mediated NAD salvage pathway and its therapeutic implications in pancreatic cancer.* Cancer Lett, 2016. **379**(1): p. 1-11.
76. Frederick, D.W., et al., *Loss of NAD Homeostasis Leads to Progressive and Reversible Degeneration of Skeletal Muscle.* Cell Metab, 2016. **24**(2): p. 269-82.

77. Tedeschi, P.M., et al., *NAD+ Kinase as a Therapeutic Target in Cancer.* Clin Cancer Res, 2016. **22**(21): p. 5189-5195.
78. Stincone, A., et al., *The return of metabolism: biochemistry and physiology of the pentose phosphate pathway.* Biological reviews of the Cambridge Philosophical Society, 2015. **90**(3): p. 927-963.
79. Campbell, K., et al., *Methionine Metabolism Alters Oxidative Stress Resistance via the Pentose Phosphate Pathway.* Antioxidants & Redox Signaling, 2016. **24**(10): p. 543-547.
80. Kurosawa, K., et al., *Kinetics of hydroperoxide degradation by NADP-glutathione system in mitochondria.* J Biochem, 1990. **108**(1): p. 9-16.
81. Rechsteiner, M., D. Hillyard, and B.M. Olivera, *Magnitude and significance of NAD turnover in human cell line D98/AH2.* Nature, 1976. **259**(5545): p. 695-6.
82. Rechsteiner, M. and V. Catanzarite, *The biosynthesis and turnover of nicotinamide adenine dinucleotide in enucleated culture cells.* J Cell Physiol, 1974. **84**(3): p. 409-22.
83. Kim, M.Y., T. Zhang, and W.L. Kraus, *Poly(ADP-ribosyl)ation by PARP-1: 'PAR-laying' NAD+ into a nuclear signal.* Genes Dev, 2005. **19**(17): p. 1951-67.
84. Hayashida, S., et al., *Fasting promotes the expression of SIRT1, an NAD+-dependent protein deacetylase, via activation of PPARα in mice.* Molecular and Cellular Biochemistry, 2010. **339**(1-2): p. 285-292.
85. Aksoy, P., et al., *Regulation of SIRT 1 mediated NAD dependent deacetylation: a novel role for the multifunctional enzyme CD38.* Biochem Biophys Res Commun, 2006. **349**(1): p. 353-9.
86. Mouchiroud, L., R.H. Houtkooper, and J. Auwerx, *NAD(+) metabolism, a therapeutic target for age-related metabolic disease.* Critical reviews in biochemistry and molecular biology, 2013. **48**(4): p. 10.3109/10409238.2013.789479.
87. Robu, M., et al., *Role of poly(ADP-ribose) polymerase-1 in the removal of UV-induced DNA lesions by nucleotide excision repair.* Proc Natl Acad Sci U S A, 2013. **110**(5): p. 1658-63.
88. Ashamu, G.A., et al., *Roles for adenosine ribose hydroxyl groups in cyclic adenosine 5'-diphosphate ribose-mediated Ca2+ release.* Biochemistry, 1997. **36**(31): p. 9509-17.
89. Braidy, N., et al., *Age Related Changes in NAD+ Metabolism Oxidative Stress and Sirt1 Activity in Wistar Rats.* PLoS ONE, 2011. **6**(4): p. e19194.
90. Laurent Mouchiroud, et al., *The NAD+/Sirtuin Pathway Modulates Longevity through Activation of Mitochondrial UPR and FOXO Signaling.* Cell, 2013. **154**(2): p. 430-441.
91. Soo Jin Yanga, et al., *Nicotinamide improves glucose metabolism and affects the hepatic NAD-sirtuin pathway in a rodent model of obesity and type 2 diabetes.* The Journal of Nutritional Biochemistry, 2014. **25**(1): p. 66-72.
92. Bai, P., et al., *PARP-1 Inhibition Increases Mitochondrial Metabolism through SIRT1 Activation.* Cell Metabolism, 2011. **13**(4): p. 461-468.
93. VanLinden, M.R., et al., *Subcellular Distribution of NAD+ between Cytosol and Mitochondria Determines the Metabolic Profile of Human Cells.* Journal of Biological Chemistry, 2015. **290**(46): p. 27644-27659.

94. Cambronne, X.A., et al., *Biosensor reveals multiple sources for mitochondrial NAD(+).* Science, 2016. **352**(6292): p. 1474-7.
95. Alano, C.C., et al., *Differences among cell types in NAD(+) compartmentalization: a comparison of neurons, astrocytes, and cardiac myocytes.* J Neurosci Res, 2007. **85**(15): p. 3378-85.
96. Pittelli, M., et al., *Inhibition of nicotinamide phosphoribosyltransferase: cellular bioenergetics reveals a mitochondrial insensitive NAD pool.* J Biol Chem, 2010. **285**(44): p. 34106-14.
97. Easlon, E., et al., *The malate-aspartate NADH shuttle components are novel metabolic longevity regulators required for calorie restriction-mediated life span extension in yeast.* Genes Dev, 2008. **22**(7): p. 931-44.
98. Graeff, R., et al., *Mechanism of cyclizing NAD to cyclic ADP-ribose by ADP-ribosyl cyclase and CD38.* J Biol Chem, 2009. **284**(40): p. 27629-36.
99. Cerutti, R., et al., *NAD(+)-dependent activation of Sirt1 corrects the phenotype in a mouse model of mitochondrial disease.* Cell Metab, 2014. **19**(6): p. 1042-9.
100. Charron, M.J. and S. Bonner-Weir, *Implicating PARP and NAD+ depletion in type I diabetes.* Nat Med, 1999. **5**(3): p. 269-70.
101. Dali-Youcef, N., et al., *Sirtuins: The 'magnificent seven', function, metabolism and longevity.* Annals of Medicine, 2007. **39**(5): p. 335-345.
102. Rahat, O., N. Maoz, and H.Y. Cohen, *Multiple Pathways Regulating the Calorie Restriction Response in Yeast.* The Journals of Gerontology Series A: Biological Sciences and Medical Sciences, 2011. **66A**(2): p. 163-169.
103. Hall, J.A., et al., *The sirtuin family's role in aging and age-associated pathologies.* The Journal of Clinical Investigation, 2013. **123**(3): p. 973-979.
104. Burnett, C., et al., *Absence of effects of Sir2 overexpression on lifespan in C. elegans and Drosophila.* Nature, 2011. **477**(7365): p. 482-485.
105. Jackson, M.D., et al., *Mechanism of nicotinamide inhibition and transglycosidation by Sir2 histone/protein deacetylases.* J Biol Chem, 2003. **278**(51): p. 50985-98.
106. Tanner, K.G., et al., *Silent information regulator 2 family of NAD- dependent histone/protein deacetylases generates a unique product, 1-O-acetyl-ADP-ribose.* Proceedings of the National Academy of Sciences, 2000. **97**(26): p. 14178-14182.
107. Frye, R.A., *Phylogenetic Classification of Prokaryotic and Eukaryotic Sir2-like Proteins.* Biochemical and Biophysical Research Communications, 2000. **273**(2): p. 793-798.
108. Houtkooper, R.H., E. Pirinen, and J. Auwerx, *Sirtuins as regulators of metabolism and healthspan.* Nat Rev Mol Cell Biol, 2012. **13**(4): p. 225-238.
109. North, B.J., et al., *The Human Sir2 Ortholog, SIRT2, Is an NAD+-Dependent Tubulin Deacetylase.* Molecular Cell, 2003. **11**(2): p. 437-444.
110. Hallows, W.C., B.N. Albaugh, and J.M. Denu, *Where in the cell is SIRT3? – functional localization of an NAD+-dependent protein deacetylase.* Biochem J, 2008. **411**(2): p. e11-e13.
111. Serrano, L., et al., *The tumor suppressor SirT2 regulates cell cycle progression and genome stability by modulating the mitotic deposition of H4K20 methylation.* Genes & Development, 2013. **27**(6): p. 639-653.
112. Mao, Z., et al., *SIRT6 Promotes DNA Repair Under Stress by Activating PARP1.* Science, 2011. **332**(6036): p. 1443-1446.

113. Nogueiras, R., et al., *Sirtuin 1 and Sirtuin 3: Physiological Modulators of Metabolism.* Physiological Reviews, 2012. **92**(3): p. 1479-1514.
114. Lee, D. and A.L. Goldberg, *SIRT1 Protein, by Blocking the Activities of Transcription Factors FoxO1 and FoxO3, Inhibits Muscle Atrophy and Promotes Muscle Growth.* Journal of Biological Chemistry, 2013. **288**(42): p. 30515-30526.
115. Li, L., et al., *Mitochondrial Biogenesis and Peroxisome Proliferator–Activated Receptor-γ Coactivator-1α (PGC-1α) Deacetylation by Physical Activity: Intact Adipocytokine Signaling Is Required.* Diabetes, 2011. **60**(1): p. 157-167.
116. Rodgers, J.T., et al., *Nutrient control of glucose homeostasis through a complex of PGC-1[alpha] and SIRT1.* Nature, 2005. **434**(7029): p. 113-118.
117. Erion, D.M., et al., *SirT1 knockdown in liver decreases basal hepatic glucose production and increases hepatic insulin responsiveness in diabetic rats.* Proceedings of the National Academy of Sciences, 2009. **106**(27): p. 11288-11293.
118. Rodgers, J.T. and P. Puigserver, *Fasting-dependent glucose and lipid metabolic response through hepatic sirtuin 1.* Proceedings of the National Academy of Sciences, 2007. **104**(31): p. 12861-12866.
119. Jing, E., et al., *Sirt3 Regulates Metabolic Flexibility of Skeletal Muscle Through Reversible Enzymatic Deacetylation.* Diabetes, 2013. **62**(10): p. 3404-3417.
120. Tallis, M., et al., *Poly(ADP-ribosyl)ation in regulation of chromatin structure and the DNA damage response.* Chromosoma, 2014. **123**(1-2): p. 79-90.
121. Durkacz, B.W., et al., *(ADP-ribose)n participates in DNA excision repair.* Nature, 1980. **283**(5747): p. 593-6.
122. Langelier, M.F., A.A. Riccio, and J.M. Pascal, *PARP-2 and PARP-3 are selectively activated by 5' phosphorylated DNA breaks through an allosteric regulatory mechanism shared with PARP-1.* Nucleic Acids Res, 2014. **42**(12): p. 7762-75.
123. El-Khamisy, S.F., et al., *A requirement for PARP-1 for the assembly or stability of XRCC1 nuclear foci at sites of oxidative DNA damage.* Nucleic Acids Res, 2003. **31**(19): p. 5526-33.
124. Andrabi, S.A., et al., *Poly(ADP-ribose) polymerase-dependent energy depletion occurs through inhibition of glycolysis.* Proc Natl Acad Sci U S A, 2014. **111**(28): p. 10209-14.
125. Kauppinen, T.M., L. Gan, and R.A. Swanson, *Poly(ADP-ribose) polymerase-1-induced NAD+ depletion promotes nuclear factor-κB transcriptional activity by preventing p65 de-acetylation.* Biochimica et Biophysica Acta (BBA) - Molecular Cell Research, 2013. **1833**(8): p. 1985-1991.
126. Sims, J.L., S.J. Berger, and N.A. Berger, *Poly(ADP-ribose) Polymerase inhibitors preserve nicotinamide adenine dinucleotide and adenosine 5'-triphosphate pools in DNA-damaged cells: mechanism of stimulation of unscheduled DNA synthesis.* Biochemistry, 1983. **22**(22): p. 5188-94.
127. Mohamed, J.S., et al., *MicroRNA-149 inhibits PARP-2 and promotes mitochondrial biogenesis via SIRT-1/PGC-1alpha network in skeletal muscle.* Diabetes, 2014. **63**(5): p. 1546-59.
128. Pillai, J.B., et al., *Poly(ADP-ribose) polymerase-1-dependent cardiac myocyte cell death during heart failure is mediated by NAD+ depletion and reduced Sir2alpha deacetylase activity.* J Biol Chem, 2005. **280**(52): p. 43121-30.
129. Bai, P., et al., *PARP-2 regulates SIRT1 expression and whole-body energy expenditure.* Cell Metab, 2011. **13**(4): p. 450-60.

130. Camacho-Pereira, J., et al., *CD38 Dictates Age-Related NAD Decline and Mitochondrial Dysfunction through an SIRT3-Dependent Mechanism.* Cell Metab, 2016. **23**(6): p. 1127-39.
131. Aksoy, P., et al., *Regulation of intracellular levels of NAD: a novel role for CD38.* Biochem Biophys Res Commun, 2006. **345**(4): p. 1386-92.
132. Naveen, K.N., et al., *Pellagra in a child--a rare entity.* Nutrition, 2013. **29**(11-12): p. 1426-8.
133. Pitche, P.T., *[Pellagra].* Sante, 2005. **15**(3): p. 205-8.
134. Hasmann, M. and I. Schemainda, *FK866, a Highly Specific Noncompetitive Inhibitor of Nicotinamide Phosphoribosyltransferase, Represents a Novel Mechanism for Induction of Tumor Cell Apoptosis.* Cancer Research, 2003. **63**(21): p. 7436-7442.
135. Yang, H., et al., *Nutrient-sensitive mitochondrial NAD+ levels dictate cell survival.* Cell, 2007. **130**(6): p. 1095-107.
136. Nikiforov, A., et al., *Pathways and Subcellular Compartmentation of NAD Biosynthesis in Human Cells: FROM ENTRY OF EXTRACELLULAR PRECURSORS TO MITOCHONDRIAL NAD GENERATION.* Journal of Biological Chemistry, 2011. **286**(24): p. 21767-21778.
137. Hara, N., et al., *Molecular identification of human glutamine- and ammonia-dependent NAD synthetases carbon-nitrogen hydrolase domain confers glutamine dependency.* Journal of Biological Chemistry, 2003.
138. Bender, D.A., B.I. Magboul, and D. Wynick, *Probable mechanisms of regulation of the utilization of dietary tryptophan, nicotinamide and nicotinic acid as precursors of nicotinamide nucleotides in the rat.* British Journal of Nutrition, 1982. **48**(1): p. 119-127.
139. Bender, D.A. and R. Olufunwa, *Utilization of tryptophan, nicotinamide and nicotinic acid as precursors for nicotinamide nucleotide synthesis in isolated rat liver cells. .* British Journal of Nutrition, 1988. **59**(1): p. 279-287.
140. Khan, J.A., X. Tao, and L. Tong, *Molecular basis for the inhibition of human NMPRTase, a novel target for anticancer agents.* Nat Struct Mol Biol, 2006. **13**(7): p. 582-588.
141. Gross, J.W., M. Rajavel, and C. Grubmeyer, *Kinetic Mechanism of Nicotinic Acid Phosphoribosyltransferase: Implications for Energy Coupling†.* Biochemistry, 1998. **37**(12): p. 4189-4199.
142. Bieganowski, P. and C. Brenner, *Discoveries of Nicotinamide Riboside as a Nutrient and Conserved NRK Genes Establish a Preiss-Handler Independent Route to NAD+ in Fungi and Humans.* Cell, 2004. **117**(4): p. 495-502.
143. Bogan, K.L. and C. Brenner, *Biochemistry: Niacin/NAD(P) A2 - Lennarz, William J*, in *Encyclopedia of Biological Chemistry*, M.D. Lane, Editor. 2013, Academic Press: Waltham. p. 172-178.
144. Collins, P.B. and S. Chaykin, *The Management of Nicotinamide and Nicotinic Acid in the Mouse.* Journal of Biological Chemistry, 1972. **247**(3): p. 778-783.
145. Canto, C., et al., *AMPK regulates energy expenditure by modulating NAD+ metabolism and SIRT1 activity.* Nature, 2009. **458**(7241): p. 1056-60.
146. Preiss, J. and P. Handler, *Biosynthesis of Diphosphopyridine Nucleotide: I. IDENTIFICATION OF INTERMEDIATES.* Journal of Biological Chemistry, 1958. **233**(2): p. 488-492.

147. Mori, V., et al., *Metabolic Profiling of Alternative NAD Biosynthetic Routes in Mouse Tissues.* PLoS ONE, 2014. **9**(11): p. e113939.
148. De Ingeniis, J., et al., *Glutamine versus ammonia utilization in the NAD synthetase family.* PLoS One, 2012. **7**(6): p. e39115.
149. Boshoff, H.I., et al., *Biosynthesis and recycling of nicotinamide cofactors in mycobacterium tuberculosis. An essential role for NAD in nonreplicating bacilli.* J Biol Chem, 2008. **283**(28): p. 19329-41.
150. Tan, B., et al., *Pharmacological Inhibition of Nicotinamide Phosphoribosyltransferase (NAMPT), an Enzyme Essential for NAD+ Biosynthesis, in Human Cancer Cells: METABOLIC BASIS AND POTENTIAL CLINICAL IMPLICATIONS.* Journal of Biological Chemistry, 2013. **288**(5): p. 3500-3511.
151. Garten, A., et al., *Nampt: linking NAD biology, metabolism and cancer.* Trends in Endocrinology & Metabolism. **20**(3): p. 130-138.
152. Bitterman, K.J., et al., *Inhibition of silencing and accelerated aging by nicotinamide, a putative negative regulator of yeast sir2 and human SIRT1.* J Biol Chem, 2002. **277**(47): p. 45099-107.
153. Wang, T., et al., *Structure of Nampt/PBEF/visfatin, a mammalian NAD+ biosynthetic enzyme.* Nat Struct Mol Biol, 2006. **13**(7): p. 661-2.
154. Samal, B., et al., *Cloning and characterization of the cDNA encoding a novel human pre-B-cell colony-enhancing factor.* Mol Cell Biol, 1994. **14**(2): p. 1431-7.
155. Fukuhara, A., et al., *Visfatin: a protein secreted by visceral fat that mimics the effects of insulin.* Science, 2005. **307**(5708): p. 426-30.
156. Harasim, E., A. Chabowski, and J. Gorski, *Lack of downstream insulin-mimetic effects of visfatin/eNAMPT on glucose and fatty acid metabolism in skeletal muscles.* Acta Physiol (Oxf), 2011. **202**(1): p. 21-8.
157. Garten, A., et al., *Physiological and pathophysiological roles of NAMPT and NAD metabolism.* Nat Rev Endocrinol, 2015. **11**(9): p. 535-46.
158. Revollo, J.R., et al., *Nampt/PBEF/Visfatin regulates insulin secretion in beta cells as a systemic NAD biosynthetic enzyme.* Cell Metab, 2007. **6**(5): p. 363-75.
159. Kitani, T., S. Okuno, and H. Fujisawa, *Growth phase-dependent changes in the subcellular localization of pre-B-cell colony-enhancing factor.* FEBS Lett, 2003. **544**(1-3): p. 74-8.
160. Hara, N., et al., *Nicotinamide Phosphoribosyltransferase/Visfatin Does Not Catalyze Nicotinamide Mononucleotide Formation in Blood Plasma.* PLOS ONE, 2011. **6**(8): p. e22781.
161. Romacho, T., et al., *Extracellular PBEF/NAMPT/visfatin activates pro-inflammatory signalling in human vascular smooth muscle cells through nicotinamide phosphoribosyltransferase activity.* Diabetologia, 2009. **52**(11): p. 2455-63.
162. Audrito, V., et al., *Extracellular nicotinamide phosphoribosyltransferase (NAMPT) promotes M2 macrophage polarization in chronic lymphocytic leukemia.* Blood, 2015. **125**(1): p. 111-23.
163. Li, Y., et al., *Extracellular Nampt promotes macrophage survival via a nonenzymatic interleukin-6/STAT3 signaling mechanism.* J Biol Chem, 2008. **283**(50): p. 34833-43.
164. Tempel, W., et al., *Nicotinamide Riboside Kinase Structures Reveal New Pathways to NAD⁺.* PLoS Biol, 2007. **5**(10): p. e263.

165. Dölle, C. and M. Ziegler, *Application of a coupled enzyme assay to characterize nicotinamide riboside kinases.* Analytical Biochemistry, 2009. **385**(2): p. 377-379.
166. Ratajczak, J., et al., *NRK1 controls nicotinamide mononucleotide and nicotinamide riboside metabolism in mammalian cells.* Nat Commun, 2016. **7**: p. 13103.
167. Sasaki, Y., T. Araki, and J. Milbrandt, *Stimulation of Nicotinamide Adenine Dinucleotide Biosynthetic Pathways Delays Axonal Degeneration after Axotomy.* The Journal of Neuroscience, 2006. **26**(33): p. 8484-8491.
168. Stein, L.R. and S. Imai, *Specific ablation of Nampt in adult neural stem cells recapitulates their functional defects during aging.* EMBO J, 2014. **33**(12): p. 1321-40.
169. Zhou, C.C., et al., *Hepatic NAD(+) deficiency as a therapeutic target for non-alcoholic fatty liver disease in ageing.* Br J Pharmacol, 2016. **173**(15): p. 2352-68.
170. Yoshino, J., et al., *Nicotinamide mononucleotide, a key NAD(+) intermediate, treats the pathophysiology of diet- and age-induced diabetes in mice.* Cell Metab, 2011. **14**(4): p. 528-36.
171. Bogan, K.L. and C. Brenner, *Nicotinic Acid, Nicotinamide, and Nicotinamide Riboside: A Molecular Evaluation of NAD+ Precursor Vitamins in Human Nutrition.* Annual Review of Nutrition, 2008. **28**(1): p. 115-130.
172. Li, J., R. Mayne, and C. Wu, *A Novel Muscle-Specific β1 Integrin Binding Protein (Mibp) That Modulates Myogenic Differentiation.* The Journal of Cell Biology, 1999. **147**(7): p. 1391-1398.
173. Goody, M.F., et al., *NAD+ Biosynthesis Ameliorates a Zebrafish Model of Muscular Dystrophy.* PLoS Biol, 2012. **10**(10): p. e1001409.
174. Koltai, E., et al., *Exercise alters SIRT1, SIRT6, NAD and NAMPT levels in skeletal muscle of aged rats.* Mech Ageing Dev, 2010. **131**(1): p. 21-8.
175. Brandauer, J., et al., *AMP-activated protein kinase regulates nicotinamide phosphoribosyl transferase expression in skeletal muscle.* J Physiol, 2013. **591**(20): p. 5207-20.
176. Neufer, P.D. and G.L. Dohm, *Exercise induces a transient increase in transcription of the GLUT-4 gene in skeletal muscle.* Am J Physiol, 1993. **265**(6 Pt 1): p. C1597-603.
177. Bori, Z., et al., *The effects of aging, physical training, and a single bout of exercise on mitochondrial protein expression in human skeletal muscle.* Experimental gerontology, 2012. **47**(6): p. 417-424.
178. Trammell, S.A., et al., *Nicotinamide Riboside Opposes Type 2 Diabetes and Neuropathy in Mice.* Sci Rep, 2016. **6**: p. 26933.
179. Brown, K.D., et al., *Activation of SIRT3 by the NAD(+) precursor nicotinamide riboside protects from noise-induced hearing loss.* Cell Metab, 2014. **20**(6): p. 1059-68.
180. Lehmann, S., et al., *Parp mutations protect against mitochondrial dysfunction and neurodegeneration in a PARKIN model of Parkinson's disease.* Cell Death Dis, 2016. **7**: p. e2166.
181. Gomes, A.P., et al., *Declining NAD(+) induces a pseudohypoxic state disrupting nuclear-mitochondrial communication during aging.* Cell, 2013. **155**(7): p. 1624-38.

182. Iannuzzi-Sucich, M., K.M. Prestwood, and A.M. Kenny, *Prevalence of sarcopenia and predictors of skeletal muscle mass in healthy, older men and women.* J Gerontol A Biol Sci Med Sci, 2002. **57**(12): p. M772-7.
183. Szulc, P., et al., *Hormonal and lifestyle determinants of appendicular skeletal muscle mass in men: the MINOS study.* Am J Clin Nutr, 2004. **80**(2): p. 496-503.
184. Morley, J.E., *Sarcopenia in the elderly.* Fam Pract, 2012. **29 Suppl 1**: p. i44-i48.
185. Sanchez-Rodriguez, D., et al., *Prevalence of malnutrition and sarcopenia in a post-acute care geriatric unit: Applying the new ESPEN definition and EWGSOP criteria.* Clin Nutr, 2016.
186. Hsu, C.P., et al., *Nicotinamide phosphoribosyltransferase regulates cell survival through NAD+ synthesis in cardiac myocytes.* Circ Res, 2009. **105**(5): p. 481-91.
187. Mohamed, J.S., et al., *Dysregulation of SIRT-1 in aging mice increases skeletal muscle fatigue by a PARP-1-dependent mechanism.* Aging (Albany NY), 2014. **6**(10): p. 820-34.
188. To, C., et al., *The PARP inhibitors, veliparib and olaparib, are effective chemopreventive agents for delaying mammary tumor development in BRCA1-deficient mice.* Cancer Prev Res (Phila), 2014. **7**(7): p. 698-707.
189. Milne, J.C., et al., *Small molecule activators of SIRT1 as therapeutics for the treatment of type 2 diabetes.* Nature, 2007. **450**(7170): p. 712-6.
190. Feige, J.N., et al., *Specific SIRT1 activation mimics low energy levels and protects against diet-induced metabolic disorders by enhancing fat oxidation.* Cell Metab, 2008. **8**(5): p. 347-58.
191. Fujitaka, K., et al., *Modified resveratrol Longevinex improves endothelial function in adults with metabolic syndrome receiving standard treatment.* Nutr Res, 2011. **31**(11): p. 842-7.
192. Trammell, S.A., et al., *Nicotinamide Riboside Is a Major NAD+ Precursor Vitamin in Cow Milk.* J Nutr, 2016. **146**(5): p. 957-63.
193. Altschul, R., A. Hoffer, and J.D. Stephen, *Influence of nicotinic acid on serum cholesterol in man.* Arch Biochem Biophys, 1955. **54**(2): p. 558-9.
194. Taskinen, M.R. and E.A. Nikkila, *Effects of acipimox on serum lipids, lipoproteins and lipolytic enzymes in hypertriglyceridemia.* Atherosclerosis, 1988. **69**(2-3): p. 249-55.
195. Benyo, Z., et al., *Nicotinic acid-induced flushing is mediated by activation of epidermal langerhans cells.* Mol Pharmacol, 2006. **70**(6): p. 1844-9.
196. van de Weijer, T., et al., *Evidence for a direct effect of the NAD+ precursor acipimox on muscle mitochondrial function in humans.* Diabetes, 2015. **64**(4): p. 1193-201.
197. Lee, S.J., et al., *Protective effect of nicotinamide on high glucose/palmitate-induced glucolipotoxicity to INS-1 beta cells is attributed to its inhibitory activity to sirtuins.* Arch Biochem Biophys, 2013. **535**(2): p. 187-96.
198. Liu, D., et al., *Nicotinamide prevents NAD+ depletion and protects neurons against excitotoxicity and cerebral ischemia: NAD+ consumption by SIRT1 may endanger energetically compromised neurons.* Neuromolecular Med, 2009. **11**(1): p. 28-42.
199. Cantó, C., et al., *The NAD+ Precursor Nicotinamide Riboside Enhances Oxidative Metabolism and Protects against High-Fat Diet-Induced Obesity.* Cell Metabolism, 2012. **15**(6): p. 838-847.

200. Uddin, G.M., et al., *Head to Head Comparison of Short-Term Treatment with the NAD(+) Precursor Nicotinamide Mononucleotide (NMN) and 6 Weeks of Exercise in Obese Female Mice.* Front Pharmacol, 2016. **7**: p. 258.
201. Trammell, S.A., et al., *Nicotinamide riboside is uniquely and orally bioavailable in mice and humans.* Nat Commun, 2016. **7**: p. 12948.
202. Ummarino, S., et al., *Simultaneous quantitation of nicotinamide riboside, nicotinamide mononucleotide and nicotinamide adenine dinucleotide in milk by a novel enzyme-coupled assay.* Food Chem, 2017. **221**: p. 161-168.
203. Mills, K.F., et al., *Long-Term Administration of Nicotinamide Mononucleotide Mitigates Age-Associated Physiological Decline in Mice.* Cell Metab, 2016. **24**(6): p. 795-806.
204. Wang, X., et al., *Nicotinamide mononucleotide protects against beta-amyloid oligomer-induced cognitive impairment and neuronal death.* Brain Res, 2016. **1643**: p. 1-9.
205. Long, A.N., et al., *Effect of nicotinamide mononucleotide on brain mitochondrial respiratory deficits in an Alzheimer's disease-relevant murine model.* BMC Neurol, 2015. **15**: p. 19.
206. de Picciotto, N.E., et al., *Nicotinamide mononucleotide supplementation reverses vascular dysfunction and oxidative stress with aging in mice.* Aging Cell, 2016. **15**(3): p. 522-30.
207. Khan, N.A., et al., *Effective treatment of mitochondrial myopathy by nicotinamide riboside, a vitamin B3.* EMBO Mol Med, 2014. **6**(6): p. 721-31.
208. Lu, S.P., M. Kato, and S.J. Lin, *Assimilation of endogenous nicotinamide riboside is essential for calorie restriction-mediated life span extension in Saccharomyces cerevisiae.* J Biol Chem, 2009. **284**(25): p. 17110-9.
209. Tan, B., et al., *Inhibition of Nicotinamide Phosphoribosyltransferase (NAMPT), an Enzyme Essential for NAD+ Biosynthesis, Leads to Altered Carbohydrate Metabolism in Cancer Cells.* J Biol Chem, 2015. **290**(25): p. 15812-24.
210. Chini, C.C., et al., *Targeting of NAD metabolism in pancreatic cancer cells: potential novel therapy for pancreatic tumors.* Clin Cancer Res, 2014. **20**(1): p. 120-30.
211. Zhang, L.Y., et al., *Anti-proliferation effect of APO866 on C6 glioblastoma cells by inhibiting nicotinamide phosphoribosyltransferase.* Eur J Pharmacol, 2012. **674**(2-3): p. 163-70.
212. Otero, M., et al., *Changes in plasma levels of fat-derived hormones adiponectin, leptin, resistin and visfatin in patients with rheumatoid arthritis.* Ann Rheum Dis, 2006. **65**(9): p. 1198-201.
213. Busso, N., et al., *Pharmacological Inhibition of Nicotinamide Phosphoribosyltransferase/Visfatin Enzymatic Activity Identifies a New Inflammatory Pathway Linked to NAD.* PLoS ONE, 2008. **3**(5): p. e2267.
214. Schilling, E., et al., *Inhibition of nicotinamide phosphoribosyltransferase modifies LPS-induced inflammatory responses of human monocytes.* Innate Immun, 2012. **18**(3): p. 518-30.
215. Yaffe, D. and O.R.A. Saxel, *Serial passaging and differentiation of myogenic cells isolated from dystrophic mouse muscle.* Nature, 1977. **270**(5639): p. 725-727.
216. Blau, H.M., C.-P. Chiu, and C. Webster, *Cytoplasmic activation of human nuclear genes in stable heterocaryons.* Cell, 1983. **32**(4): p. 1171-1180.

217. Burattini, S., et al., *C2C12 murine myoblasts as a model of skeletal muscle development: morpho-functional characterization.* Eur J Histochem, 2004. **48**(3): p. 223-33.
218. Rosenblatt, J.D., et al., *Culturing satellite cells from living single muscle fiber explants.* In Vitro Cellular & Developmental Biology - Animal, 1995. **31**(10): p. 773-779.
219. Schmittgen, T.D. and K.J. Livak, *Analyzing real-time PCR data by the comparative CT method.* Nat. Protocols, 2008. **3**(6): p. 1101-1108.
220. Schuster, S., et al., *Resveratrol differentially regulates NAMPT and SIRT1 in Hepatocarcinoma cells and primary human hepatocytes.* PLoS One, 2014. **9**(3): p. e91045.
221. Thompson, J.D., D.G. Higgins, and T.J. Gibson, *CLUSTAL W: improving the sensitivity of progressive multiple sequence alignment through sequence weighting, position-specific gap penalties and weight matrix choice.* Nucleic Acids Res, 1994. **22**(22): p. 4673-80.
222. Myers, E.W. and W. Miller, *Optimal alignments in linear space.* Comput Appl Biosci, 1988. **4**(1): p. 11-7.
223. Bioscience, S. http://www.seahorsebio.com/products/xfconsumables/xfcellmito.php. 2015.
224. Trammell, S.A.J. and C. Brenner, *Targeted, LCMS-based Metabolomics for Quantitative Measurement of NAD(+) Metabolites.* Computational and Structural Biotechnology Journal, 2013. **4**: p. e201301012.
225. http://www.jax.org/index.html. 2015.
226. Dolle, C., et al., *NAD biosynthesis in humans--enzymes, metabolites and therapeutic aspects.* Curr Top Med Chem, 2013. **13**(23): p. 2907-17.
227. Kim, J.S., C.S. Yoon, and D.R. Park, *NAMPT regulates mitochondria biogenesis via NAD metabolism and calcium binding proteins during skeletal muscle contraction.* J Exerc Nutrition Biochem, 2014. **18**(3): p. 259-66.
228. Samal, B., et al., *Cloning and characterization of the cDNA encoding a novel human pre-B-cell colony-enhancing factor.* Molecular and Cellular Biology, 1994. **14**(2): p. 1431-1437.
229. Mendelsohn, A.R. and J.W. Larrick, *Partial reversal of skeletal muscle aging by restoration of normal NAD(+) levels.* Rejuvenation Res, 2014. **17**(1): p. 62-9.
230. Lavery, G.G., et al., *Deletion of hexose-6-phosphate dehydrogenase activates the unfolded protein response pathway and induces skeletal myopathy.* J Biol Chem, 2008. **283**(13): p. 8453-61.
231. Hara, N., et al., *Molecular identification of human glutamine- and ammonia-dependent NAD synthetases. Carbon-nitrogen hydrolase domain confers glutamine dependency.* J Biol Chem, 2003. **278**(13): p. 10914-21.
232. Tomczak, K.K., et al., *Expression profiling and identification of novel genes involved in myogenic differentiation.* FASEB J, 2004. **18**(2): p. 403-5.
233. Meyer, A. and M. Schartl, *Gene and genome duplications in vertebrates: the one-to-four (-to-eight in fish) rule and the evolution of novel gene functions.* Curr Opin Cell Biol, 1999. **11**(6): p. 699-704.
234. Kimmel, C.B., et al., *Stages of embryonic development of the zebrafish.* Dev Dyn, 1995. **203**(3): p. 253-310.

235. Gordon, J.W., et al., *Selected contribution: Effects of contractile activity on mitochondrial transcription factor A expression in skeletal muscle.* Journal of Applied Physiology, 2001. **90**(1): p. 389-396.
236. Kulikova, V., et al., *Generation, Release, and Uptake of the NAD Precursor Nicotinic Acid Riboside by Human Cells.* J Biol Chem, 2015. **290**(45): p. 27124-37.
237. Nagatomo, F., et al., *PGC-1alpha and FOXO1 mRNA levels and fiber characteristics of the soleus and plantaris muscles in rats after hindlimb unloading.* Histol Histopathol, 2011. **26**(12): p. 1545-53.
238. Okamoto, T., S. Torii, and S. Machida, *Differential gene expression of muscle-specific ubiquitin ligase MAFbx/Atrogin-1 and MuRF1 in response to immobilization-induced atrophy of slow-twitch and fast-twitch muscles.* J Physiol Sci, 2011. **61**(6): p. 537-46.
239. Westerblad, H., J.D. Bruton, and A. Katz, *Skeletal muscle: Energy metabolism, fiber types, fatigue and adaptability.* Experimental Cell Research, 2010. **316**(18): p. 3093-3099.
240. Frederick, D.W., et al., *Increasing NAD synthesis in muscle via nicotinamide phosphoribosyltransferase is not sufficient to promote oxidative metabolism.* J Biol Chem, 2015. **290**(3): p. 1546-58.
241. Lin, S.-J. and L. Guarente, *Nicotinamide adenine dinucleotide, a metabolic regulator of transcription, longevity and disease.* Current Opinion in Cell Biology, 2003. **15**(2): p. 241-246.
242. Ryu, D., et al., *NAD⁺ repletion improves muscle function in muscular dystrophy and counters global PARylation.* Science Translational Medicine, 2016. **8**(361): p. 361ra139-361ra139.
243. Elkalaf, M., M. Anděl, and J. Trnka, *Low Glucose but Not Galactose Enhances Oxidative Mitochondrial Metabolism in C2C12 Myoblasts and Myotubes.* PLOS ONE, 2013. **8**(8): p. e70772.
244. Fulco, M., et al., *Glucose Restriction Inhibits Skeletal Myoblast Differentiation by Activating SIRT1 through AMPK-Mediated Regulation of Nampt.* Developmental Cell, 2008. **14**(5): p. 661-673.
245. Ramsey, K.M., et al., *Circadian Clock Feedback Cycle Through NAMPT-Mediated NAD⁺ Biosynthesis.* Science, 2009. **324**(5927): p. 651-654.
246. Pirinen, E., et al., *Pharmacological Inhibition of poly(ADP-ribose) polymerases improves fitness and mitochondrial function in skeletal muscle.* Cell Metab, 2014. **19**(6): p. 1034-41.
247. Gille, A., et al., *Nicotinic Acid: Pharmacological Effects and Mechanisms of Action.* Annual Review of Pharmacology and Toxicology, 2008. **48**(1): p. 79-106.
248. Wielgus-Kutrowska, B., et al., *Nicotinamide riboside, an unusual, non-typical, substrate of purified purine-nucleoside phosphorylases.* Eur J Biochem, 1997. **243**(1-2): p. 408-14.
249. Aksoy, S., C.L. Szumlanski, and R.M. Weinshilboum, *Human liver nicotinamide N-methyltransferase. cDNA cloning, expression, and biochemical characterization.* J Biol Chem, 1994. **269**(20): p. 14835-40.
250. Sims, J.L., S.J. Berger, and N.A. Berger, *Effects of nicotinamide on NAD and poly(ADP-ribose) metabolism in DNA-damaged human lymphocytes.* J Supramol Struct Cell Biochem, 1981. **16**(3): p. 281-8.

251. Lagouge, M., et al., *Resveratrol Improves Mitochondrial Function and Protects against Metabolic Disease by Activating SIRT1 and PGC-1&#x3b1.* Cell. **127**(6): p. 1109-1122.
252. Goody, M.F., et al., *Nrk2b-mediated NAD+ production regulates cell adhesion and is required for muscle morphogenesis in vivo: Nrk2b and NAD+ in muscle morphogenesis.* Dev Biol, 2010. **344**(2): p. 809-26.
253. Belenky, P., et al., *Nicotinamide riboside promotes Sir2 silencing and extends lifespan via Nrk and Urh1/Pnp1/Meu1 pathways to NAD+.* Cell, 2007. **129**(3): p. 473-84.
254. Ishihara, K. and T. Hirano, *BST-1/CD157 regulates the humoral immune responses in vivo.* Chem Immunol, 2000. **75**: p. 235-55.
255. Podesta, M., et al., *Extracellular cyclic ADP-ribose increases intracellular free calcium concentration and stimulates proliferation of human hemopoietic progenitors.* FASEB J, 2000. **14**(5): p. 680-90.
256. Pheiffer, C., et al., *Expression of UCP2 in Wistar rats varies according to age and the severity of obesity.* J Physiol Biochem, 2016. **72**(1): p. 25-32.
257. Toda, C. and S. Diano, *Mitochondrial UCP2 in the central regulation of metabolism.* Best Pract Res Clin Endocrinol Metab, 2014. **28**(5): p. 757-64.
258. Andrews, Z.B., et al., *Ghrelin promotes and protects nigrostriatal dopamine function via an UCP2-dependent mitochondrial mechanism.* The Journal of neuroscience : the official journal of the Society for Neuroscience, 2009. **29**(45): p. 14057-14065.
259. Finck, B.N. and D.P. Kelly, *PGC-1 coactivators: inducible regulators of energy metabolism in health and disease.* Journal of Clinical Investigation, 2006. **116**(3): p. 615-622.
260. Rao, N., et al., *Fibroblasts influence muscle progenitor differentiation and alignment in contact independent and dependent manners in organized co-culture devices.* Biomedical microdevices, 2013. **15**(1): p. 161-169.
261. Danoviz, M.E. and Z. Yablonka-Reuveni, *Skeletal Muscle Satellite Cells: Background and Methods for Isolation and Analysis in a Primary Culture System.* Methods in Molecular Biology (Clifton, N.j.), 2012. **798**: p. 21-52.
262. Kaeberlein, M., et al., *Sir2-Independent Life Span Extension by Calorie Restriction in Yeast.* PLOS Biology, 2004. **2**(9): p. e296.
263. Bruss, M.D., et al., *Calorie restriction increases fatty acid synthesis and whole body fat oxidation rates.* Am J Physiol Endocrinol Metab, 2010. **298**(1): p. E108-16.
264. Zhang, L.Q., D.P. Heruth, and S.Q. Ye, *Nicotinamide Phosphoribosyltransferase in Human Diseases.* Journal of bioanalysis & biomedicine, 2011. **3**: p. 013-025.
265. Stromsdorfer, K.L., et al., *NAMPT-mediated NAD(+) biosynthesis in adipocytes regulates adipose tissue function and multi-organ insulin sensitivity in mice.* Cell reports, 2016. **16**(7): p. 1851-1860.
266. Zhang, H., et al., *NAD⁺ repletion improves mitochondrial and stem cell function and enhances life span in mice.* Science, 2016. **352**(6292): p. 1436-1443.
267. Xu, F., et al., *Diet-induced obesity and insulin resistance are associated with brown fat degeneration in SIRT1-deficient mice.* Obesity (Silver Spring), 2016. **24**(3): p. 634-42.

268. Simonson, D.C. and R.A. DeFronzo, *Indirect calorimetry: methodological and interpretative problems.* American Journal of Physiology - Endocrinology And Metabolism, 1990. **258**(3): p. E399-E412.
269. Peronnet, F. and D. Massicotte, *Table of nonprotein respiratory quotient: an update.* Can J Sport Sci, 1991. **16**(1): p. 23-9.
270. Jequier, E., K. Acheson, and Y. Schutz, *Assessment of energy expenditure and fuel utilization in man.* Annu Rev Nutr, 1987. **7**: p. 187-208.
271. Brown, J.D., S.P. Naples, and F.W. Booth, *Effects of voluntary running on oxygen consumption, RQ, and energy expenditure during primary prevention of diet-induced obesity in C57BL/6N mice.* Journal of Applied Physiology, 2012. **113**(3): p. 473-478.
272. Cummins, T.D., et al., *Metabolic remodeling of white adipose tissue in obesity.* Am J Physiol Endocrinol Metab, 2014. **307**(3): p. E262-77.
273. Keim, N.L. and W.F. Horn, *Restrained eating behavior and the metabolic response to dietary energy restriction in women.* Obes Res, 2004. **12**(1): p. 141-9.
274. Bergman, B.C. and G.A. Brooks, *Respiratory gas-exchange ratios during graded exercise in fed and fasted trained and untrained men.* J Appl Physiol (1985), 1999. **86**(2): p. 479-87.
275. Oosterman, J.E., et al., *Timing of fat and liquid sugar intake alters substrate oxidation and food efficiency in male Wistar rats.* Chronobiol Int, 2015. **32**(2): p. 289-98.
276. Shi, W., et al., *Effects of a wide range of dietary nicotinamide riboside (NR) concentrations on metabolic flexibility and white adipose tissue (WAT) of mice fed a mildly obesogenic diet.* Mol Nutr Food Res, 2017.
277. Aguilar, C.A., et al., *In vivo Monitoring of Transcriptional Dynamics After Lower-Limb Muscle Injury Enables Quantitative Classification of Healing.* Scientific Reports, 2015. **5**: p. 13885.
278. Xu, W., et al., *Lethal cardiomyopathy in mice lacking transferrin receptor in the heart.* Cell reports, 2015. **13**(3): p. 533-545.
279. Smith, L.R., et al., *Transcriptional Abnormalities of Hamstring Muscle Contractures in Children with Cerebral Palsy.* PLOS ONE, 2012. **7**(8): p. e40686.
280. Zielinska, A., *Investigations into the integrated metabolism of glucocorticoids and glucose in skeletal muscle.* etheses, University of Birmingham, 2015.
281. Cordain, L., et al., *Origins and evolution of the Western diet: health implications for the 21st century.* The American Journal of Clinical Nutrition, 2005. **81**(2): p. 341-354.
282. Hamity, M.V., et al., *Nicotinamide riboside, a form of vitamin B3 and NAD+ precursor, relieves the nociceptive and aversive dimensions of paclitaxel-induced peripheral neuropathy in female rats.* PAIN, 2017. **158**(5): p. 962-972.
283. Caton, P.W., et al., *Nicotinamide mononucleotide protects against pro-inflammatory cytokine-mediated impairment of mouse islet function.* Diabetologia, 2011. **54**(12): p. 3083-3092.
284. Ramsey, K.M., et al., *Age-associated loss of Sirt1-mediated enhancement of glucose-stimulated insulin secretion in beta cell-specific Sirt1-overexpressing (BESTO) mice.* Aging Cell, 2008. **7**(1): p. 78-88.
285. Cynamon, M.H., T.B. Sorg, and A. Patapow, *Utilization and metabolism of NAD by Haemophilus parainfluenzae.* J Gen Microbiol, 1988. **134**(10): p. 2789-99.